ADVANCES IN SPACE MAPPING OPTIMIZATION OF MICROWAVE CIRCUITS

By

MOHAMED H. BAKR, M.Sc.

A Thesis

Submitted to the School of Graduate Studies

in Partial Fulfillment of the Requirements

for the Degree

Doctor of Philosophy

McMaster University

September 2000

ADVANCES IN SPACE MAPPING OPTIMIZATION OF MICROWAVE CIRCUITS

To My Parents

DOCTOR OF PHILOSOPHY (2000) McMASTER UNIVERSITY
(Electrical Engineering) Hamilton, Ontario

TITLE: **Advances in Space Mapping Optimization of Microwave Circuits**

AUTHORS: Mohamed H. Bakr
M.Sc.
(Faculty of Engineering, Cairo University)

SUPERVISOR: J.W. Bandler
Professor, Department of Electrical and Computer Engineering
B.Sc. (Eng.), Ph.D., D.Sc. (Eng.) (University of London)
D.I.C. (Imperial College)
P.Eng. (Province of Ontario)
C.Eng. F.I.E.E. (United Kingdom)
Fellow, I.E.E.E.
Fellow, Royal Society of Canada
Fellow, E.I.C.

NUMBER OF PAGES: clxxx, 180

ABSTRACT

This thesis concerns itself with advances in Space Mapping optimization of microwave circuits and with the developments in Parameter Extraction.

Space Mapping (SM) optimization aims at efficiently optimizing microwave circuits using the accurate and time-intensive electromagnetic simulators. Such simulators represent "fine" models of the circuit under consideration. SM exploits the existence of a less accurate but fast "coarse" model, e.g., an empirical model. A mapping is established between the parameter spaces of the coarse and fine models. The fine model design is the inverse mapping of the optimal coarse model design. A crucial step for any SM-based optimization algorithm is Parameter Extraction (PE). In this step a coarse model point that corresponds to a given fine model response is obtained through an optimization process. The nonuniqueness of PE can lead to divergence or oscillation of the optimization iterates.

We introduced the Trust Region Aggressive Space Mapping (TRASM) algorithm. This algorithm integrates a trust region methodology with SM optimization. The iterate is confined to a trust region in which the utilized linearization can be trusted. TRASM also exploits a recursive multi-point parameter extraction step to enhance the uniqueness of PE.

The Aggressive Parameter Extraction (APE) algorithm addresses the optimal selection of parameter perturbations used to increase trust in PE uniqueness. We establish an appropriate criterion for the generation of these perturbations. The APE algorithm classifies possible solutions for the PE problem. Two different approaches for obtaining subsequent perturbations are utilized based on a classification of the extracted parameters. The algorithm is demonstrated through parameter extraction of microwave filters and transformers.

The Hybrid Aggressive Space Mapping (HASM) algorithm addresses the case of a poor coarse model. HASM utilizes SM optimization as long as it is converging. Otherwise, it

switches to a direct optimization phase. We developed a relationship that relates the established mapping and the first order derivatives of the coarse and fine models. This relationship is utilized in switching between the SM phase and the direct optimization phase.

We also present a Surrogate Model-based Space Mapping (SMSM) optimization algorithm. SMSM integrates two approaches for efficient optimization: SM optimization and surrogate model optimization. It exploits a surrogate model in predicting new iterates. This model is a convex combination between a mapped coarse model and a linearized fine model. The mapped coarse model exploits a frequency-sensitive mapping. During the optimization iterates, the coarse and fine models are simulated at two different sets of frequencies. Utilizing a frequency sensitive mapping is shown to enhance the uniqueness of PE. It also overcomes severe frequency misalignments between the responses of both models.

ACKNOWLEDGEMENTS

The author wishes to express his sincere appreciation for Dr. J.W. Bandler of Bandler Corporation for his expert guidance and supervision throughout the course of this work. In addition to his constant encouragement and inspiration the author derived from him, the opportunity given by Dr. Bandler to be involved in relevant industrial projects and research is thankfully acknowledged. In particular, he spent a year with Optimization Systems Associates Inc. as a student intern.

The author offers his gratitude to Dr. R.M. Biernacki, currently with Agilent Technologies, for his expert advice and fruitful discussions during the early phase of this work.

The author would like also to express his appreciation to Dr. K. Madsen of the Institute of Mathematical Modeling, the Technical University of Denmark, for his expert advice in addition to lectures and discussions at both McMaster University and the Technical University of Denmark.

The author thanks Sonnet Software, Inc., Liverpool, NY for making *em* available for this work. He also thanks HP EESof, now Agilent Technologies, Santa Rosa, CA, for making HP HFSS and HP Empipe3D available. Thanks are also due to Optimization Systems Associates Inc., Dundas, ON, for making OSA90/hope available. The author wishes to thank Ansoft Corporation for making Maxwell Eminence available at an early stage of this work.

The author would like to thank his colleagues Dr. N. Georgieva, M.A. Ismail, J.E. Rayas-Sánchez and J. Søndergaard (Technical University of Denmark) for productive collaboration and stimulating discussions. He also acknowledges their nice company that made many of the tough times bearable.

Support has been provided in part by the Natural Sciences and Engineering Research Council of Canada through grants OGP0007239, STP0201832, the Micronet Network of Centres

of Excellence, TRIO and Bandler Corporation in addition to an Ontario Graduate Scholarship (OGS). The author also extends his gratitude to the Department of Electrical and Computer Engineering, McMaster University, for a Teaching Assistantship, a Research Assistantship and Scholarship.

Finally, thanks are due to my parents for their continuous encouragement, understanding, patience and support.

CONTENTS

ABSTRACT.....iii

ACKNOWLEDGEMENTS.....v

LIST OF FIGURES.....ix

LIST OF TABLES.....xvii

LIST OF SYMBOLS.....xix

1.0 INTRODUCTION.....1
- 1.1 Motivation.....1
- 1.2 Contributions.....2
- 1.3 Outline of Thesis.....2

2.0 REVIEW OF SOME CONCEPTS IN CIRCUIT OPTIMIZATION.....5
- 2.1 Introduction.....5
- 2.2 Design Specifications and Error Functions.....6
- 2.3 Norms and Optimization Methods.....10
- 2.4 Space Mapping Optimization: the Basic Concept.....14
- 2.5 The Original SM Optimization Algorithm.....14
- 2.6 The ASM Algorithm.....18
- 2.7 Three-Section Microstrip Transformer.....22
- 2.8 Conclusions.....26

3.0 THE TRUST REGION AGGRESSIVE SPACE MAPPING ALGORITHM.....27
- 3.1 Introduction.....27
- 3.2 Trust Region Methodologies in Optimization.....28
- 3.3 The TRASM algorithm.....29
- 3.4 Examples.....35
  - 3.4.1 Double-Folded Stub Filter.....35
  - 3.4.2 HTS Filter.....36
  - 3.4.3 Waveguide Transformers.....46
  - 3.4.4 A Three-Section Transformer with Rounded Corners.....58
- 3.5 Monte Carlo Analysis Using Space Mapping.....62
- 3.6 Conclusions.....65

4.0 THE AGGRESSIVE PARAMETER EXTRACTION ALGORITHM.....67
- 4.1 Introduction.....67
- 4.2 The Parameter Extraction Problem.....68
- 4.3 The Selection of Perturbations.....71
- 4.4 The APE Algorithm.....77
- 4.5 Examples.....78
  - 4.5.1 The Rosenbrock Function.....78
  - 4.5.2 A 10:1 Impedance Transformer.....83

4.5.3 The HTS Filter....85
4.5.4 Double-Folded Stub Filter....90
4.6 Conclusions....102

5.0 THE HYBRID AGGRESSIVE SPACE MAPPING ALGORITHM....103
5.1 Introduction....103
5.2 The Motivation for a Hybrid Algorithm....104
5.3 Space Mapping and Direct Optimization....106
5.4 Selection of the Starting Point for Parameter Extraction....112
5.5 The HASM Algorithm....112
5.6 Examples....119
5.6.1 Three-Section Waveguide Transformer....119
5.6.2 Six-Section H-Plane Waveguide Filter....119
5.6.3 Seven-Section Waveguide Transformer....123
5.6.4 Double-Folded Stub Filter....127
5.7 Conclusions....134

6.0 SURROGATE MODEL-BASED-SPACE MAPPING OPTIMIZATION 135
6.1 Introduction....135
6.2 Space Mapping Optimization vs. Surrogate-Based Optimization....136
6.3 The Surrogate Model....137
6.4 The SMSM Algorithm....141
6.5 Examples....144
6.5.1 The Rosenbrock Example....144
6.5.2 A Capacitively-Loaded 10:1 Impedance Transformer....147
6.5.3 The Double-Folded Stub Filter....155
6.5.4 The HTS Filter....158
6.6 Conclusions....166

7.0 CONCLUSIONS....167

Bibliography....171

Subject Index....179

LIST OF FIGURES

2.1. Illustration of some basic engineering optimization concepts; (a) the responses at a feasible design x_1 and an infeasible design x_2, (b) the error functions at sampled values of the independent parameter ω and (c) a possible location of the two designs with respect to the feasible region for a two-dimensional case.....9

2.2. Illustration of design centering and yield for a two-dimensional problem with manufacturing tolerances of Δx_1 and Δx_2. Three different designs are shown; a centered design where all possible outcomes are feasible (yield=1), an infeasible design where possible outcomes are infeasible (yield=0) and non centered feasible design where possible outcomes may be feasible or infeasible (0<yield<1).....13

2.3. Illustration of the SPE procedure.....16

2.4. Illustration of the original SM optimization algorithm; (a) a new point $x_f^{(m_i+1)}$ is obtained using the current mapping $P^{(i)}$, (b) the point $x_f^{(m_i+1)}$ does not satisfy the stopping criterion and the sets $S_f^{(i)}$ and $S_c^{(i)}$ are augmented by $x_f^{(m_i+1)}$ and $x_c^{(m_i+1)}$, respectively, and (c) a new mapping $P^{(i+1)}$ is estimated and is used to obtain a new iterate $x_f^{(m_i+2)}$.....19

2.5. Illustration of ASM; (a) a new iterate $x_f^{(i+1)}$ is obtained, (b) by applying parameter extraction we find that the stopping criterion is not satisfied ($\|f^{(i+1)}\| > \varepsilon$) and (c) the updated matrix $B^{(i+1)}$ is used to predict a new iterate $x_f^{(i+2)}$.....21

2.6. The three-section 3:1 microstrip impedance transformer.....23

2.7 The coarse model of the three-section 3:1 microstrip impedance transformer.....23

2.8 The optimal coarse model response (—) and the fine model response (o) at the initial design for the three-section microstrip transformer.....25

2.9 The optimal coarse model response (—) and the fine model response (o) at the space-mapped design for the three-section microstrip transformer.....25

3.1 Illustration of the RMPE procedure; a) the current state at the ith iteration, b) initial parameter extraction at the suggested point $x_f^{(i+1)}$ and c) parameter extraction fails; an additional point $x_t^{(1)}$ is obtained and multi-point parameter extraction is carried out to sharpen the solution.....32

3.2 The DFS filter.....38

3.3 The optimal coarse model response (—) and the fine model response (o) at the starting point for the DFS filter.....38

3.4 The optimal coarse model response (—) and the space-mapped fine model response (o) for the DFS filter.....38

3.5 The structure of the HTS filter.....41

3.6 The coarse model of the HTS filter.....41

3.7 The optimal coarse model response (—) and the fine model response (o) at the starting point for the HTS filter.....42

3.8 The variation of two of the extracted coarse model parameters in the first iteration with the number of points used for parameter extraction where (1) is obtained using a single fine model point, (2) is obtained using two fine model points and (3) is obtained using three fine model points.....43

3.9 The coarse model response (—) and the fine model response (o) corresponding to the three extracted points in Fig. 3.8 where (a) is obtained using a single fine model, (b) is obtained using two fine model points and (c) is obtained using three fine model points.....43

3.10 The coarse model response (—) at the extracted point and the fine model response (o) corresponding to (a) the second iteration, (b) the third iteration, (c) the fourth iteration and (d) the fifth iteration.....44

3.11 The optimal coarse model response (—) and the final fine model response (o) for the HTS filter.....45

3.12 The optimal coarse model response (—) and the final fine model response (o) for the HTS filter in the passband.....45

3.13 A typical two-section waveguide transformer.....48

3.14 The optimal response of the ideal analytical model (—) and the response of the nonideal analytical model (o) at the starting point for the two-section waveguide transformer.....48

3.15 The optimal response of the ideal analytical model (—) and the final response of the nonideal analytical model (o) for the two-section waveguide transformer.....48

3.16 The optimal response of the ideal analytical model (—) and the response of Maxwell Eminence (o) at the starting point for the two-section waveguide transformer.....49

3.17 The optimal response of the ideal analytical model (—) and the final Maxwell Eminence response (o) for the two-section waveguide transformer.....49

3.18 The optimal response of the ideal analytical model (—) and the response of the nonideal analytical model (o) at the starting point for the three-section waveguide transformer.....52

3.19 The optimal response of the ideal analytical model (—) and the final response of the nonideal analytical model (o) for the three-section waveguide transformer..... 52

3.20 The optimal response of the ideal analytical model (—) and the response of Maxwell Eminence (o) at the starting point for the three-section waveguide transformer..... .53

3.21 The optimal response of the ideal analytical model (—) and the final Maxwell Eminence response (o) for the three-section waveguide transformer.....53

3.22 The optimal ideal analytical model response (—) and the response of the nonideal analytical model (o) at the starting point for the seven-section waveguide transformer..... ..56

3.23 The optimal response of the ideal analytical model (—) and the final response of the nonideal analytical model (o) for the seven-section waveguide transformer..... ..56

3.24 The optimal response of the ideal analytical model (—) and the response of Maxwell Eminence (o) at the starting point for the seven-section waveguide transformer..... 57

3.25 The optimal response of the ideal analytical model (—) and the final Maxwell Eminence response (o) for the seven-section waveguide transformer.....57

3.26 The simulated part of the three-section waveguide transformer with rounded corners.....59

3.27 The optimal response of the ideal analytical model (—) and the response of HP HFSS (o) at the starting point for the three-section waveguide transformer with rounded corners.....59

3.28 The optimal response of the ideal analytical model (—) and the final HP HFSS response (o) for the three-section waveguide transformer with rounded corners.....60

3.29 Monte Carlo analysis for the three-section waveguide transformer with rounded corners assuming 1% uniformly distributed parameters.....63

3.30 Monte Carlo analysis for the three-section waveguide transformer with rounded corners assuming 2% uniformly distributed parameters.....63

3.31 Monte Carlo analysis for the three-section waveguide transformer with rounded corners assuming 5% uniformly distributed parameters.....64

4.1 Illustration of the MPE procedure.....70

4.2 Illustration of the relationship between the generated sets $V^{(i)}$, the fine model points $x_f^{(i)}$ and the extracted coarse model points $x_c^{\varepsilon(i)}$ generated by the APE algorithm..... .79

4.3 The flowchart of the APE algorithm.....80

4.4 The contours of $Q(x, V^{(1)})$ for the Rosenbrock function.....81

4.5 The contours of $Q(x, V^{(2)})$ for the Rosenbrock function.....81

4.6 The contours of $Q(x, V^{(3)})$ for the Rosenbrock function.....82

4.7 The responses of the given fine model point (o) and the coarse model response (–) at the point $x_c^{s(1)}$ for the 10:1 impedance transformer.....86

4.8 The contours of $Q(x, V^{(1)})$ for the 10:1 impedance transformer.....86

4.9 The fine model response (o) and the corresponding coarse model response (–); (a) at the first point and (b) at the second point utilized in the DPE for the 10:1 impedance transformer.....87

4.10 The contours of $Q(x, V^{(2)})$ for the 10:1 impedance transformer.....87

4.11 The fine model response (o) and the corresponding coarse model response (–) ; (a) at the first point, (b) at the second point and (c) at the third point utilized in the three-point parameter extraction for the 10:1 impedance transformer.....88

4.12 The contours of $Q(x, V^{(3)})$ for the 10:1 impedance transformer.....89

4.13 The decomposed HTS filter.....91

4.14 The fine model response (o) and the corresponding coarse model response (–) at the point utilized in the SPE for the HTS filter. Note that only points in the range 3.967 GHz to 4.099 GHz were actually used.....92

4.15 The fine model response (o) and the corresponding coarse model response (–), (a) at the first point, and (b) at the second point utilized in the DPE for the HTS filter. Note that only points in the range 3.967 GHz to 4.099 GHz were actually used.....92

4.16 The fine model response (o) and the corresponding coarse model response (–), (a) at the first point, (b) at the second point, and (c) at the third point utilized in the three-point parameter extraction for the HTS filter. Note that only points in the range 3.967 GHz to 4.099 GHz were actually used.....93

4.17 The fine model response (o) and the corresponding coarse model response (–), (a) at the first point, (b) at the second point, (c) at the third point, and (d) at the fourth point utilized in the four-point parameter extraction for the HTS filter. Note that only points in the range 3.967 GHz to 4.099 GHz were actually used.....94

4.18 The coarse model of the DFS filter.....98

4.19 The optimal coarse model response (—) and the fine model response (o) at the optimal coarse model design for the DFS filter.....98

4.20 The fine model response (o) and the corresponding coarse model response (–) at the point $x_c^{e(1)}$ for the DFS filter.....99

4.21 The fine model response (o) and the corresponding coarse model response (–) at the point $x_c^{e(9)}$ for the DFS filter.....99

4.22 The variation of $Q(x,V^{(i)})$ for the DFS filter at the point $x_c^{e(1)}$ (— * —) and at the point $x_c^{e(9)}$ (— o —) with the number of points utilized for parameter extraction.....100

5.1 Different contour plots for the Rosenbrock problem for the case $\alpha = [-0.1 \quad -0.1]^T$; (a) the contour plot of $\|x_f+\alpha-x_c^*\|_2^2$, (b) the contour plot of $\|P(x_f)-x_c^*\|_2^2$ obtained through parameter extraction and (c) contours of the fine model Rosenbrock function.....107

5.2 Different contour plots for the Rosenbrock problem for the case $\alpha = [-1.5 \quad -1.5]^T$; (a) the contour plot of $\|x_f+\alpha-x_c^*\|_2^2$, (b) the contour plot of $\|P(x_f)-x_c^*\|_2^2$ obtained through parameter extraction and (c) contours of the fine model Rosenbrock function.....108

5.3 Illustration of the connection between SM optimization and direct optimization.....111

5.4 A flowchart of the first phase of the HASM algorithm.....118

5.5 The coarse response R_c^* (—) and the fine response $R_f(x_c^*)$ (o) for the three-section waveguide transformer.....120

5.6 The coarse response R_c^* (—) and the fine response R'_f (o) for the three-section waveguide transformer.....120

5.7 The coarse response R_c^* (—) and the fine response R''_f (o) for the three-section waveguide transformer.....121

5.8 The coarse response R_c^* (—) and the fine response R_f^* (o) for the three-section waveguide transformer.....121

5.9 The fine model of the six-section H-plane waveguide filter.....124

5.10 The coarse model of the six-section H-plane waveguide filter.....124

5.11 The coarse response R_c^* (—) and the fine response $R_f(x_c^*)$ (o) for the six-section H-plane waveguide filter.....124

5.12 The coarse response R_c^* (—) and the fine response R''_f (o) for the six-section H-plane waveguide filter.....125

5.13 The coarse response $\boldsymbol{R}_c^*$ (—) and the fine response $\boldsymbol{R}_f^*$ (o) for the six-section H-plane waveguide filter.....125

5.14 The seven-section waveguide transformer.....128

5.15 The coarse response $\boldsymbol{R}_c^*$ (—) and the fine response $\boldsymbol{R}_f(\boldsymbol{x}_c^*)$ (o) for the seven-section waveguide transformer.....128

5.16 The coarse response $\boldsymbol{R}_c^*$ (—) and the fine response $\boldsymbol{R}'_f$ (o) for the seven-section waveguide transformer.....129

5.17 The coarse response $\boldsymbol{R}_c^*$ (—) and the fine response $\boldsymbol{R}''_f$ (o) for the seven-section waveguide transformer.....129

5.18 The coarse response $\boldsymbol{R}_c^*$ (—) and the fine response $\boldsymbol{R}_f^*$ (o) for the seven-section waveguide transformer.....130

5.19 The coarse response $\boldsymbol{R}_c^*$ (—) and the fine response $\boldsymbol{R}_f(\boldsymbol{x}_c^*)$ (o) for the DFS filter.....132

5.20 The coarse response $\boldsymbol{R}_c^*$ (—) and the fine response $\boldsymbol{R}'_f$ (o) for the DFS filter.....132

5.21 The coarse response $\boldsymbol{R}_c^*$ (—) and the fine response $\boldsymbol{R}''_f$ (o) for the DFS filter.....133

5.22 The coarse response $\boldsymbol{R}_c^*$ (—) and the fine response $\boldsymbol{R}_f^*$ (o) for the DFS filter.....133

6.1 Illustration of the frequency-sensitive mapping concept; (a) a significant frequency band shift exists between fine and coarse model responses at the initial iteration and (b) the coarse model frequency is transformed such that both responses match.....140

6.2 Illustration of the selection of the parameter extraction points; (a) in the $(i-1)$th iteration, we have the point $\boldsymbol{x}_f^{(i-1)}$ and the set $V^{(i-1)}$, (b) a new point is generated by the algorithm that does not satisfy the success criterion, (c) $\boldsymbol{x}_f^{(i-1)}$ becomes $\boldsymbol{x}_f^{(i)}$, the previous perturbation $\boldsymbol{h}^{(i)}$ is excluded from $V^{(i)}$ and the algorithm generates an alternative perturbation and (d) the set $V^{(i)}$ is used to extract new mapping parameters and predict a successful iterate.....142

6.3 Illustration of the ith iteration of the SMSM algorithm.....145

6.4 A flowchart of the SMSM algorithm.....146

6.5 The contours of U for the fine model of the Rosenbrock example.....148

6.6 The contours of U for the coarse model of the Rosenbrock example.....148

6.7 The value of U in each iteration for the Rosenbrock example.....149

6.8 The fine model of the capacitively-loaded 10:1 impedance transformer.....150

6.9 The coarse model of the capacitively-loaded 10:1 impedance transformer.....150

6.10 The optimal coarse model response (—) and the fine model response (o) at the starting point for the capacitively-loaded 10:1 impedance transformer.....153

6.11 The optimal coarse model response (—) and the fine model response (o) at the end of the first successful iteration for the capacitively-loaded 10:1 impedance transformer.....153

6.12 The optimal coarse model response (—) and the fine model response (o) at the end of the second successful iteration for the capacitively-loaded 10:1 impedance transformer.....154

6.13 The change of U with each iteration for the 10:1 impedance transformer.....154

6.14 The optimal coarse model response (—) and the fine model response (o) at the starting design for the DFS filter.....156

6.15 The optimal coarse model response (—) and the fine model response (o) at the final design for the DFS filter.....156

6.16 The value of U in every iteration for the DFS filter.....157

6.17 The optimal coarse model response (—) and the fine model response (o) at the initial design for the HTS filter (first case).....161

6.18 The optimal coarse model response (—) and the fine model response (o) at the final design for the HTS filter (first case).....161

6.19 The value of U in every iteration for the HTS filter (first case).....162

6.20 The optimal coarse model response (—) and the fine model response (o) at the end of the first iteration for the HTS filter (first case).....162

6.21 The optimal coarse model response (—) and the fine model response (o) at the initial design for the HTS filter (second case).....164

6.22 The optimal coarse model response (—) and the fine model response (o) at the final design for the HTS filter (second case).....164

6.23 The value of U in every iteration for the HTS filter (second case).....165

LIST OF TABLES

2.1 The initial and final designs for the three-section microstrip impedance transformer.....24

3.1 Material and physical parameters for the coarse and fine ***em*** models of the DFS filter.....37

3.2 Values of designable parameters at each iteration for the DFS filter.....37

3.3 Material and physical parameters for the HTS filter.....40

3.4 The initial and final designs of the fine model for the HTS filter.....40

3.5 Values of designable parameters at each iteration for the two-section waveguide transformer using two analytical models.....47

3.6 Values of designable parameters at each iteration for the two-section waveguide transformer using Maxwell Eminence and an ideal analytical model.....47

3.7 Values of designable parameters at each iteration for the three-section waveguide transformer using two analytical models.....51

3.8 Values of designable parameters at each iteration for the three-section waveguide transformer using Maxwell Eminence and an ideal analytical model.....51

3.9 Values of designable parameters at the initial and final design for the seven-section waveguide transformer using two analytical models.....54

3.10 Values of designable parameters at the initial and final design for the seven-section waveguide transformer using Maxwell Eminence and an ideal analytical model.....55

3.11 Values of designable parameters at each iteration for the three-section waveguide transformer with round corners using HP HFSS and an ideal analytical model.....61

4.1 The variation of the extracted parameters for the Rosenbrock function with the number of points used for extraction.....84

4.2 The variation of the extracted parameters for the 10:1 impedance transformer with the number of points used for extraction.....84

4.3 Material and physical parameters for the coarse and fine models of the HTS filter.....95

4.4 The optimal coarse model design for the HTS filter.....95

4.5 The fine model points used in the APE algorithm for the HTS filter.....96

4.6 The variation in the extracted parameters for the HTS filter with the number of fine model points.....96

4.7 The optimal coarse model design for the DFS filter.....101

4.8 The fine model points used in the APE algorithm for the DFS filter.....101

4.9 The variation in the extracted parameters for the DFS filter with the number of fine model points.....101

5.1 The optimal coarse model design and the designs obtained during different phases of the HASM algorithm for the three-section waveguide transformer.....122

5.2 The optimal coarse model design, the final space-mapped and the optimal fine model designs for the six-section H-plane waveguide filter.....126

5.3 The optimal coarse model design and the designs obtained during different phases of the HASM algorithm for the seven-section waveguide transformer.....131

5.4 The optimal coarse model design, the final space-mapped and the optimal fine model designs for the DFS filter.....131

6.1 Initial and final fine model designs for the Rosenbrock function.....151

6.2 The fine model capacitances for the capacitively-loaded impedance transformer.....151

6.3 The characteristic impedances for the capacitively-loaded impedance transformer.....152

6.4 The first three designs for the capacitively-loaded impedance transformer.....152

6.5 The initial and final designs for the DFS filter without interpolation.....159

6.6 Material and physical parameters for the HTS filter.....159

6.7 The initial and final designs of the fine model for the HTS filter (first case).....160

6.8 The initial and final designs of the fine model for the HTS filter (second case).....160

LIST OF SYMBOLS

x – Vector of designable parameters

N_r – Number of circuit response functions

ξ_i – Vector of independent parameters associated with the ith response

$R^i(x, \xi_i)$ – The value of the ith response at a given point x and a vector of independent parameter ξ_i

m – The total number of samples of the circuit response functions

n – The number of designable parameters

i, j, k – General index variables

μ_i – Number of samples associated with the ith circuit response function

$\Re^{m \times n}$ – Space of matrices of dimension $m \times n$

$\boldsymbol{R}$ – The vector of sampled circuit response functions

ξ_i^j – The jth sample of the vector of independent parameters of the ith circuit response function

e_k – The kth error function

Γ_k – The kth target specification

w_k – The weight associated with the kth target specification

N_c – The total number of design specifications

Γ_{uk} – The kth upper design specification

Γ_{lk} – The kth lower design specification

K_s – The set of indices of the target specifications

K_u – The set of indices of the upper specifications

K_l – The set of indices for the lower specifications

w_{uk} – The weight associated with the kth upper specification

w_{lk} – The weight associated with the kth lower specification

$\boldsymbol{e}$ – The vector of all error functions

$U(\boldsymbol{x})$ – The value of the scalar objective function U for a vector of designable parameters $\boldsymbol{x}$

$\boldsymbol{x}^*$ – Vector of optimal values of the designable parameters

$\|\boldsymbol{e}\|_p$ – The l_p norm of the vector of error functions $\boldsymbol{e}$

$\|\boldsymbol{e}\|_H$ – The Huber norm of the vector of error functions $\boldsymbol{e}$

$\psi_\beta(e_k)$ – The Huber function with Huber threshold β corresponding to the error function e_k

β – The Huber threshold

ℓ_p^+ – One-sided l_p function that considers only positive error functions

ℓ_p^- – One-sided l_p function that considers only negative error functions

$\boldsymbol{x}_f$ – Vector of fine model parameters

$\boldsymbol{x}_c$ – Vector of coarse model parameters

$\boldsymbol{x}_c^*$ – Vector of optimal coarse model parameters

$\boldsymbol{R}_c^*$ – Vector of optimal coarse model responses

$\boldsymbol{P}$ – The vector of nonlinear mapping relating the fine and coarse model parameters

ε – A small positive number

$\boldsymbol{P}^{(i)}$ – An approximation of the nonlinear mapping $\boldsymbol{P}$ in the ith iteration

$\overline{\boldsymbol{x}}_f$ – The vector of space-mapped fine model parameters

$S_f^{(i)}$ – A set of fine model points in the ith iteration

$S_c^{(i)}$ – A set of coarse model points in the ith iteration

$x_f^{(i)}$ – The ith vector of fine model parameters

$x_c^{(i)}$ – The ith vector of coarse model parameters

m_i – The number of utilized fine model points in the ith iteration of the original SM algorithm

N_φ – A constant related to the predefined and fixed functions used in the original SM algorithm; the number of these functions is $N_\varphi+1$

$\varphi_k(x_f)$ – The kth function used to approximate the mapping in the original SM algorithm

$\boldsymbol{\varphi}(x_f)$ – The vector of expansion functions utilized by the original SM algorithm

$A^{(i)}$ – The matrix of mapping unknowns obtained in the ith iteration of the original SM algorithm

$B^{(i)}$ – A matrix that approximates the Jacobian of the mapping P in the ith iteration

$c^{(i)}$ – A vector that approximates the shift between the fine and coarse models parameters

$x_{f,k}$ – The kth fine model parameter

D, X – Two matrices utilized in obtaining the mapping parameters in the original SM algorithm

x_f^* – Vector of optimal fine model parameters

$f(x_f)$ – A residual vector that represents the difference between the coarse model point corresponding to x_f and the optimal coarse model parameters

$h^{(i)}$ – The step taken by the respective algorithm in the ith iteration

$J_m(x_f)$ – The Jacobian of the coarse model parameters with respect to the fine model parameters at the point x_f

I – The identity matrix

$\overline{B}$ – The space mapped approximation of the matrix J_m at the space mapped design $\overline{x}_f$

$f(x)$ – A scalar objective function

$L^{(i)}(x)$: An approximation of the function $f(x)$ in the ith iteration

δ – The trust region size

$\delta^{(i)}$ – The trust region size in the ith iteration

λ – A parameter correlated to the trust region size that is used by the TRASM algorithm

V – Set of fine model points used for either extracting coarse model points or extracting mapping parameters

$\Delta \boldsymbol{x}_f$ – A perturbation in the fine model parameters

$\boldsymbol{g}^{(i)}$ – The difference vector between the fine model response at the point $\boldsymbol{x}_f^{(i)}$ and the optimal coarse model response

$\boldsymbol{x}_t^{(k)}$ – The kth temporary fine point utilized by the TRASM algorithm

$\boldsymbol{g}_t^{(k)}$ – The difference vector between the fine model response at the temporary point $\boldsymbol{x}_t^{(i)}$ and the optimal coarse model response

$\boldsymbol{J}_f$ – The Jacobian of fine model responses with respect to the fine model parameters

δ_f – The termination trust region size for the TRASM algorithm

$|V|$ – The cardinality of the set V

$\boldsymbol{x}_c^e$ – Vector of extracted coarse model parameters

$\Delta \boldsymbol{x}_c^{(i)}$ – The ith perturbation of the coarse model parameters

$\boldsymbol{e}_i$ – The error vector corresponding to the ith point utilized by the APE algorithm

V_p – The set of coarse model perturbations utilized by the APE algorithm

N_p – The number of coarse model perturbations utilized by the APE algorithm

$\boldsymbol{R}_T$ – The vector of target responses utilized by the APE algorithm

m_T – The dimensionality of the vector of target responses $\boldsymbol{R}_T$

$\boldsymbol{J}_T$ – The Jacobian of the vector of target responses with respect to coarse model parameters

ϑ – The rank of the Jacobian matrix $\boldsymbol{J}_T$

S, S_a – Sets of gradients utilized by the APE algorithm

$\boldsymbol{y}^{(k)}$, $\boldsymbol{y}_a^{(i)}$ – gradients utilized by the APE algorithm

$G^{(i)}$ – The Hessian matrix of the ith response

Z – A matrix utilized by the APE algorithm for predicting a new perturbation in the case of a locally nonunique extracted parameters

c_y – A vector utilized by the APE algorithm for predicting a new perturbation in the case of a locally nonunique extracted parameters

H_i – The Hessian matrix of the least-squares objective function at the ith solution to the parameter extraction problem

$x_c^{e,i}$ – The ith solution to the least-squares parameter extraction problem

$Q(x,V)$ – The value of the least-squares objective function for the parameter extraction problem using the points in the set V at the point x

$q_i(\Delta x,V)$ – A local approximation of the least squares objective function in the neighborhood of the point $x_c^{e,i}$

θ – The Lagrange multiplier utilized by the APE algorithm

ΔR_i – The perturbation in the coarse model response corresponding to a perturbation Δx in the neighborhood of the point $x_c^{e,i}$

$J_c(x_c^{e,i})$ – The Jacobian of the coarse model responses at the point $x_c^{e,i}$

$v^{(k)}$ – The kth eigenvector obtained by the APE algorithm for the case of a locally unique extracted parameters

π_s – A factor used to scale the trust region size in the APE algorithm

$V^{(i)}$ – The set of fine model points utilized by the APE algorithm in the ith iteration

$x_c^{e(i)}$ – The solution to the parameter extraction problem obtained by the APE algorithm in the ith iteration

α_i – A scalar shift in the ith parameter

α – A vector of shifts

R_f^* – The optimal fine model design

x_n – A fine model point in the neighborhood of a point x_f

$x_c^{(p)}$ – A prediction of the parameter extraction solution that is utilized by the Hybrid Aggressive Space Mapping (HASM) algorithm

x'_f – The design obtained at the end of the first phase of the HASM algorithm

R'_f – The fine model response corresponding to the point x'_f

x''_f – The design obtained at the end of the first phase of the HASM algorithm

R''_f – The fine model response corresponding to the point x''_f

h_t – A temporary perturbation utilized by the HASM algorithm

ω – The real frequency variable

$R_f(x_f, \omega)$ – The fine model responses at a point x_f and frequency ω

N_ω – Number of frequency samples

$R_s^{(i)}(x_f)$ – The vector of the ith iteration surrogate model responses at the point x_f

$R_m^{(i)}(x_f)$ – The vector of the ith iteration mapped coarse model responses at the point x_f

$\eta^{(i)}$ – The surrogate model parameter in the ith iteration

$B^{(i)}$, $c^{(i)}$, $s^{(i)}$, $t^{(i)}$, $\sigma^{(i)}$, $\gamma^{(i)}$ – The mapping parameters extracted in the ith iteration of the SMSM algorithm

ω_j – The jth frequency sample

$P^{(i)}(x_f, \omega_j)$ – The coarse model point corresponding to a fine model point x_f and frequency ω_j obtained in the ith iteration of the SMSM algorithm

$P_\omega^{(i)}(x_f, \omega_j)$ – The coarse model frequency corresponding to a fine model point x_f and frequency ω_j obtained in the ith iteration of the SMSM algorithm

$R_c(x_c, \omega)$ – The coarse model responses at a point x_c and frequency ω

N – Total number of error vectors where $N=N_p N_\omega$

δ_e – The extraction radius parameter used by the SMSM algorithm

S_v – Set of scaled eigenvectors utilized by the SMSM in generating alternative perturbations

$\tau^{(k)}$ – The kth eigenvalue corresponding to the kth eigenvector in the set S_v

r_a - The actual reduction in the objective function

r_p – The predicted reduction in the objective reduction

ρ – The ratio between the actual reduction and the expected reduction in the objective function

π_i – the ith factor utilized for scaling the trust region size in the SMSM algorithm

$E_m^{(i)}$ – The prediction error of the mapped coarse model in the ith iteration of the SMSM algorithm

$E_l^{(i)}$ – The prediction error of the linearized fine model in the ith iteration of the SMSM algorithm

1

INTRODUCTION

1.1 MOTIVATION

During the past three decades, several robust optimization techniques [1-26] have been developed. These techniques supplied designers with strong and reliable tools necessary for the complex and demanding needs of modern circuit design. They utilize the circuit responses and possibly derivative information in the optimization loop.

Recently, commercial software packages, for example [27-29], have been developed that solve Maxwell's equations for circuits of arbitrary geometrical shapes. Such simulators are denoted as Electromagnetic (EM) simulators. They utilize different methods of the analysis of microwave circuits such as the Finite Element Method (FEM), the Method of Moments (MoM), etc. These simulators are accurate but they require intensive CPU time. The models presented by these simulators are denoted as "fine" models.

Utilizing EM simulators for optimizing microwave circuits can be formidable. The initial use of these simulators was limited to validating designs obtained through traditional optimization of empirical/analytical models. Over the years, empirical and circuit theoretic models of many microwave circuits have been developed and accumulated. The empirical and circuit-theoretic models are denoted as "coarse" models. Advances in the technology of workstations and PCs enabled traditional EM optimization of simple structures. However, the increasing complexity of microwave circuits still makes traditional EM optimization a formidable task.

Space Mapping (SM) optimization aims at solving this problem. It combines the computational efficiency of empirical/circuit-theoretic models with the accuracy of the EM

simulators. A mathematical link (mapping) is established between the spaces of the parameters of the empirical and EM models. This approach directs the bulk of the required CPU time to the fast model while preserving the accuracy and confidence supplied by few EM analyses. The first SM algorithms were introduced in [30, 31].

An essential step of SM optimization is Parameter Extraction (PE). In this step, the coarse model parameters corresponding to a given fine model response are obtained. In general, PE is formulated as an optimization problem. The solution of this problem may be nonunique. This nonuniqueness may affect the convergence of SM optimization [32].

1.2 CONTRIBUTIONS

The author contributed substantially to the following original developments presented in this thesis

(1) An algorithm that integrates a trust region methodology with Aggressive Space Mapping.

(2) An algorithm for the selection of perturbations utilized in enhancing the uniqueness of parameter extraction.

(3) A hybrid algorithm that utilizes both Space Mapping optimization and direct optimization.

(4) A new formulation of Space Mapping optimization as a general optimization problem.

(5) The integration of frequency-sensitive mappings in Space Mapping optimization.

(6) An algorithm that integrates Space Mapping optimization and surrogate model-based optimization.

1.3 OUTLINE OF THESIS

The objective of this thesis is to review recent developments in SM optimization and in PE approaches. These developments include the Trust Region Aggressive Space Mapping

(TRASM) algorithm [33-37], the Hybrid Aggressive Space Mapping (HASM) algorithm [38-40], the Aggressive Parameter Extraction (APE) algorithm [41-42] and the Surrogate Model-based Space Mapping (SMSM) optimization [43, 44].

In Chapter 2 we review some concepts of the field of circuit optimization. We show how the design problem is formulated as an optimization problem. The different norms and their properties are briefly reviewed. The motivation for SM-based optimization is discussed. Two of the previously developed SM algorithms, the original SM algorithm and Aggressive Space Mapping (ASM), are reviewed. The limitations of these algorithms are discussed.

Chapter 3 addresses the Trust Region Aggressive Space Mapping (TRASM) algorithm. TRASM integrates a trust region methodology with the Aggressive Space Mapping (ASM) technique [31]. The trust region methodology utilized by the algorithm is explained. To improve the uniqueness of the extraction phase we developed a recursive multi-point parameter extraction. TRASM was successfully used to design a number of microwave circuits. The examples addressed include the EM optimization of a Double-Folded Stub (DFS) filter and of a High-Temperature Superconducting (HTS) filter using Sonnet's ***em*** [27]. The proposed algorithm was also used to design two-section, three-section and seven-section waveguide transformers exploiting Maxwell Eminence [28]. The design of a three-section waveguide transformer with rounded corners was carried out using HP HFSS [29].

Chapter 4 presents the Aggressive Parameter Extraction (APE) algorithm. APE addresses the optimal selection of parameter perturbations used to increase trust in parameter extraction uniqueness. The appropriate criterion for the generation of these perturbations is reviewed. APE classifies possible solutions for the parameter extraction problem. Two different approaches for obtaining subsequent perturbations are utilized based on a classification of the extracted parameters. These two approaches are discussed and their theory is explained. A number of examples illustrate the APE algorithm. The examples include the parameter

extraction of a decomposed electromagnetic model of an HTS filter. Also, the parameter extraction of an empirical model of a DFS filter is carried out.

In Chapter 5, we review the Hybrid Aggressive Space Mapping (HASM) optimization algorithm. HASM exploits both the TRASM strategy and direct optimization. We start by illustrating the motive for a hybrid algorithm. A lemma that enables switching from TRASM optimization to direct optimization is explained. This lemma relates the mapping and the fine and coarse model derivatives. The approach utilized by the HASM algorithm for choosing a good starting point for the parameter extraction is also reviewed. HASM has been tested on designs of several microwave filters and transformers. The examples include a three-section and a seven-section waveguide transformer as well as the design of an H-plane waveguide filter and an DFS filter.

Chapter 6 presents a Surrogate Model-based Space Mapping (SMSM) optimization algorithm. It draws upon recent developments in both surrogate-based optimization [45-49] and modeling of microwave devices [50, 51]. It integrates two different approaches for efficient optimization; SM and surrogate model-based optimization. SM optimization is formulated as a general optimization problem of a surrogate model. We start this chapter by giving a comparison between SM formulation and surrogate model formulation. The construction of the utilized surrogate model is explained in detail. The utilization of a frequency-sensitive mapping by the algorithm is also addressed. This approach is shown to be especially powerful if significant response shift exists. SMSM is illustrated through a number of examples.

We conclude in Chapter 7 with suggestions for further research.

2

REVIEW OF SOME CONCEPTS IN CIRCUIT OPTIMIZATION

2.1 INTRODUCTION

The target of circuit optimization is to determine a set of values for the circuit parameters such that certain design specifications are satisfied. These specifications represent constraints on the circuit responses. Usually, a model of the physical circuit is utilized in simulating and thus optimizing the circuit.

Traditional optimization techniques [1-26] utilize the simulated circuit responses directly and possibly available derivatives. Engineering models used in simulating the circuit responses vary in accuracy and speed. Usually, accurate models are computationally expensive and less accurate models are fast. In some engineering problems, applying traditional optimization using the accurate models directly may be prohibitively impractical. On the other hand, applying optimization using the less accurate models may indicate feasibility of the design but could lead to unreliable results. These results must be validated using the accurate models or even using measurements. It follows that alternative optimization approaches must be utilized.

Space Mapping (SM) establishes a mathematical link (mapping) between the spaces of the parameters of two different models of the same physical circuit. The accurate and time-intensive model is denoted as a "fine" model. The less accurate but fast model is denoted as a "coarse" model. For example, a fine model may be a time-intensive finite element solution of Maxwell's equations while the coarse model may be a circuit-theoretic model with empirical algebraic formulas.

All the SM-based optimization algorithms we will review in this Chapter utilize two steps. The first step optimizes the design parameters of the coarse model to satisfy the original design specifications. The second step establishes a mapping between the parameter spaces of the two models. The space-mapped design is then taken as the mapped image of the optimal coarse model design.

The first SM-based optimization algorithm was introduced in [30]. This method assumes a linear mapping between the parameter spaces. This assumption may not be accurate if significant misalignment exists between the two spaces. An initialization overhead of fine model simulations is required.

Aggressive Space Mapping (ASM) [31] eliminates the simulation overhead required in [30]. It exploits a quasi-Newton step in predicting the new iterates. The algorithm does not assume that the mapping is necessarily linear. However, the nonuniqueness of the parameter extraction step may lead to divergence or oscillations of the process [32].

2.2 DESIGN SPECIFICATIONS AND ERROR FUNCTIONS

The performance of the circuit is described in terms of some measurable quantities. We denote these measurable quantities as the circuit response functions. The response functions are manipulated by adjusting certain designable parameters. For example, the electrical response of a microstrip line can be adjusted by changing the physical width and length of the strip. Usually, some or all physical parameters are selected as designable parameters and thus can be optimized. We denote the vector of designable parameters by $\boldsymbol{x}$.

Each response function is also dependent on some other independent parameters, such as frequency, time and temperature [52]. In some cases we are confronted with response functions

that are dependent on a number of independent parameters. We denote the ith response function by $R^i(\boldsymbol{x}, \boldsymbol{\xi}_i)$, i=1, 2, ..., N_r, where $\boldsymbol{\xi}_i$ is the vector of associated independent parameters.

The desired performance of the circuit is expressed by a set of specifications. These specifications represent constraints on the responses that are functions of some of the independent parameters. In practice, only a discrete set of samples of the independent parameters is considered [52, 53]. Satisfying the specifications at these sampled values implies satisfying them almost everywhere.

Let μ_i be the number of discrete samples of the ith response. We define $\boldsymbol{R} \in \Re^{m\times 1}$ as the vector of sampled response functions. The kth component of $\boldsymbol{R}$ is given by

$$R_k = R^i(\boldsymbol{x}, \boldsymbol{\xi}_i^j) \tag{2.1}$$

where $k = \sum_{\rho=1}^{i-1} \mu_\rho + j$ for $i = 1, 2, \ldots, N_r$ and j=1, 2, ..., μ_i. Here $\boldsymbol{\xi}_i^j$ is the jth sample of $\boldsymbol{\xi}_i$ and m is the total number of sampled response functions.

An error function defines the difference between the specification and the corresponding response. In some problems the specifications define a target response that should be reached. These types of specifications are denoted as single specifications [52]. In other problems, specifications define upper and lower bounds on the respective response. For the case of single specifications the error functions are given by

$$e_k = w_k |R_k - \Gamma_k| \tag{2.2}$$

where Γ_k is the kth specification, $k \in K_s = \{k_1, k_2, \ldots, k_{N_c}\}$, the set of indices for the constrained responses, w_k is a nonnegative weight and N_c is the number of specifications.

In the case of upper and lower specifications, we classify the constraints on the response functions. We denote by Γ_{uk} and Γ_{lk} the kth upper and lower specification, respectively. Here, the error functions are given by

$$e_k = w_{uk}\left(R_k - \Gamma_{uk}\right),\ k \in K_u \tag{2.3}$$

and

$$e_k = w_{lk}\left(\Gamma_{lk} - R_k\right),\ k \in K_l \tag{2.4}$$

where K_u and K_l are sets of indices for the constrained responses and w_{uk} and w_{lk} are nonnegative weights. It is worth mentioning that simultaneous upper and lower specifications can be imposed on the same sampled response function, i.e., K_u and K_l may not be disjoint. Here $|K_u| + |K_l| = N_c$ and $|\ |$ denotes the set cardinality. We denote by $\boldsymbol{e}$ the vector whose components are the error functions given by (2.2) or by (2.3) and (2.4).

It is clear from (2.3) and (2.4) that upper and lower specifications are meaningful only in the case of a real response while (2.2) is valid in general for complex responses. Also, a positive, negative or zero value of an error function indicates that the corresponding specification is violated, exceeded or just satisfied, respectively. A set of designable parameters for which $\boldsymbol{e}$ is nonpositive is denoted a feasible design. The set of all feasible designs defines a feasible region in the space of designable parameters. Fig. 2.1 illustrates the concepts of error functions, feasible design and feasible region.

The error vector $\boldsymbol{e}$ is evaluated for a given $\boldsymbol{x}$ using the vector of sampled responses $\boldsymbol{R}$. $\boldsymbol{R}$ may be obtained by measuring the circuit responses. However, this approach is expensive and time consuming. Alternatively, $\boldsymbol{R}$ may be obtained by using a model of the circuit. This model utilizes the knowledge available about the physical processes taking place within the circuit. Usually, different models exist for the same circuit. These models vary in their accuracy and the speed with which $\boldsymbol{R}$ is obtained. In the discussion that follows we assume that the responses are obtained through simulation.

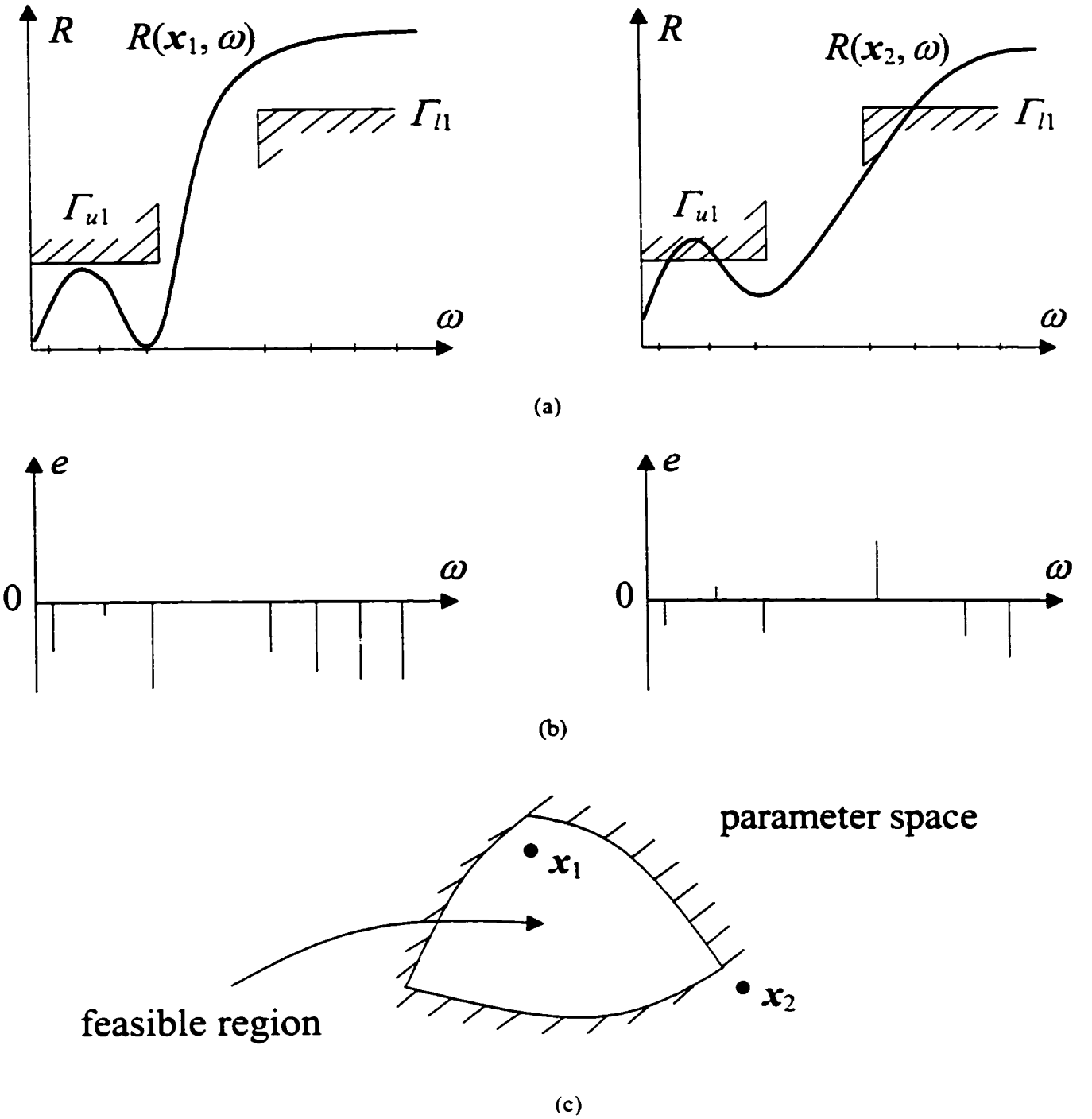

Fig. 2.1. Illustration of some basic engineering optimization concepts: (a) the responses at a feasible design x_1 and an infeasible design x_2, (b) the error functions at sampled values of the independent parameter ω and (c) a possible location of the two designs with respect to the feasible region for a two-dimensional case.

2.3 NORMS AND OPTIMIZATION METHODS

The problem of circuit design can be formulated as

$$\boldsymbol{x}^* = arg\left\{\min_{\boldsymbol{x}} U(\boldsymbol{x})\right\} \tag{2.5}$$

where $U(\boldsymbol{x})$ is a scalar objective function that is dependent on the error functions. $U(\boldsymbol{x})$ should offer a measure of the specifications' violation or satisfaction. A possible choice of $U(\boldsymbol{x})$ is the l_p norm [54], Huber norm [55, 56] or the generalized l_p function [25, 57]. The l_p norm of $\boldsymbol{e}$ is given by

$$\|\boldsymbol{e}\|_p = \left[\sum_{k=1}^{N_c} |e_k|^p\right]^{1/p} \tag{2.6}$$

The most commonly used norm is the l_2 norm, i.e., p=2. This norm is widely used because of its differentiability and its statistical properties. A large number of optimization techniques exist for least-squares optimization [9]. Solutions obtained using least-squares optimization can be altered significantly by the existence of a few wild data points.

Setting p=1 we have the l_1 norm

$$\|\boldsymbol{e}\|_1 = \sum_{k=1}^{N_c} |e_k| \tag{2.7}$$

This norm is robust to outliers. It finds wide application in data-fitting in the presence of gross errors [21], in analog fault location [58] and device modeling [24].

Setting p=∞ we have the l_∞ norm

$$\|\boldsymbol{e}\|_\infty = \max_k |e_k| \tag{2.8}$$

which considers only the worst violated error function. Many circuit design problems can be formulated as a minimax optimization problem [12].

The l_1 and l_∞ norms are both nondifferentiable. Corresponding optimization algorithms are more involved than least-squares algorithms. In general, the algorithms used to minimize the l_1 and l_∞ norms follow similar strategies. These algorithms solve the minimization problem in an iterative way. In [10, 11], the problem is formulated as a nonlinear program. Some methods utilize first-order derivatives of the error functions to construct linearization of the nonlinear program. Such methods are denoted as first-order methods. For example, in [19, 23] the linearization is used to construct a linear program that returns a suggested search direction. A line search is then executed in that direction. A trust region methodology [59] is integrated with the linear program formulation in [60]. Some of these first-order methods assure global convergence to a stationary point, for example [60]. However, they may become very slow in the neighborhood of a solution if the problem is singular [61].

Another class of methods for the minimization of l_1 and l_∞ norms utilizes approximate second-order information. These methods solve the first-order optimality conditions using quasi-Newton methods [5, 6, 9]. They are usually fast in the neighborhood of a solution. However, pure second-order methods do not guarantee convergence from a bad starting point. Hybrid methods [12, 21] combine both first-order and second-order methods. A first-order method is used far from the solution. Once the solution is approached, a switch to a second-order method is executed. Several switches can take place between the two methods.

Another norm that can be utilized as an objective function is the Huber norm [55, 56]. This norm is a hybrid combination between the l_1 and l_2 norms. It is defined by

$$\|e\|_H = \sum_{k=1}^{N_c} \psi_\beta(e_k) \tag{2.9}$$

where

$$\psi_\beta(e_k)=\begin{cases}\dfrac{e_k^2}{2} & \text{if } |e_k|\le\beta\\ \beta|e_k|-\dfrac{e_k^2}{2} & \text{if } |e_k|>\beta\end{cases} \tag{2.10}$$

where β is a threshold called the Huber threshold. This norm treats small errors in the l_2 sense while it treats large errors in the l_1 sense. Huber optimization [26] is more robust against gross errors than least-squares optimization. It also offers less biased designs than those obtained using l_1 optimization [26].

The previously discussed norms, can be used to minimize the error functions towards zero. A design that corresponds to a zero error vector would be satisfactory if it were not for manufacturing tolerances. These tolerances are inevitable and may cause the manufactured circuit to violate the specifications. It follows that optimization should continue to center the design within the feasible region [62-64]. The yield is defined as the percentage of the manufactured circuits that satisfy the design constraints. Fig. 2.2 Illustrates the concepts of design centering and yield. Several algorithms have been developed with the aim of maximizing the yield [65-67].

The generalized l_p function [25, 57] was developed to enable optimization towards a better centered design. It makes use of the one-sided functions

$$\ell_p^+=\left[\sum_k |e_k|^p\right]^{1/p},\ \forall e_k\ge 0 \tag{2.11}$$

and

$$\ell_p^-=-\left[\sum_k (-e_k)^{-p}\right]^{-1/p},\ \forall e_k<0 \tag{2.12}$$

The generalized l_p function is equal to (2.11) if at least one of the specifications is violated. Otherwise, it is equal to (2.12).

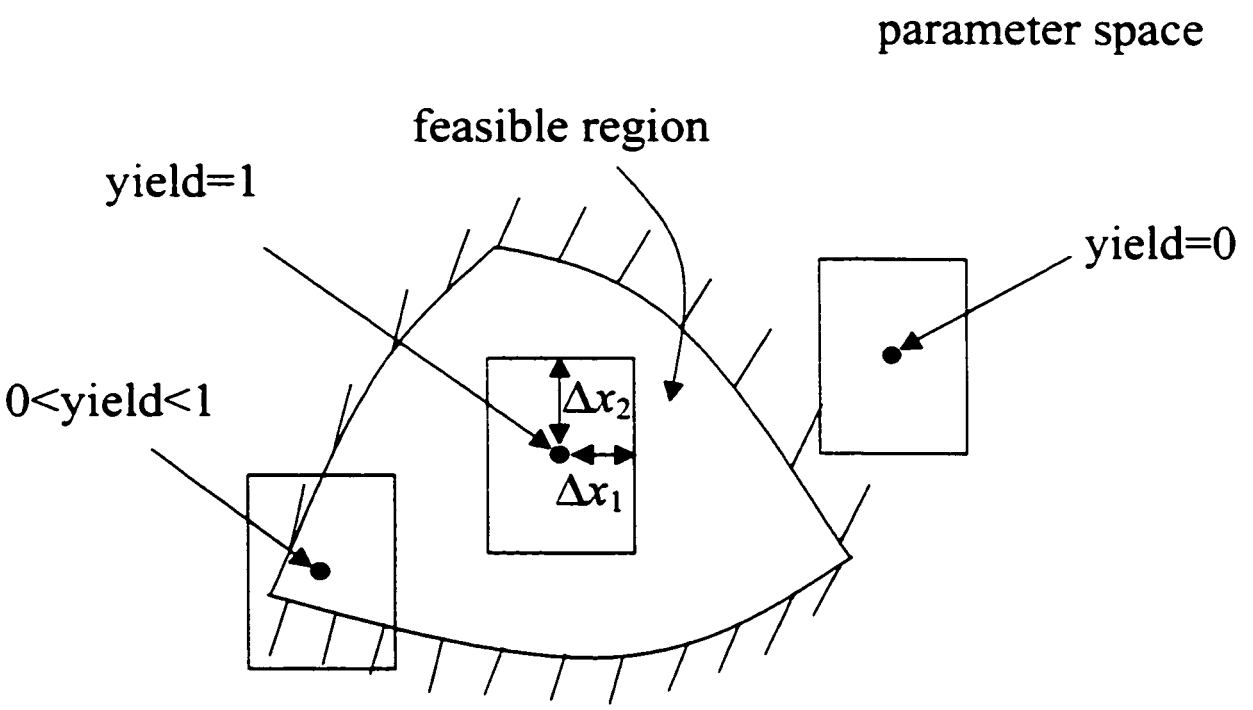

Fig. 2.2. Illustration of design centering and yield for a two-dimensional problem with manufacturing tolerances of Δx_1 and Δx_2. Three different designs are shown; a centered design where all possible outcomes are feasible (yield=1), an infeasible design where possible outcomes are infeasible (yield=0) and non centered feasible design where possible outcomes may be feasible or infeasible (0<yield<1).

We denote the optimization algorithms discussed thus far as 'direct optimization' algorithms. They utilize simulations of the optimized circuit and can be applied if the model simulation time is not extensive. Otherwise, direct optimization becomes formidable and alternative methods should be used. SM optimization was introduced as such an alternative.

2.4 SPACE MAPPING OPTIMIZATION: THE BASIC CONCEPT

We refer to the vectors of fine model parameters and corresponding coarse model parameters as $x_f \in \Re^n$ and $x_c \in \Re^n$, respectively. The optimal coarse model design x_c^* is obtained using only coarse model simulations. The corresponding response is denoted by R_c^*. A minimax algorithm [12], if appropriate, may be used.

SM establishes a mathematical link (mapping) P between the two spaces [31]

$$x_c = P(x_f) \tag{2.13}$$

such that

$$\left\| R_f(x_f) - R_c(x_c) \right\| \le \varepsilon \tag{2.14}$$

The mapping P is valid over a region in the parameter space. It is established in an iterative way. We denote by $P^{(i)}$ the available approximation to P at the ith iteration. The corresponding design is given by

$$x_f^{(i+1)} = P^{(i)^{-1}}(x_c^*) \tag{2.15}$$

If it satisfies a certain termination criterion, it is accepted as the space mapped design $\bar{x}_f$. Otherwise, the mapping is updated and a new design is calculated.

2.5 THE ORIGINAL SM OPTIMIZATION ALGORITHM [30]

At the ith iteration, the algorithm utilizes a set of fine model points $S_f^{(i)}$ defined by

$$S_f^{(i)} = \left\{ \boldsymbol{x}_f^{(1)}, \boldsymbol{x}_f^{(2)}, \ldots, \boldsymbol{x}_f^{(m_i)} \right\} \tag{2.16}$$

where $m_i = \left| S_f^{(i)} \right|$. The fine model response for every point in the set $S_f^{(i)}$ is simulated. A corresponding set of coarse model points $S_c^{(i)}$ defined by

$$S_c^{(i)} = \left\{ \boldsymbol{x}_c^{(1)}, \boldsymbol{x}_c^{(2)}, \ldots, \boldsymbol{x}_c^{(m_i)} \right\} \tag{2.17}$$

is then constructed. The points $\boldsymbol{x}_c^{(j)} \in S_c^{(i)}$, j=1, 2, ..., m_i are obtained through the Single-Point Extraction (SPE) process (see Fig. 2.3)

$$\boldsymbol{x}_c^{(j)} = arg \left\{ \min_{\boldsymbol{x}_c} \left\| \boldsymbol{R}_f(\boldsymbol{x}_f^{(j)}) - \boldsymbol{R}_c(\boldsymbol{x}_c) \right\| \right\} \tag{2.18}$$

$\boldsymbol{P}^{(i)}$ is then obtained using $S_f^{(i)}$ and $S_c^{(i)}$. Here, every coarse model parameter is expressed as a linear combination of some predefined and fixed functions $\varphi_k(\boldsymbol{x}_f)$, k=0, 1, ..., N_φ. It follows that

$$\boldsymbol{x}_c = \boldsymbol{P}^{(i)}(\boldsymbol{x}_f) = \boldsymbol{A}^{(i)} \boldsymbol{\varphi}(\boldsymbol{x}_f) \tag{2.19}$$

where $\boldsymbol{A}^{(i)} \in \Re^{n \times (N_\varphi + 1)}$ is a matrix of constant coefficients and $\boldsymbol{\varphi}(\boldsymbol{x}_f)$ is given by

$$\boldsymbol{\varphi}(\boldsymbol{x}_f) = \begin{bmatrix} \varphi_0(\boldsymbol{x}_f) \\ \varphi_1(\boldsymbol{x}_f) \\ \vdots \\ \varphi_{N_\varphi}(\boldsymbol{x}_f) \end{bmatrix} \tag{2.20}$$

Relation (2.19) must be satisfied for every pair of corresponding points in $S_f^{(i)}$ and $S_c^{(i)}$. It follows that $\boldsymbol{A}^{(i)}$ should satisfy

$$\left[\boldsymbol{x}_c^{(1)} \; \boldsymbol{x}_c^{(2)} \ldots \boldsymbol{x}_c^{(m_i)} \right] = \boldsymbol{A}^{(i)} \left[\boldsymbol{\varphi}(\boldsymbol{x}_f^{(1)}) \; \boldsymbol{\varphi}(\boldsymbol{x}_f^{(2)}) \ldots \boldsymbol{\varphi}(\boldsymbol{x}_f^{(m_i)}) \right] \tag{2.21}$$

In [30] it is assumed that the mapping between the two spaces is linear, i.e.,

$$\boldsymbol{x}_c = \boldsymbol{P}^{(i)}(\boldsymbol{x}_f) = \boldsymbol{B}^{(i)} \boldsymbol{x}_f + \boldsymbol{c}^{(i)} \tag{2.22}$$

$$\boldsymbol{R}_c(\boldsymbol{x}_c^{(j)}) \approx \boldsymbol{R}_f(\boldsymbol{x}_f^{(j)})$$

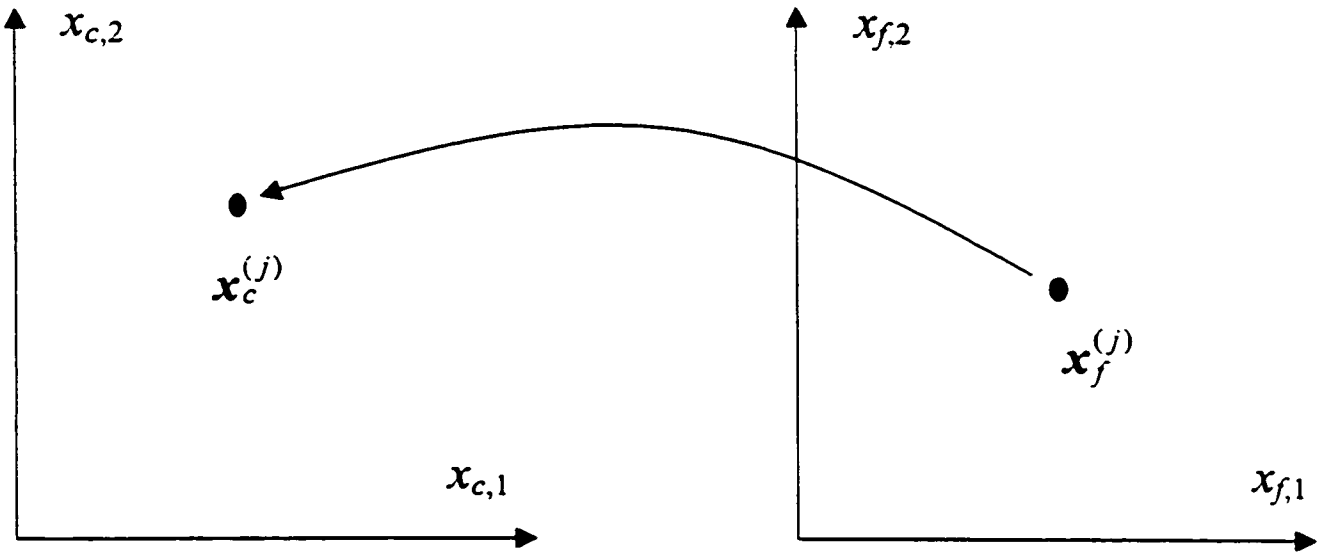

Fig. 2.3. Illustration of the SPE procedure.

where $\boldsymbol{B}^{(i)} \in \Re^{n \times n}$ and $\boldsymbol{c}^{(i)} \in \Re^{n \times 1}$. The linear mapping (2.22) is equivalent to (2.19) with $\boldsymbol{A}^{(i)} = \left[\boldsymbol{c}^{(i)} \quad \boldsymbol{B}^{(i)}\right]$ and $\varphi_k(\boldsymbol{x}_f) = x_{f.k}$, k=1, 2, ..., n, the kth component of the vector $\boldsymbol{x}_f$. $\varphi_0(\boldsymbol{x}_f) = 1$ and N_φ=n. It follows that (2.21) can be written as

$$\left[\boldsymbol{x}_c^{(1)} \; \boldsymbol{x}_c^{(2)} \ldots \boldsymbol{x}_c^{(m_i)}\right] = \boldsymbol{A}^{(i)} \begin{bmatrix} 1 & 1 & \ldots & 1 \\ \boldsymbol{x}_f^{(1)} & \boldsymbol{x}_f^{(2)} & \ldots & \boldsymbol{x}_f^{(m_i)} \end{bmatrix} \tag{2.23}$$

A least-squares solution for $\boldsymbol{A}^{(i)T}$ is thus given by

$$\boldsymbol{A}^{(i)T} = \left(\boldsymbol{D}^T \boldsymbol{D}\right)^{-1} \boldsymbol{D}^T \boldsymbol{X} \tag{2.24}$$

where

$$\boldsymbol{D} = \begin{bmatrix} 1 & 1 & \ldots & 1 \\ \boldsymbol{x}_f^{(1)} & \boldsymbol{x}_f^{(2)} & \ldots & \boldsymbol{x}_f^{(m_i)} \end{bmatrix}^T \tag{2.25}$$

and

$$\boldsymbol{X} = \left[\boldsymbol{x}_c^{(1)} \; \boldsymbol{x}_c^{(2)} \ldots \boldsymbol{x}_c^{(m_i)}\right]^T \tag{2.26}$$

Once $\boldsymbol{A}^{(i)}$ is obtained, the suggested space-mapped design is

$$\boldsymbol{x}_f^{(m_i+1)} = \boldsymbol{P}^{(i)-1}(\boldsymbol{x}_c^*) = \boldsymbol{B}^{(i)-1}\left(\boldsymbol{x}_c^* - \boldsymbol{c}^{(i)}\right) \tag{2.27}$$

Here, the mapping is assumed to be one to one. The new point $\boldsymbol{x}_f^{(m_i+1)}$ is taken as an approximation to the optimal fine model design $\boldsymbol{x}_f^*$ if the condition

$$\left\| \boldsymbol{R}_f(\boldsymbol{x}_f^{(m_i+1)}) - \boldsymbol{R}_c(\boldsymbol{x}_c^*) \right\| \le \varepsilon \tag{2.28}$$

is satisfied. In this case, we take $\overline{\boldsymbol{x}}_f = \boldsymbol{x}_f^{(m_i+1)}$. Otherwise, the set $S_f^{(i)}$ is augmented by $\boldsymbol{x}_f^{(m_i+1)}$ and the set $S_c^{(i)}$ is augmented by $\boldsymbol{x}_c^{(m_i+1)}$ obtained using (2.18). The algorithm steps using (2.23)-

(2.28) are then repeated using the augmented sets. Fig. 2.4 illustrates one iteration of the algorithm.

This algorithm is simple but it suffers from a number of drawbacks. First, to have the algorithm started an initial set of fine model points $S_f^{(0)}$ must be created. The points in $S_f^{(0)}$ are localized in the vicinity of a reasonable candidate for the fine model design. In [30] it was suggested that $|S_f^{(0)}| \geq n+1$. Simulating $S_f^{(0)}$ represents a significant overhead for the algorithm. The mapping is assumed to be linear, which may not be true for significantly misaligned models. Also, coarse model points are obtained through SPE. Nonuniqueness of the extracted parameters may lead to an erroneous mapping estimation and divergence of the algorithm. These drawbacks led to the development of the ASM algorithm [31].

2.6 THE ASM ALGORITHM

The space-mapped design $\bar{x}_f$ is a solution to the system of nonlinear equations

$$f = P(x_f) - x_c^* = 0 \tag{2.29}$$

ASM solves (2.29) in an iterative manner. Let $x_f^{(i)}$ be the ith iterate in the solution of (2.29). The next iterate $x_f^{(i+1)}$ is found by a quasi-Newton iteration

$$x_f^{(i+1)} = x_f^{(i)} + h^{(i)} \tag{2.30}$$

where $h^{(i)}$ is the solution of

$$B^{(i)} h^{(i)} = -f^{(i)} \tag{2.31}$$

where $f^{(i)} = P^{(i)}(x_f^{(i)}) - x_c^*$. $B^{(i)}$ is an approximation to the Jacobian J_m of f with respect to x_f at $x_f^{(i)}$. J_m is defined by

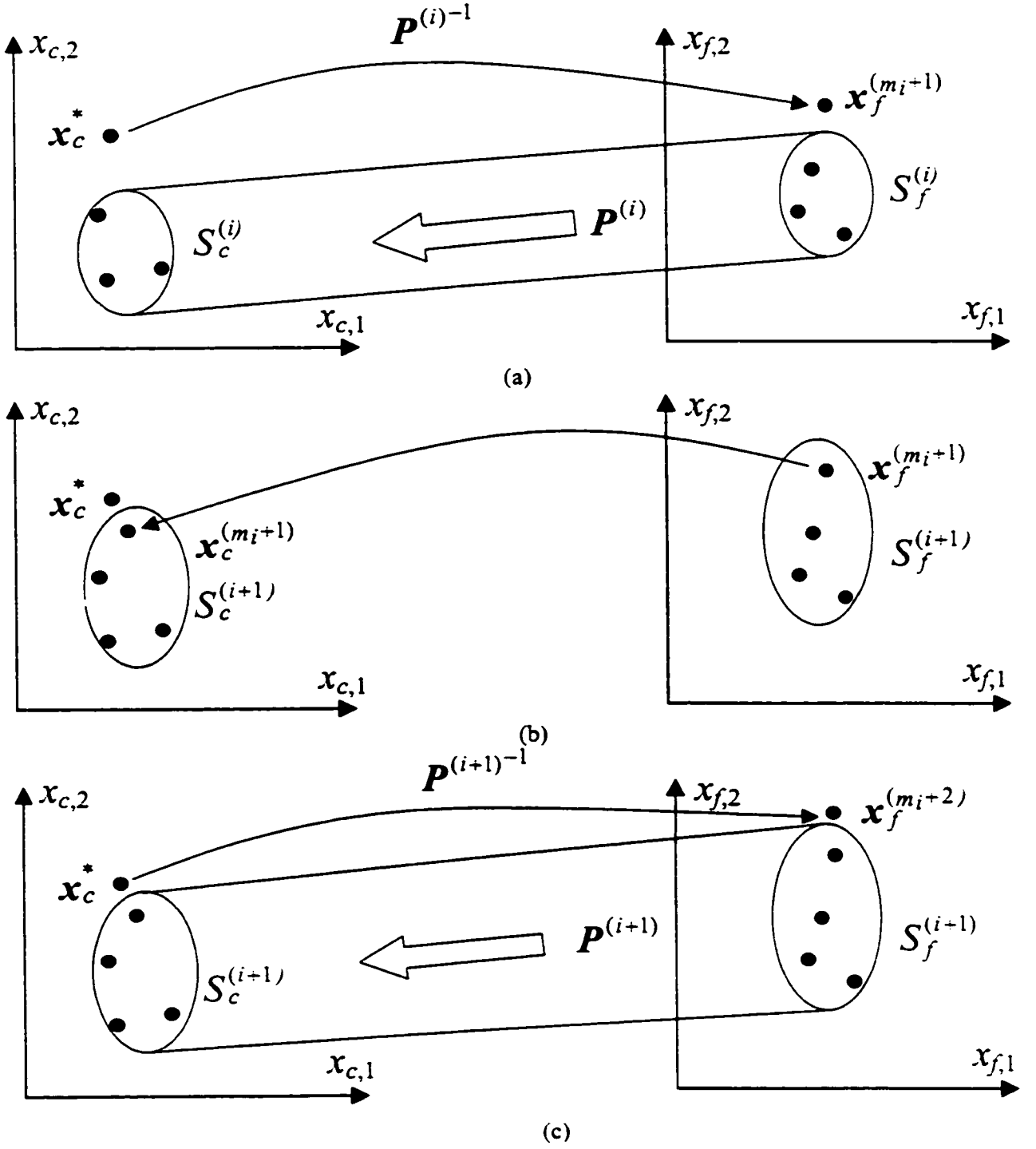

Fig. 2.4. Illustration of the original SM optimization algorithm: (a) a new point $x_f^{(m_i+1)}$ is obtained using the current mapping $P^{(i)}$, (b) the point $x_f^{(m_i+1)}$ does not satisfy the stopping criterion and the sets $S_f^{(i)}$ and $S_c^{(i)}$ are augmented by $x_f^{(m_i+1)}$ and $x_c^{(m_i+1)}$, respectively, and (c) a new mapping $P^{(i+1)}$ is estimated and is used to obtain a new iterate $x_f^{(m_i+2)}$.

$$J_m(x_f^{(i)}) = \left(\frac{\partial f^T(x_f)}{\partial x_f} \right)^T_{x_f = x_f^{(i)}} \tag{2.32}$$

If the mapping between the two spaces is linear, similar to (2.22), the matrix J_m is constant. Otherwise, it is a function of the fine model parameters. The initial approximation to J_m is taken as $B^{(0)} = I$, the identity matrix. $B^{(i)}$ is updated at each iteration using Broyden's update [6]

$$B^{(i+1)} = B^{(i)} + \frac{f^{(i+1)} - f^{(i)} - B^{(i)} h^{(i)}}{h^{(i)T} h^{(i)}} h^{(i)T} \tag{2.33}$$

The formula (2.33) can be simplified using (2.31) to

$$B^{(i+1)} = B^{(i)} + \frac{f^{(i+1)}}{h^{(i)T} h^{(i)}} h^{(i)T} \tag{2.34}$$

The error vector $f^{(i)}$ is obtained by evaluating $P^{(i)}(x_f^{(i)})$, which is done indirectly through SPE. The algorithm terminates if $\left\| f^{(i)} \right\|$ becomes sufficiently small. A complete iteration of the algorithm is shown in Fig. 2.5.

The ASM algorithm solves the problem of the overhead encountered in the original SM optimization algorithm. Also, while (2.23) assumes that the mapping is linear, ASM does not make this assumption. The output of the ASM algorithm is the space-mapped design $\bar{x}_f$ and the matrix $\bar{B}$, which approximates the Jacobian J_m at $\bar{x}_f$. However, the nonuniqueness problem of the SPE process remains. An incorrect value for the vector $P^{(i)}(x_f^{(i)})$ may cause the algorithm to diverge or exhibit oscillatory behavior.

Two interesting, intuitive, variants of the ASM algorithm are suggested in [68, 69]. The basic idea of both algorithms is essentially the same. The iterate is given by (2.31) with the matrix $B^{(i)}$ fixed at $B^{(i)} = I$. Here, Broyden's updating formula is not utilized. These "steepest-

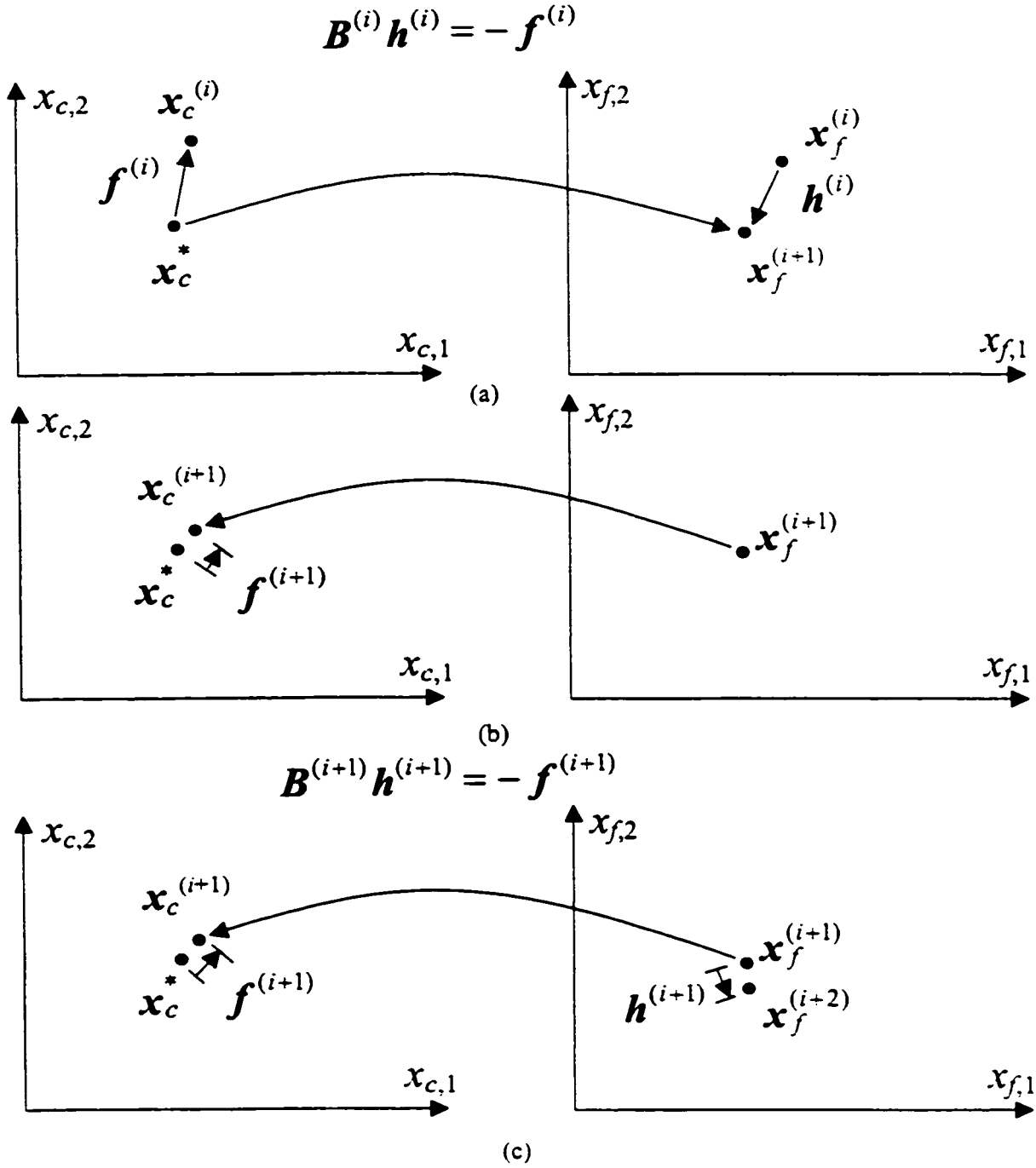

Fig. 2.5. Illustration of ASM; (a) a new iterate $x_f^{(i-1)}$ is obtained, (b) by applying parameter extraction we find that the stopping criterion is not satisfied ($\left\| f^{(i-1)} \right\| > \varepsilon$) and (c) the updated matrix $B^{(i+1)}$ is used to predict a new iterate $x_f^{(i-2)}$.

descent" approaches may succeed if the mapping between the two spaces is substantially represented by a shift.

2.7 THREE-SECTION MICROSTRIP TRANSFORMER

An example of ASM optimization is the three-section microstrip impedance transformer [70]. The filter structure is shown in Fig. 2.6. The fine model utilizes a full-wave electromagnetic simulator (Sonnet's ***em*** [27]). The coarse model utilizes the empirical microstrip line and microstrip step models available in the circuit simulator OSA90/hope [71]. The coarse model is shown in Fig. 2.7. The design specifications are

$$|S_{11}| \leq 0.11 \quad \text{for } 5 \text{ GHz} \leq \omega \leq 15 \text{ GHz} \tag{2.35}$$

The designable parameters are the width and physical length of each microstrip line. Here, the reflection coefficient $|S_{11}|$ is used to match the two model responses. ASM terminated using only 9 fine model simulations. The initial and final designs are given in Table 2.1. The corresponding responses are shown in Figs. 2.8 and 2.9, respectively. Simulating the fine model requires about one hour of CPU time on an HP workstation model 715/33. The coarse model simulation time is a fraction of a second.

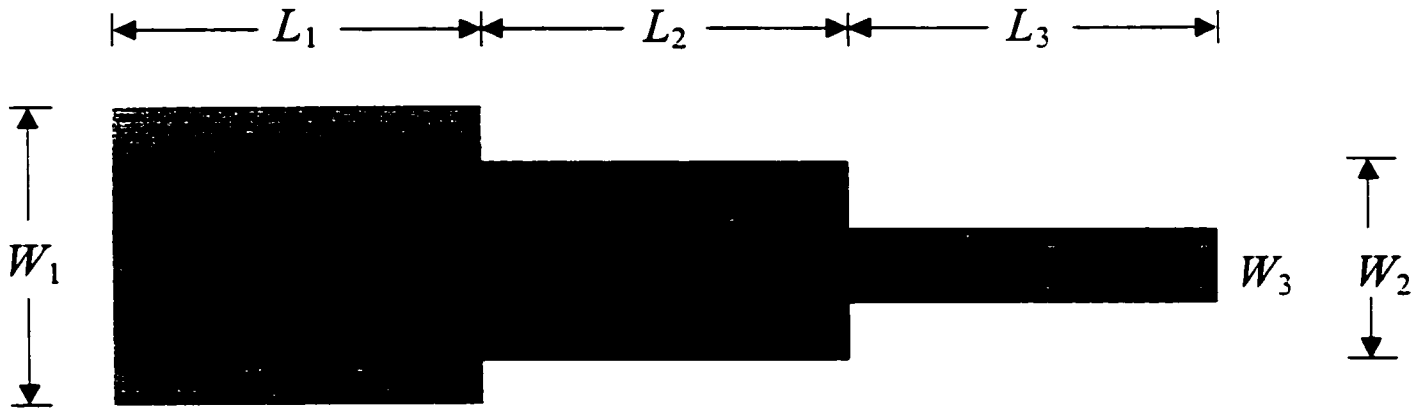

Fig. 2.6. The three-section 3:1 microstrip impedance transformer.

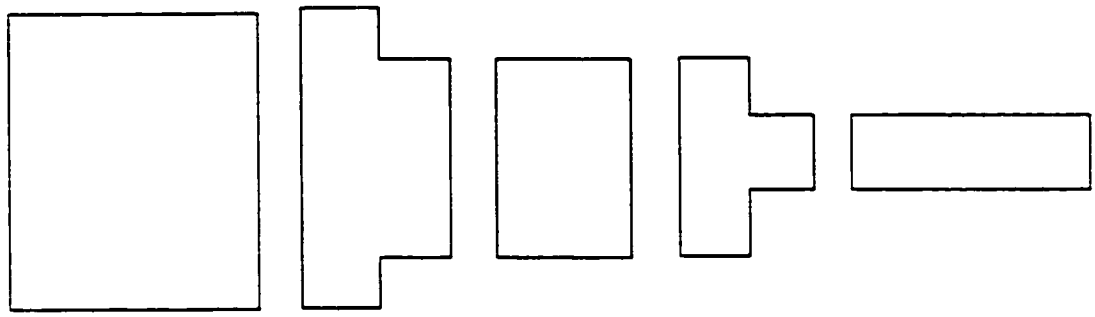

Fig. 2.7. The coarse model of the three-section 3:1 microstrip impedance transformer.

TABLE 2.1
THE INITIAL AND FINAL DESIGNS FOR THE THREE-SECTION MICROSTRIP IMPEDANCE TRANSFORMER

Parameter	$x_f^{(0)}$	$\bar{x}_f$
W_1	0.38145	0.35760
L_1	2.78208	2.97243
W_2	0.15126	0.14241
L_2	3.00255	3.04148
W_3	0.04227	0.04215
L_3	3.08801	3.08122
all values are in mm		

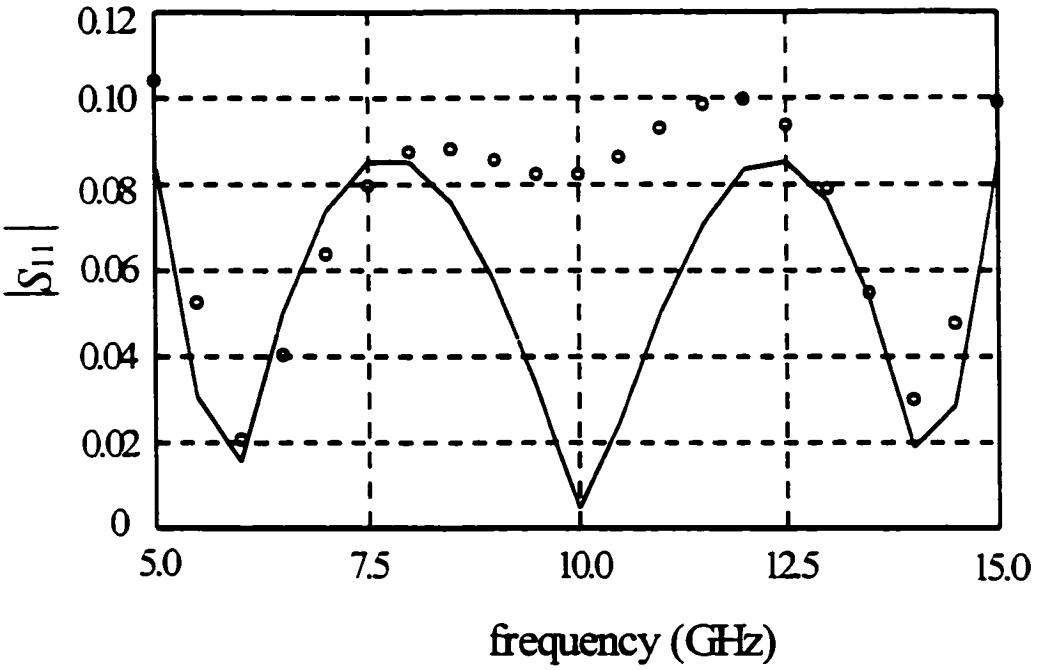

Fig. 2.8. The optimal coarse model response (—) and the fine model response (o) at the initial design for the three-section microstrip transformer.

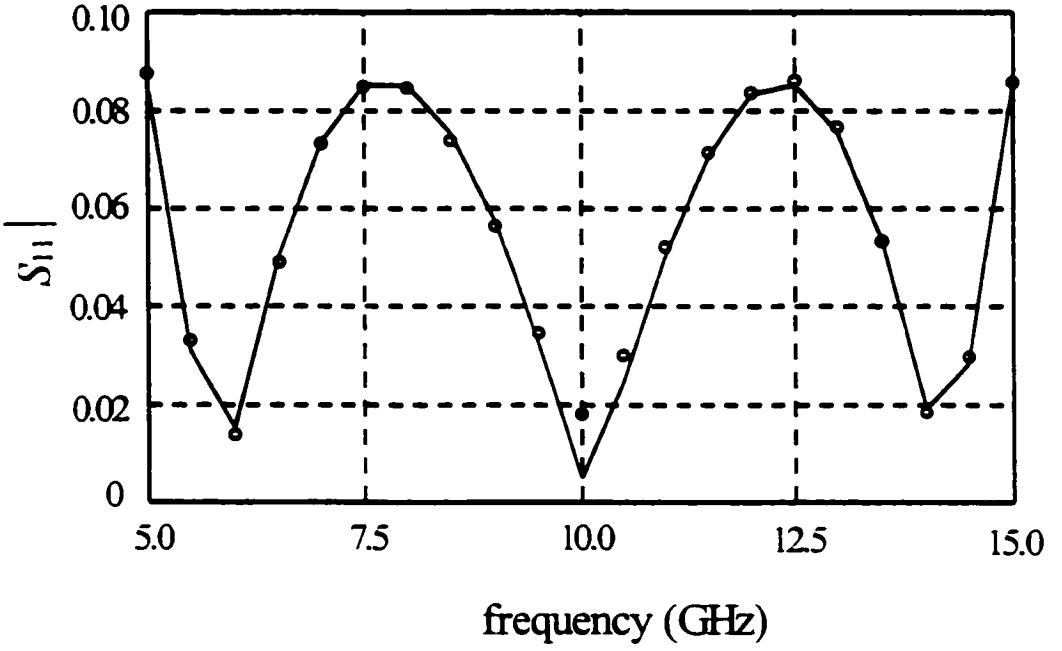

Fig. 2.9. The optimal coarse model response (—) and the fine model response (o) at the space-mapped design for the three-section microstrip transformer.

2.8 CONCLUSIONS

In this Chapter we reviewed some of the basic concepts in circuit optimization. We showed how a nominal circuit design problem can be formulated as an optimization problem. A general formulation that minimizes a suitable norm is reviewed. This norm is a measure of the errors between the given specifications and the related responses. We addressed different types of models that can be used in the design problems. These models vary in their accuracy and speed. Applying traditional optimization approaches using time-intensive models is shown to be formidable.

The concept of Space Mapping (SM) optimization was also presented. Two of the first SM-based optimization algorithms are reviewed. We showed that SM optimization can be efficient in optimizing circuits using time-intensive simulators. The Parameter Extraction (PE) problem is an essential step in SM optimization. We reviewed the formulation of this problem as an optimization problem. A microwave transformer example was used to illustrate ASM optimization.

3

THE TRUST REGION AGGRESSIVE SPACE MAPPING ALGORITHM

3.1 INTRODUCTION

Space mapping (SM) optimization aims at aligning two different simulation models: a coarse model, typically an empirical circuit simulation and a fine model, typically a full wave EM simulation. SM combines the accuracy of the fine model with the speed of the coarse model. Parameter Extraction (PE) is a crucial part of the technique. In this step the parameters of the coarse model whose responses match the fine model responses are obtained. The nonuniqueness of PE may lead to divergence or oscillation of SM optimization.

Multi-Point parameter Extraction (MPE) concept was proposed [32] to enhance the uniqueness of the extraction step at the expense of an increased number of fine model simulations. The selection of points was arbitrary, not automated and no information about the mapping between the two spaces was taken into account.

The Trust Region Aggressive Space Mapping (TRASM) algorithm, the main focus of this chapter, integrates a trust region methodology [59] with the ASM technique. The step taken in each iteration is constrained by a suitable trust region. TRASM also automates the selection of fine model points used for the MPE process. A Recursive Multi-Point parameter Extraction (RMPE) procedure utilizes all the fine model points simulated since the last successful iteration. Also, the current approximation to the mapping between the two spaces is integrated into this extraction step.

The TRASM algorithm is applied to a number of examples. The EM solver ***em*** [27] is used successfully to optimize the design of an HTS filter and a Double-Folded Stub (DFS) filter. Maxwell Eminence [28] through Empipe3D [72] is used as a fine model to design two-section, three-section and seven-section waveguide transformers. HP HFSS ver. 5 [29] is used to carry out the optimization of a three-section waveguide transformer with rounded corners. The coarse models for these examples exploit either a coarse grid EM model or circuit-theoretic/analytical models. The different types of models used illustrate the flexibility of selection of coarse and fine models.

The required number of fine model simulations to obtain the final design, as demonstrated by the examples, is of the order of the problem dimension. Such designs would otherwise be obtained by computationally very expensive direct optimizations of the fine models.

3.2 TRUST REGION METHODOLOGIES IN OPTIMIZATION [59]

One of the goals of modern nonlinear programming algorithms is to achieve global convergence. By global convergence we mean the mathematical assurance that the optimization iterates produced by the algorithm, starting from an arbitrary initial iterate, will converge to a stationary point or local minimizer of the problem. Trust region strategies can be used to achieve this property.

Assume that it is required to minimize a scalar function $f(\boldsymbol{x})$. In the ith iteration, an approximate model $L^{(i)}(\boldsymbol{x})$ is used to approximate $f(\boldsymbol{x})$. This model may be a linearized or quadratic approximation of $f(\boldsymbol{x})$. It is expected to approximate well the behavior of $f(\boldsymbol{x})$ in the neighborhood of the current iterate $\boldsymbol{x}^{(i)}$. Consequently, the step taken using $L^{(i)}(\boldsymbol{x})$ model is confined to a region in which the approximate model can be trusted, whence the name "trust

region". This is done by adding a constraint on the length of the step allowed, resulting in the trust region subproblem

$$\underset{\boldsymbol{h}^{(i)}}{\text{minimize}}\, L^{(i)}(\boldsymbol{x}^{(i)} + \boldsymbol{h}^{(i)}) \tag{3.1}$$

$$\text{Subject to } \left\|\boldsymbol{h}^{(i)}\right\| \le \delta^{(i)} \tag{3.2}$$

Where $\delta^{(i)}$ is the trust region size. In (3.2) different types of norms may be used. Also, scaling can be applied to some of the parameters to improve the conditioning of the problem.

The step $\boldsymbol{h}^{(i)}$ obtained by (3.2) is accepted if it satisfies

$$f(\boldsymbol{x}^{(i)} + \boldsymbol{h}^{(i)}) < f(\boldsymbol{x}^{(i)}) \tag{3.3}$$

In this case, we set $\boldsymbol{x}^{(i+1)} = \boldsymbol{x}^{(i)} + \boldsymbol{h}^{(i)}$. Otherwise, we set $\boldsymbol{x}^{(i+1)} = \boldsymbol{x}^{(i)}$.

The trust region size is adjusted at the end of each iteration based on how well the actual reduction in the objective function compares to the expected reduction. If there is good agreement between both reductions we conclude that $L^{(i)}(\boldsymbol{x})$ is a good approximation of $f(\boldsymbol{x})$ in the vicinity of $\boldsymbol{x}^{(i)}$. In this case, the trust region size can be increased to allow for larger steps and thus faster convergence. Similarly, the trust region size is shrunk if there is poor agreement between both reductions. In this case, $L^{(i)}(\boldsymbol{x})$ is not a good approximation of $f(\boldsymbol{x})$.

3.3 THE TRASM ALGORITHM

At the ith iteration, the residual vector $\boldsymbol{f}^{(i)} = \boldsymbol{P}(\boldsymbol{x}_f^{(i)}) - \boldsymbol{x}_c^*$ defines the difference between the vector of extracted coarse model parameters $\boldsymbol{x}_c^{(i)} = \boldsymbol{P}(\boldsymbol{x}_f^{(i)})$ and the optimal coarse model design. The space-mapped design is reached if this residual vector is driven to zero. It follows that $\left\|\boldsymbol{f}^{(i)}\right\|$ serves as a measure of the misalignment between the two spaces.

TRASM [33-37] integrates a trust region methodology [59] with the ASM technique. Similar to ASM, TRASM aims at solving (2.29). However, instead of utilizing a quasi-Newton step the problem is solved as a least-squares problem. In the ith iteration, the objective of TRASM is to minimize $\left\| f^{(i+1)} \right\|_2^2$ within a certain trust region. To achieve this, TRASM utilizes a linearization of the vector $f^{(i+1)}$. The linearized objective function is thus given by

$$L^{(i)}(x^{(i)} + h^{(i)}) = \left\| f^{(i)} + B^{(i)} h^{(i)} \right\|_2^2 \tag{3.4}$$

The suggested step is obtained by solving

$$h^{(i)} = arg\left\{ \min_{h} \left\| f^{(i)} + B^{(i)} h \right\|_2^2 \right\} \tag{3.5}$$

$$\text{subject to } \left\| h^{(i)} \right\|_2 \le \delta^{(i)} \tag{3.6}$$

where $\delta^{(i)}$ is the size of the trust region. The solution of (3.5)-(3.6) is obtained by solving [73, 74]

$$(B^{(i)T} B^{(i)} + \lambda I) h^{(i)} = - B^{(i)T} f^{(i)} \tag{3.7}$$

where $B^{(i)}$ is an approximation to the Jacobian (2.32) at the ith iteration. The parameter λ is selected such that the step obtained satisfies $\left\| h^{(i)} \right\|_2 \le \delta^{(i)}$, where $\delta^{(i)}$ is the size of the trust region. This is done utilizing the iterative algorithm suggested in [75]. The point suggested for the next iteration is $x_f^{(i+1)} = x_f^{(i)} + h^{(i)}$. SPE is then applied at the point $x_f^{(i+1)}$ to get $f^{(i+1)} = P(x_f^{(i+1)}) - x_c^*$. The point $x_f^{(i+1)}$ is accepted and the matrix $B^{(i)}$ is updated using Broyden's formula [6] if a success criterion related to the reduction in $\| f \|$ is satisfied. In our implementation, this success criterion is given by

$$\left(\left\| f^{(i)} \right\| - \left\| f^{(i+1)} \right\| \right) > 0.01 \left(\left\| f^{(i)} \right\| - \left\| f^{(i)} + B^{(i)} h^{(i)} \right\| \right). \tag{3.8}$$

The success criterion (3.8) ensures that the ratio between the actual reduction in the ℓ_2 norm of $\boldsymbol{f}$ and the predicted reduction is greater than a certain value. Otherwise, the validity of the extraction process leading to $\boldsymbol{f}^{(i+1)}$ is suspect. The residual vector $\boldsymbol{f}^{(i+1)}$ is then used to construct a candidate point from the point $\boldsymbol{x}_f^{(i+1)}$ by using (3.7). This candidate point is then added to the set of points employed for MPE at the point $\boldsymbol{x}_f^{(i+1)}$: a new value for $\boldsymbol{f}^{(i+1)}$ is obtained by solving

$$\underset{\boldsymbol{x}_c}{minimize} \left\| \boldsymbol{R}_c(\boldsymbol{x}_c + \boldsymbol{B}^{(i)}(\boldsymbol{x}_f - \boldsymbol{x}_f^{(i+1)})) - \boldsymbol{R}_f(\boldsymbol{x}_f) \right\|, \tag{3.9}$$

simultaneously for all $\boldsymbol{x}_f \in V$, where V is the set of fine model points used for MPE. This multi-point parameter extraction step differs from that suggested in [32] in one important aspect. A perturbation in the fine model space of $\Delta\boldsymbol{x}_f$ corresponds to a perturbation in the coarse model space of $\boldsymbol{B}^{(i)}\Delta\boldsymbol{x}_f$. This is logical since $\boldsymbol{B}^{(i)}$ represents the most up-to-date approximation to the mapping between the two spaces. Thus, the available information about the mapping between the two spaces is exploited.

The new extracted coarse model parameters either satisfy the success criterion (3.8) or they are used to obtain another candidate point which is then added to the set V and the whole process is repeated. See Fig. 3.1. This RMPE process is expected to improve the uniqueness of the extraction step. This may lead to the satisfaction of (3.8) or the step is declared a failure. Failure is declared in one of two cases: either the vector of extracted parameters approaches a limiting value with (3.8) not satisfied, or the number of fine model simulations since the last successful iteration has reached $n+1$. In the first case, the vector $\boldsymbol{f}^{(i+1)}$ is trusted and the accuracy of the linearization used to predict $\boldsymbol{h}^{(i)}$ is suspected. Thus, to ensure a successful step

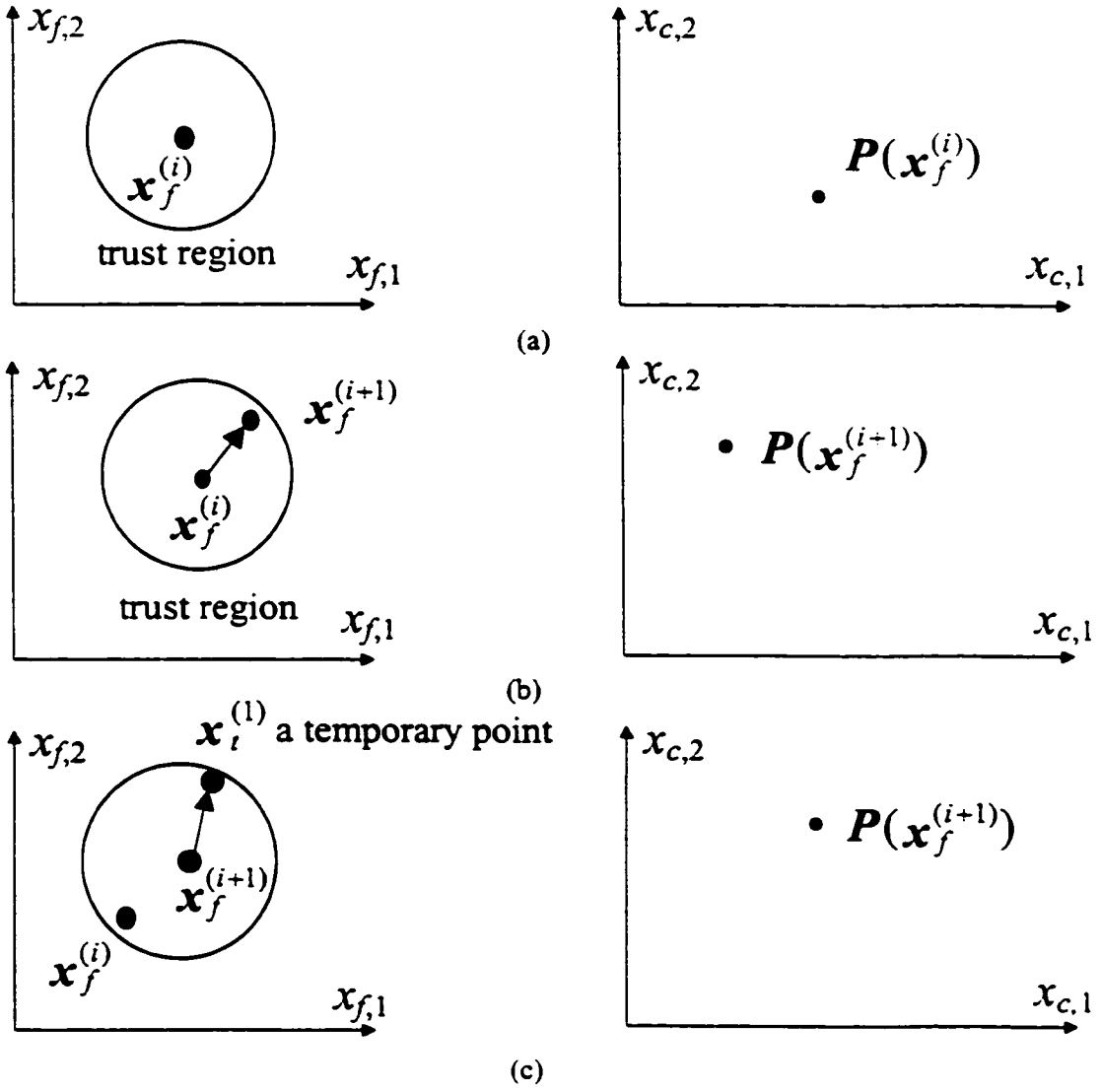

Fig. 3.1. Illustration of the RMPE procedure: (a) the current state at the ith iteration, (b) initial parameter extraction at the suggested point $x_f^{(i+1)}$ and (c) parameter extraction fails; an additional point $x_t^{(1)}$ is obtained and multi-point parameter extraction is carried out to sharpen the solution.

from the current point $x_f^{(i)}$, $\delta^{(i)}$ is shrunk and a new suggested point $x_f^{(i+1)}$ is obtained. In the latter case, sufficient information is available to obtain an estimate for the Jacobian of the fine model responses with respect to the fine model parameters. This is done by solving the system of linear equations

$$\begin{pmatrix} (x_f^{(i)}-x_f^{(i-1)})^T \\ (x_f^{(i)}-x_t^{(1)})^T \\ \vdots \\ (x_f^{(i)}-x_t^{(n-1)})^T \end{pmatrix} J_f^T = \begin{pmatrix} (g^{(i)}-g^{(i-1)})^T \\ (g^{(i)}-g_t^{(1)})^T \\ \vdots \\ (g^{(i)}-g_t^{(n-1)})^T \end{pmatrix}, \tag{3.10}$$

where $x_t^{(k)}$ is the kth candidate point used for MPE and $g_t^{(k)}$ is the corresponding error between the fine model response and the optimal coarse model response. This matrix is then used to obtain a step $h^{(i)}$ in the parameter space by solving the system of equations

$$(J_f^T J_f + \lambda I) h^{(i)} = -J_f^T g^{(i)}, \tag{3.11}$$

varying the parameter λ until $\|h^{(i)}\| \le \delta^{(i)}$. If there is no reduction in the ℓ_2 norm of the vector function g, the trust region is shrunk and (3.11) is resolved. This is repeated until either the size of the trust region has shrunk significantly and hence the algorithm terminates or a successful step is taken. The successful step is then used instead of the step obtained by (3.7).

At the end of each iteration, the ratio between the actual reduction in the ℓ_2 norm of the vector f and the predicted reduction using linearization is used to check the accuracy of the linearization. The criterion

$$\left(\|f^{(i)}\| - \|f^{(i-1)}\|\right) \ge 0.80 \left(\|f^{(i)}\| - \|f^{(i)} + B^{(i)} h^{(i)}\|\right) \tag{3.12}$$

is utilized in our implementation. If (3.12) is satisfied then we exploit the accuracy of the linearization and increase the size of the trust region.

In the initialization phase we assign $x_f^{(0)} = x_c^*$ and $B^{(0)} = I$, the identity matrix. Also, we assign values to the two parameters δ_f and ε. These two parameters are used to determine the termination condition of the algorithm.

To ensure the uniqueness of $f^{(0)}$, the multi-point parameter extraction at the first point is repeated for an increasing number of points in the set V until it approaches a limiting value. This limiting value can then be trusted and the algorithm proceeds. For any iteration $i > 0$, the basic steps taken are as follows.

Step 0 Given $x_f^{(i)}$, $f^{(i)}$, $B^{(i)}$ and $\delta^{(i)}$. Set $\delta^{(i-1)} = \delta^{(i)}$.

Step 1 Obtain $h^{(i)}$ by solving (3.7). Let $\delta^{(i+1)} = \|h^{(i)}\|_2$.

Step 2 If $\delta^{(i+1)} \le \delta_f$ stop else evaluate $x_f^{(i-1)}$ using (2.30) and set $V = \{x_f^{(i-1)}\}$.

Step 3 Apply multi-point parameter extraction using the points in the set V to obtain $f^{(i-1)}$.

Step 4 If the success criterion (3.8) is satisfied go to Step 9.

Step 5 If $|V|$ is equal to one go to Step 8.

Comment $|V|$ denotes the cardinality of the set V.

Step 6 Compare $f^{(i-1)}$ obtained using $|V|$ fine model points with that previously obtained using $|V|-1$ fine model points. If $f^{(i-1)}$ is approaching a limiting value shrink the trust region size $\delta^{(i-1)}$ and go to Step 1.

Step 7 If $|V|$ is equal to n obtain the Jacobian J_f, shrink the trust region size $\delta^{(i-1)}$, evaluate a new step $h^{(i)}$ by solving (3.11) with $\delta = \delta^{(i-1)}$ for a suitable value of λ that results in the reduction in the ℓ_2 norm of the vector g and go to Step 2.

Comment The trust region is shrunk to ensure a successful step.

Step 8 Obtain a temporary point using $x_f^{(i+1)}$, $f^{(i+1)}$ and $\delta^{(i+1)}$. Add this point to the set V and go to Step 3.

Step 9 Update the matrix $B^{(i)}$ to $B^{(i+1)}$ using Broyden's formula [6].

Step 10 If $\left\| R_f(x_f^{(i-1)}) - R_f(x_f^{(i)}) \right\| \leq \varepsilon$ stop.

Step 11 Increase the trust region size $\delta^{(i-1)}$ if (3.12) is satisfied.

Step 12 Let $i=i+1$. Go to Step 0.

The algorithm terminates if the condition $\delta^{(i+1)} \leq \delta_f$ is satisfied or if there is no significant change in the fine model responses in two consecutive iterations. The algorithm produces two main results. These results are the space-mapped design $\bar{x}_f$ and the matrix $\bar{B}$ which represents the mapping between the two spaces.

In our implementation, proper scaling is applied to the optimizable parameters to make them of the same order. The initial trust region size is taken as 2% to 10% of the ℓ_∞ norm of the vector of scaled parameters.

3.4 EXAMPLES

3.4.1 Double-Folded Stub Filter

We consider the design of the DFS microstrip structure shown in Fig. 3.2 (Bandler *et al.* [30]). Folding the stubs reduces the filter area w.r.t. the conventional double stub structure (Rautio [76]). The filter is characterized by five parameters : W_1 , W_2 , S, L_1 and L_2 (see Fig. 3.2). L_1, L_2 and S are chosen as optimization variables. W_1 and W_2 are fixed at 4.8 mil. The design specifications are given by $|S_{21}| \geq$ -3 dB in the passband and $|S_{21}| \leq$ -30 dB in the stopband, where the passband includes frequencies below 9.5 GHz and above 16.5 GHz and the

stopband lies in the range [12 GHz, 14 GHz]. The structure is simulated by Sonnet's ***em*** [27] through Empipe [77]. The coarse model is a coarse-grid ***em*** model with cell size 4.8 mil by 4.8 mil. The fine model is a fine-grid ***em*** model with cell size 1.6 mil by 1.6 mil. Other parameters are summarized in Table 3.1.

Fig. 3.3 shows the response $\boldsymbol{R}_f(\boldsymbol{x}_c^*)$ along with the optimal coarse model response. The time needed to simulate the structure (coarse model) at a single frequency is only 5 CPU seconds on a Sun SPARCstation 10. This includes the automatic response interpolation carried out to accommodate off-grid geometries.

It is clear from Fig. 3.3 that the fine model response violates the design specifications at the starting point. The TRASM algorithm required only two iterations to reach the final design. The algorithm's progress is shown in Table 3.2. The number of fine model points needed is 5. Linear response interpolation was enabled to simulate the off-grid fine model points. The fine model response $\boldsymbol{R}_f(\bar{\boldsymbol{x}}_f)$ is shown in Fig. 3.4. The CPU time needed for the fine model is approximately 70 seconds per frequency point.

3.4.2 HTS Filter

We consider optimization of a high-temperature superconducting (HTS) filter [31,78]. This filter is shown in Fig. 3.5. The specifications are $|S_{21}| \geq 0.95$ in the passband and $|S_{21}| \leq 0.05$ in the stopband, where the stopband includes frequencies below 3.967 GHz and above 4.099 GHz and the passband lies in the range [4.008 GHz, 4.058 GHz]. The design variables for this problem are L_1, L_2, L_3, S_1, S_2 and S_3. We take $L_0 = 50$ mil and $W = 7$ mil. The coarse model exploits the empirical models of microstrip lines, coupled lines and open stubs available in

TABLE 3.1
MATERIAL AND PHYSICAL PARAMETERS FOR THE COARSE AND FINE *em* MODELS OF THE DFS FILTER

Model Parameter	Value
substrate dielectric constant	9.9
substrate thickness (mil)	5
shielding cover height (mil)	∞
conducting material thickness	3.0E-6
substrate dielectric loss tangent	2.0E-3
resistivity of metal (Ωm)	1.72E-8
magnetic loss tangent	0
surface reactance (Ω/sq)	0
lower frequency limit (GHz)	5
upper frequency limit (GHz)	20
frequency increment size (GHz)	0.25

TABLE 3.2
VALUES OF DESIGNABLE PARAMETERS AT EACH ITERATION FOR THE DFS FILTER

Parameter	$x_f^{(0)}$	$x_f^{(1)}$	$x_f^{(2)}$
L_1	88.8	89.5	94.3
L_2	84.1	84.6	85.4
S	3.9	4.7	4.7

all values are in mils

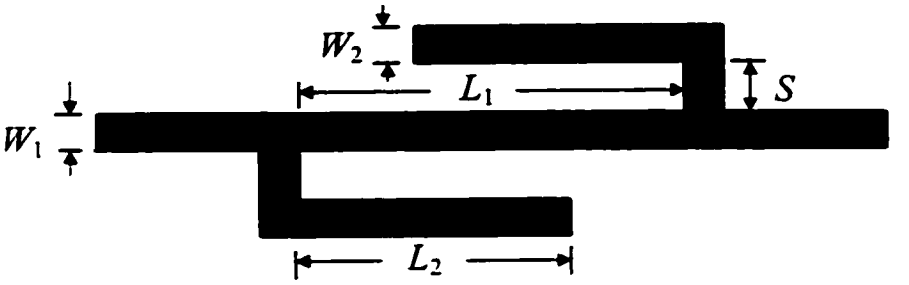

Fig. 3.2. The DFS filter.

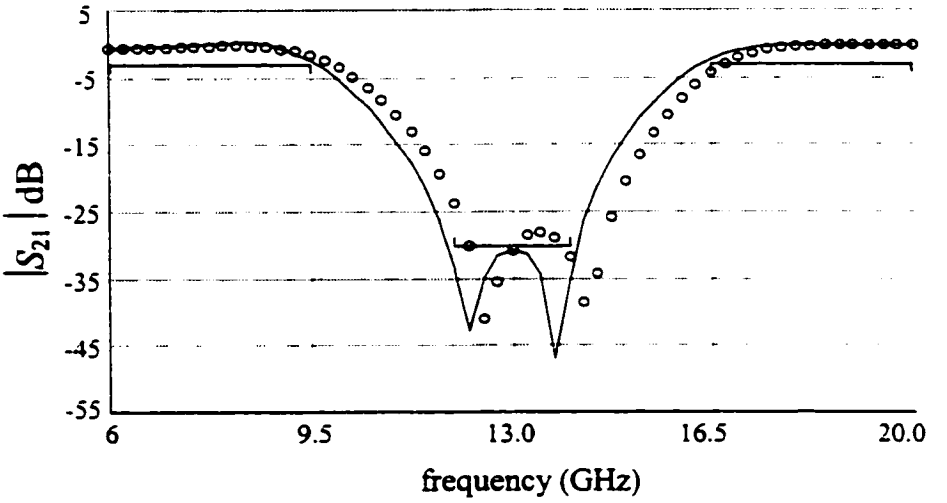

Fig. 3.3. The optimal coarse model response (—) and the fine model response (o) at the starting point for the DFS filter.

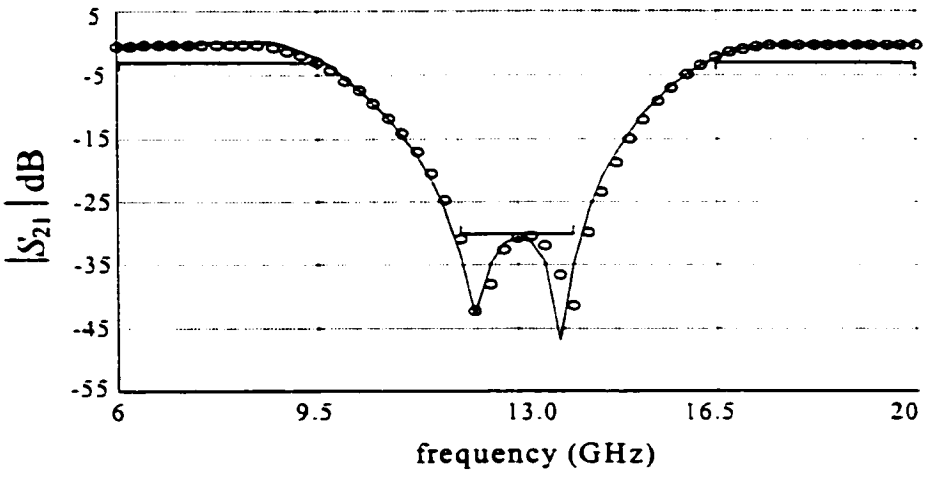

Fig. 3.4. The optimal coarse model response (—) and the space-mapped fine model response (o) for the DFS filter.

OSA90/hope (see Fig. 3.6). The fine model employs a fine-grid ***em*** simulation. The material and physical parameters values used in both OSA90/hope and in ***em*** are shown in Table 3.3. The coarse model is first optimized using the OSA90/hope minimax optimizer. The fine model response $\boldsymbol{R}_f(x_c^*)$ is shown in Fig. 3.7.

Fig. 3.8 shows how two of the extracted coarse model parameters change with the number of points used for parameter extraction in the first iteration. The first point (1) is obtained using SPE. These extracted values would have caused the original ASM technique to diverge. TRASM automatically generates a candidate point which is then used together with the original point to carry out a Double-Point parameter Extraction (DPE) and the second point (2) is obtained. To confirm that this point is the required one a third candidate point is generated. Three-point extraction is then carried out to obtain the third extracted point (3). The second and third extracted points show that the extracted vector of coarse model parameters is approaching a limiting value and can thus be trusted. The coarse model responses corresponding to the three extracted points of Fig. 3.8 are shown in Fig. 3.9.

For the remaining iterations, single point parameter extraction worked well. The fine model responses and the coarse model responses for the corresponding extracted points are shown in Fig. 3.10. The space-mapped fine model design was obtained in 5 iterations which required 8 fine model simulations. The final fine model design is given in Table 3.4. The fine model response at this design is shown in Fig. 3.11. The passband ripples are shown in Fig. 3.12.

In the original space mapping approaches [30, 31] this example required significant manual intervention to successfully complete the parameter extraction phase. Furthermore, without such intervention the previous approaches would not work.

TABLE 3.3
MATERIAL AND PHYSICAL PARAMETERS
FOR THE HTS FILTER

Model Parameter	OSA90/hope	*em*
substrate dielectric constant	23.425	23.425
substrate thickness (mil)	19.9516	19.9516
shielding cover height (mil)	∞	250
conducting material thickness	1.968E-2	0
substrate dielectric loss tangent	3.0E-5	3.0E-5
resistivity of metal (Ωm)	0	4.032E-8
surface roughness of metal	0	—
magnetic loss tangent	—	0
surface reactance (Ω/sq)	—	0
x-grid cell size (mil)	—	1.00
y-grid cell size (mil)	—	1.75

TABLE 3.4
THE INITIAL AND FINAL DESIGNS OF THE FINE MODEL
FOR THE HTS FILTER

Parameter	$x_f^{(0)}$	$x_f^{(5)}$
L_1	188.33	181.43
L_2	197.98	200.51
L_3	188.58	180.49
S_1	21.97	19.44
S_2	99.12	80.52
S_3	111.67	83.41
all values are in mils		

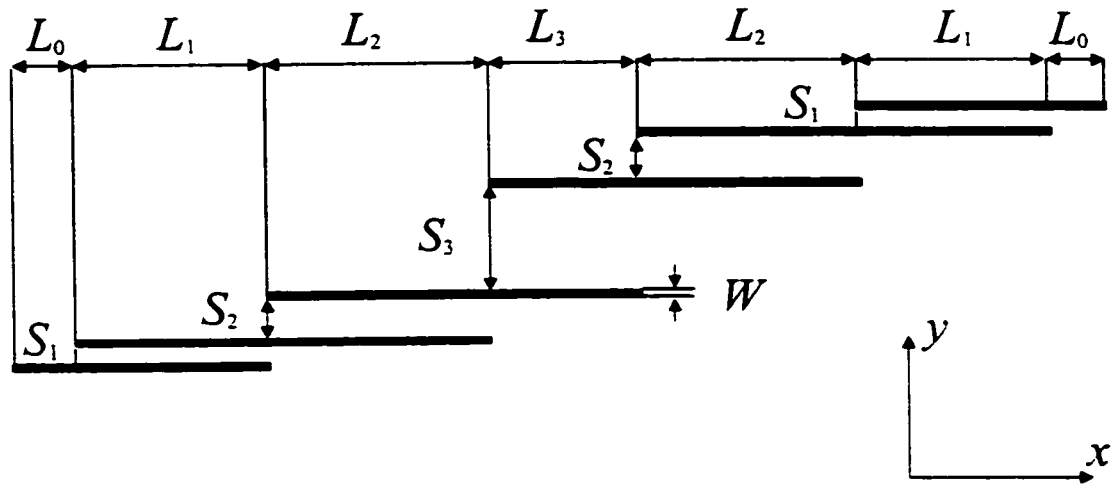

Fig. 3.5. The structure of the HTS filter.

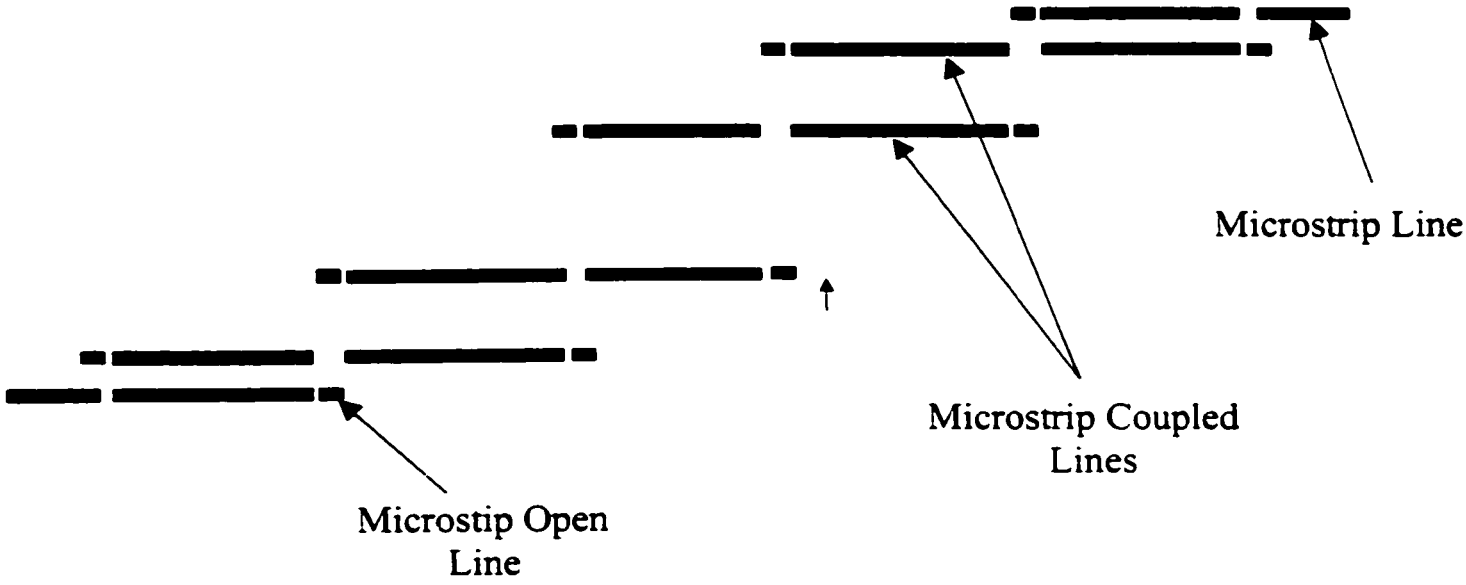

Fig. 3.6. The coarse model of the HTS filter.

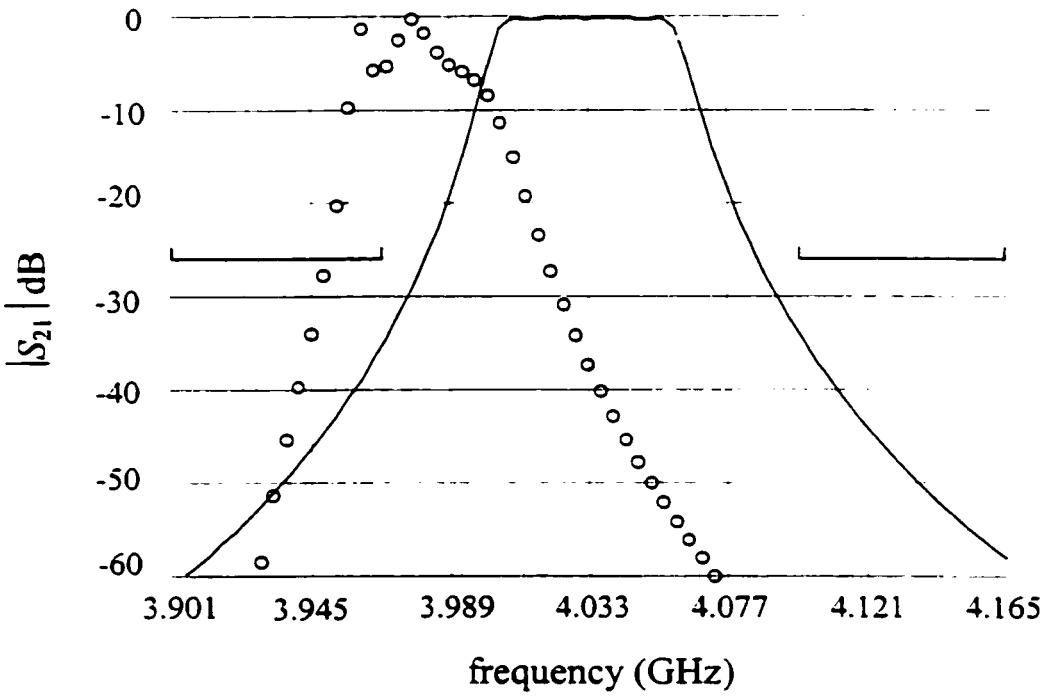

Fig. 3.7. The optimal coarse model response (—) and the fine model response (o) at the starting point for the HTS filter.

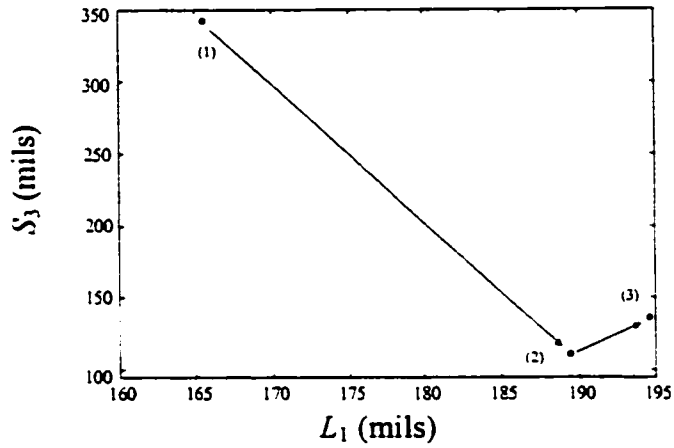

Fig. 3.8. The variation of two of the extracted coarse model parameters in the first iteration with the number of points used for parameter extraction where (1) is obtained using a single fine model point, (2) is obtained using two fine model points and (3) is obtained using three fine model points.

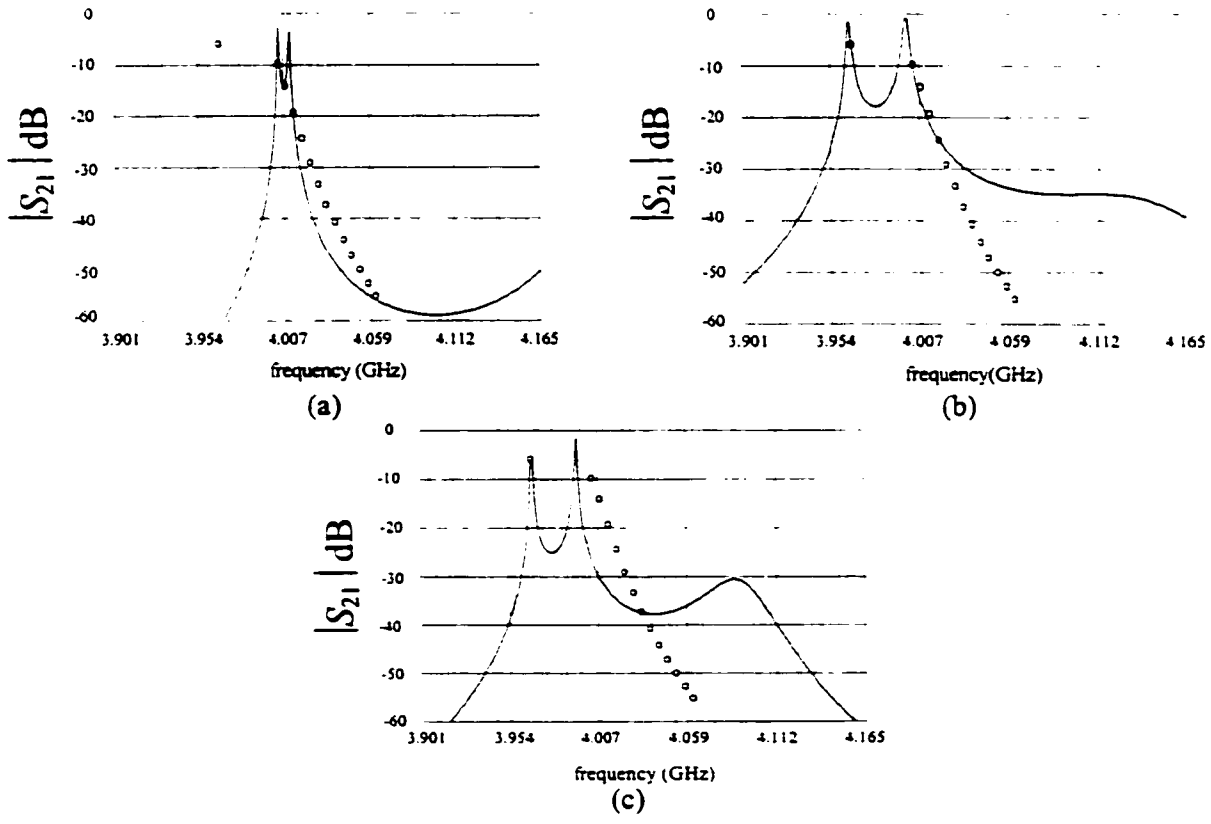

Fig. 3.9. The coarse model response (—) and the fine model response (o) corresponding to the three extracted points in Fig. 3.8 where (a) is obtained using a single fine model, (b) is obtained using two fine model points and (c) is obtained using three fine model points.

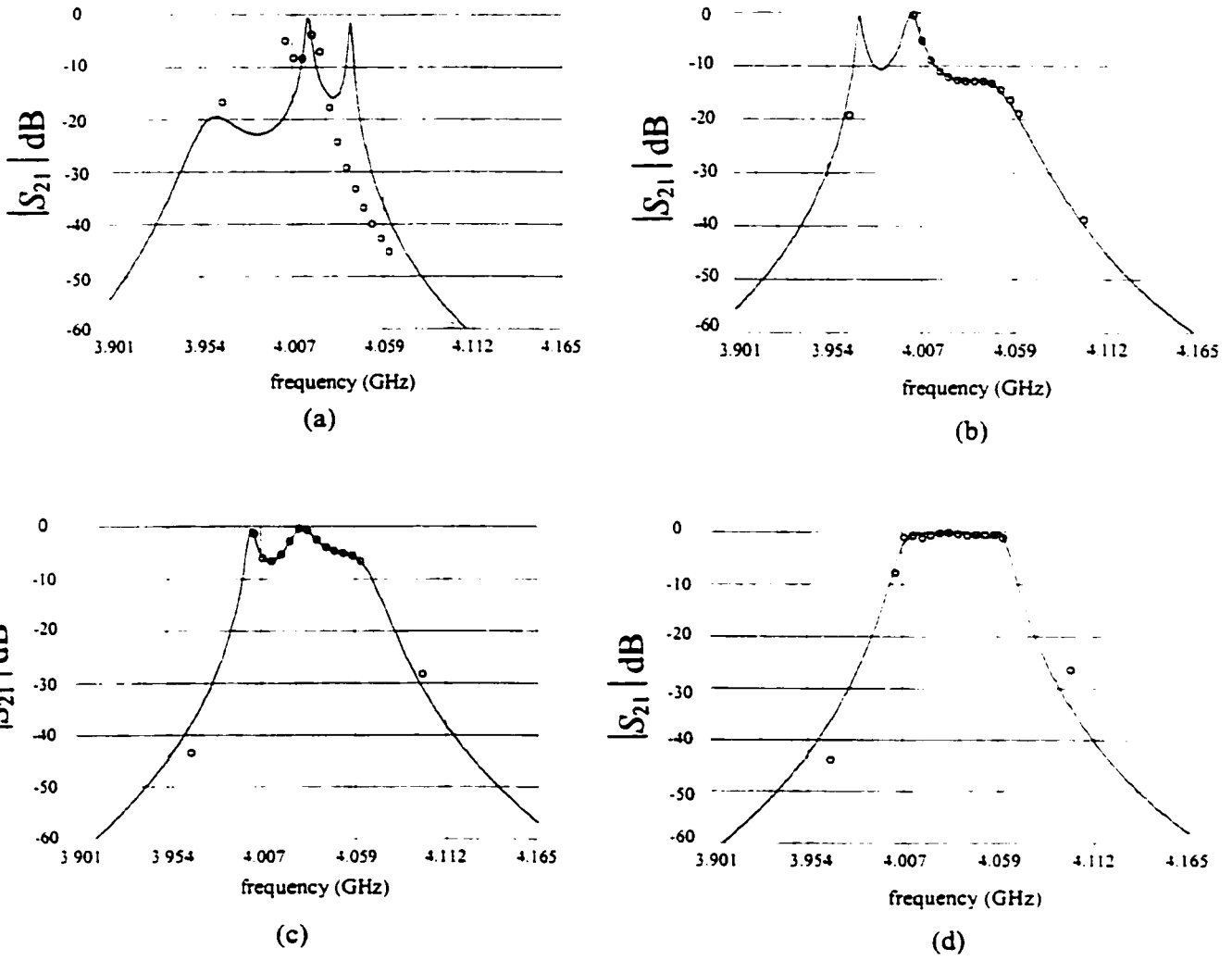

Fig. 3.10. The coarse model response (—) at the extracted point and the fine model response (o) corresponding to (a) the second iteration, (b) the third iteration, (c) the fourth iteration and (d) the fifth iteration.

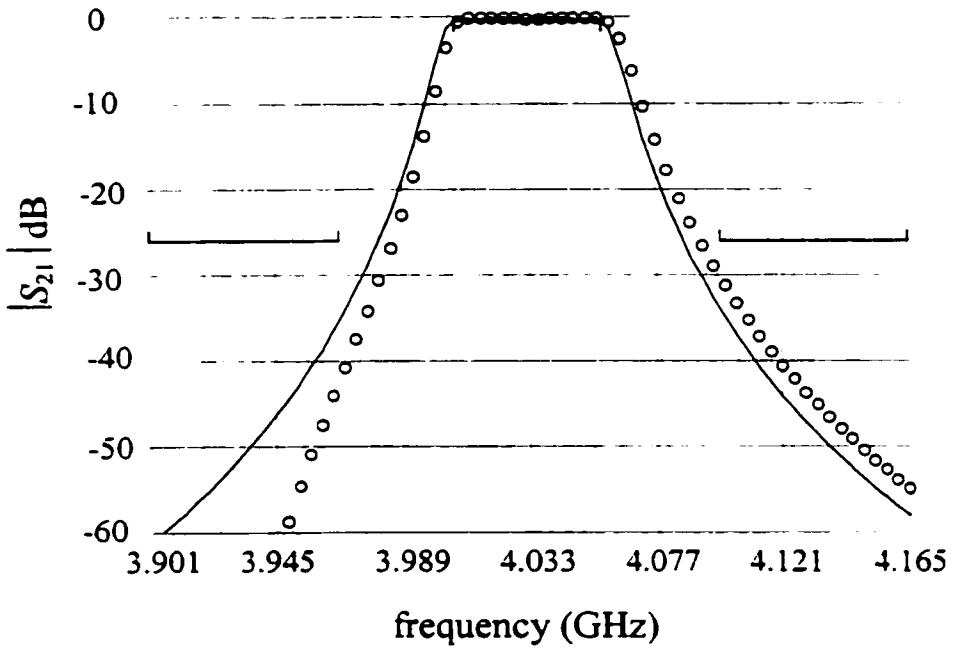

Fig. 3.11. The optimal coarse model response (—) and the final fine model response (o) for the HTS filter.

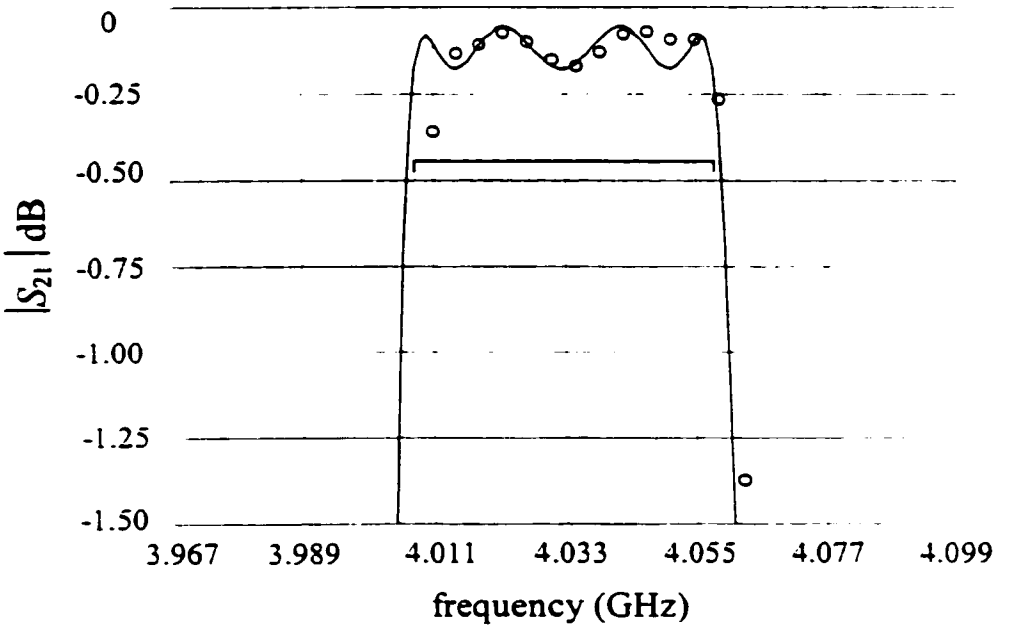

Fig. 3.12. The optimal coarse model response (—) and the final fine model response (o) for the HTS filter in the passband.

3.4.3 Waveguide Transformers

Three designs, of two, three and seven-section waveguide transformers were considered. The two-section waveguide transformer is shown in Fig. 3.13. These examples are classical microwave circuit design problems [79]. Two different sets of models were used. The first set exploits two empirical models: an "ideal" analytical model which neglects the junction discontinuity and a more accurate "nonideal" analytical model which includes the junction discontinuity effects [79]. The second set uses the ideal analytical model of the first set as the coarse model while Maxwell Eminence [28] is used as the fine model. The designable parameters for these design problems are the height and length of each waveguide section.

The two-section transformer is optimized using the two analytical models. The optimum ideal model response is shown in Fig. 3.14 along with the nonideal model response at the same point. TRASM terminated in three iterations, requiring 5 fine model simulations. The final nonideal model design is given in Table 3.5. The corresponding nonideal model response is shown in Fig. 3.15. This example is known to have more than one minimum for the parameter extraction step [32]. However, our new algorithm converged successfully. The number of simulations needed to align the two models is smaller than that reported in [32]. The same transformer is then optimized using Maxwell Eminence and the ideal analytical model. Nine adaptive passes were allowed for Maxwell Eminence with allowable delta S set to 0.0001. The initial fine model response is shown in Fig. 3.16. The space-mapped design is obtained in three iterations which required five Maxwell Eminence fine model simulations. This is one half the number of fine model simulations reported in [32]. The Maxwell Eminence fine model design is shown in Table 3.6 and the corresponding fine model response is shown in Fig. 3.17.

The previous steps were repeated for the three-section waveguide transformer. The initial fine model response is shown in Fig. 3.18. Using the two analytical models the final

TABLE 3.5
VALUES OF DESIGNABLE PARAMETERS AT EACH ITERATION FOR THE TWO-SECTION WAVEGUIDE TRANSFORMER USING TWO ANALYTICAL MODELS

Parameter	$x_f^{(0)}$	$x_f^{(1)}$	$x_f^{(2)}$	$x_f^{(3)}$
b_1	0.712	0.715	0.716	0.716
b_2	1.395	1.400	1.402	1.402
L_1	1.657	1.591	1.560	1.560
L_2	1.590	1.541	1.518	1.518
all values are in cm				

TABLE 3.6
VALUES OF DESIGNABLE PARAMETERS AT EACH ITERATION FOR THE TWO-SECTION WAVEGUIDE TRANSFORMER USING MAXWELL EMINENCE AND AN IDEAL ANALYTICAL MODEL

Parameter	$x_f^{(0)}$	$x_f^{(1)}$	$x_f^{(2)}$	$x_f^{(3)}$
b_1	0.712	0.713	0.719	0.716
b_2	1.395	1.397	1.408	1.402
L_1	1.657	1.595	1.565	1.567
L_2	1.590	1.535	1.517	1.517
all values are in cm				

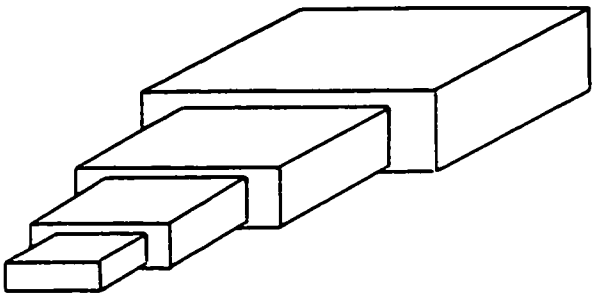

Fig. 3.13. A typical two-section waveguide transformer.

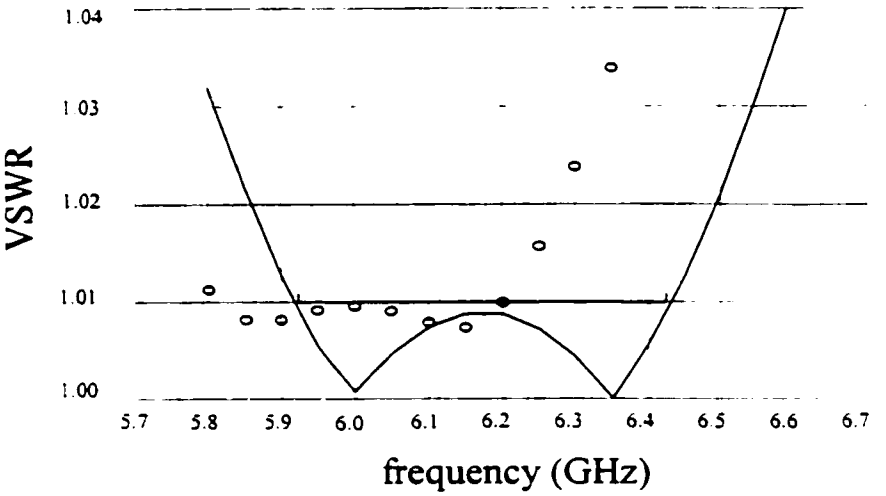

Fig. 3.14. The optimal response of the ideal analytical model (—) and the response of the nonideal analytical model (o) at the starting point for the two-section waveguide transformer.

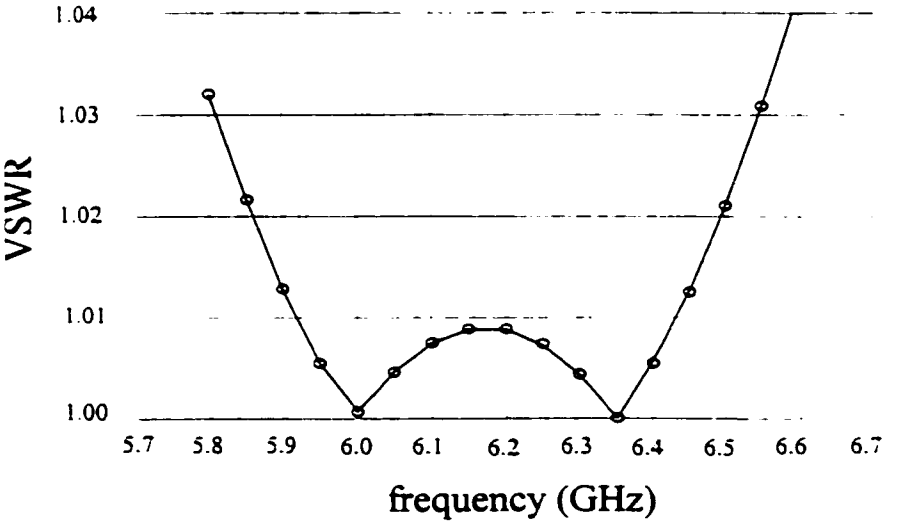

Fig. 3.15. The optimal response of the ideal analytical model (—) and the final response of the nonideal analytical model (o) for the two-section waveguide transformer.

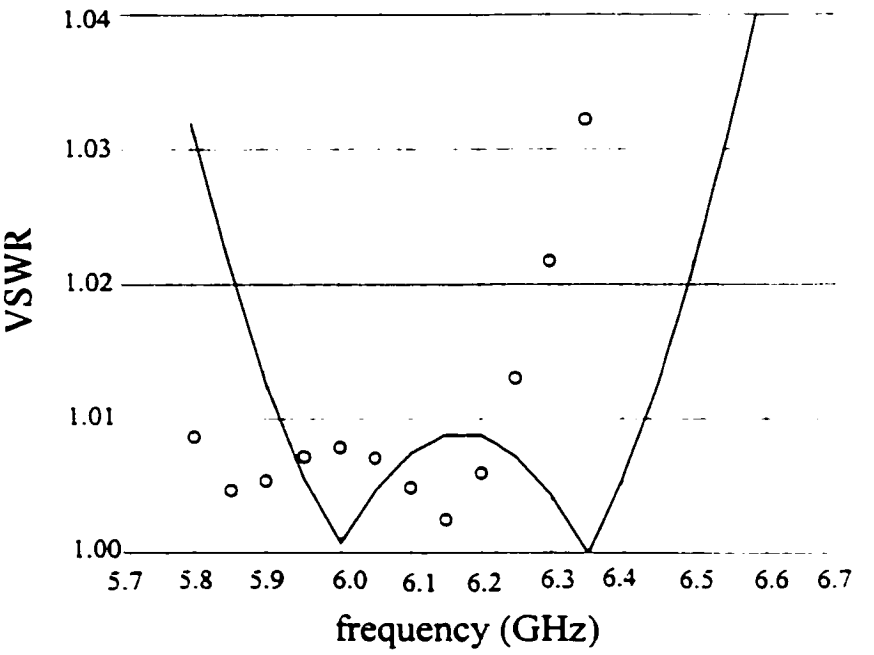

Fig. 3.16. The optimal response of the ideal analytical model (—) and the response of Maxwell Eminence (o) at the starting point for the two-section waveguide transformer.

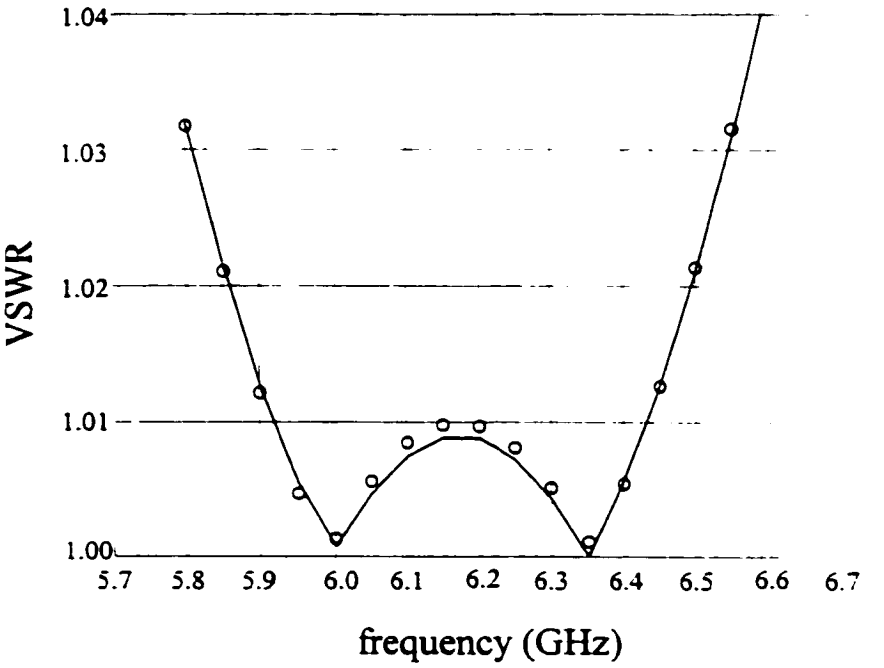

Fig. 3.17. The optimal response of the ideal analytical model (—) and the final Maxwell Eminence response (o) for the two-section waveguide transformer.

design was obtained in four iterations which required six fine model simulations. This final design is shown in Table 3.7. The corresponding fine model response is indistinguishable from the optimal coarse model response as shown in Fig. 3.19.

The design of the three-section transformer is then repeated using Maxwell Eminence and the ideal analytical model. We allowed only five adaptive passes with the same value of allowable delta S as before. The initial Maxwell Eminence fine model response is shown in Fig. 3.20. The algorithm terminated in two iterations with a total number of nine fine model simulations. Most of these fine model simulations were used to shrink the trust region around the final design. The final design is shown in Table 3.8. The corresponding Maxwell Eminence fine model response is shown in Fig. 3.21.

The design of a seven-section waveguide transformer was also considered. Using the two analytical models, the final design was obtained in three iterations which required six fine model simulations. The initial fine model response is shown in Fig. 3.22. The fine model response corresponding to the final design is almost identical to the optimal coarse model response as shown in Fig. 3.23. Table 3.9 shows the space-mapped design.

Finally, the design of the seven-section transformer was carried out using Maxwell Eminence and an ideal analytical model. We allowed ten refinement passes with allowable delta S of 0.001. The algorithm terminated in three iterations which required eleven Maxwell Eminence fine model simulations. The initial Maxwell Eminence response is shown in Fig. 3.24. The final fine model response is shown in Fig. 3.25. Table 3.10 shows the corresponding Maxwell Eminence fine model design.

TABLE 3.7
VALUES OF DESIGNABLE PARAMETERS AT EACH ITERATION FOR THE THREE-SECTION WAVEGUIDE TRANSFORMER USING TWO ANALYTICAL MODELS

Parameter	$x_f^{(0)}$	$x_f^{(1)}$	$x_f^{(2)}$	$x_f^{(3)}$	$x_f^{(4)}$
b_1	0.903	0.905	0.881	0.891	0.892
b_2	1.371	1.363	1.298	1.325	1.325
b_3	1.736	1.718	1.692	1.701	1.702
L_1	1.549	1.500	1.500	1.489	1.489
L_2	1.584	1.575	1.575	1.575	1.577
L_3	1.646	1.768	1.880	1.853	1.850

all values are in cm

TABLE 3.8
VALUES OF DESIGNABLE PARAMETERS AT EACH ITERATION FOR THE THREE-SECTION WAVEGUIDE TRANSFORMER USING MAXWELL EMINENCE AND AN IDEAL ANALYTICAL MODEL

Parameter	$x_f^{(0)}$	$x_f^{(1)}$	$x_f^{(2)}$
b_1	0.903	0.898	0.893
b_2	1.371	1.340	1.327
b_3	1.736	1.707	1.703
L_1	1.549	1.514	1.495
L_2	1.584	1.566	1.568
L_3	1.646	1.810	1.848

all values are in cm

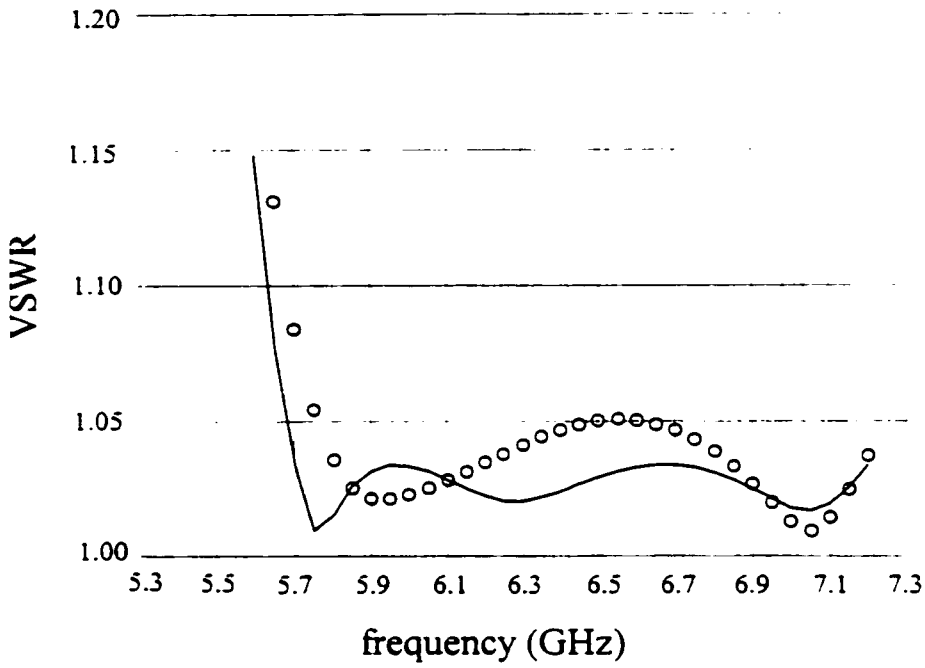

Fig. 3.18. The optimal response of the ideal analytical model (—) and the response of the nonideal analytical model (o) at the starting point for the three-section waveguide transformer.

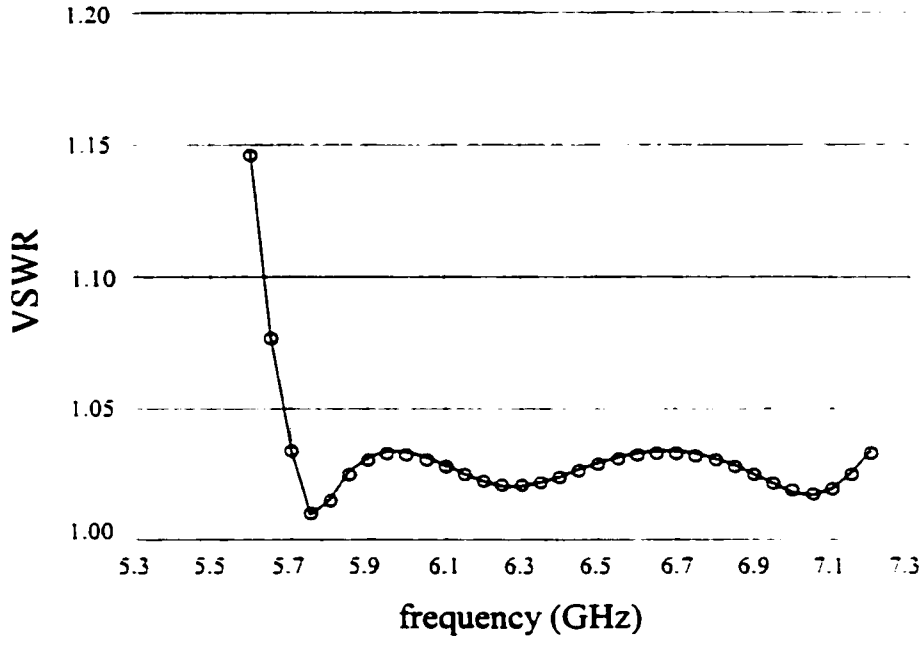

Fig. 3.19. The optimal response of the ideal analytical model (—) and the final response of the nonideal analytical model (o) for the three-section waveguide transformer.

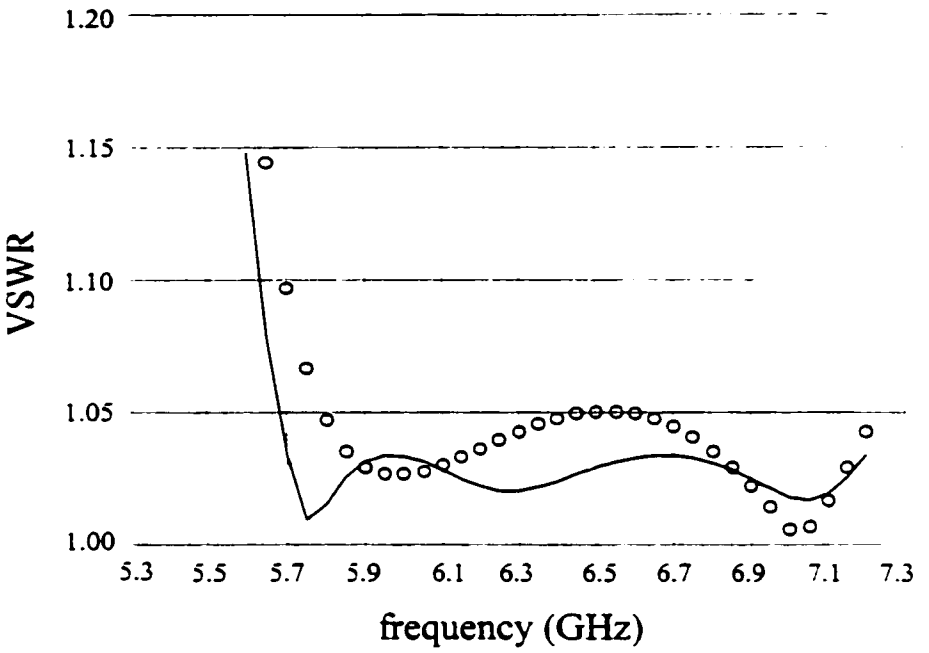

Fig. 3.20. The optimal response of the ideal analytical model (—) and the response of Maxwell Eminence (o) at the starting point for the three-section waveguide transformer.

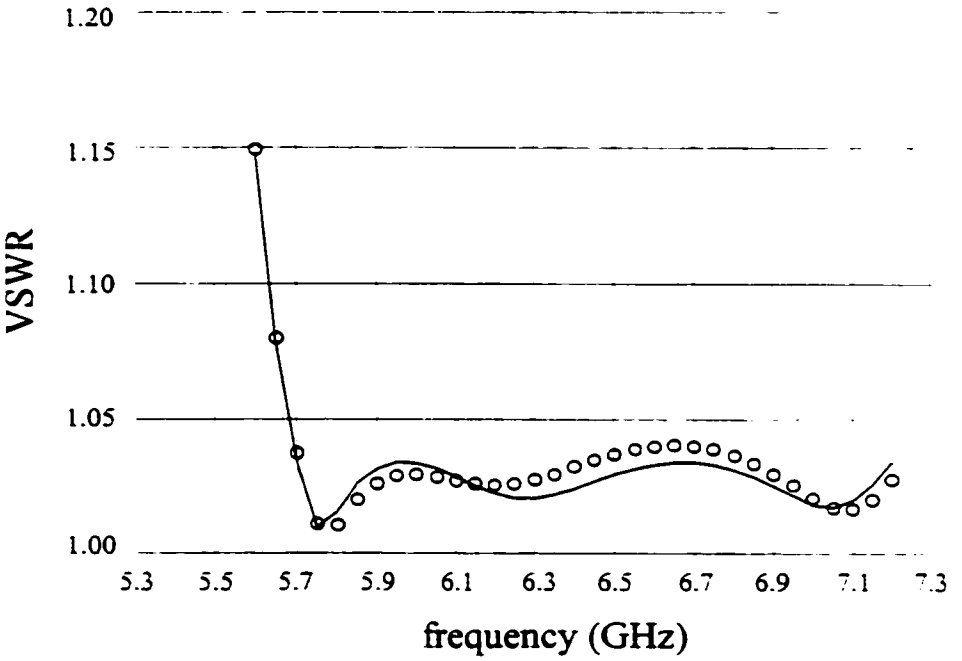

Fig. 3.21. The optimal response of the ideal analytical model (—) and the final Maxwell Eminence response (o) for the three-section waveguide transformer.

TABLE 3.9
VALUES OF DESIGNABLE PARAMETERS AT THE INITIAL AND FINAL DESIGNS FOR THE SEVEN-SECTION WAVEGUIDE TRANSFORMER USING TWO ANALYTICAL MODELS

Parameter	$x_f^{(0)}$	$x_f^{(3)}$
b_1	7.86732	7.87152
b_2	6.61888	6.64855
b_3	4.68540	4.74039
b_4	2.91987	2.96613
b_5	1.81412	1.83659
b_6	1.27658	1.28401
b_7	1.06847	1.06967
L_1	7.10588	7.24590
L_2	7.12201	7.08753
L_3	7.11760	6.91817
L_4	7.12331	6.90979
L_5	7.12815	6.98383
L_6	7.12154	7.03845
L_7	7.12945	7.07431
all values are in cm		

TABLE 3.10
VALUES OF DESIGNABLE PARAMETERS AT THE INITIAL AND FINAL DESIGNS FOR THE SEVEN-SECTION WAVEGUIDE TRANSFORMER USING MAXWELL EMINENCE AND AN IDEAL ANALYTICAL MODEL

Parameter	$x_f^{(0)}$	$x_f^{(3)}$
b_1	7.86732	7.87494
b_2	6.61888	6.65247
b_3	4.68540	4.74347
b_4	2.91987	2.97030
b_5	1.81412	1.84134
b_6	1.27658	1.28891
b_7	1.06847	1.07201
L_1	7.10588	7.18744
L_2	7.12201	7.03537
L_3	7.11760	6.89166
L_4	7.12331	6.89697
L_5	7.12815	6.98825
L_6	7.12154	7.05869
L_7	7.12945	7.12572
all values are in cm		

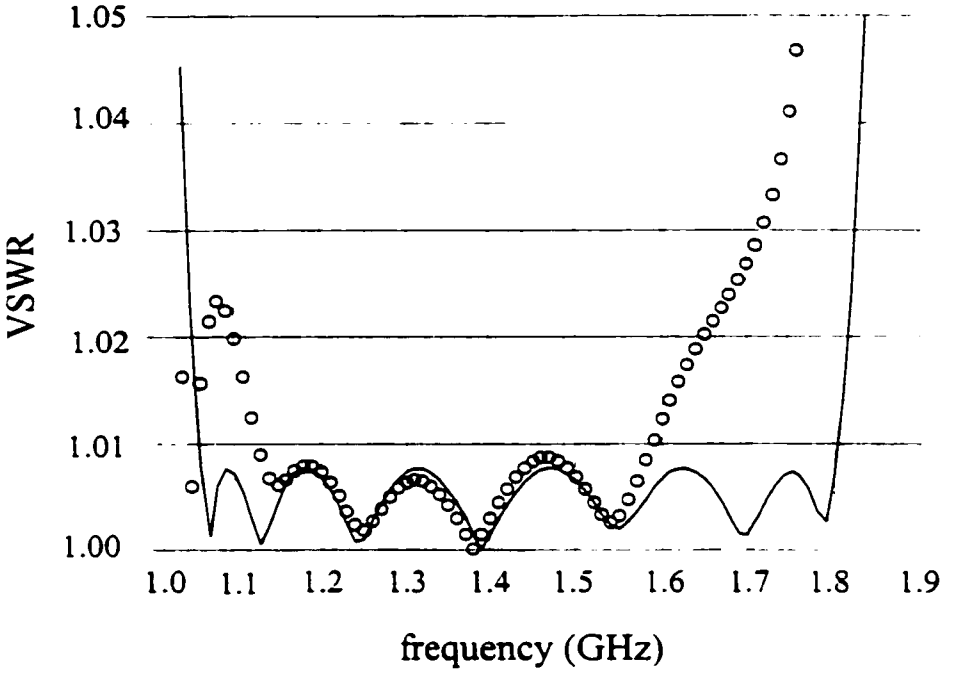

Fig. 3.22. The optimal ideal analytical model response (—) and the response of the nonideal analytical model (o) at the starting point for the seven-section waveguide transformer.

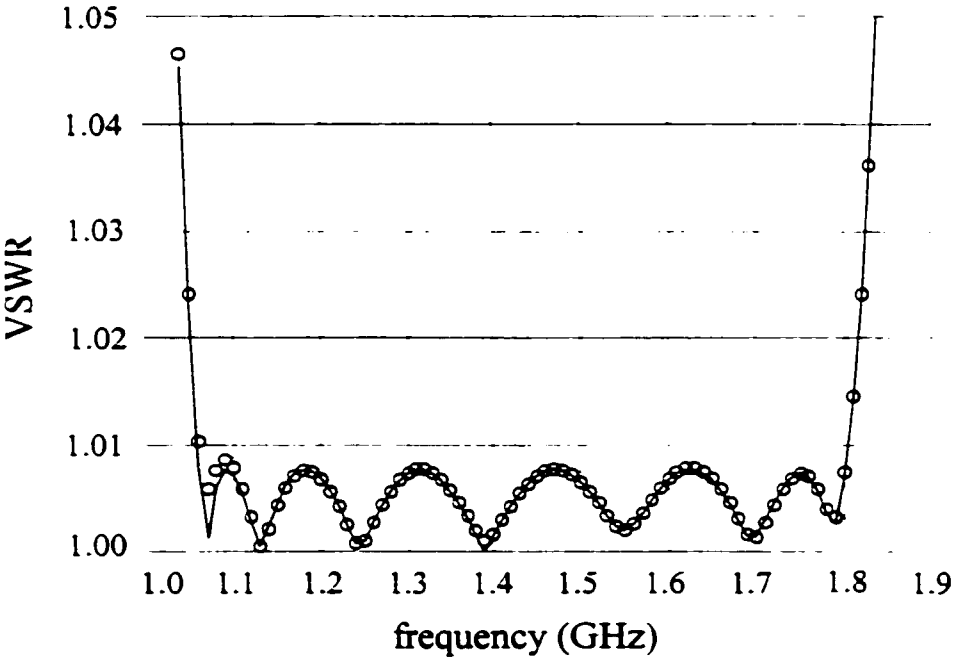

Fig. 3.23. The optimal response of the ideal analytical model (—) and the final response of the nonideal analytical model (o) for the seven-section waveguide transformer.

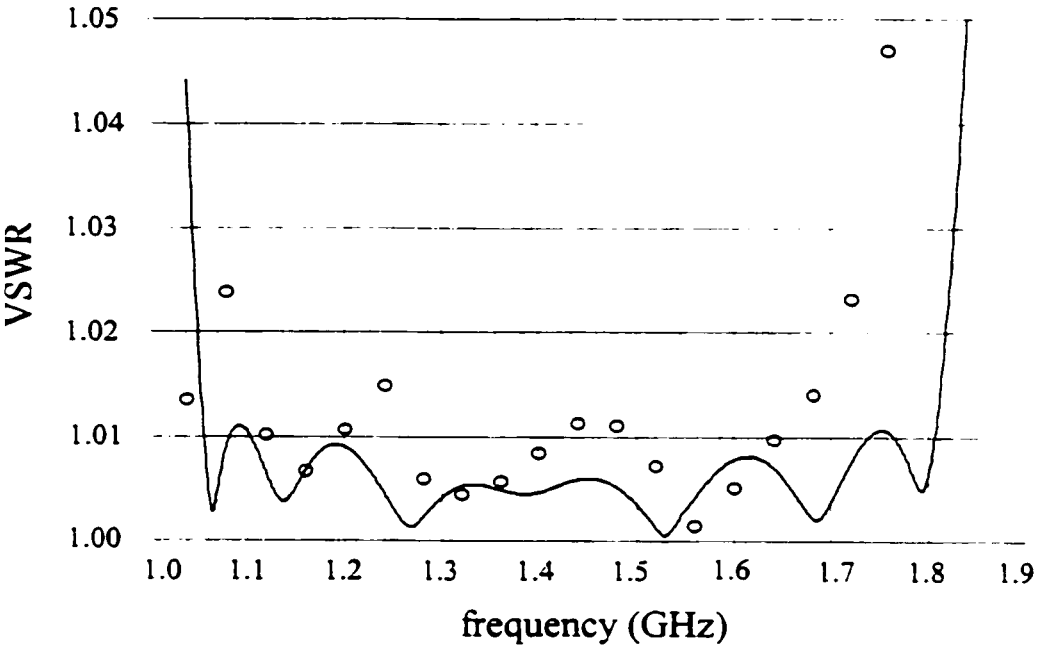

Fig. 3.24. The optimal response of the ideal analytical model (—) and the response of Maxwell Eminence (o) at the starting point for the seven-section waveguide transformer.

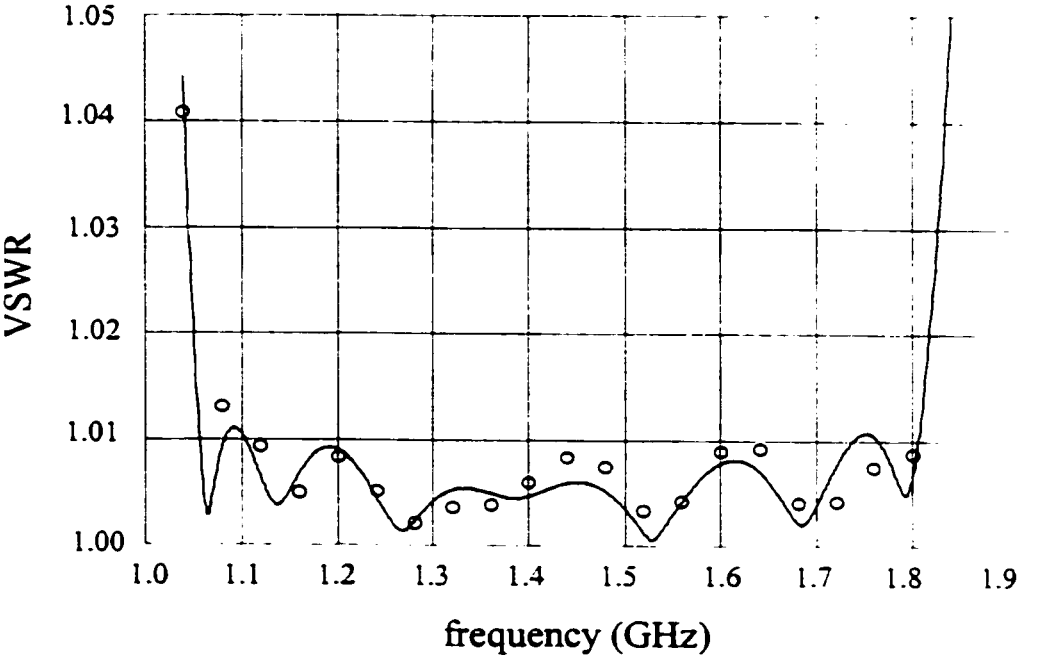

Fig. 3.25. The optimal response of the ideal analytical model (—) and the final Maxwell Eminence response (o) for the seven-section waveguide transformer.

3.4.4 A Three-section Waveguide Transformer with Rounded Corners [80]

In this example we considered the design of a three-section transformer with rounded corners. The designable parameters for this problem are the height and length of each waveguide section. The specifications are $|S_{11}| \leq$ -30 dB for a range of frequencies extending from 9.5 GHz to 15 GHz. The fine model of this circuit exploits HP HFSS ver. 5 [29]. The coarse model exploits an ideal empirical model that does not take into account the rounding of the corners. One quadrant of the transformer is shown in Fig. 3.26. We exploited the geometrical symmetry of the problem to reduce the required CPU time of HP HFSS.

Each time a new HP HFSS simulation is requested by the algorithm a new project is created using the new values for the length and height of each section. To facilitate this process, a MATLAB ver. 5 [81] program was developed that converts the values of the designable parameters into the corresponding HP HFSS drawing commands with the appropriate values. This approach accelerates the generation of new HP HFSS projects and eliminates the possibility of wrong dimensions.

The initial fine model response at the optimal coarse model design is shown in Fig. 3.27. Clearly, the specifications are slightly violated at this point. Only one iteration was needed to reach the final fine model design. The required number of HP HFSS simulations is seven. The first three of these simulations were needed to trust the parameter extraction at the first point. The other fine model points were needed to contract the size of the trust region to the termination size. The final HP HFSS fine model design is given in Table 3.11. The corresponding fine model response is shown in Fig. 3.28.

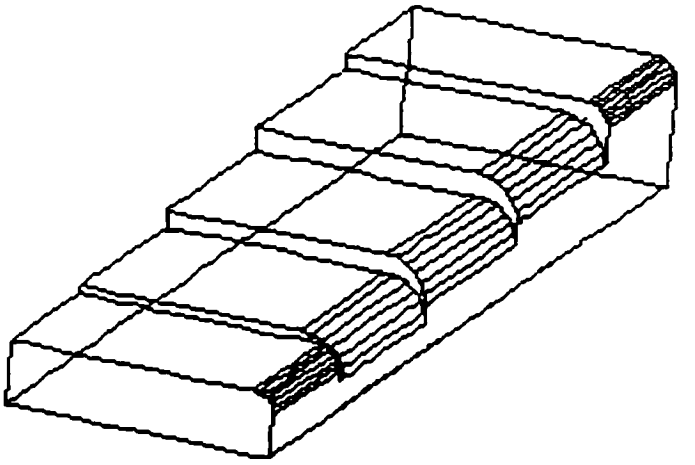

Fig. 3.26. The simulated part of the three-section waveguide transformer with rounded corners.

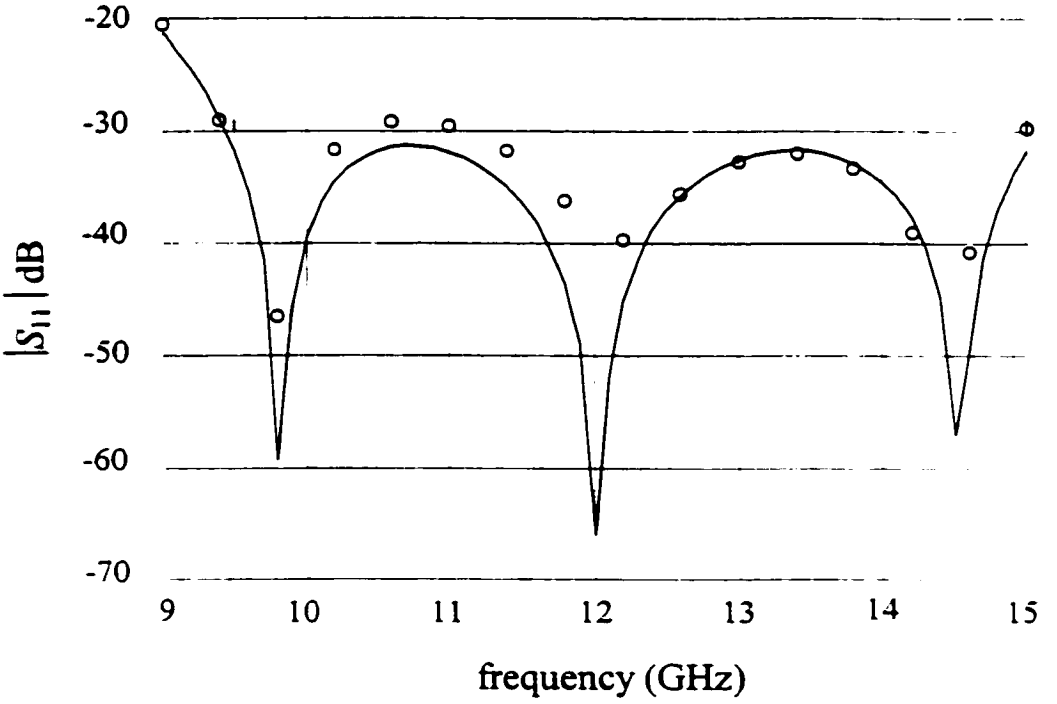

Fig. 3.27. The optimal response of the ideal analytical model (—) and the response of HP HFSS (o) at the starting point for the three-section waveguide transformer with rounded corners.

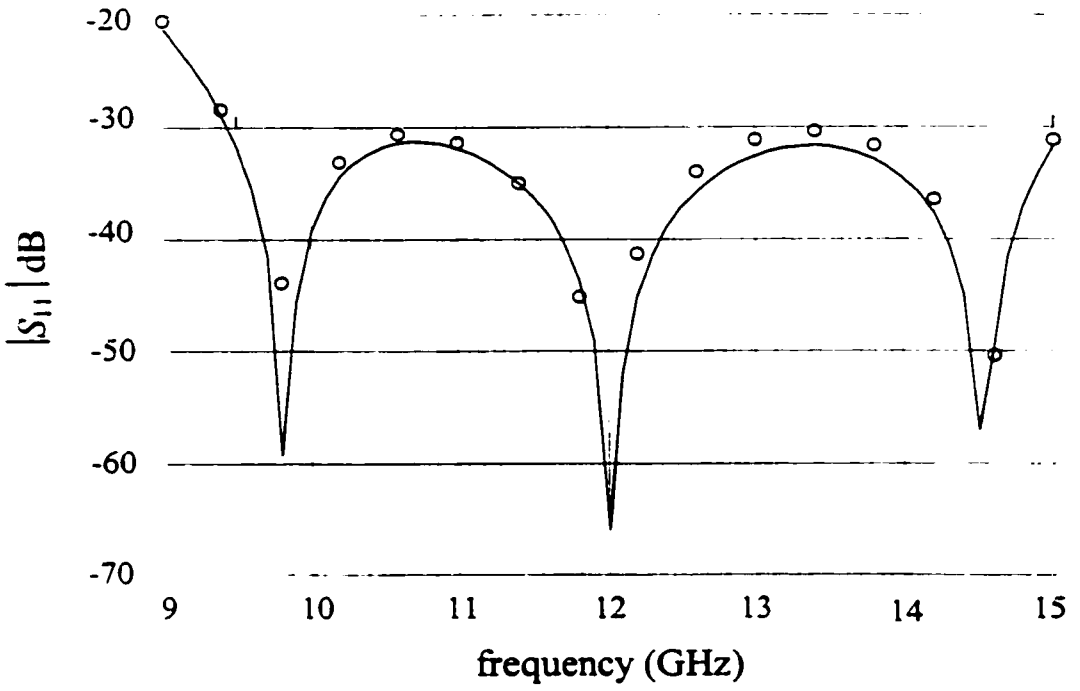

Fig. 3.28. The optimal response of the ideal analytical model (—) and the final HP HFSS response (o) for the three-section waveguide transformer with rounded corners.

TABLE 3.11
VALUES OF DESIGNABLE PARAMETERS AT EACH ITERATION FOR THE THREE-SECTION WAVEGUIDE TRANSFORMER WITH ROUND CORNERS USING HP HFSS AND AN IDEAL ANALYTICAL MODEL

Parameter	$x_f^{(0)}$	$x_f^{(1)}$
b_1	0.33276	0.32971
b_2	0.26551	0.26396
b_3	0.21186	0.20978
L_1	0.32556	0.33208
L_2	0.32640	0.32335
L_3	0.32556	0.32192
all values are in inch		

3.5. MONTE CARLO ANALYSIS USING SPACE MAPPING

The final matrix $\overline{\boldsymbol{B}}$ obtained by the TRASM algorithm represents the best available information about the mapping between the two spaces. A small perturbation of $\Delta \boldsymbol{x}_f$ in the fine model space is mapped to a perturbation of $\Delta \boldsymbol{x}_c$ in the coarse model space by

$$\Delta \boldsymbol{x}_c = \overline{\boldsymbol{B}} \Delta \boldsymbol{x}_f \tag{3.13}$$

The perturbations in the coarse model space and fine model space are with respect to $\boldsymbol{x}_c^*$ and $\overline{\boldsymbol{x}}_f$, respectively. The established mapping can be used to perform a space-mapped Monte Carlo analysis [31] for the problem under consideration. The random points generated in the fine model space are mapped to the coarse model space using (3.13). Coarse model simulations are then used instead of the CPU intensive fine model points. This statistical analysis should enjoy the speed of the coarse model and the accuracy of the fine model.

To demonstrate this approach we carried out a Monte Carlo analysis of the three-section waveguide transformer with rounded corners. The fine model parameters are assumed to be uniformly distributed with tolerances of 1%, 2% and 5%. The corresponding responses are shown in Figs. 3.29, 3.30 and 3.31. The estimated yields for these tolerances are 39%, 4% and 0%.

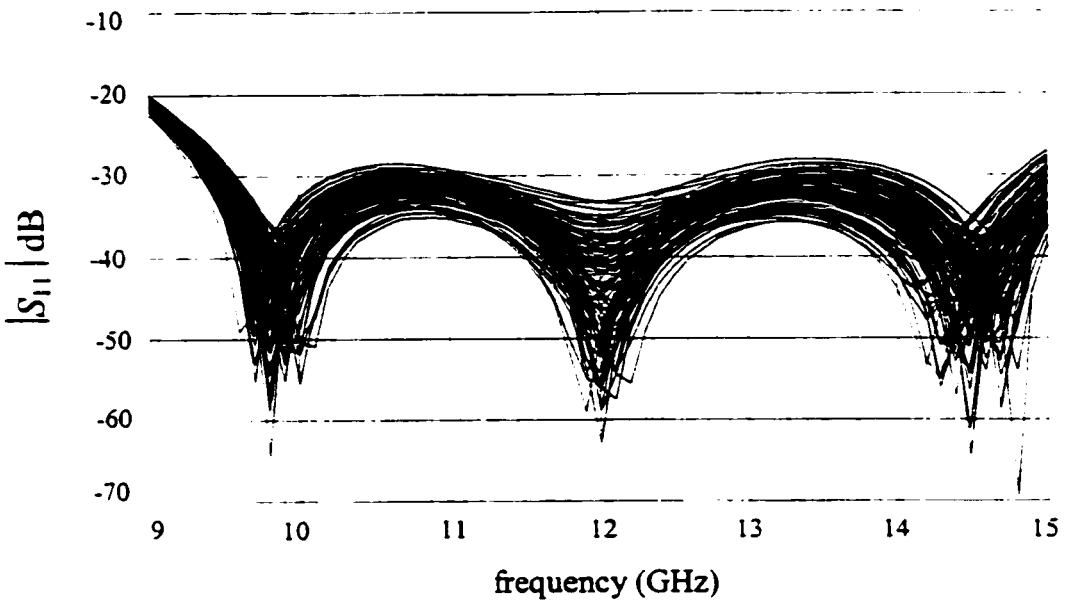

Fig. 3.29. Monte Carlo analysis for the three-section waveguide transformer with rounded corners assuming 1% uniformly distributed parameters.

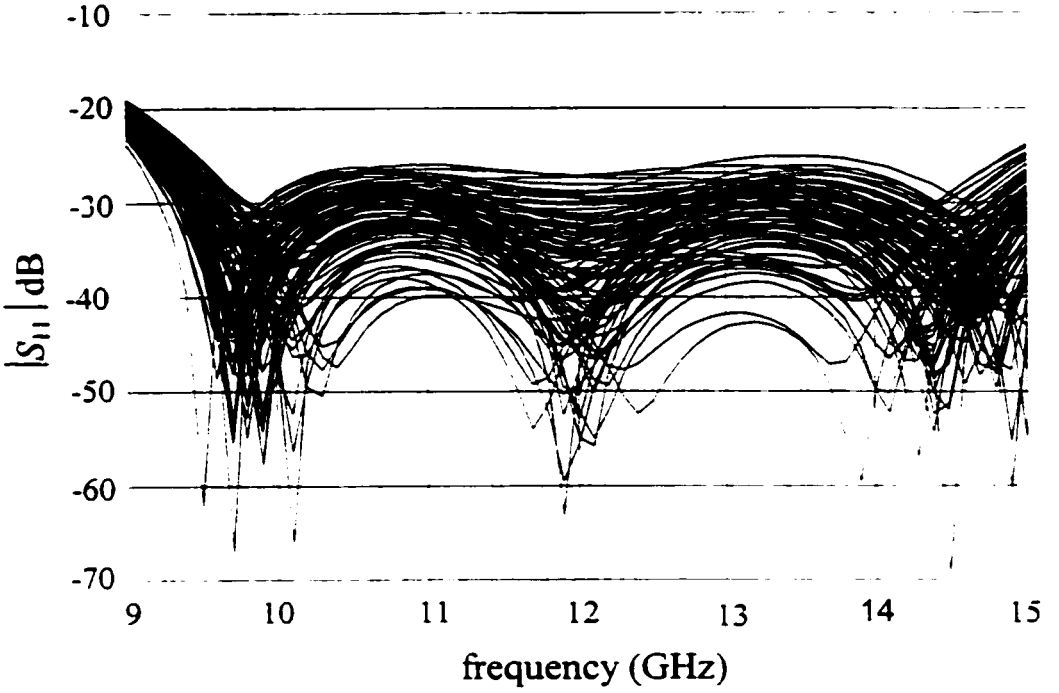

Fig. 3.30. Monte Carlo analysis for the three-section waveguide transformer with rounded corners assuming 2% uniformly distributed parameters.

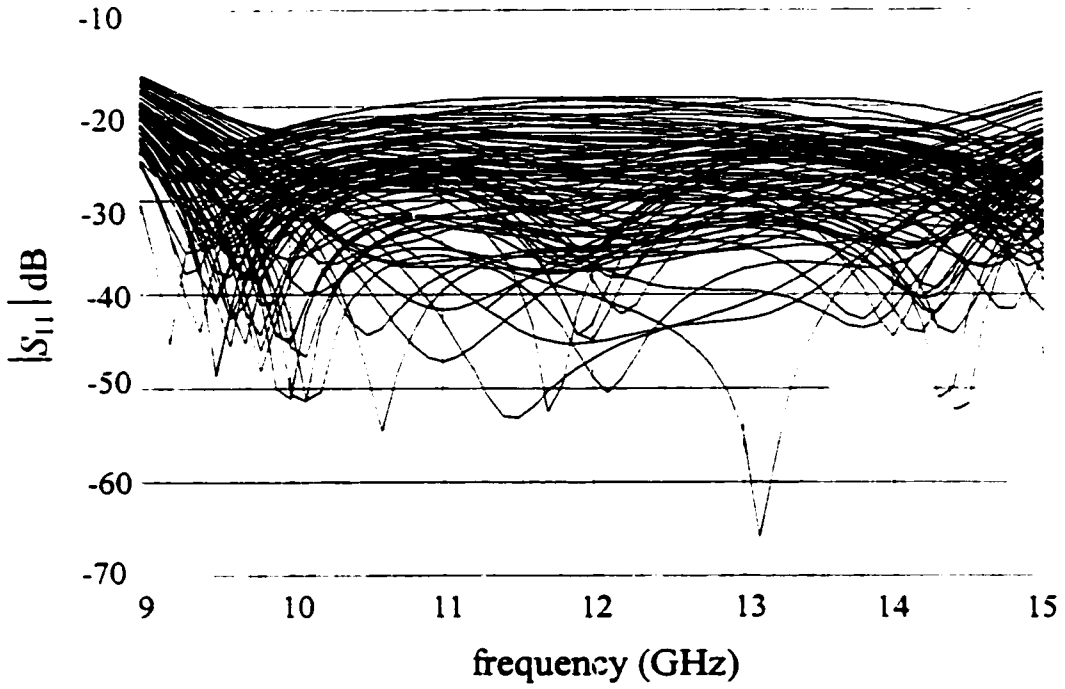

Fig. 3.31. Monte Carlo analysis for the three-section waveguide transformer with rounded corners assuming 5% uniformly distributed parameters.

3.6 CONCLUSIONS

In this Chapter, we reviewed the Trust Region Aggressive Space Mapping (TRASM) optimization algorithm. TRASM integrates a trust region methodology with the Aggressive Space Mapping (ASM) technique. It improves the uniqueness of the parameter extraction step, the most critical step in the space mapping process, and exploits all available fine model simulations. A Recursive Multi-Point parameter Extraction (RMPE) procedure is utilized by the algorithm. This procedure makes use of the available information about the mapping between the two spaces. TRASM is successfully illustrated through the design of a number of microwave circuits. The examples include the design of a High Temperature Superconducting (HTS) filter and the design of an Double Folded Stub (DFS) filter. Also, the design of a number of waveguide transformers was also considered. A space-mapped Monte Carlo analysis of a waveguide filter illustrates the statistical analysis applications of SM. We showed that the number of fine model simulations needed is of the order of problem dimensionality.

4

THE AGGRESSIVE PARAMETER EXTRACTION ALGORITHM

4.1 INTRODUCTION

In previous chapters we discussed three of the SM-based optimization algorithms. The importance of the Parameter Extraction (PE) step for SM optimization was illustrated. Usually, PE is formulated as an optimization problem. Optimization approaches to PE often yield nonunique solutions. We showed that this nonuniqueness may cause SM optimization to diverge or exhibit oscillatory behavior.

In this chapter, we discuss the PE extraction problem in more detail. We present an "aggressive" approach to parameter extraction. While generally applicable, the algorithm presented is discussed in the context of SM technology. We assume the existence of a fine model that generates the target response and a coarse model whose parameters are to be extracted.

Several authors have addressed nonuniqueness in parameter extraction. For example, Bandler *et. al.* [24] proposed the idea of making unknown perturbations to a certain system whose parameters are to be extracted. Later Bandler *et al.* [32] suggested that Multi-Point Extraction (MPE) be used to match the first-order derivatives of the two models to ensure a global minimum. The perturbations used in that approach are predefined and arbitrary. The optimality of the selection of those perturbations was not addressed. A Recursive Multi-Point Extraction (RMPE) procedure was presented in Chapter 3 in the context of the TRASM

algorithm [33]. This procedure employs a mapping between the two models to enhance uniqueness.

The algorithm presented in this chapter aims at minimizing the number of fine simulations used in the MPE process. This is done by utilizing perturbations that significantly improve the uniqueness in each iteration. Consequently, the algorithm is designated as an Aggressive Parameter Extraction (APE) algorithm. Each perturbation requires an additional fine model simulation which could be very CPU intensive. We classify the different solutions returned by the MPE process and, based on this classification, a new perturbation that is likely to sharpen the result is suggested.

4.2 THE PARAMETER EXTRACTION PROBLEM

The objective of parameter extraction is to find a set of parameters of a model whose response matches a given set of measurements. The Single Point Extraction (SPE) procedure is given by (2.18). Here, the coarse and fine models are matched using the response of a single point. The solution to this problem may be nonunique. SPE was illustrated by Fig. 2.3.

An MPE procedure [32] was suggested to improve the uniqueness of the step. The vector of extracted coarse model parameters x_c^e corresponding to a fine model point x_f is obtained by solving

$$x_c^e = arg\left\{ \min_{x_c} \left\| \begin{bmatrix} e_0^T & e_1^T & \cdots & e_{N_p}^T \end{bmatrix}^T \right\| \right\} \tag{4.1}$$

where

$$e_0 = R_c(x_c) - R_f(x_f) \tag{4.2}$$

and

$$\boldsymbol{e}_i = \boldsymbol{R}_c(\boldsymbol{x}_c + \Delta \boldsymbol{x}_c^{(i)}) - \boldsymbol{R}_f(\boldsymbol{x}_f + \Delta \boldsymbol{x}_f^{(i)}) \tag{4.3}$$

The set of perturbations in the coarse model space is represented by $\Delta \boldsymbol{x}_c^{(i)} \in V_p$, where i=1, 2, . . . , N_p and $|V_p| = N_p$. $\Delta \boldsymbol{x}_f^{(i)}$ is the corresponding perturbation in the fine model space. The perturbations $\Delta \boldsymbol{x}_c^{(i)}$ and $\Delta \boldsymbol{x}_f^{(i)}$ in this MPE procedure [32] are related by

$$\Delta \boldsymbol{x}_c^{(i)} = \Delta \boldsymbol{x}_f^{(i)} \tag{4.4}$$

It follows that its solution simultaneously matches the responses of a set of corresponding points in both spaces. The number of fine model points needed for this process is arbitrary. There is no clear way of how to select the set of perturbations. Also, the available information about the mapping between the two spaces was not utilized.

The RMPE procedure [36] suggested that the perturbations utilized in (4.1)-(4.3) should satisfy

$$\Delta \boldsymbol{x}_c^{(i)} = \boldsymbol{B} \Delta \boldsymbol{x}_f^{(i)} \tag{4.5}$$

The matrix $\boldsymbol{B}$ approximates the mapping between the two spaces. The TRASM algorithm generates the perturbations used for the RMPE process. These perturbations are not guaranteed to result in significant improvement in the uniqueness of the extracted parameters. A large number of additional fine model simulations may be needed to ensure the uniqueness of the step.

For both (4.4) and (4.5) the set V of fine model points utilized in MPE is

$$V = \{\boldsymbol{x}_f\} \cup \left\{ \boldsymbol{x}_f + \Delta \boldsymbol{x}_f^{(i)} \middle| \, \forall \, \Delta \boldsymbol{x}_c^{(i)} \in V_p \right\} \tag{4.6}$$

Fig. 4.1 illustrates the MPE procedure.

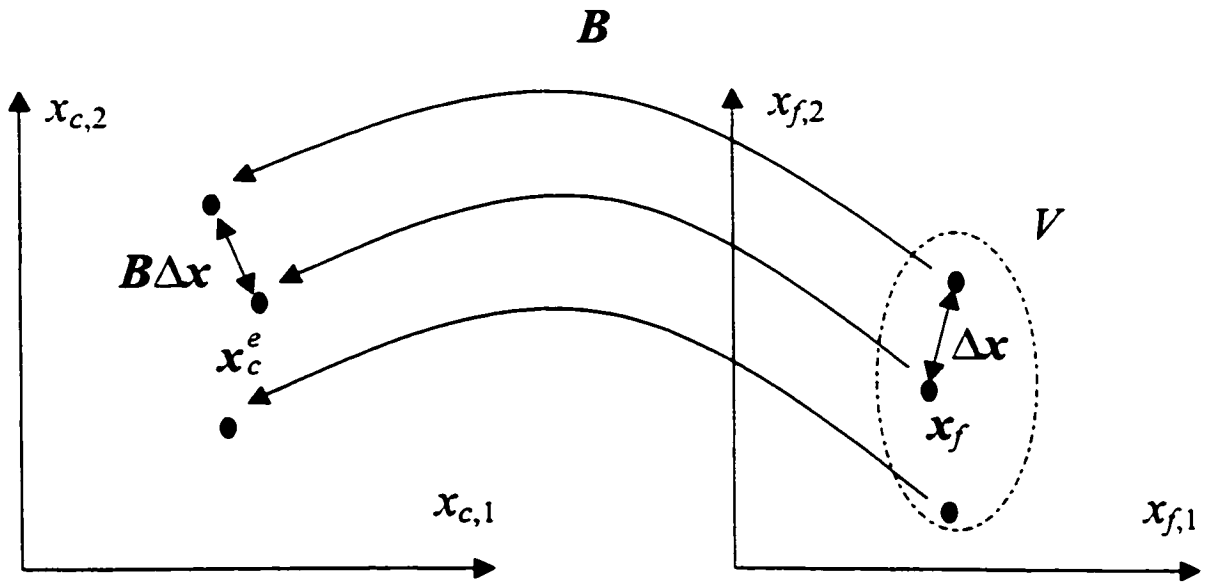

Fig. 4.1. Illustration of the MPE procedure.

4.3 THE SELECTION OF PERTURBATIONS

The vector of target coarse model responses $\boldsymbol{R}_T$ used to match the two models is given by

$$\boldsymbol{R}_T = \begin{bmatrix} \boldsymbol{R}_c(\boldsymbol{x}_c) \\ \boldsymbol{R}_c(\boldsymbol{x}_c + \Delta \boldsymbol{x}_c^{(1)}) \\ . \\ . \\ \boldsymbol{R}_c(\boldsymbol{x}_c + \Delta \boldsymbol{x}_c^{(N_p)}) \end{bmatrix} \tag{4.7}$$

The dimensionality of $\boldsymbol{R}_T$ is m_T, where $m_T=(N_p+1)m$ and m is the dimensionality of both $\boldsymbol{R}_c$ and $\boldsymbol{R}_f$. Vector $\boldsymbol{x}_c^e$ is labeled locally unique [58] if there exists an open neighborhood of $\boldsymbol{x}_c^e$ containing no other point $\boldsymbol{x}_c$ such that $\boldsymbol{R}_T(\boldsymbol{x}_c) = \boldsymbol{R}_T(\boldsymbol{x}_c^e)$. Otherwise, it is labeled locally nonunique. It was shown in [58] that local uniqueness is equivalent to the condition that the Jacobian of $\boldsymbol{R}_T$ has rank n where n is the number of parameters.

To achieve local uniqueness, it was suggested in the context of system identification [24] that increasing the number of perturbations enhances the possibility that the Jacobian matrix $\boldsymbol{J}_T$ of $\boldsymbol{R}_T$ becomes full rank. The perturbations suggested by Daijavad [24] were unidentified perturbations and thus result in an increase in the number of the optimizable parameters. However, it was pointed out that the improvement in the rank of $\boldsymbol{J}_T$ outweighs the increase in the number of parameters.

In a later work, the idea of using known perturbations to achieve global uniqueness of parameter extraction was introduced [32]. By global uniqueness we mean that there exists only one minimum $\boldsymbol{x}_c^e$ for the MPE problem. It was also pointed out in [32] that using MPE is equivalent to matching the first-order derivatives of the coarse and fine models.

We suggest two types of perturbation depending on whether the solution of the MPE is locally unique or locally nonunique. If the solution obtained is locally nonunique we choose a perturbation that is likely to make the new extracted parameters locally unique.

Assume that a locally nonunique minimum x_c^e is obtained using the current set of coarse model perturbations V_p. Here, the rank of the Jacobian $J_T(x_c^e)$ is ϑ where $\vartheta < n$. We suggest a perturbation Δx that attempts to increase the rank of the Jacobian of the responses corresponding to the augmented set $\{V_p \cup \Delta x\}$ at x_c^e by at least one. This is achieved by imposing the condition that the gradients of $n-\vartheta$ of the coarse model responses in the new response vector $R_c(x_c^e + \Delta x)$ be normal to a linearly independent set of gradients of cardinality ϑ of the responses in the vector R_T at the point x_c^e. We denote the set of linearly independent gradients by S where

$$S = \left\{ y^{(1)}, \ldots, y^{(\vartheta)} \right\} \tag{4.8}$$

We denote the set of the gradients of the newly selected $n-\vartheta$ responses in $R_c(x_c^e + \Delta x)$ by S_a, where

$$S_a = \left\{ y_a^{(\vartheta+1)}, \ldots, y_a^{n} \right\} \tag{4.9}$$

Each of these gradients is approximated by

$$y_a^{(i)} = y^{(i)} + G^{(i)} \Delta x, \qquad i = \vartheta+1, \ldots, n \tag{4.10}$$

where $y^{(i)}$ is the gradient of the ith response at the point x_c^e and $G^{(i)}$ is the corresponding Hessian. The imposed condition on the perturbation is that

$$y_a^{(i)T} y^{(j)} = 0 \quad \forall\, y^{(j)} \in S \text{ and } \forall\, y_a^{(i)} \in S_a \tag{4.11}$$

Using (4.10) and (4.11), the perturbation Δx is obtained by solving the system of linear equations

$$Z^T \Delta x = -c_y \tag{4.12}$$

where the matrix Z is given by

$$Z=[\, G^{(\vartheta-1)} y^{(1)} \ldots G^{(n)} y^{(1)} \ldots G^{(n)} y^{(\vartheta)} \,] \tag{4.13}$$

and the vector c_y is given by

$$c_y = \begin{bmatrix} y^{(\vartheta-1)T} y^{(1)} \\ \vdots \\ y^{(n)T} y^{(1)} \\ \vdots \\ y^{(n)T} y^{(\vartheta)} \end{bmatrix} \tag{4.14}$$

It should be noted that the system of linear equations (4.12) may be an over-determined, under-determined or well-determined system of equations depending on ϑ and n. The pseudoinverse of the matrix Z^T obtains the solution with minimum ℓ_2 norm in all cases. The fact that this solution is a minimum length solution is of importance since (4.12) is based on a linear approximation of the gradients which can only be trusted within a certain trust region. If the perturbation Δx is outside this trust region, it is rescaled.

If the minimum obtained by the MPE is locally unique we still have to ensure that this is the true solution to the extraction problem. The following lemma leads to a robust way to weaken any other existing locally unique minimum.

Lemma

Assume that there exist two locally unique minima $x_c^{\epsilon,1}$ and $x_c^{\epsilon,2}$ for the MPE problem obtained using least squares optimization and a set of perturbations V_p. A possible perturbation Δx that can be added to the set V_p and can be used to weaken one of these minima as a solution for the MPE is in the direction of an eigenvector for the matrix $H_1 - H_2$ where H_1 and H_2 are the Hessian matrices for the ℓ_2 objective function at the points $x_c^{\epsilon,1}$ and $x_c^{\epsilon,2}$, respectively.

Proof

We denote by $Q(\boldsymbol{x},V)$ the value of the ℓ_2 objective function of the MPE problem at a coarse model point $\boldsymbol{x}$ using a set of fine model points V, where V is given by (4.6). The quadratic approximations of $Q(\boldsymbol{x},V)$ in a neighborhood centered at the two locally unique minima $\boldsymbol{x}_c^{\epsilon,1}$ and $\boldsymbol{x}_c^{\epsilon,2}$, respectively are given by

$$q_1(\Delta\boldsymbol{x},V) = Q(\boldsymbol{x}_c^{\epsilon,1},V) + 0.5\,\Delta\boldsymbol{x}^T \boldsymbol{H}_1\,\Delta\boldsymbol{x} \tag{4.15}$$

$$q_2(\Delta\boldsymbol{x},V) = Q(\boldsymbol{x}_c^{\epsilon,2},V) + 0.5\,\Delta\boldsymbol{x}^T \boldsymbol{H}_2\,\Delta\boldsymbol{x} \tag{4.16}$$

The perturbation $\Delta\boldsymbol{x}$ that results in the maximum difference between the two quadratic models (4.15) and (4.16) for a specific trust region δ is obtained by formulating the Lagrangian

$$L(\boldsymbol{x},\lambda) = (Q(\boldsymbol{x}_c^{\epsilon,2},V) - Q(\boldsymbol{x}_c^{\epsilon,1},V)) + 0.5\,\Delta\boldsymbol{x}^T(\boldsymbol{H}_2 - \boldsymbol{H}_1)\Delta\boldsymbol{x} + \theta(\Delta\boldsymbol{x}^T\Delta\boldsymbol{x} - \delta^2) \tag{4.17}$$

Taking the derivative with respect to $\Delta\boldsymbol{x}$ gives

$$(\boldsymbol{H}_1 - \boldsymbol{H}_2)\Delta\boldsymbol{x} = 2\theta\Delta\boldsymbol{x} \tag{4.18}$$

It follows that $\Delta\boldsymbol{x}$ is an eigenvector of the matrix $\boldsymbol{H}_1 - \boldsymbol{H}_2$. $\Delta\boldsymbol{x}$ provides a direction that maximizes the difference between the quadratic models. In other words, it provides a perturbation that maximizes the contrast between the changes of the coarse model responses at these two minima. It follows that the true minimum is the one whose response changes match better the changes of the fine model responses obtained using the perturbation $\Delta\boldsymbol{x}$.

A similar result to (4.18) can be obtained using a different approach. A perturbation $\Delta\boldsymbol{x}$ results in a perturbation of the coarse model responses at the two minima by

$$\Delta\boldsymbol{R}_1 = \boldsymbol{J}_c(\boldsymbol{x}_c^{\epsilon,1})\Delta\boldsymbol{x} \tag{4.19}$$

and

$$\Delta\boldsymbol{R}_2 = \boldsymbol{J}_c(\boldsymbol{x}_c^{\epsilon,2})\Delta\boldsymbol{x} \tag{4.20}$$

Where $J_c(x_c)$ is the Jacobian of the coarse model response R_c. We impose the condition that the difference between the ℓ_2 norms of these two response perturbations be maximized subject to certain trust region size. Therefore, the following Lagrangian can be formed

$$L(\Delta x, \lambda) = \Delta x^T J_c(x_c^{c,1})^T J_c(x_c^{c,1})\Delta x - \Delta x^T J_c(x_c^{c,2})^T J_c(x_c^{c,2})\Delta x + \theta(\Delta x^T \Delta x - \delta^2) \quad (4.21)$$

Using a similar approach to that used in deriving (4.18) it can be shown that the perturbation Δx is obtained by solving the eigenvalue problem

$$(J_c(x_c^{c,1})^T J_c(x_c^{c,1}) - J_c(x_c^{c,2})^T J_c(x_c^{c,2}))\Delta x = \theta \Delta x \quad (4.22)$$

The two perturbations (4.18) and (4.22) can be shown to be almost identical by writing the Hessian matrix of $Q(x,V)$ in terms of the Jacobian of the coarse model responses [82]. However, the perturbation calculated in (4.22) is more computionally efficient than that of (4.18).

There is one substantial difficulty in the exact evaluation of the perturbation given by (4.22). Once a locally unique minimum is reached the Hessian of Q at this point can be obtained while no information is available about the Hessian at the other locally unique minima that may exist. In such a case, a reasonable assumption is to take $H_2=I$, the identity matrix or alternatively take $J_c(x_c^{c,2})^T J_c(x_c^{c,2})$ as the identity matrix in (4.22). This assumption implies that no information is available about the curvature of the objective function at the other minima. It follows that Δx is an eigenvector of the matrix $J_c(x_c^{c,1})^T J_c(x_c^{c,1})$.

The perturbation given by (4.22) is a suggested perturbation in the coarse model space. The new fine model point that should be added to the set V is $x_f + \Delta x_f$ where Δx_f is obtained by solving the system of linear equations

$$\Delta x = B \Delta x_f \quad (4.23)$$

The relation (4.23) is used if some information is available about the mapping between the two spaces. However, in most cases we make the assumption that $\boldsymbol{B}=\boldsymbol{I}$.

The scheme that we utilized for the selection of points in (4.22) is as follows. First, the eigenvalue problem is solved. The eigenvector $\boldsymbol{v}^{(1)}$ with the largest eigenvalue in modulus is initially selected as the candidate eigenvector. The suggested perturbation in this case is

$$\Delta \boldsymbol{x}_c = \frac{\delta}{\left\|\boldsymbol{v}^{(1)}\right\|}\boldsymbol{v}^{(1)} \tag{4.24}$$

where δ is the current size of the trust region. This perturbation is tested to see whether it belongs to the current set of perturbations. It follows that $\Delta \boldsymbol{x}_c$ is rejected if the condition

$$\frac{\Delta \boldsymbol{x}_c^T \Delta \boldsymbol{x}_c^{(i)}}{\left\|\Delta \boldsymbol{x}_c\right\|^2} > (1-\varepsilon) \tag{4.25}$$

is satisfied for a perturbation $\Delta \boldsymbol{x}_c^{(i)} \in V_p$, where $\varepsilon > 0$ is a small number. In this case the alternative perturbation

$$\Delta \boldsymbol{x}_c = \frac{-\delta}{\left\|\boldsymbol{v}^{(1)}\right\|}\boldsymbol{v}^{(1)} \tag{4.26}$$

is tested against the condition (4.25). If it also fails, we switch to the eigenvector with second largest eigenvalue in modulus and repeat steps (4.24) – (4.26). This is repeated until either a perturbation is found such that condition (4.25) is not satisfied or all the eigenvectors are exhausted for perturbations of length δ. In this case the trust region size δ is scaled by π_s, where $\pi_s > 1.0$. The perturbation is then taken in the direction of eigenvector with largest eigenvalue in modulus.

4.4 THE APE ALGORITHM

In this section we present the APE algorithm for the MPE process. This algorithm is based on the two methods discussed in the previous section. It is given by the following steps.

Step 0 Given $\boldsymbol{x}_f$, δ and n. Initialize $V^{(1)} = \{\boldsymbol{x}_f^{(1)}\}$, where $\boldsymbol{x}_f^{(1)} = \boldsymbol{x}_f$ and set i=1.

Comment The set $V^{(i)}$ contains the points used for the MPE in the ith iteration. The index i is equal to $|V^{(i)}|$, the cardinality of $V^{(i)}$.

Step 1 Apply MPE using the set $V^{(i)}$ to get $\boldsymbol{x}_c^{e(i)}$.

Comment The point $\boldsymbol{x}_c^{e(i)}$ is the solution to the MPE problem obtained using the set $V^{(i)}$.

Step 2 If $\boldsymbol{J}_T(\boldsymbol{x}_c^{e(i)})$ has full rank, go to Step 4.

Step 3 Obtain a new perturbation $\Delta\boldsymbol{x}$ using (4.12), use (4.23) to get $\Delta\boldsymbol{x}_f$ and let $V^{(i+1)} = V^{(i)} \cup \{\boldsymbol{x}_f^{(i+1)}\}$, where $\boldsymbol{x}_f^{(i+1)} = \boldsymbol{x}_f + \Delta\boldsymbol{x}_f$. Set i=i+1 and go to Step 1.

Comment The perturbation $\Delta\boldsymbol{x}$ is rescaled to satisfy the trust region condition $\|\Delta\boldsymbol{x}\| = \delta$.

Step 4 If $|V^{(i)}|$ is equal to one, go to Step 6.

Step 5 If $\|\boldsymbol{x}_c^{e(i)} - \boldsymbol{x}_c^{e(i-1)}\| \le \varepsilon$, stop.

Step 6 Obtain a new perturbation $\Delta\boldsymbol{x}$ using (4.22) and use (4.23) to get $\Delta\boldsymbol{x}_f$. Update δ and let $V^{(i+1)} = V^{(i)} \cup \{\boldsymbol{x}_f^{(i+1)}\}$, where $\boldsymbol{x}_f^{(i+1)} = \boldsymbol{x}_f + \Delta\boldsymbol{x}_f$. Set i=i+1 and go to Step 1.

Comment In Step 6 the eigenvalue problem is solved and the perturbation $\Delta\boldsymbol{x}$ is selected according to the scheme discussed in the previous section. This scheme may result in updating the trust region size. The algorithm terminates if the vector of extracted coarse model parameters obtained using i fine model points is close enough in terms

of some norm to the vector of extracted parameters obtained using $i-1$ fine model points.

Fig. 4.2 illustrates the relationship between the generated sets $V^{(i)}$, the fine model points $x_f^{(i)}$ and the extracted coarse model points $x_c^{e(i)}$. A flowchart of the APE algorithm is shown in Fig. 4.3.

4.5 EXAMPLES

4.5.1 The Rosenbrock Function

The first example utilizes the famous Rosenbrock function [82]. The coarse model for this problem is given by

$$R_c = 100(u_2 - u_1^2)^2 + (1-u_1)^2 \tag{4.27}$$

The fine model is another "Rosenbrock" function but with a shift applied to the parameters

$$R_f = 100((u_2+0.2) - (u_1-0.2)^2)^2 + (1-(u_1-0.2))^2 \tag{4.28}$$

It is required to extract the coarse model parameters corresponding to the fine model point $[1.0 \quad 1.0]^T$. The result of the SPE at this point is $x_c^{e(1)} = [1.21541 \quad 0.91728]^T$. The contours of $Q(x, V^{(1)})$ are shown in Fig. 4.4. It is clear from the contour plot that the minimum obtained is a locally nonunique minimum. The algorithm detects this and generates a perturbation that attempts to improve the rank of the Jacobian of R_T in the Double Point Extraction (DPE) using (4.12). Utilizing a trust region size of 0.25 the set $V^{(2)}$ is given by

$$V^{(2)} = \left\{ [1.0 \quad 1.0]^T, [0.7643 \quad 1.0833]^T \right\} \tag{4.29}$$

The contours of $Q(x, V^{(2)})$ are shown in Fig. 4.5. It is clear that by using only one additional fine model simulation the uniqueness of the problem has improved dramatically. Actually, the only

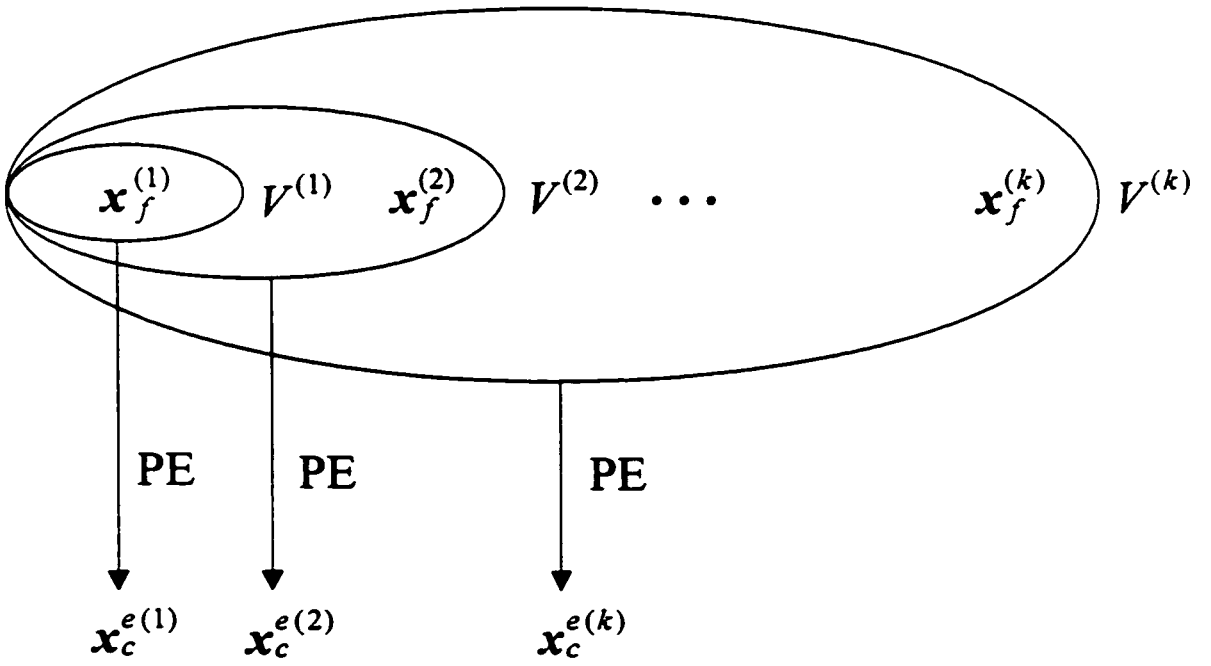

Fig. 4.2. Illustration of the relationship between the generated sets $V^{(i)}$, the fine model points $x_f^{(i)}$ and the extracted coarse model points $x_c^{e(i)}$ generated by the APE algorithm.

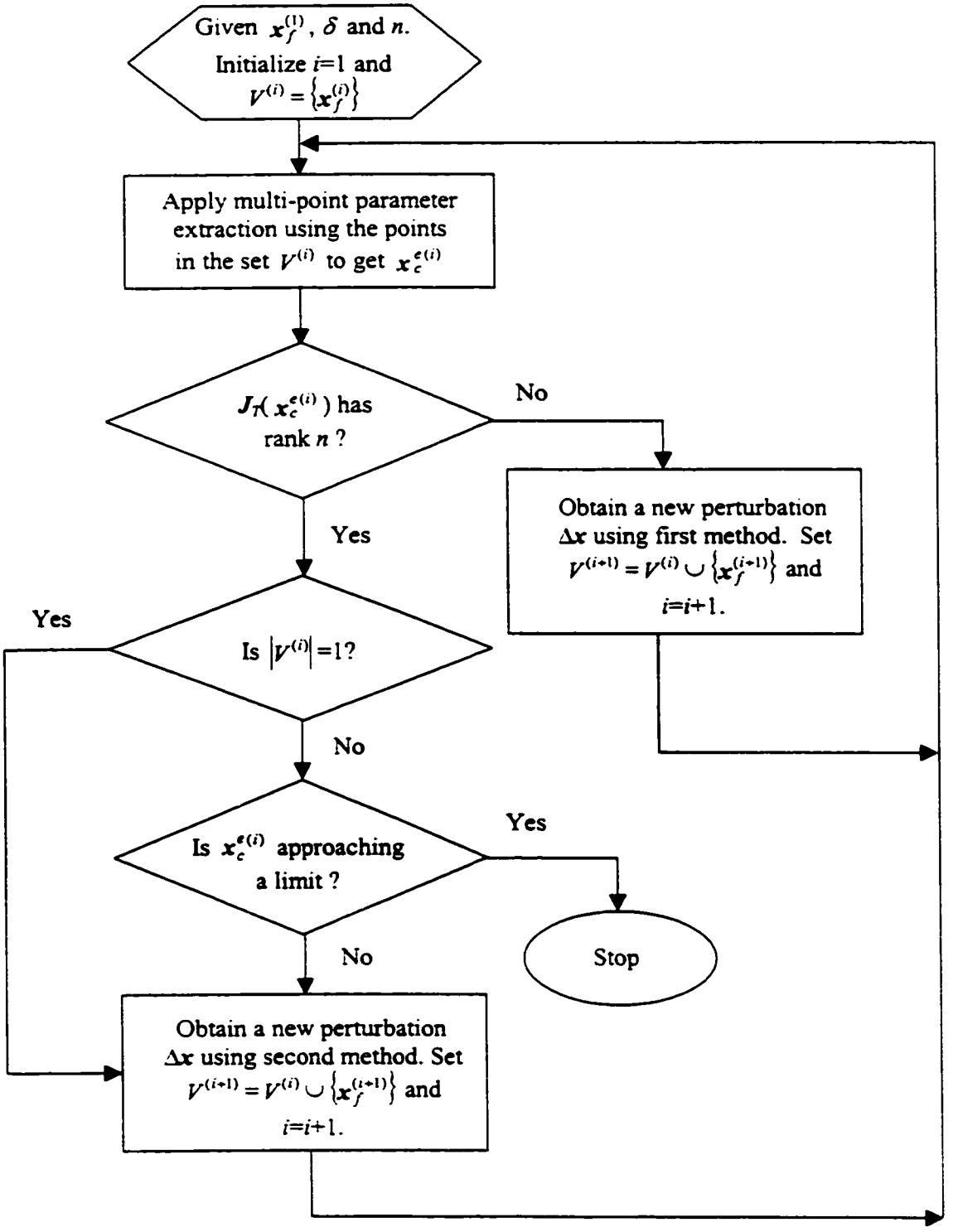

Fig. 4.3. A flowchart of the APE algorithm.

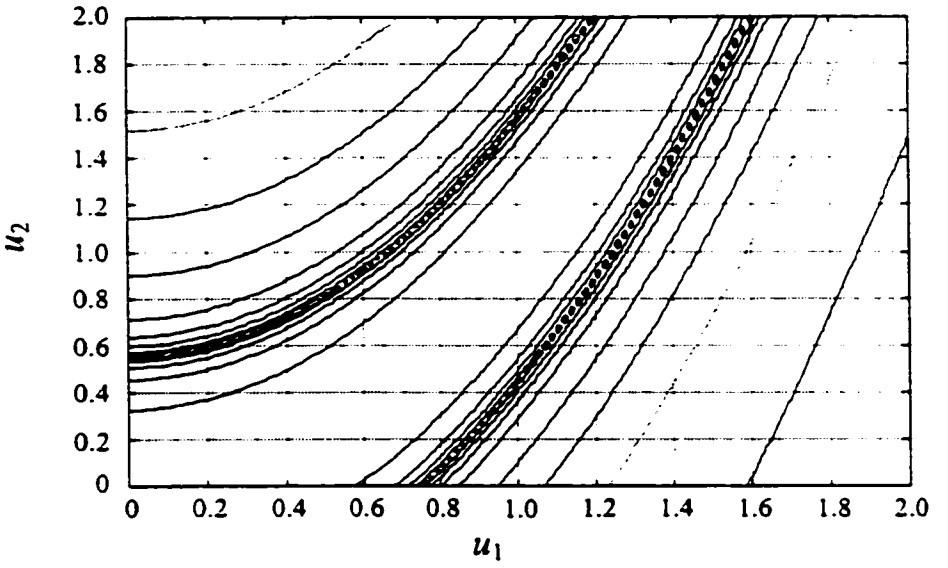

Fig. 4.4. The contours of $Q(\boldsymbol{x}, V^{(1)})$ for the Rosenbrock function.

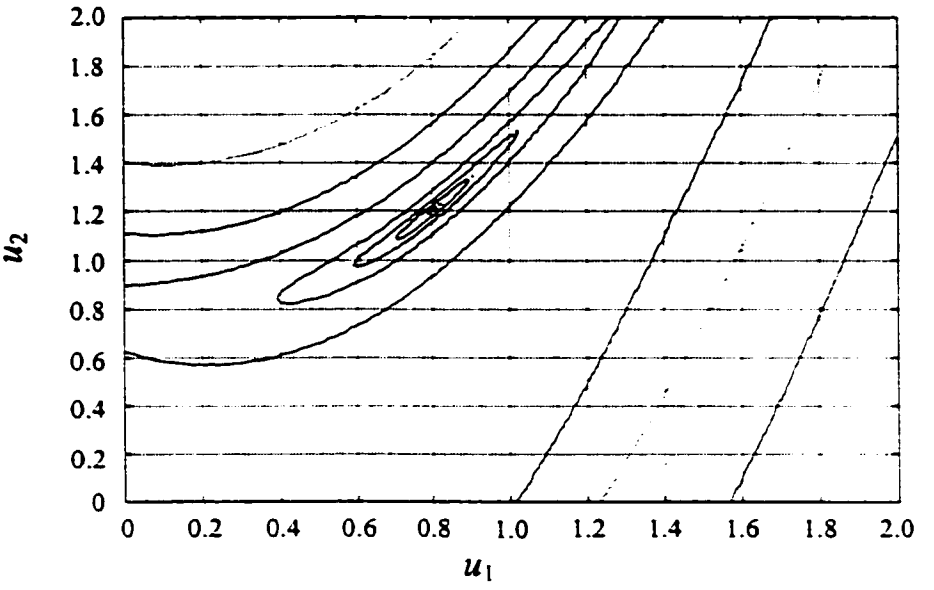

Fig. 4.5. The contours of $Q(\boldsymbol{x}, V^{(2)})$ for the Rosenbrock function.

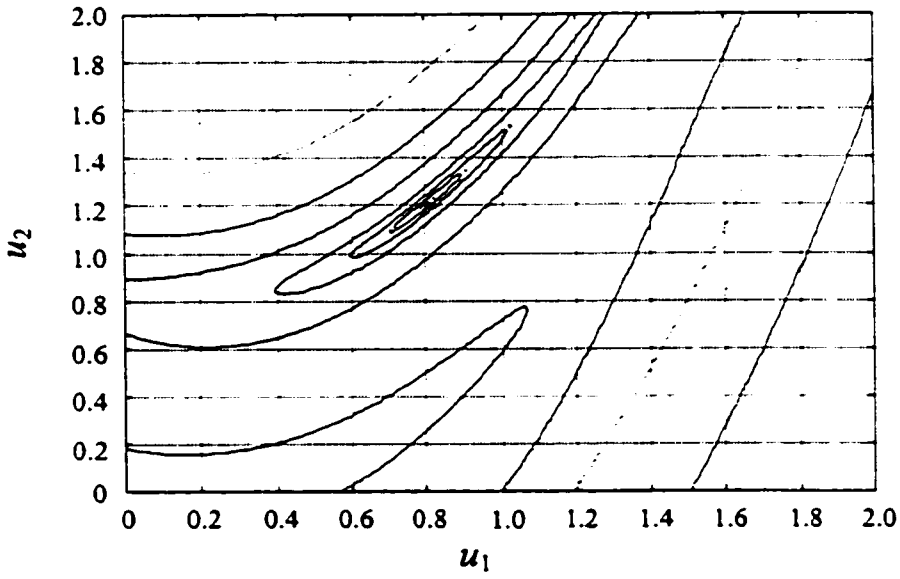

Fig. 4.6. The contours of $Q(x, V^{(3)})$ for the Rosenbrock function.

existing minimum is a global unique minimum. To ensure uniqueness a third point is generated by solving the eigenvalue problem (4.22). Thus we have

$$V^{(3)} = \left\{ [1.0 \quad 1.0]^T, [0.7643 \quad 1.0833]^T, [0.8185 \quad 0.8281]^T \right\} \tag{4.30}$$

The contours of $Q(x, V^{(3)})$ are shown in Fig. 4.6. The algorithm then terminates as it detects that the extracted parameters are approaching a limit. It returns the last set of extracted parameters as the solution for the MPE problem. The variation of the extracted parameters obtained using the ℓ_2 optimizer with the number of fine model points used is shown in Table 4.1.

4.5.2 A 10:1 Impedance Transformer

The second example is the well-known 10:1 impedance transformer [83]. The parameters for this problem are the characteristic impedance of the two transmission lines Z_1 and Z_2 while the two lengths of the transmission lines are kept fixed at their optimal values (quarter wave length). The coarse model utilizes nonscaled parameters while a "fine" model scales each of the two impedances by a factor of 1.6.

It is required in this synthetic problem to extract the coarse model parameters whose response matches the fine model response at the point $[2.2628 \quad 4.5259]^T$. This point is the optimal coarse model design according to the specifications in [83]. The two models are matched using the reflection coefficients at eleven equally spaced frequencies in the frequency range 0.5 GHz $\leq \omega \leq$ 1.5 GHz. The fine model response at $x_f^{(1)}$ and the coarse model response at the point $x_c^{e(1)}$ are shown in Fig. 4.7. The contours of $Q(x, V^{(1)})$ are shown in Fig. 4.8. It is clear from this figure that there exist three locally unique minima for the extraction problem. The algorithm then generates a second perturbation using (4.22). The set $V^{(2)}$ is given by

TABLE 4.1
THE VARIATION OF THE EXTRACTED PARAMETERS FOR THE ROSENBROCK FUNCTION WITH THE NUMBER OF POINTS USED FOR EXTRACTION

Parameter	$x_c^{e(1)}$	$x_c^{e(2)}$	$x_c^{e(3)}$
u_1	1.21541	0.80008	0.80008
u_2	0.91728	1.20012	1.20014

TABLE 4.2
THE VARIATION OF THE EXTRACTED PARAMETERS FOR THE 10:1 IMPEDANCE TRANSFORMER WITH THE NUMBER OF POINTS USED FOR EXTRACTION

Parameter	$x_c^{e(1)}$	$x_c^{e(2)}$	$x_c^{e(3)}$
Z_1	3.62043	3.47160	3.60357
Z_2	7.24147	7.43214	7.35052

$$V^{(2)} = \left\{ [2.26277 \quad 4.52592]^T, [1.49975 \quad 4.76634]^T \right\} \tag{4.31}$$

The fine model response for every point in $V^{(2)}$ and the coarse response at the corresponding extracted coarse model point are shown in Fig. 4.9. The corresponding contours of $Q(x, V^{(2)})$ are shown in Fig. 4.10. It is clear that there still exist two locally unique minima. Using (4.22) we have

$$V^{(3)} = \left\{ [2.26277 \quad 4.52592]^T, [1.49975 \quad 4.76634]^T, [3.02024 \quad 4.26855]^T \right\} \tag{4.32}$$

The fine model response for each point in the set $V^{(3)}$ and the coarse model response at the corresponding extracted coarse model point are shown in Fig. 4.11. The contours of $Q(x, V^{(3)})$ are shown in Fig. 4.12. The algorithm terminates as the termination condition is satisfied. The variation of the extracted coarse model point with $|V^{(i)}|$ is given in Table 4.2.

4.5.3 The HTS Filter

The fine model for the HTS filter is simulated as a whole using Sonnet's ***em***. The "coarse" model is a decomposed Sonnet version of the fine model (see Fig. 4.13). This model exploits a coarser grid than that used for the fine model. The physical parameters of the coarse and fine models are given in Table 4.3.

It is required to extract the coarse model parameters corresponding to the fine model parameters given in Table 4.4. The values in this table are the optimal coarse model design obtained using the minimax optimizer in OSA90/hope according to specifications given in [78]. We utilize the responses at 15 discrete frequencies in the range [3.967 GHz, 4.099 GHz] in the parameter extraction process.

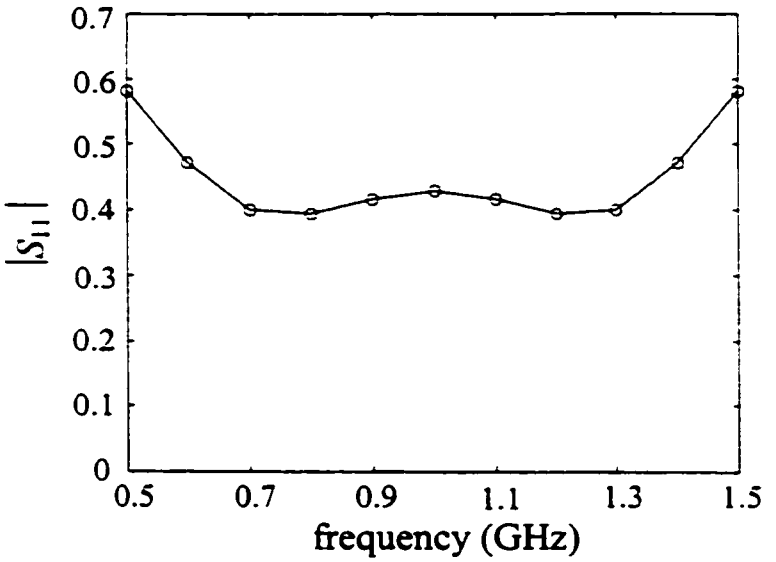

Fig. 4.7. The responses of the given fine model point (o) and the coarse model response (–) at the point $x_c^{(1)}$ for the 10:1 impedance transformer.

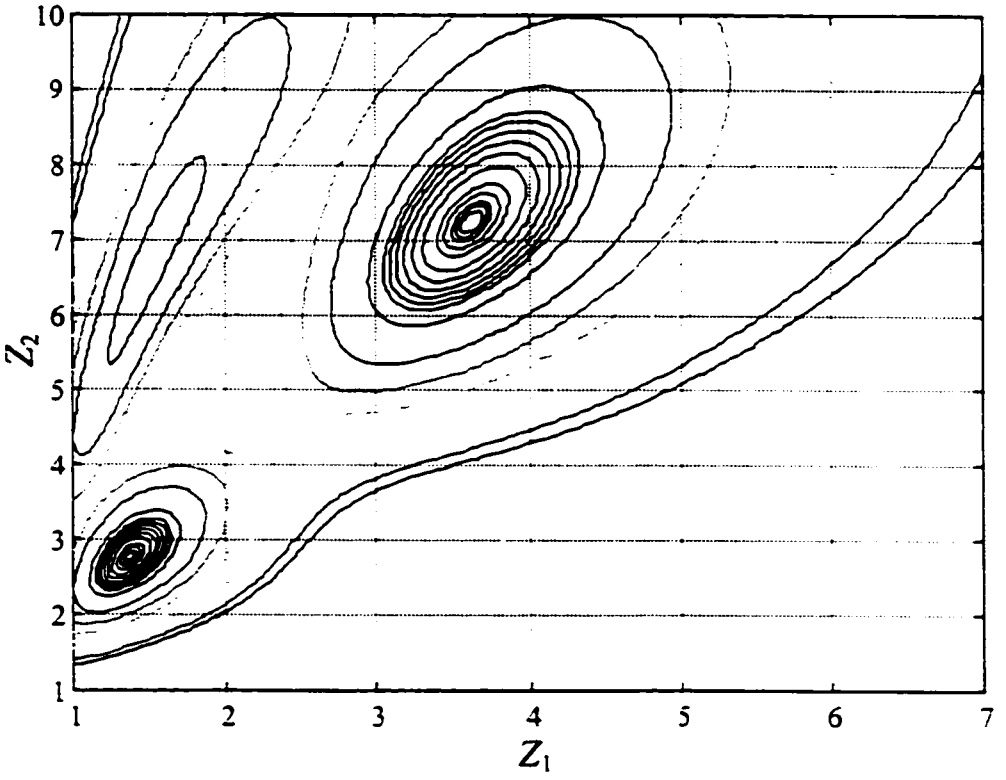

Fig. 4.8. The contours of $Q(x, V^{(1)})$ for the 10:1 impedance transformer.

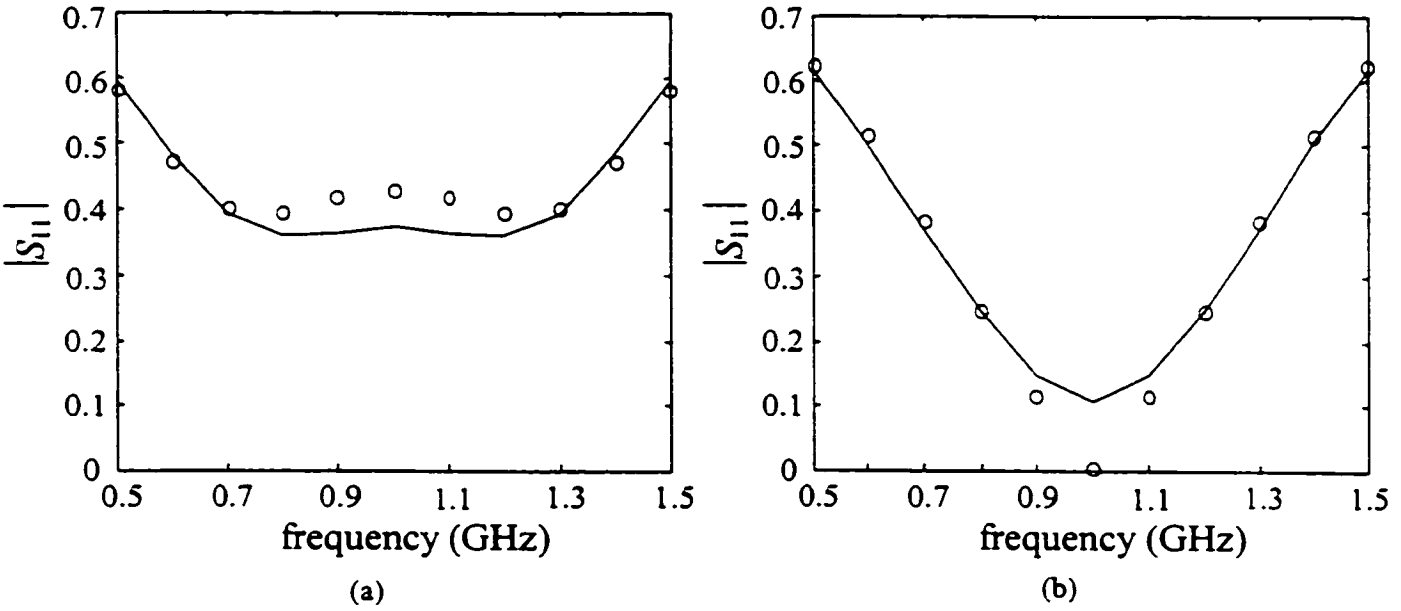

Fig. 4.9. The fine model response (o) and the corresponding coarse model response (–); (a) at the first point and (b) at the second point utilized in the DPE for the 10:1 impedance transformer.

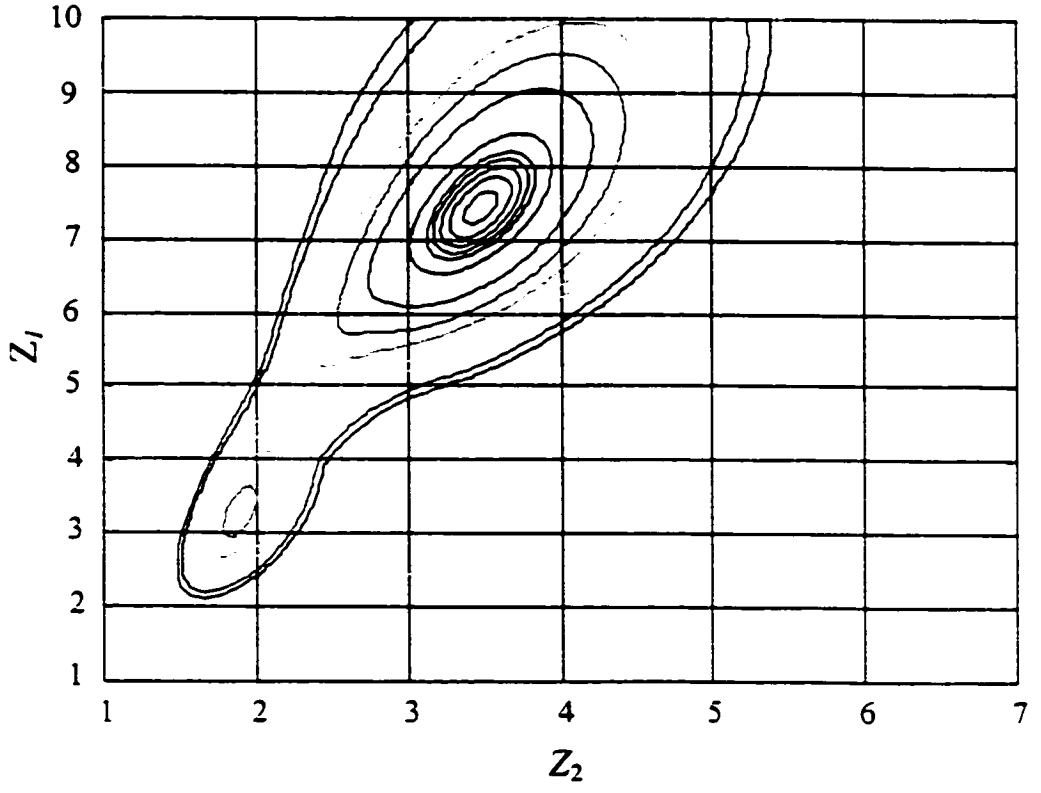

Fig. 4.10. The contours of $Q(x, V^{(2)})$ for the 10:1 impedance transformer.

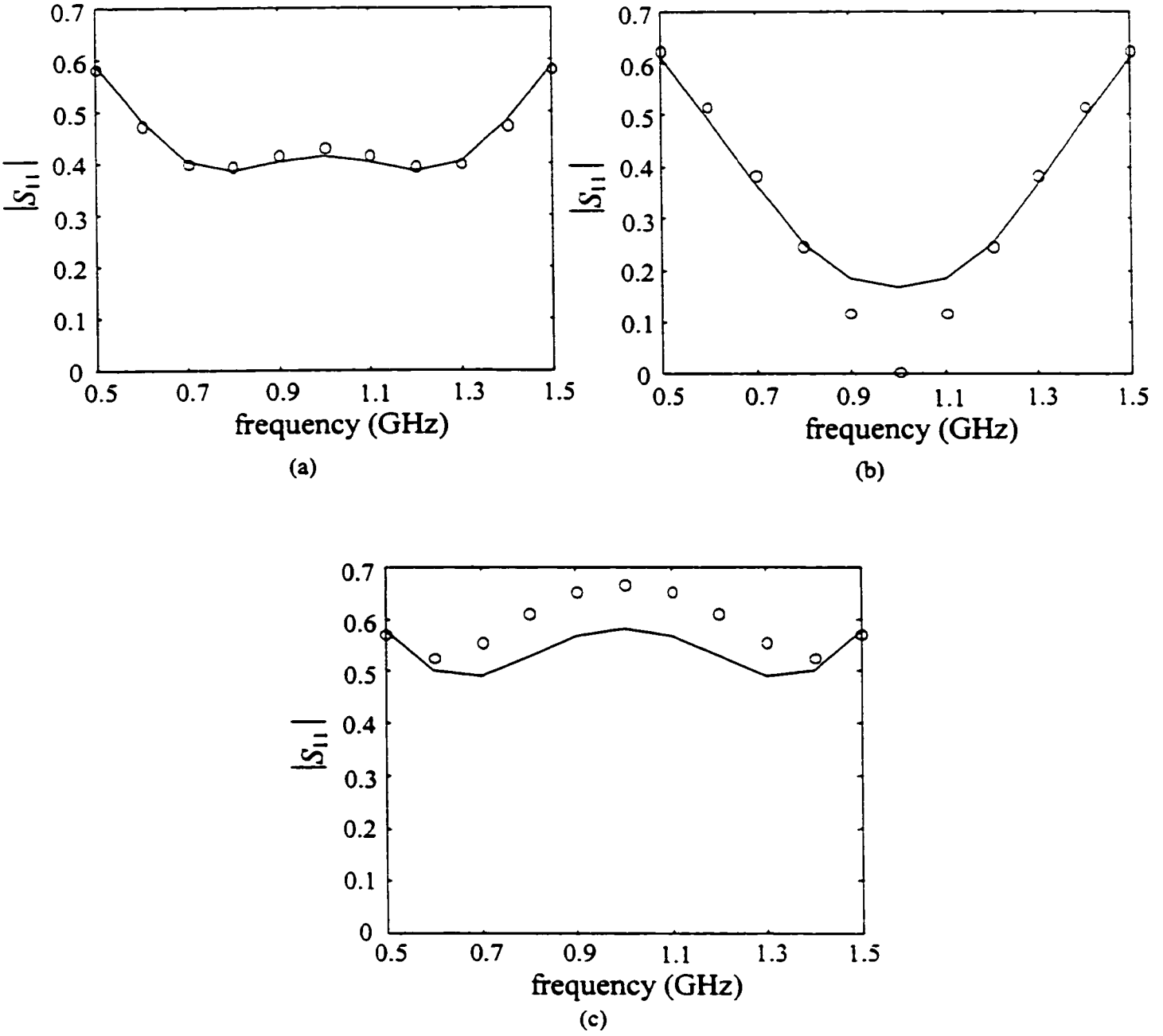

Fig. 4.11. The fine model response (o) and the corresponding coarse model response (–) : (a) at the first point, (b) at the second point and (c) at the third point utilized in the three-point parameter extraction for the 10:1 impedance transformer.

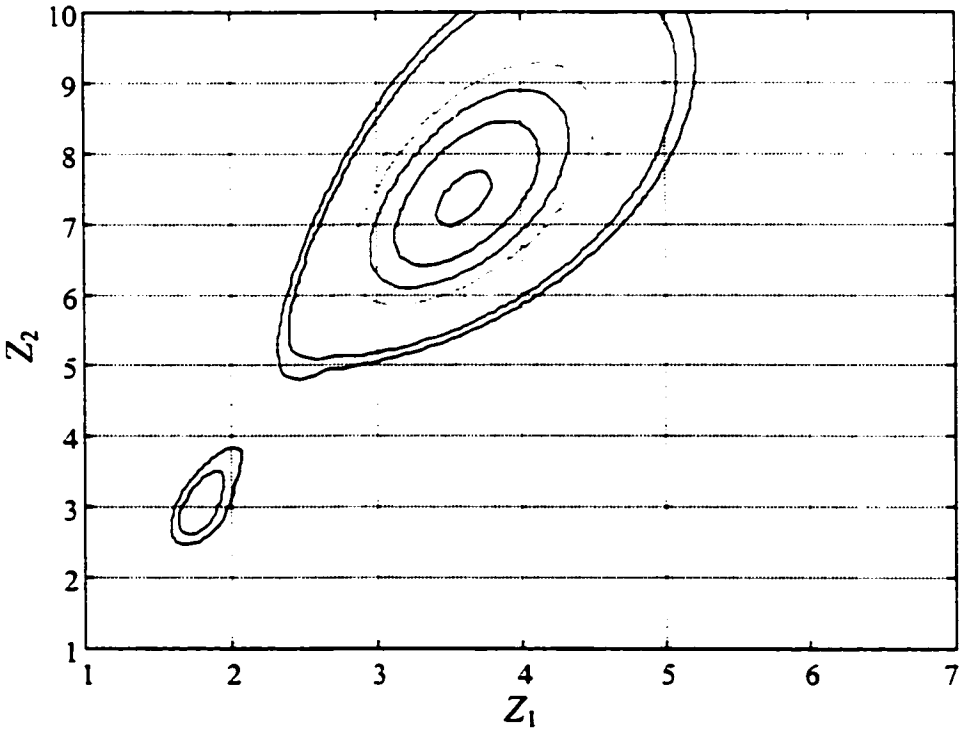

Fig. 4.12. The contours of $Q(x, V^{(3)})$ for the 10:1 impedance transformer.

The algorithm first started by applying SPE where $V^{(1)}$ contains only the point $x_f^{(1)}$ given in Table 4.5. The point $x_c^{e(1)}$ is given in Table 4.6. Fig. 4.14 shows the fine model response at $x_f^{(1)}$ and the coarse model response at $x_c^{e(1)}$.

The algorithm detected that this extracted point is a locally unique minimum. A new fine model point is then generated by solving the eigenvalue problem (4.22). A DPE step is then carried out. The set $V^{(2)}$ includes the points given in the second and third columns of Table 4.5. The point $x_c^{e(2)}$ is given in Table 4.6. Fig. 4.15 shows the fine model responses at the two utilized fine model points and the responses at the corresponding extracted coarse model points, respectively. Again the algorithm detected that the extracted point is locally unique and a new fine model point is generated and added to the set of points. The same steps were then repeated for three-point and four-point parameter extraction. The points utilized are given in Table 4.5. The results are shown in the fourth and fifth columns of Table 4.6. It is clear that the extracted parameters are approaching a limit. The fine model responses and the responses at the corresponding extracted coarse model points for the last two iterations are shown in Figs. 4.16 and 4.17, respectively. Fig. 4.17(a) demonstrates that a good match between the responses of both models over a wider range of frequencies than that used for parameter extraction is achieved.

4.5.4 Double-Folded Stub Filter

We consider the design of the double-folded stub (DFS) microstrip structure shown in Fig. 3.2. The filter is characterized by five parameters : W_1 , W_2 , S, L_1 and L_2. L_1, L_2 and S are chosen as optimization variables. W_1 and W_2 are fixed at 4.8 mil. The fine model is simulated

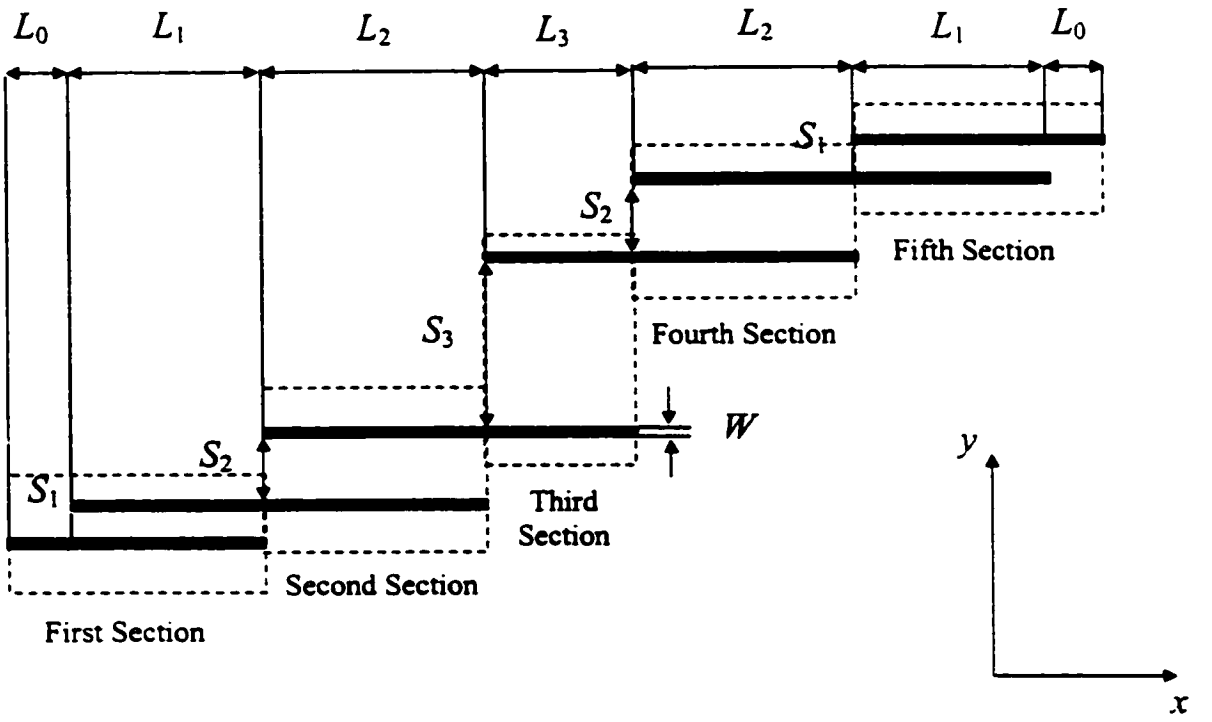

Fig. 4.13. The decomposed HTS filter.

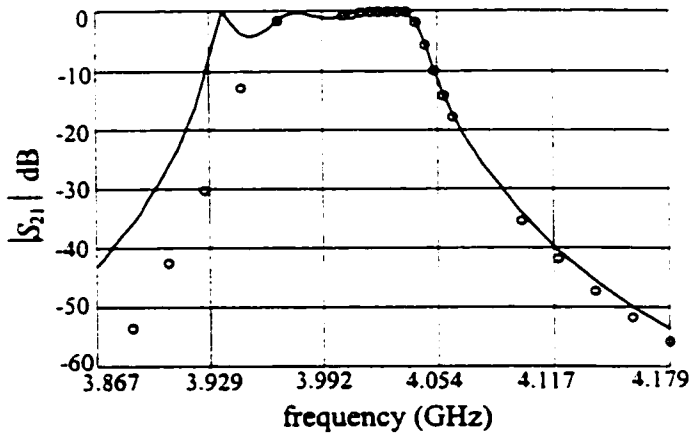

Fig. 4.14. The fine model response (o) and the corresponding coarse model response (–) at the point utilized in the SPE for the HTS filter. Note that only points in the range 3.967 GHz to 4.099 GHz were actually used.

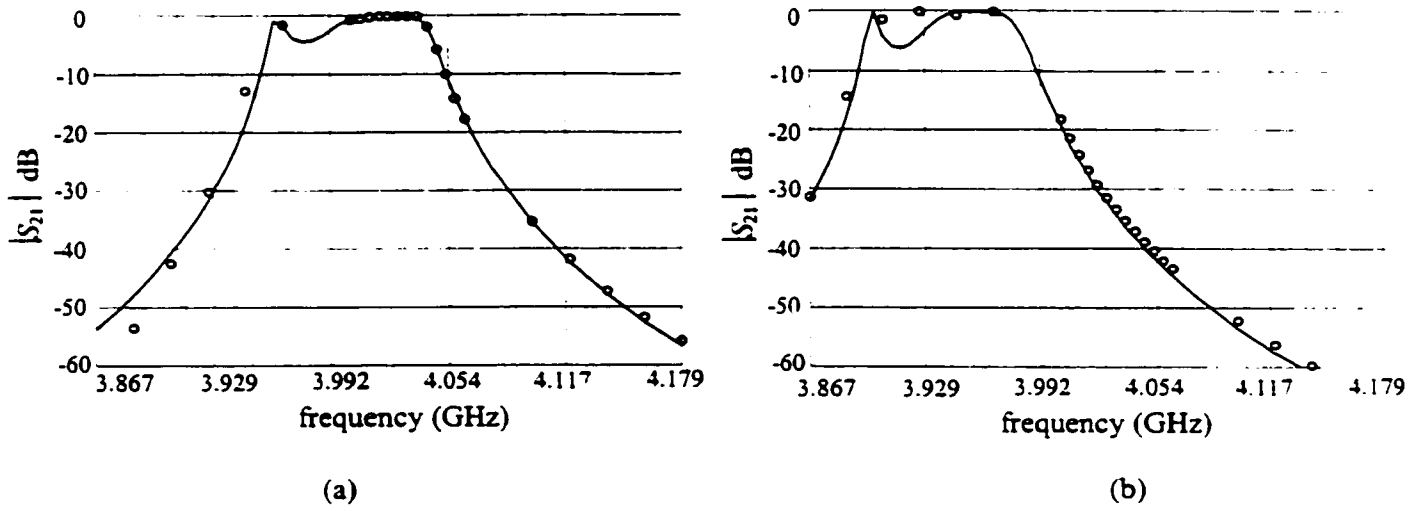

Fig. 4.15. The fine model response (o) and the corresponding coarse model response (–), (a) at the first point, and (b) at the second point utilized in the DPE for the HTS filter. Note that only points in the range 3.967 GHz to 4.099 GHz were actually used.

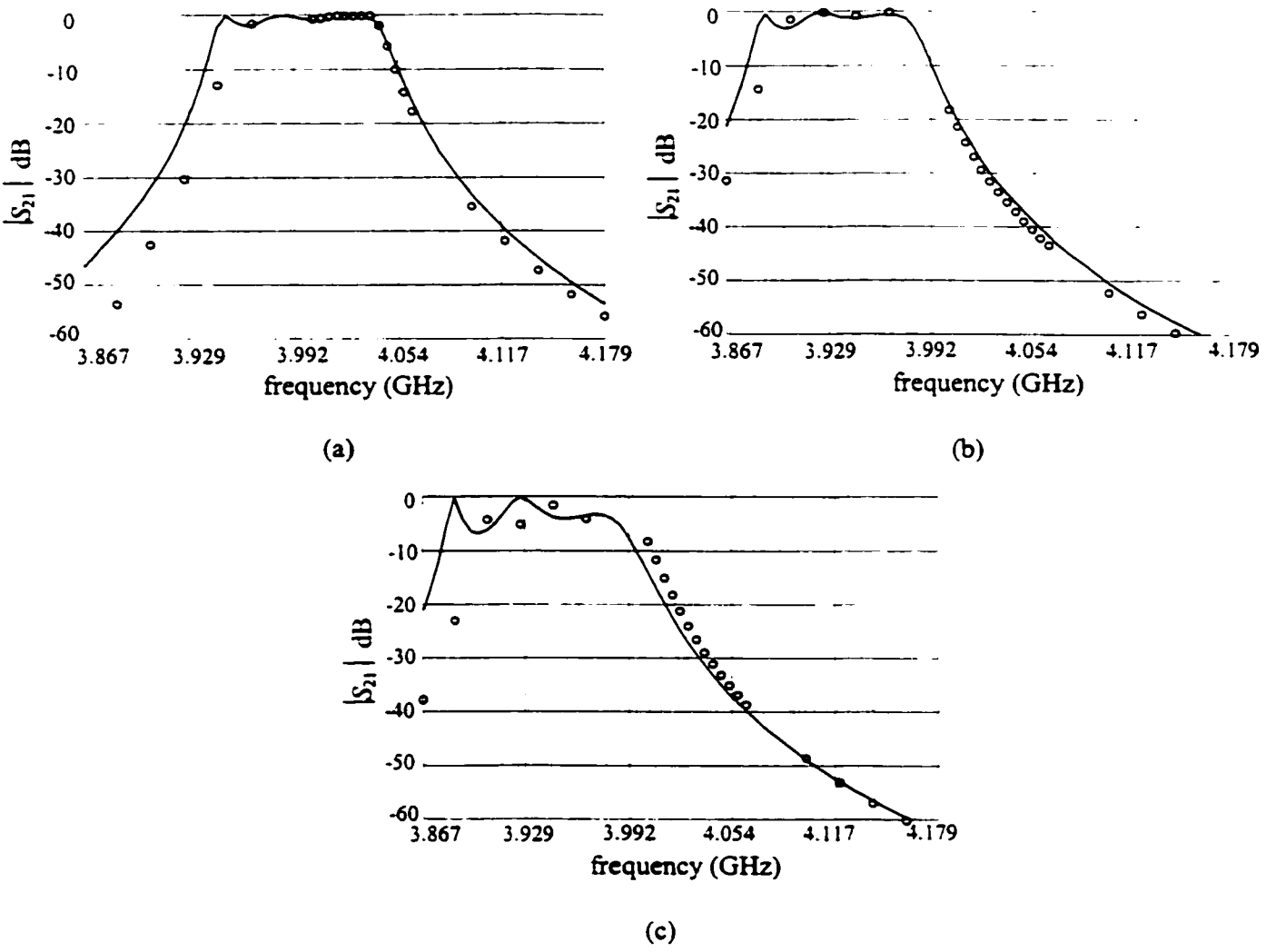

Fig. 4.16. The fine model response (o) and the corresponding coarse model response (–), (a) at the first point, (b) at the second point, and (c) at the third point utilized in the three-point parameter extraction for the HTS filter. Note that only points in the range 3.967 GHz to 4.099 GHz were actually used.

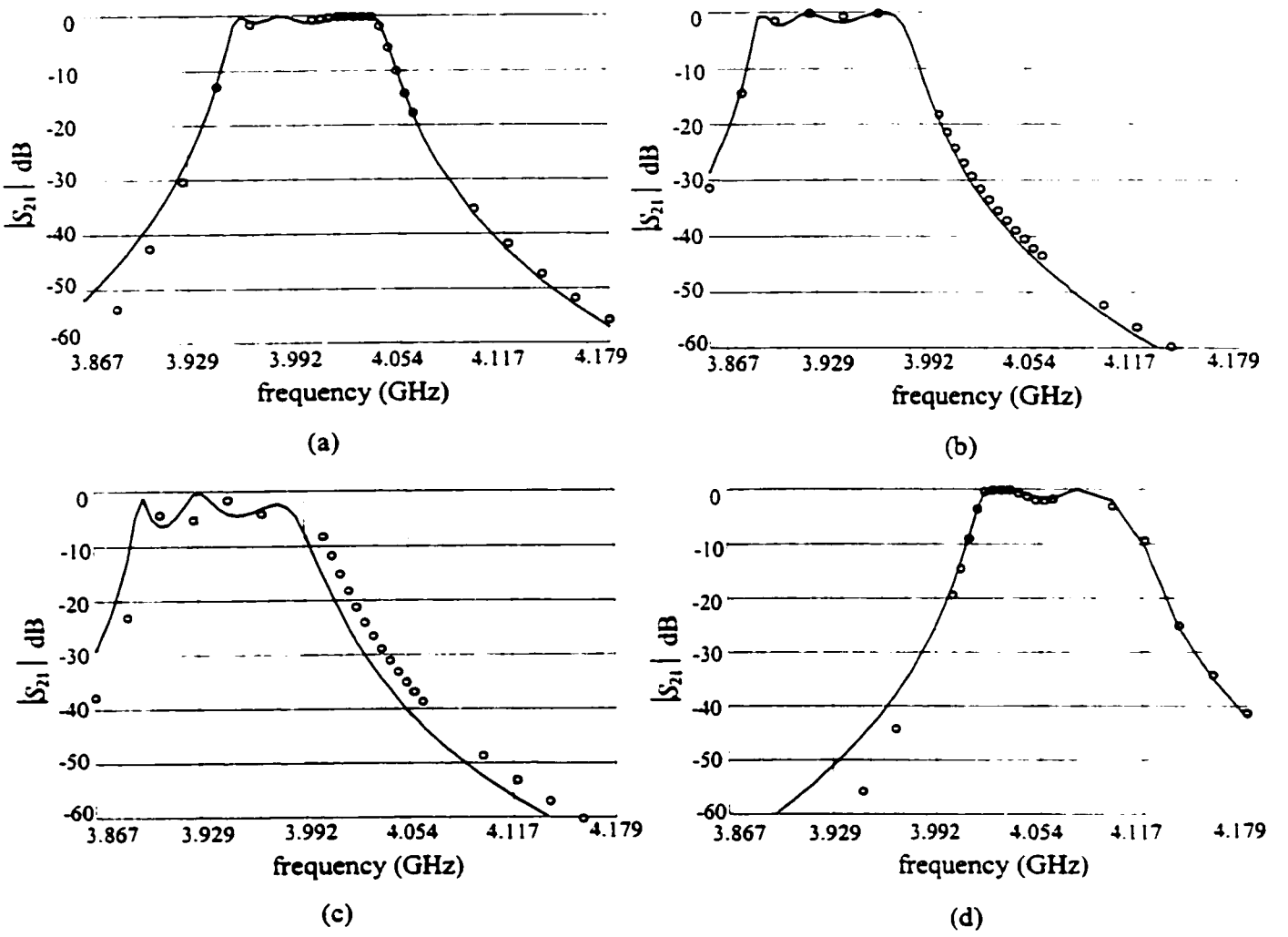

Fig. 4.17. The fine model response (o) and the corresponding coarse model response (–), (a) at the first point, (b) at the second point, (c) at the third point, and (d) at the fourth point utilized in the four-point parameter extraction for the HTS filter. Note that only points in the range 3.967 GHz to 4.099 GHz were actually used.

TABLE 4.3
MATERIAL AND PHYSICAL PARAMETERS
FOR THE COARSE AND FINE MODELS OF THE HTS FILTER

Model Parameter	Coarse Model	Fine Model
substrate dielectric constant	23.425	23.425
substrate thickness (mil)	19.9516	19.9516
shielding cover height (mil)	100	250
conducting material thickness	0	0
substrate dielectric loss tangent	0	0
resistivity of metal (Ωm)	0	0
magnetic loss tangent	0	0
surface reactance (Ω/sq)	0	0
x-grid cell size (mil)	2.00	1.00
y-grid cell size (mil)	1.75	1.75

TABLE 4.4
THE OPTIMAL COARSE MODEL DESIGN
FOR THE HTS FILTER

Parameter	Value
L_1	181.00
L_2	201.59
L_3	180.97
S_1	20.12
S_2	67.89
S_3	66.85
all values are in mils	

TABLE 4.5
THE FINE MODEL POINTS USED IN THE APE ALGORITHM FOR THE HTS FILTER

Parameter	$x_f^{(1)}$	$x_f^{(2)}$	$x_f^{(3)}$	$x_f^{(4)}$
L_1	181.00	182.55	181.34	179.86
L_2	201.59	205.64	205.38	197.74
L_3	180.97	183.36	184.20	178.08
S_1	20.12	20.05	20.07	20.46
S_2	67.89	68.40	68.08	67.35
S_3	66.85	67.25	66.98	66.46

all values are in mils

TABLE 4.6
THE VARIATION IN THE EXTRACTED PARAMETERS FOR THE HTS FILTER WITH THE NUMBER OF FINE MODEL POINTS

Parameter	$x_c^{e(1)}$	$x_c^{e(2)}$	$x_c^{e(3)}$	$x_c^{e(4)}$
L_1	188.31	179.99	176.67	178.50
L_2	197.69	204.52	208.52	206.78
L_3	189.72	181.23	178.00	179.09
S_1	19.34	17.13	17.21	18.99
S_2	52.67	63.44	56.52	57.99
S_3	52.06	53.18	53.47	56.77

all values are in mils

by HP HFSS ver. 5.2 through HP Empipe3D [84]. The coarse model exploits the microstrip line and microstrip T-junction models available in OSA90/hope. The coupling between the folded stubs and the microstrip line is simulated using equivalent capacitors. The values of these capacitors is determined using Walker's formulas [85]. Jansen's microstrip bend model [86] is used to model the folding effect of the stub. The coarse model is shown in Fig. 4.18.

It is required in this example to extract the coarse model parameters corresponding to the fine model parameters given in Table 4.7. This vector is the optimal design of the coarse model obtained by minimax optimization. The optimal coarse model response and the fine model response at the optimal coarse model design are shown in Fig. 4.19. This figure shows clearly the large misalignment between the two models which implies nonuniqueness of the extracted parameters.

The algorithm started by applying SPE using the fine model point given in Table 4.7. Fig. 4.20 shows the fine model response at $x_f^{(1)}$ and the coarse model response at the point $x_c^{e(1)}$. The algorithm detected that the extracted parameters are locally unique. A new fine model point is generated using (4.22) and added to the set of fine model points used for the MPE. The algorithm needed nine iterations to trust the extracted coarse model parameters. The fine model points utilized are given in Table 4.8 and the extracted coarse model points are given in Table 4.9. Fig. 4.21 shows the fine model response at $x_f^{(1)}$ and the coarse model response at the point $x_c^{e(9)}$.

Table 4.9 shows the large relative change in parameter values between the first set of extracted parameters $x_c^{e(1)}$ and the trusted set of parameters $x_c^{e(9)}$. If the step taken by any SM optimization algorithm utilizes $x_c^{e(1)}$, the algorithm would have probably failed. Fig. 4.22 shows the change of $Q(x_c^{e(1)}, V^{(i)})$ and of $Q(x_c^{e(9)}, V^{(i)})$ with $|V^{(i)}|$. The value of $Q(x_c^{e(9)}, V^{(i)})$ remains

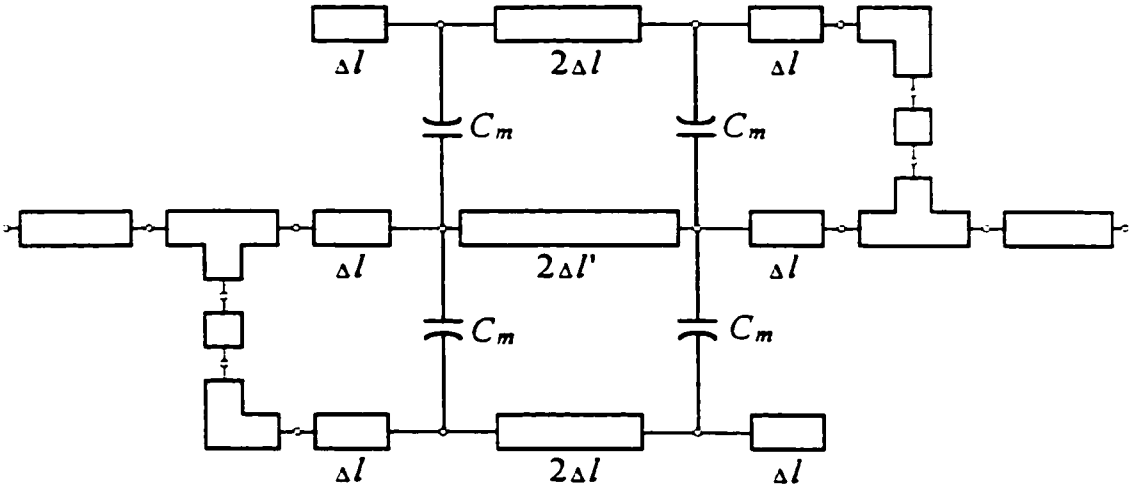

Fig. 4.18. The coarse model of the DFS filter.

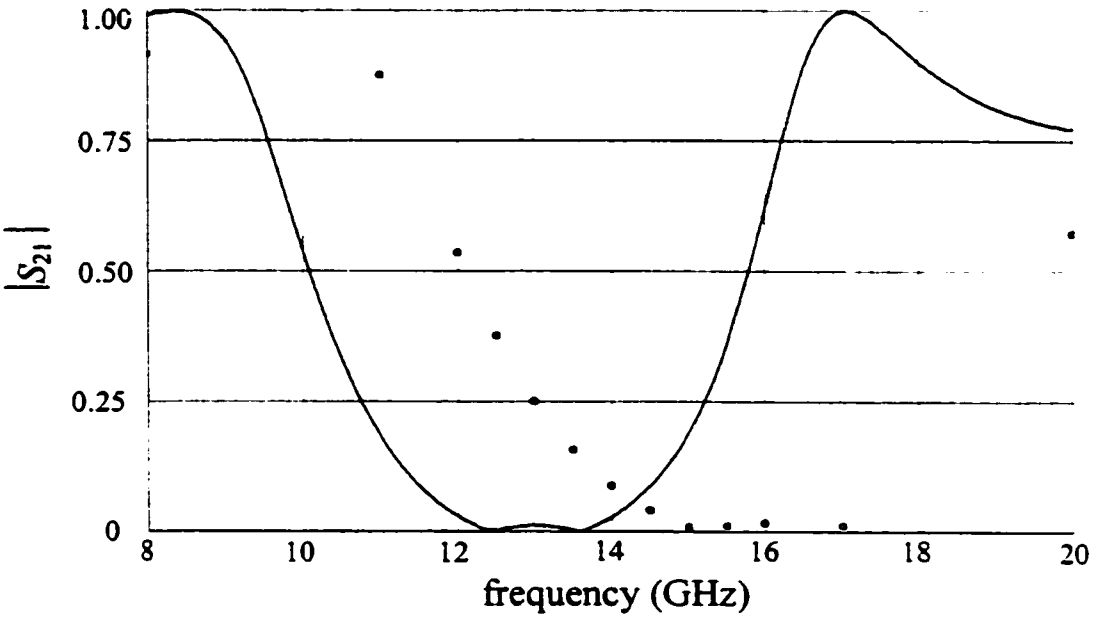

Fig. 4.19. The optimal coarse model response (—) and the fine model response (o) at the optimal coarse model design for the DFS filter.

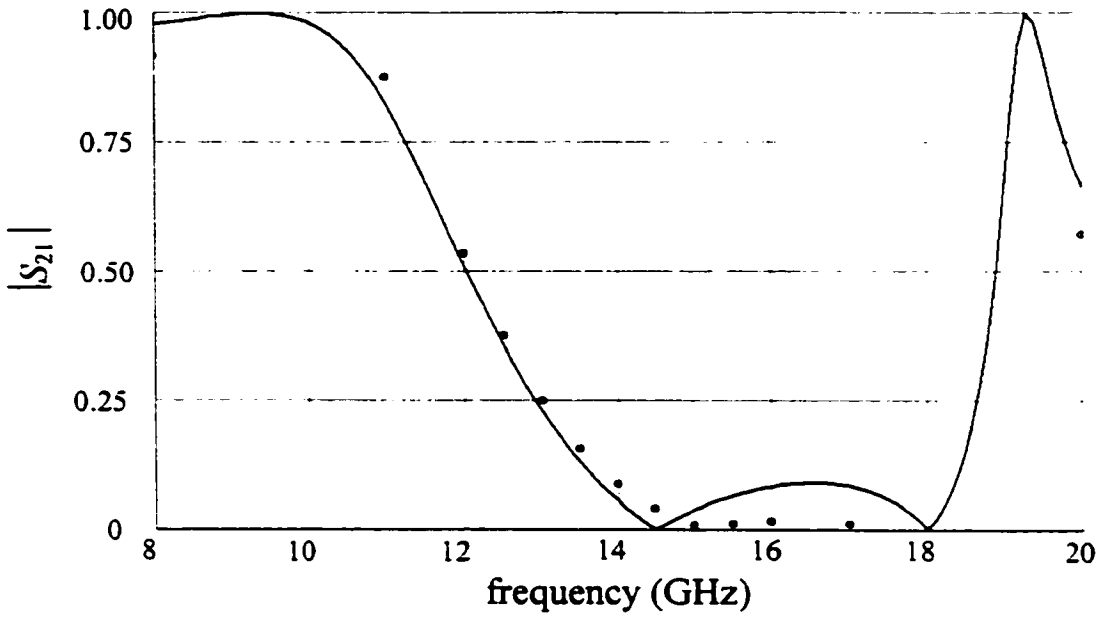

Fig. 4.20. The fine model response (o) and the corresponding coarse model response (–) at the point $x_c^{\epsilon(1)}$ for the DFS filter.

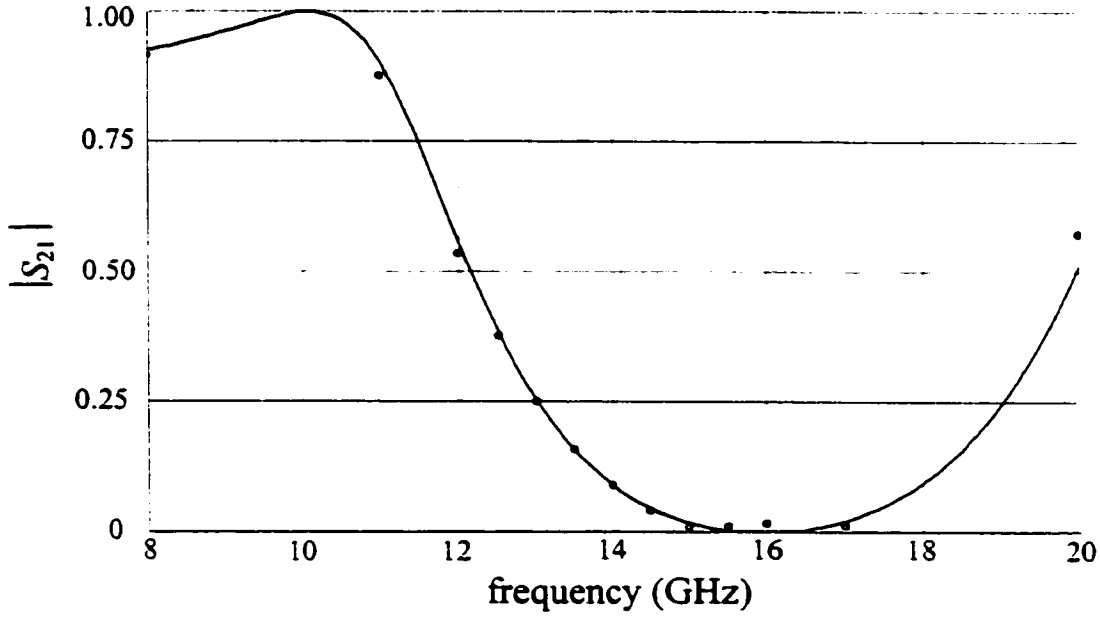

Fig. 4.21. The fine model response (o) and the corresponding coarse model response (–) at the point $x_c^{\epsilon(9)}$ for the DFS filter.

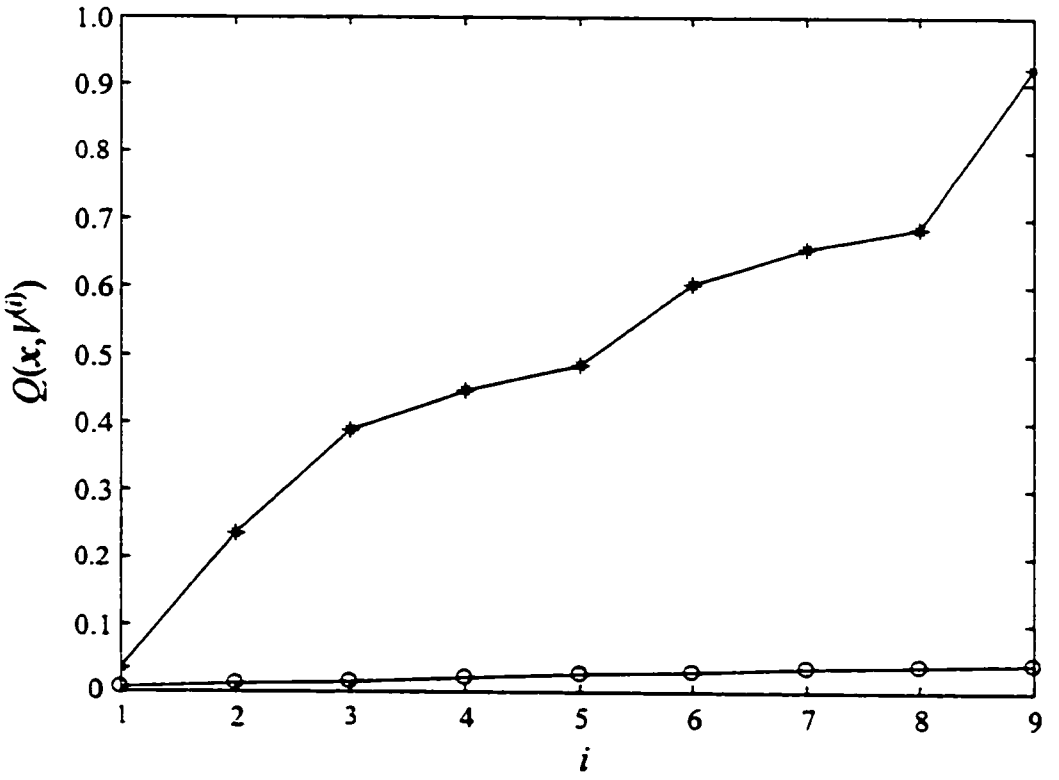

Fig. 4.22. The variation of $Q(x, V^{(i)})$ for the DFS filter at the point $x_c^{\epsilon(1)}$ (— * —) and at the point $x_c^{\epsilon(9)}$ (— o —) with the number of points utilized for parameter extraction.

TABLE 4.7
THE OPTIMAL COARSE MODEL DESIGN FOR THE DFS FILTER

Parameter	Value
L_1	66.73
L_2	60.23
S	9.59

all values are in mils

TABLE 4.8
THE FINE MODEL POINTS USED IN THE APE ALGORITHM FOR THE DFS FILTER

Parameter	$x_f^{(1)}$	$x_f^{(2)}$	$x_f^{(3)}$	$x_f^{(4)}$	$x_f^{(5)}$	$x_f^{(6)}$	$x_f^{(7)}$	$x_f^{(8)}$	$x_f^{(9)}$
L_1	66.73	67.72	67.32	66.15	70.60	67.66	62.82	65.80	66.57
L_2	60.23	63.58	64.13	56.33	59.48	64.10	60.88	56.36	59.85
S	9.59	9.27	9.48	9.71	9.71	9.66	9.50	9.52	10.26

all values are in mils

TABLE 4.9
THE VARIATION IN THE EXTRACTED PARAMETERS FOR THE DFS FILTER WITH THE NUMBER OF FINE MODEL POINTS

Parameter	$x_c^{e(1)}$	$x_c^{e(2)}$	$x_c^{e(3)}$	$x_c^{e(4)}$	$x_c^{e(5)}$	$x_c^{e(6)}$	$x_c^{e(7)}$	$x_c^{e(8)}$	$x_c^{e(9)}$
L_1	58.01	67.05	66.11	64.36	56.46	66.10	56.50	56.39	56.59
L_2	38.40	40.47	40.40	43.28	42.94	42.02	42.81	43.00	43.02
S	3.24	6.86	6.64	8.83	18.10	7.99	18.25	17.93	17.87

all values are in mils

almost constant and small in value. On the other hand the value of $Q(x_c^{(i)}, V^{(i)})$ increases significantly with each new point added to the set of utilized fine model points signaling a false minimum.

4.6 CONCLUSIONS

The Aggressive Parameter Extraction (APE) algorithm was presented in this chapter. APE addresses the optimal selection of parameter perturbations used to improve the uniqueness of the multi-point parameter extraction procedure. The nonuniqueness of the parameter extraction problem may lead to the divergence or oscillation of the SM approach to circuit design. New parameter perturbations are generated based on the nature of the minimum reached in the previous iteration. We consider possibly locally unique and locally nonunique minima. The suggested perturbations in each of these two cases are obtained either by solving a system of linear equations or by solving an eigenvalue problem. The APE algorithm continues until the extracted coarse model parameters can be trusted. The algorithm is demonstrated through the parameter extraction of microwave filters and impedance transformers.

5

THE HYBRID AGGRESSIVE SPACE MAPPING ALGORITHM

5.1 INTRODUCTION

In this chapter, the Hybrid Aggressive Space Mapping (HASM) algorithm is presented. The HASM algorithm addresses the case of a poor coarse model. The previously discussed SM-based optimization algorithms assume that the coarse model has sufficient accuracy. The information supplied by the coarse model is used to guide the fine mode optimization iterates. However, if the coarse model is severely different from the fine model, SM-based optimization is unlikely to converge.

We present a lemma that relates the developed mapping with the coarse and fine model derivatives. We show that all SM-based optimization algorithms utilize coarse model derivatives and the mapping to indirectly estimate the fine model derivatives. However, if the coarse model is poor, the estimated fine model derivatives may be inaccurate. This may lead the TRASM optimization to be trapped in local minima.

The HASM algorithm exploits two phases. The first phase utilizes the TRASM strategy while the second phase utilizes direct optimization. HASM utilizes SM optimization as long as it is converging. Otherwise, it switches to the direct optimization phase. The lemma that relates the established mapping and the first order derivatives of the coarse and fine models is utilized in the switching process.

Another motive for a hybrid algorithm is the optimality of the space-mapped design. This design in most cases is very near optimal. However, the optimality of the final design can not be guaranteed. This is because the final space-mapped response matches the optimal coarse model response, which may be different from the optimal fine model response obtained by solving the original design problem in the fine model space.

We start by discussing some properties of SM optimization in Section 5.2. These properties motivate the utilization of a hybrid algorithm. The lemma is introduced in Section 5.3. In Section 5.4, we address a prediction approach for a good starting point for MPE. This approach is used by the HASM algorithm to improve PE uniqueness. The HASM algorithm is presented in Section 5.5. The algorithm is applied to the design of microwave transformers and filters. The examples include the design of a three-section waveguide transformer, a seven-section waveguide transformer, an H-plane waveguide filter and a double-folded stub microstrip filter. These examples are given in Section 5.6. Finally, the conclusions are given in Section 5.7.

5.2 THE MOTIVATION FOR A HYBRID ALGORITHM

ASM and TRASM are efficient algorithms. The number of fine model simulations needed to obtain the space-mapped design is of the order of the problem dimensionality. However, both algorithms depend on the existence of a coarse model that is fast and has enough accuracy.

If the coarse model is bad (i.e., very different from the fine model) space mapping may not work. To illustrate this we consider the Rosenbrock function [82]. We form an artificial problem in which the "coarse" model is given by

$$R_c = 100\,(x_2 - x_1^2)^2 + (1 - x_1)^2 \tag{5.1}$$

and the "fine" model by

$$R_f = 100\,((x_2+\alpha_2)-(x_1+\alpha_1)^2)^2 + (1-(x_1+\alpha_1))^2 \tag{5.2}$$

where α_1 and α_2 are constant shifts. The target of the direct optimization problem is to minimize R_f. Considering (5.1) and (5.2) we notice that $\boldsymbol{x}_c^* = [1.0 \quad 1.0]^T$ and $\boldsymbol{x}_f^* = (\boldsymbol{x}_c^* - \boldsymbol{\alpha})$ where $\boldsymbol{\alpha} = [\alpha_1 \quad \alpha_2]^T$. The misalignment between the two models is thus given by the two shifts α_1 and α_2.

We discuss two sets of values for the shifts. First, we consider $\boldsymbol{\alpha} = [-0.1 \quad -0.1]^T$. Using (5.1) and (5.2) we notice that the coarse model point corresponding to a fine model point $\boldsymbol{x}_f$ is $\boldsymbol{x}_c = (\boldsymbol{x}_f + \boldsymbol{\alpha})$. It follows that the mapping between the two spaces is given by $\boldsymbol{P}(\boldsymbol{x}_f) = \boldsymbol{x}_f + \boldsymbol{\alpha}$. The contours of $\|\boldsymbol{x}_f + \boldsymbol{\alpha} - \boldsymbol{x}_c^*\|_2^2$ are shown in Fig. 5.1(a). The mapping $\boldsymbol{P}(\boldsymbol{x}_f)$ is then approximated through MPE. Only one perturbed fine model point is utilized. The contours of $\|\boldsymbol{P}(\boldsymbol{x}_f) - \boldsymbol{x}_c^*\|_2^2$ obtained in this manner are shown in Fig. 5.1(b). Figs. 5.1(a) and 5.1(b) show that $\|\boldsymbol{f}\|_2^2$ has a single minimum which is the solution that would have been obtained by direct optimization. The differences between the two plots are attributed to the nonuniqueness of the parameter extraction process. Taking the point $\boldsymbol{x}_c^*$ as the initial solution of the fine model, the TRASM algorithm is expected to converge to $\boldsymbol{x}_f^*$. The corresponding contours of R_f are shown in Fig. 5.1(c), whose minimum value is at $[1.1 \quad 1.1]^T$ as expected.

The same steps are repeated for the case $\boldsymbol{\alpha} = [-1.5 \quad -1.5]^T$. The contour plot of $\|\boldsymbol{x}_f + \boldsymbol{\alpha} - \boldsymbol{x}_c^*\|_2^2$ is shown in Fig. 5.2(a). The contour plot of $\|\boldsymbol{P}(\boldsymbol{x}_f) - \boldsymbol{x}_c^*\|_2^2$ obtained using MPE is shown in Fig. 5.2(b). Fig. 5.2(b) illustrates the existence of a minimum of $\|\boldsymbol{P}(\boldsymbol{x}_f) - \boldsymbol{x}_c^*\|_2^2$ other

than x_f^* which is closer to the starting point of the TRASM algorithm x_c^*. It follows that the TRASM algorithm is unlikely to converge to x_f^*. The corresponding contours of R_f for this case are shown in Fig. 5.2(c), whose minimum value is at $[2.5 \quad 2.5]^T$.

Another motive for a hybrid algorithm is the optimality of the space-mapped design. The space-mapped design is very near optimal if $\boldsymbol{R}_c^*$ is similar to the optimal fine model response $\boldsymbol{R}_f^*$. However, this can not be guaranteed. For example, consider

$$R_f = 100\,(x_2 - x_1^2)^2 + (1 - x_1)^2 \tag{5.3}$$

Assume also that

$$R_c = R_f + \varepsilon \tag{5.4}$$

where $\varepsilon > 0$. It is clear that R_c^* is equal to ε while R_f^* is zero. It follows that space mapping may converge to a solution other than x_f^*.

5.3 SPACE MAPPING AND DIRECT OPTIMIZATION

The properties of space mapping suggest that a hybrid algorithm be used. This algorithm exploits the efficiency of space mapping and defaults to direct optimization when space mapping fails. The HASM algorithm utilizes a lemma that enables switching between the TRASM optimization and direct optimization and vice versa.

Lemma Assume that x_c corresponds to x_f through a parameter extraction process. Then the Jacobian J_f of the fine model response at x_f and the Jacobian J_c of the coarse model response at x_c are related by

$$\boldsymbol{J}_f = \boldsymbol{J}_c \boldsymbol{B} \tag{5.5}$$

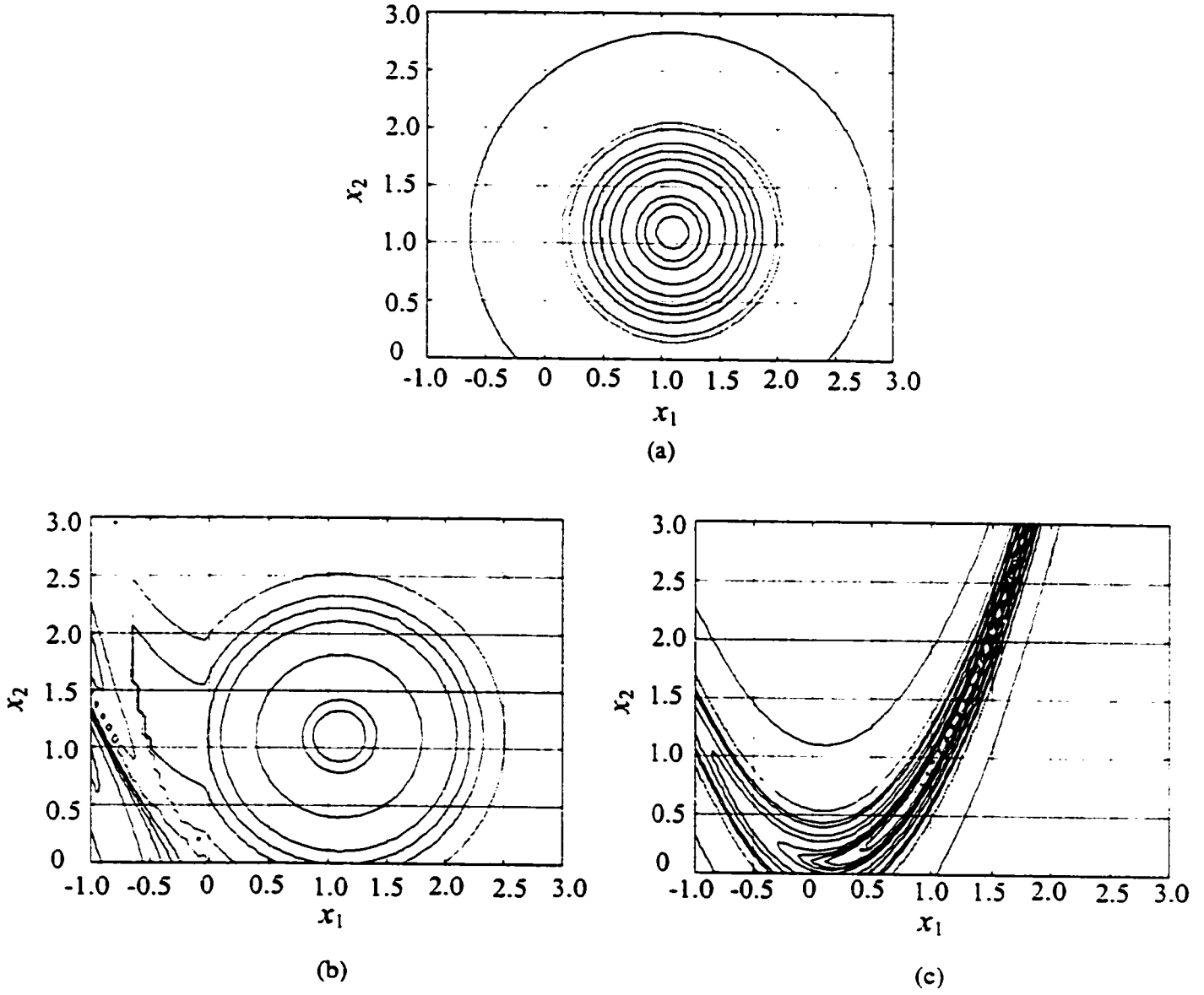

Fig. 5.1. Different contour plots for the Rosenbrock problem for the case $\boldsymbol{\alpha} = [-0.1 \quad -0.1]^T$; (a) the contour plot of $\left\|\boldsymbol{x}_f + \boldsymbol{\alpha} - \boldsymbol{x}_c^*\right\|_2^2$, (b) the contour plot of $\left\|\boldsymbol{P}(\boldsymbol{x}_f) - \boldsymbol{x}_c^*\right\|_2^2$ obtained through parameter extraction and (c) contours of the fine model Rosenbrock function.

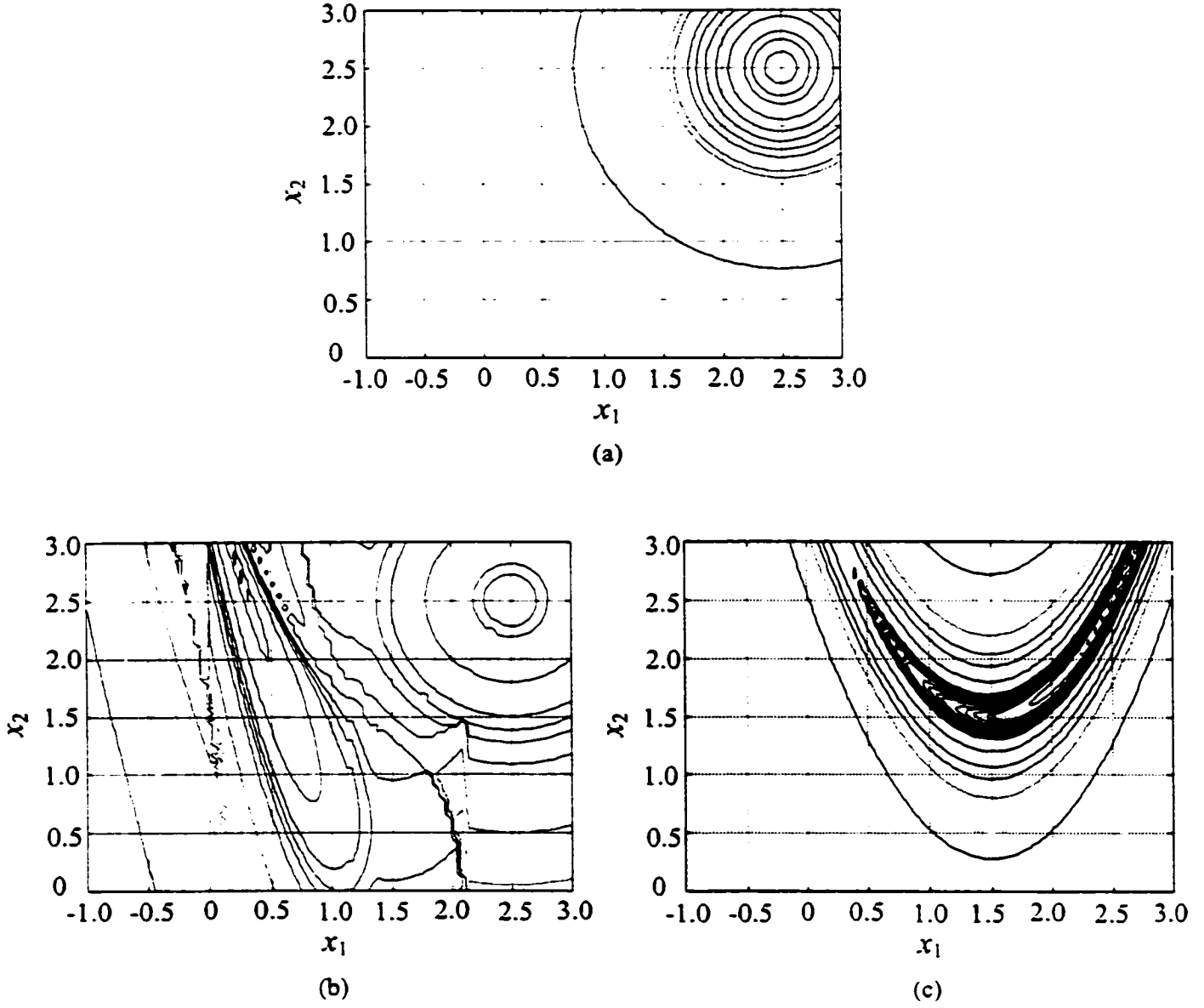

Fig. 5.2. Different contour plots for the Rosenbrock problem for the case $\boldsymbol{\alpha} = [-1.5 \quad -1.5]^T$; (a) the contour plot of $\left\|\boldsymbol{x}_f + \boldsymbol{\alpha} - \boldsymbol{x}_c^*\right\|_2^2$, (b) the contour plot of $\left\|\boldsymbol{P}(\boldsymbol{x}_f) - \boldsymbol{x}_c^*\right\|_2^2$ obtained through parameter extraction and (c) contours of the fine model Rosenbrock function.

where $\boldsymbol{B}$ is a valid mapping between the two spaces at $\boldsymbol{x}_c$ and $\boldsymbol{x}_f$.

Proof

As the points $\boldsymbol{x}_f$ and $\boldsymbol{x}_c$ correspond to each other, it follows that their responses match, i.e.,

$$\boldsymbol{R}_f(\boldsymbol{x}_f) = \boldsymbol{R}_c(\boldsymbol{x}_c) \tag{5.6}$$

Now define a new fine model point $\boldsymbol{x}_n = \boldsymbol{x}_f + \Delta \boldsymbol{x}_f$ where $\Delta \boldsymbol{x}_f$ is a small perturbation. The response at this new point is perturbed from the response at the point $\boldsymbol{x}_f$ by

$$\Delta \boldsymbol{R} = \boldsymbol{J}_f \Delta \boldsymbol{x}_f \tag{5.7}$$

The point $\boldsymbol{x}_n$ corresponds to a coarse model point $\boldsymbol{x}_c + \Delta \boldsymbol{x}_c$ that satisfies

$$\Delta \boldsymbol{R} = \boldsymbol{J}_f \Delta \boldsymbol{x}_f = \boldsymbol{J}_c \Delta \boldsymbol{x}_c \tag{5.8}$$

Also, by definition of the mapping $\boldsymbol{B}$ the two perturbations $\Delta \boldsymbol{x}_f$ and $\Delta \boldsymbol{x}_c$ are related by

$$\boldsymbol{B} \Delta \boldsymbol{x}_f = \Delta \boldsymbol{x}_c \tag{5.9}$$

multiplying both sides of (5.9) by $\boldsymbol{J}_c$ we get

$$\boldsymbol{J}_c \boldsymbol{B} \Delta \boldsymbol{x}_f = \boldsymbol{J}_c \Delta \boldsymbol{x}_c \tag{5.10}$$

Comparing (5.10) with (5.8) we conclude that

$$\boldsymbol{J}_f = \boldsymbol{J}_c \boldsymbol{B} \tag{5.11}$$

Relation (5.11) is interesting. It shows that by having the matrix $\boldsymbol{B}$ and the coarse model Jacobian $\boldsymbol{J}_c$ we are able to obtain a good estimate of the Jacobian of the fine model response without any further fine model simulations. It follows that when SM optimization fails to converge we can switch to direct optimization and supply it with the available first order derivatives given by (5.11).

Another relationship which can be easily obtained from (5.11) is

$$\boldsymbol{B} = \left(\boldsymbol{J}_c^T \boldsymbol{J}_c\right)^{-1} \boldsymbol{J}_c^T \boldsymbol{J}_f \tag{5.12}$$

Relation (5.12) assumes that $\boldsymbol{J}_c$ is full rank and $m \geq n$. It is used for switching back from direct optimization to SM optimization. Fig. 5.3 illustrates the switching between SM optimization and direct optimization.

We illustrate the lemma as follows. Consider

$$R_f = (0.9x_1 + 0.1x_2)^2 + (0.1x_1 + 0.9x_2)^2 \tag{5.13}$$

and

$$R_c = x_1^2 + x_2^2 \tag{5.14}$$

Take $\boldsymbol{x}_f = [2.0 \quad 1.0]^T$. Here $R_f = 4.82$. The solution for the parameter extraction problem is $\boldsymbol{x}_c = [1.90 \quad 1.10]^T$. The Jacobian $\boldsymbol{J}_c$ at $\boldsymbol{x}_c$ is

$$\boldsymbol{J}_c = \begin{bmatrix} 3.8 & 2.2 \end{bmatrix} \tag{5.15}$$

From (5.13) and (5.14) it is seen that

$$\boldsymbol{B} = \begin{bmatrix} 0.9 & 0.1 \\ 0.1 & 0.9 \end{bmatrix} \tag{5.16}$$

It follows that $\boldsymbol{J}_f$ at $\boldsymbol{x}_f$ is estimated by

$$\boldsymbol{J}_f = \begin{bmatrix} 3.8 & 2.2 \end{bmatrix} \begin{bmatrix} 0.9 & 0.1 \\ 0.1 & 0.9 \end{bmatrix} = \begin{bmatrix} 3.64 & 2.36 \end{bmatrix} \tag{5.17}$$

which is the exact Jacobian of the fine model response.

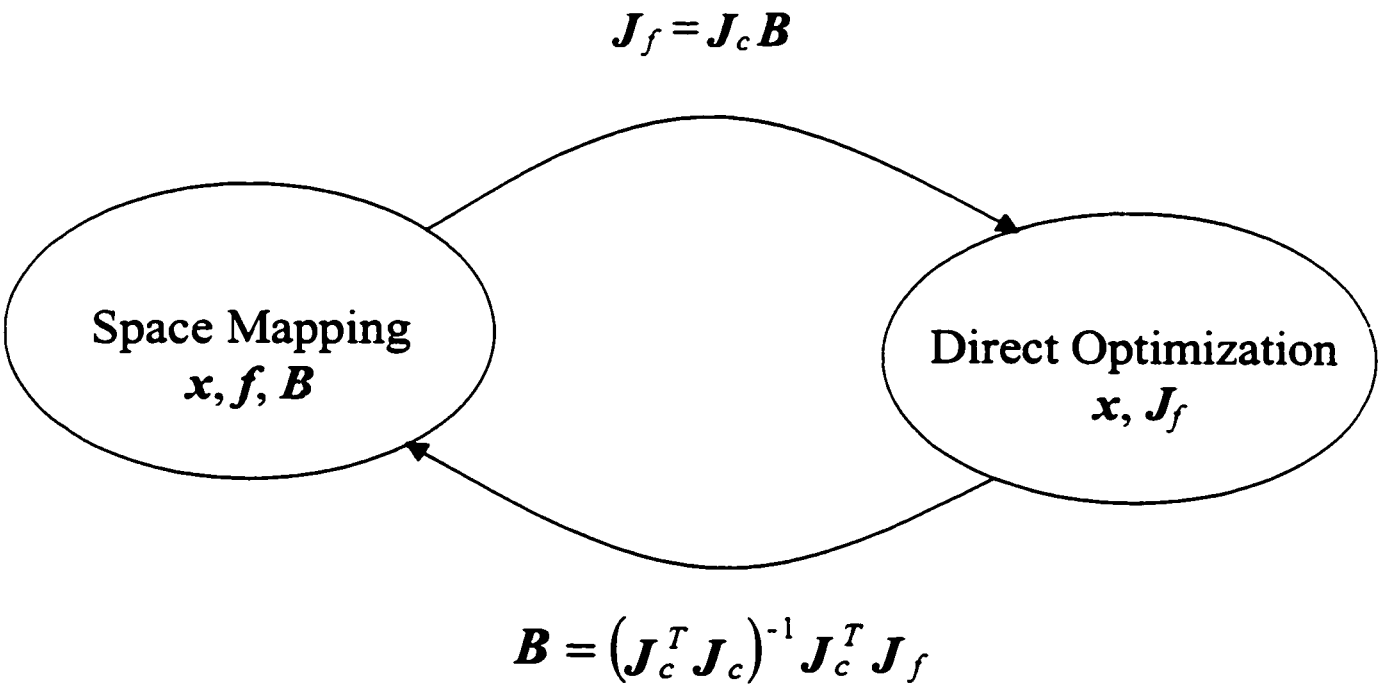

Fig. 5.3. Illustration of the connection between SM optimization and direct optimization.

5.4 SELECTION OF THE STARTING POINT FOR PARAMETER EXTRACTION

The discussion in Section 5.2 reveals how the nonuniqueness of the PE process can affect the convergence of SM optimization. The uniqueness of this procedure can be improved by utilizing a good starting point. In the first iteration of the algorithm there is no available information about the mapping between the two spaces. A reasonable assumption is to take $\boldsymbol{x}_c^*$ as the starting point for the PE optimization problem. As the algorithm proceeds the matrix $\boldsymbol{B}^{(i)}$ approximates the mapping between the two spaces. A prediction of the extracted parameters in the ith iteration is given by

$$\boldsymbol{x}_c^{(p)} = \boldsymbol{x}_c^{(i)} + \boldsymbol{B}^{(i)}\left(\boldsymbol{x}_f^{(i+1)} - \boldsymbol{x}_f^{(i)}\right) \tag{5.18}$$

This predicted point is then taken as a starting point for the PE optimization problem. It supplies a good starting point provided that $\boldsymbol{x}_c^{(i)}$ is a valid solution to the parameter extraction in the previous iteration and $\boldsymbol{B}^{(i)}$ approximates the mapping between the two spaces.

5.5 THE HASM ALGORITHM

The HASM algorithm exploits SM when effective, otherwise it defaults to direct optimization. Two objective functions are utilized by the algorithm. The first objective function is

$$\|\boldsymbol{f}\|_2^2 = \left\|\boldsymbol{P}(\boldsymbol{x}_f) - \boldsymbol{x}_c^*\right\|_2^2 \tag{5.19}$$

while the second function is

$$\|\boldsymbol{g}\|_2^2 = \left\|\boldsymbol{R}_f(\boldsymbol{x}_f) - \boldsymbol{R}_c(\boldsymbol{x}_c^*)\right\|_2^2 \tag{5.20}$$

While (5.19) aims at matching the extracted coarse model parameters to x_c^* in the parameter space, (5.20) aims at matching the same points mapped through the appropriate responses in the response space.

The HASM algorithm consists of two phases: the first phase follows the TRASM strategy while the second phase exploits direct optimization. It utilizes (5.11) and (5.12) for switching between phases as dictated by the convergence of the iterates.

In the ith iteration we assume the existence of a trusted extracted coarse model parameters $x_c^{(i)} = P(x_f^{(i)})$. The step taken in this iteration is given by (3.7), where $x_f^{(i+1)} = x_f^{(i)} + h^{(i)}$. SPE is then applied at the point $x_f^{(i+1)}$ to get $f^{(i+1)} = P(x_f^{(i+1)}) - x_c^*$.

The first phase utilizes two success criteria related to the reduction in (5.19) and (5.20). The SM success criterion is given by (3.8). It indicates that the actual reduction in the objective function (5.19) should be greater than a certain fraction of the predicted reduction. The direct optimization success criterion is

$$\left\| g^{(i+1)} \right\| < \left\| g^{(i)} \right\| \tag{5.21}$$

which implies that the new iterate $x_f^{(i+1)}$ is a descent iterate of (5.20).

The new point $x_f^{(i+1)}$ is accepted and the first phase resumes if this point satisfies both (3.8) and (5.21). $B^{(i)}$ is then updated. The vector $f^{(i+1)}$ satisfying (3.8) is either obtained through SPE or through RMPE that approaches a limit satisfying (3.8). We denote by x_f' and R_f' the solution obtained at the end of the first phase and the corresponding fine model response, respectively.

Switching to the second phase takes place in two cases. The first case is that (5.21) is not satisfied which means that we have to reject the new point $x_f^{(i+1)}$. The Jacobian of the fine model response at the point $x_f^{(i)}$ is then evaluated. This is done by first evaluating the Jacobian of the coarse model response $J_c^{(i)}$ at the previously extracted coarse model point $x_c^{(i)}=P(x_f^{(i)})$. $J_f^{(i)}$ is then approximated using (5.11). The second phase is then supplied by $x_f^{(i)}$, $J_f^{(i)}$ and $f^{(i)}$.

The second case occurs when the new point $x_f^{(i+1)}$ satisfies (5.21) but does not satisfy (3.8). In this case the point $x_f^{(i+1)}$ is better than the previous point $x_f^{(i)}$ and is accepted. As the vector of extracted parameters does not satisfy (3.8), the vector $f^{(i+1)}$ can not be trusted. In order to trust this vector, RMPE is applied at the point $x_f^{(i+1)}$ until either $f^{(i+1)}$ approaches a limiting value or the number of additional points used for MPE reaches n. If $f^{(i+1)}$ approaches a limit that does not satisfy (3.8), $B^{(i+1)}$ is updated, $J_c^{(i+1)}$ at the extracted coarse model point $x_c^{(i+1)}=P(x_f^{(i+1)})$ is evaluated and $J_f^{(i+1)}$ is then approximated using (5.11). Otherwise, $J_f^{(i+1)}$ is approximated using the $n+1$ fine model points used for MPE. The second phase is then supplied by the point $x_f^{(i+1)}$, $f^{(i+1)}$ and the Jacobian estimate $J_f^{(i+1)}$, which is either calculated using (5.11) or through finite differences.

The second phase utilizes the first-order derivatives supplied by SM to carry out a number of successful iterations. By a successful iteration we mean an iteration that satisfies the success criterion

$$\left(\left\|g^{(k)}\right\|-\left\|g^{(k+1)}\right\|\right)>0.01\left(\left\|g^{(k)}\right\|-\left\|g^{(k)}+J_f^{(k)}h^{(k)}\right\|\right) \tag{5.22}$$

which indicates that the actual reduction in the objective function (5.20) should be greater than a certain fraction of the predicted reduction. Notice that the superscript k is used as an index for the successful iterates of the direct optimization phase. At the end of each successful iteration PE is applied at the new iterate $\boldsymbol{x}_f^{(k)}$ and is used to check whether a switch back to the first phase can take place. The criterion for such a switch is

$$\left\| \boldsymbol{f}^{(k+1)} \right\| < \left\| \boldsymbol{f}^{(k)} \right\| \tag{5.23}$$

If it is satisfied $\boldsymbol{J}_c^{(k+1)}$ is evaluated at the point $\boldsymbol{x}_c^{(k+1)} = \boldsymbol{P}(\boldsymbol{x}_f^{(k+1)})$, $\boldsymbol{B}$ is reevaluated using (5.12) and the algorithm switches back to the first phase. Otherwise, the second phase continues. We denote by $\boldsymbol{x}^*_f$ and $\boldsymbol{R}^*_f$ the solution obtained at the end of the second phase and the corresponding fine model response, respectively.

For any iteration $i > 0$, the two phases are given by the following steps.

Phase 1

Step 0 Given $\boldsymbol{x}_f^{(i)}$, $\boldsymbol{f}^{(i)}$, $\boldsymbol{B}^{(i)}$ and $\delta^{(i)}$. Set $\delta^{(i+1)} = \delta^{(i)}$.

Comment $\delta^{(i)}$ is the utilized trust region size.

Step 1 Obtain $\boldsymbol{h}^{(i)}$ by solving (3.7). Let $\delta^{(i+1)} = \left\| \boldsymbol{h}^{(i)} \right\|_2$.

Step 2 Evaluate $\boldsymbol{x}_f^{(i+1)}$ and set $V = \{\boldsymbol{x}_f^{(i+1)}\}$.

Step 3 Apply MPE using the points in the set V to obtain $\boldsymbol{f}^{(i+1)}$.

Comment The prediction given in (5.18) is used as a starting point for the MPE.

Step 4 If both (3.8) and (5.21) are satisfied update the matrix $\boldsymbol{B}^{(i)}$ to $\boldsymbol{B}^{(i+1)}$ using Broyden's formula [6] and update $\delta^{(i+1)}$. Go to Step 10.

Comment The trust region size is updated based on how the predicted reduction in $\|f\|_2$ agrees with the actual reduction [36].

Step 5 If (5.21) is not satisfied, obtain $J_c^{(i)}$ and evaluate $J_f^{(i)} = J_c^{(i)} B^{(i)}$. Switch to the second phase.

Comment The second phase takes as arguments $x_f^{(i)}$, $f^{(i)}$ and $J_f^{(i)}$ and returns $x_f^{(k)}$, $B^{(k)}$ and $f^{(k)}$. It should be clear that several iterations might be executed in the second phase before switching back to the first phase at Step 10.

Step 6 If $|V|$ is equal to one, go to Step 9.

Comment $|V|$ denotes the cardinality of the set V.

Step 7 Compare $f^{(i+1)}$ obtained using $|V|$ fine model points with that previously obtained using $|V|-1$ fine model points. If $f^{(i+1)}$ is approaching a limit, update the matrix $B^{(i)}$ to get $B^{(i+1)}$, obtain $J_c^{(i+1)}$, evaluate $J_f^{(i+1)} = J_c^{(i+1)} B^{(i+1)}$ and switch to the second phase.

Step 8 If $|V|$ is equal to n+1, obtain the matrix $J_f^{(i+1)}$ by finite differences using the set V. Switch to the second phase.

Step 9 Obtain a temporary point $x_t = x_f^{(i+1)} + h_t$, where

$$(B^{(i)T} B^{(i)} + \lambda I) h_t = -B^{(i)T} f^{(i+1)}$$

and $\|h_t\| \le \delta^{(i+1)}$. Add this point to the set V and go to Step 3.

Step 10 Let i=i+1. Go to Step 0.

The second phase can be summarized by the following steps.

Phase 2

Step 0 Given the current iterate of the space mapping technique $\boldsymbol{x}_f^{(k)}$, the corresponding Jacobian matrix $\boldsymbol{J}_f^{(k)}$ and $\boldsymbol{f}^{(k)}$.

Step 1 Obtain a successful iterate $\boldsymbol{x}_f^{(k+1)}$ by solving

$$(\boldsymbol{J}_f^{(k)T}\boldsymbol{J}_f^{(k)} + \lambda \boldsymbol{I})\Delta \boldsymbol{x} = -\boldsymbol{J}_f^{(k)T}\boldsymbol{g}^{(k)}$$

for a suitable value of λ that satisfies the direct optimization success criterion.

Step 2 Update $\boldsymbol{J}_f^{(k)}$ to $\boldsymbol{J}_f^{(k+1)}$.

Step 3 Apply PE at $\boldsymbol{x}_f^{(k+1)}$ to get $\boldsymbol{f}^{(k+1)}$.

Step 4 If (5.23) is satisfied obtain $\boldsymbol{J}_c^{(k+1)}$ at the point $\boldsymbol{x}_c^{(k+1)} = \boldsymbol{P}(\boldsymbol{x}_f^{(k+1)})$, evaluate the matrix $\boldsymbol{B} = \left(\boldsymbol{J}_c^{(k+1)T}\boldsymbol{J}_c^{(k+1)}\right)^{-1}\boldsymbol{J}_c^{(k+1)T}\boldsymbol{J}_f^{(k+1)}$ and switch to the first phase.

Step 5 If the termination condition is satisfied invoke the minimax optimizer else set $k=k+1$ and go to Step 1.

A flowchart of the first phase of the HASM algorithm is shown in Fig. 5.4.

To ensure optimality, direct optimization is used to solve the original design problem using a minimax optimizer [12] starting from $\boldsymbol{x}_f^*$.

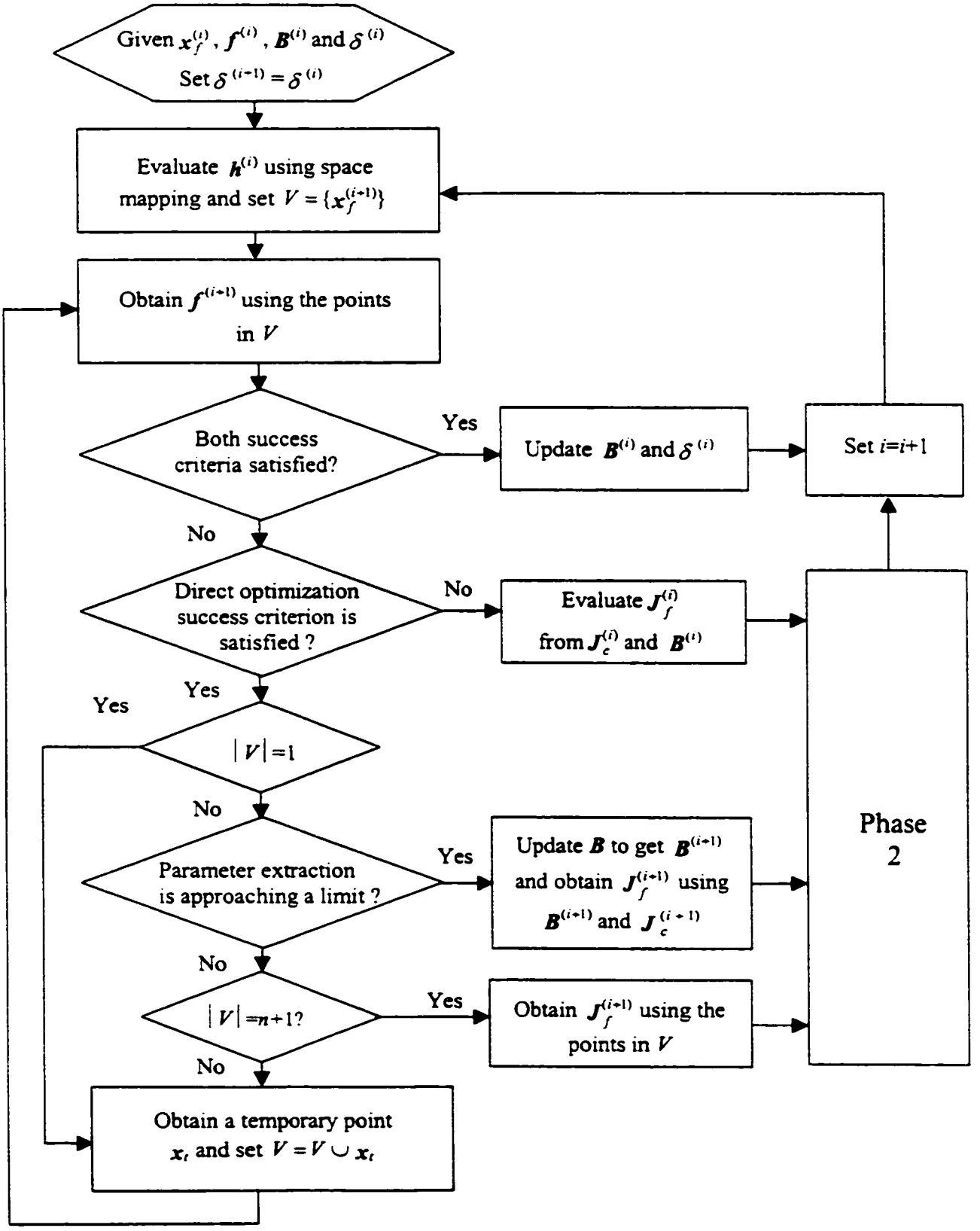

Fig. 5.4. A flowchart of the first phase of the HASM algorithm.

5.6 EXAMPLES

5.6.1 Three-Section Waveguide Transformer

We consider the design of a three-section waveguide transformer [79]. The design specifications are

$$VSWR \le 1.04 \text{ for } 5.7 \text{ GHz} \le \omega \le 7.2 \text{ GHz} \tag{5.24}$$

The designable parameters are the heights of the waveguide sections b_1, b_2 and b_3 and the lengths of waveguide sections L_1, L_2 and L_3. The fine model exploits HP HFSS ver. 5.2 through HP Empipe3D. The coarse analytical model does not take into account the junction discontinuity effects [79].

The vector $\boldsymbol{x}_c^*$ is taken as the initial fine model design (Fig. 5.5). The HASM algorithm switched to the second phase after two iterations of the first phase that required 4 fine model simulations. The response $\boldsymbol{R}'_f$ is shown in Fig. 5.6. The second phase carried out only one iteration which required 2 fine model simulations. The response $\boldsymbol{R}''_f$ is shown in Fig. 5.7.

Direct minimax optimization is then applied to the original design problem. The optimal fine model response $\boldsymbol{R}_f^*$ is shown in Fig. 5.8. Figs. 5.6 and 5.8 show that in this example $\boldsymbol{R}'_f$ is different from $\boldsymbol{R}_f^*$. The designs $\boldsymbol{x}_c^*, \boldsymbol{x}'_f, \boldsymbol{x}''_f$ and $\boldsymbol{x}_f^*$ are shown in Table 5.1.

5.6.2 Six-Section H-Plane Waveguide Filter

We consider a six-section H-plane waveguide filter [87, 88]. Design specifications are taken as

$$|S_{11}| \le 0.16 \text{ for } 5.4 \text{ GHz} \le \omega \le 9.0 \text{ GHz} \tag{5.25}$$

$$|S_{11}| \ge 0.85 \text{ for } \omega \le 5.2 \text{ GHz and } |S_{11}| \ge 0.5 \text{ for } 9.5 \text{ GHz} \le \omega \tag{5.26}$$

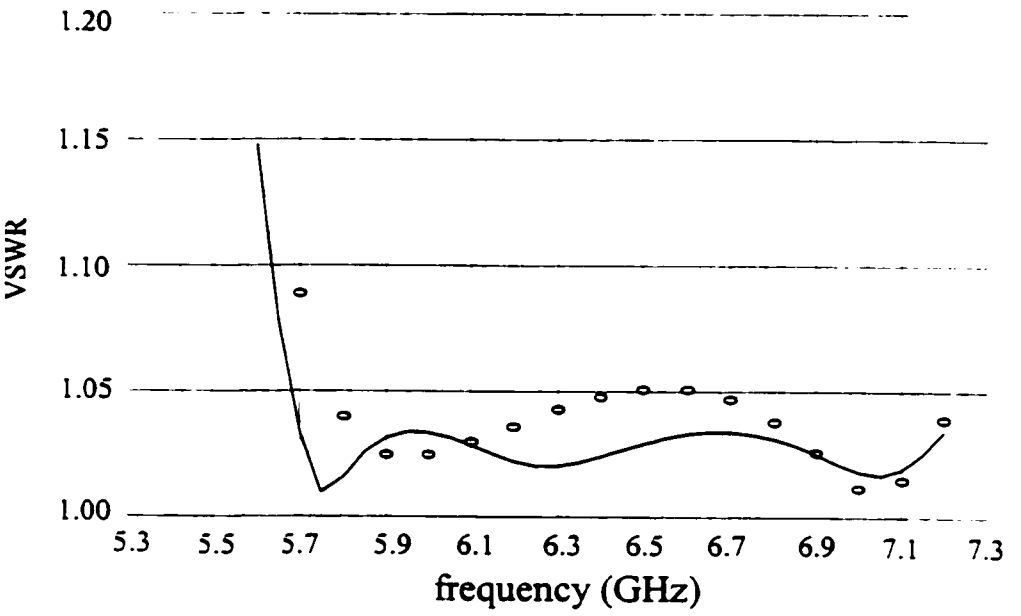

Fig. 5.5. The coarse response $\boldsymbol{R}_c^*$ (—) and the fine response $\boldsymbol{R}_f(\boldsymbol{x}_c^*)$ (o) for the three-section waveguide transformer.

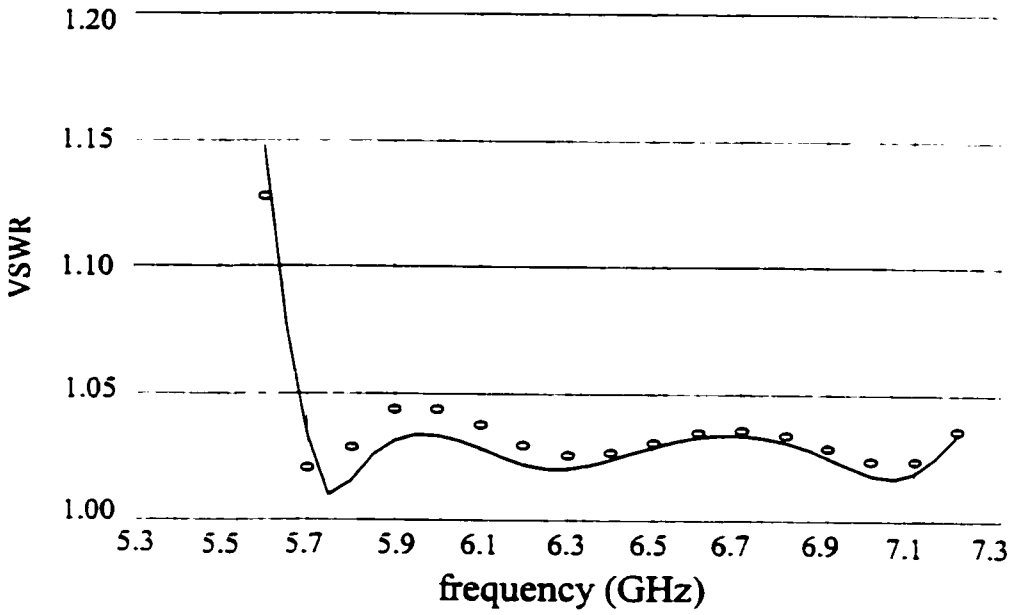

Fig. 5.6. The coarse response $\boldsymbol{R}_c^*$ (—) and the fine response $\boldsymbol{R}'_f$ (o) for the three-section waveguide transformer.

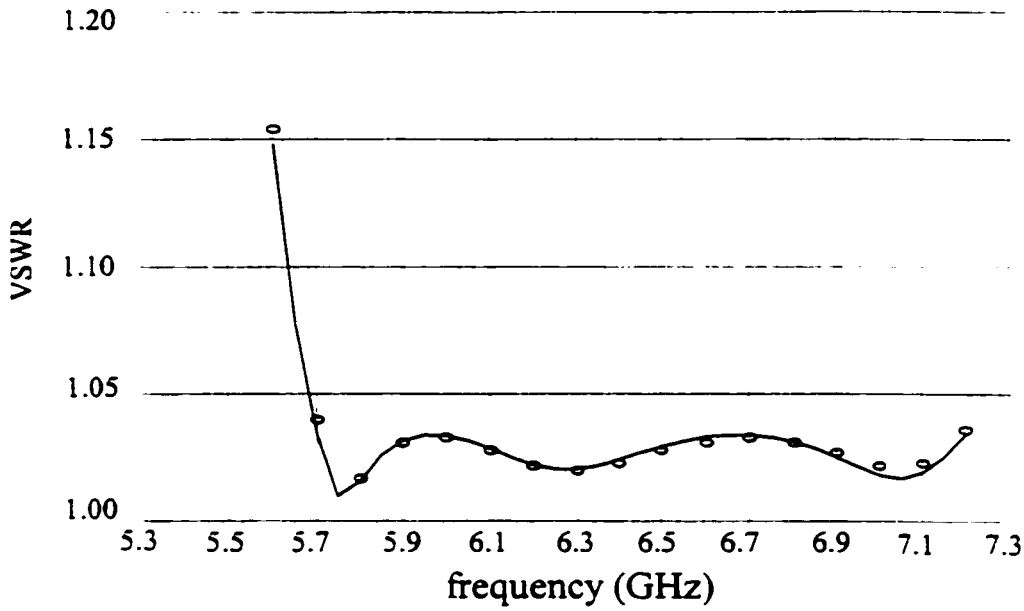

Fig. 5.7. The coarse response $\boldsymbol{R}_c^*$ (—) and the fine response $\boldsymbol{R}_f^*$ (o) for the three-section waveguide transformer.

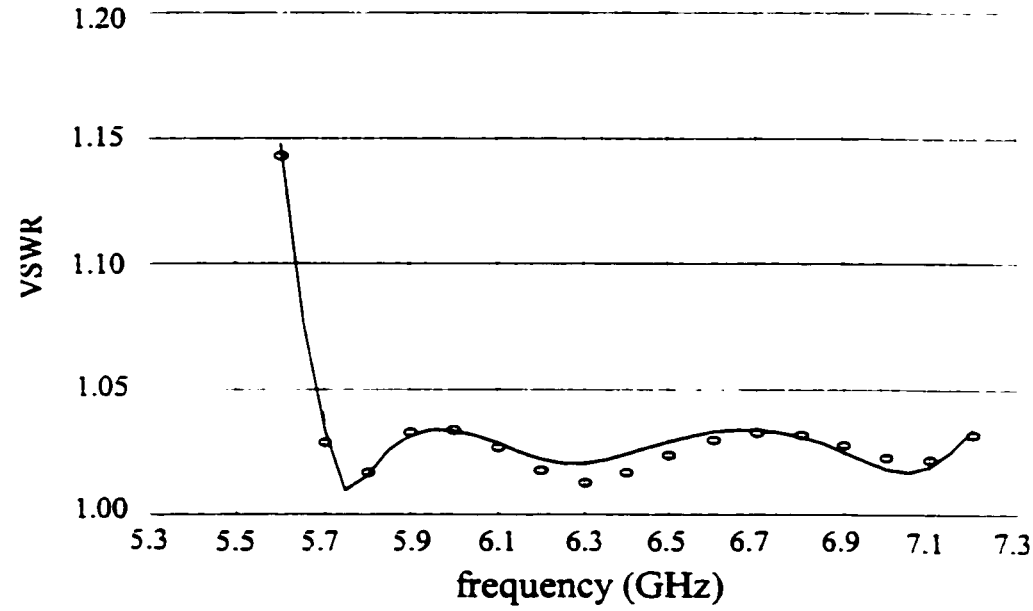

Fig. 5.8. The coarse response $\boldsymbol{R}_c^*$ (—) and the fine response $\boldsymbol{R}_f^*$ (o) for the three-section waveguide transformer.

TABLE 5.1
THE OPTIMAL COARSE MODEL DESIGN AND THE DESIGNS OBTAINED DURING DIFFERENT PHASES OF THE HASM ALGORITHM FOR THE THREE-SECTION WAVEGUIDE TRANSFORMER

Parameter	x_c^*	x_f'	x_f''	x_f^*
b_1	0.90318	0.90331	0.90114	0.90549
b_2	1.37093	1.36436	1.35687	1.35777
b_3	1.73609	1.73208	1.72470	1.71866
L_1	1.54879	1.46991	1.47203	1.47008
L_2	1.58375	1.56402	1.56521	1.57587
L_3	1.64590	1.79666	1.77744	1.78286

all values are in cm

A waveguide with a cross-section of 1.372 inches by 0.622 inches (3.485 cm by 1.58 cm) is used. The six sections are separated by seven H-plane septa, which have a finite thickness of 0.02 inches (0.508 mm). The filter is shown in Fig. 5.9.

The optimizable parameters are the four septa widths W_1, W_2, W_3 and W_4 and the three waveguide-section lengths L_1, L_2 and L_3. The coarse model consists of lumped inductances and dispersive transmission line sections. It is simulated using OSA90/hope. There are various approaches to calculate the equivalent inductive susceptance corresponding to an H-plane septum. We utilize a simplified version of a formula due to Marcuvitz [89] in evaluating the inductances. The coarse model is shown in Fig. 5.10. The fine model exploits HP HFSS ver. 5.2 through HP Empipe3D.

The fine model response at the starting point x_c^* is shown in Fig. 5.11. The first phase required 4 iterations to reach the design x'_f. A total of 5 fine model simulations were needed. The second phase did not carry out any successful iteration. The response R''_f is shown in Fig. 5.12.

The response R_f^* is obtained through direct minimax optimization (see Fig. 5.13). The different fine model designs are given in Table 5.2. It is clear that the convergence of the first phase is smooth as $R'_f \approx R_f^* \approx R_c^*$.

5.6.3 Seven-Section Waveguide Transformer

The design of a seven-section waveguide transformer is also considered. The transformer is shown in Fig. 5.14. This example is a classical microwave circuit design problem [79]. The fine model is simulated using HP HFSS ver. 5.2 through HP Empipe3D. The coarse model is an analytical model which neglects the junction discontinuity [79]. The design

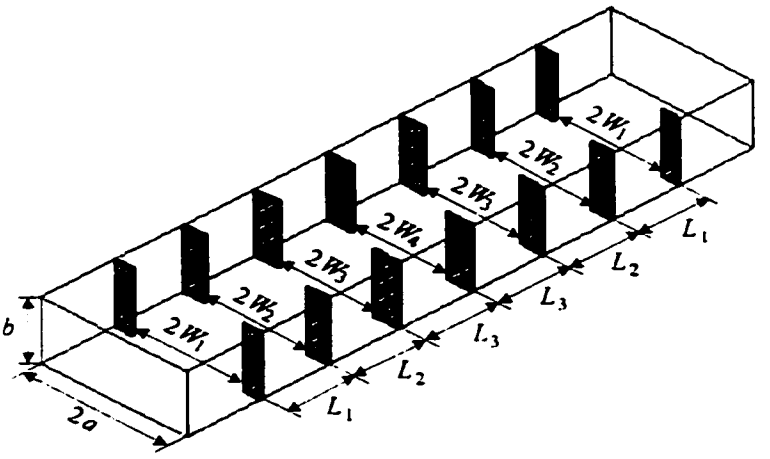

Fig. 5.9. The fine model of the six-section H-plane waveguide filter.

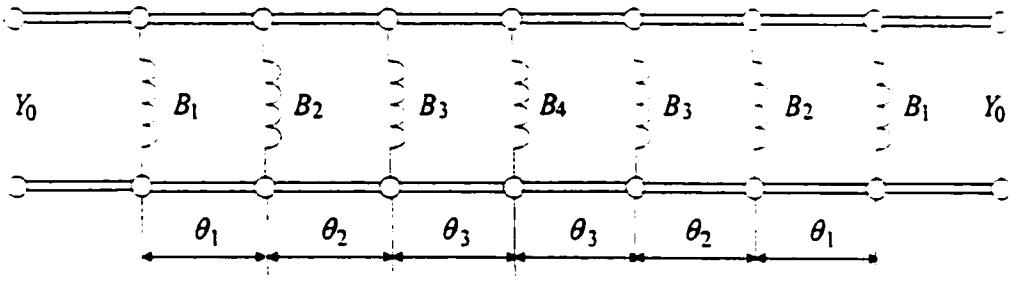

Fig. 5.10. The coarse model of the six-section H-plane waveguide filter.

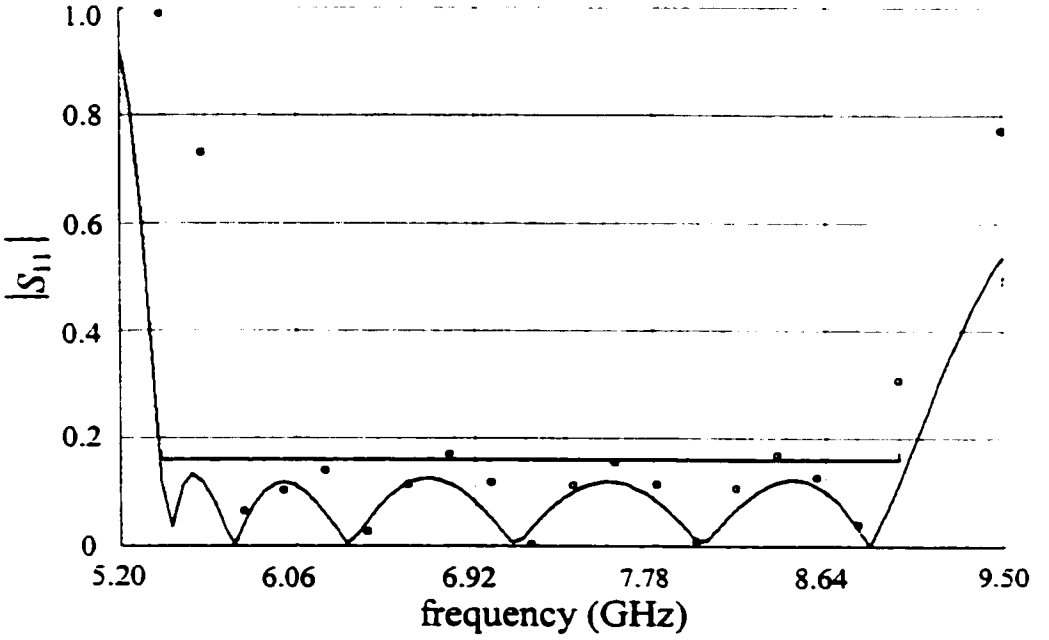

Fig. 5.11. The coarse response $\boldsymbol{R}_c^{\bullet}$ (—) and the fine response $\boldsymbol{R}_f(\boldsymbol{x}_c^{\bullet})$ (o) for the six-section H-plane waveguide filter.

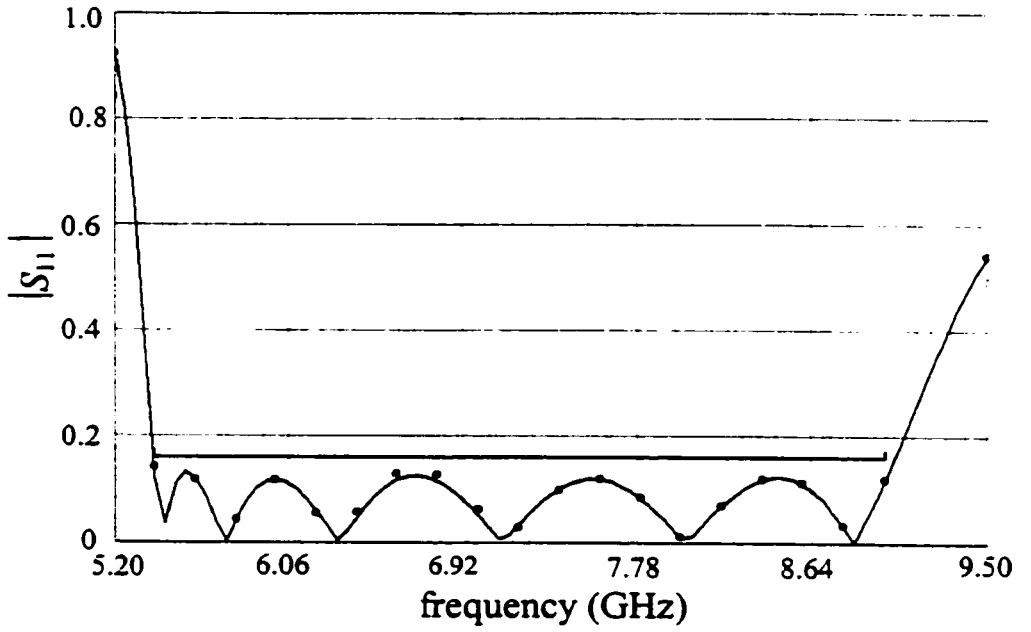

Fig. 5.12. The coarse response $\boldsymbol{R}_c^*$ (—) and the fine response $\boldsymbol{R}_f^*$ (o) for the six-section H-plane waveguide filter.

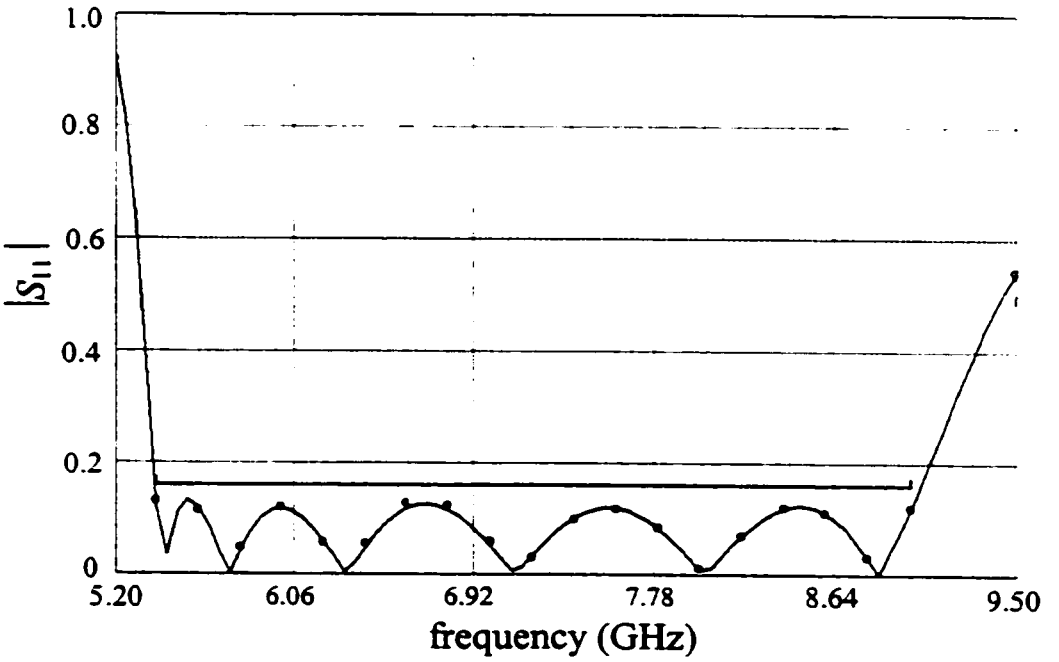

Fig. 5.13. The coarse response $\boldsymbol{R}_c^*$ (—) and the fine response $\boldsymbol{R}_f^*$ (o) for the six-section H-plane waveguide filter.

TABLE 5.2
THE OPTIMAL COARSE MODEL DESIGN, THE FINAL SPACE-MAPPED AND THE OPTIMAL FINE MODEL DESIGNS FOR THE SIX-SECTION H-PLANE WAVEGUIDE FILTER

Parameter	x_c^*	x'_f, x''_f	x_f^*
W_1	0.48583	0.51326	0.51344
W_2	0.43494	0.47379	0.47396
W_3	0.40433	0.45091	0.45100
W_4	0.39796	0.44675	0.44664
L_1	0.65585	0.63701	0.63695
L_2	0.65923	0.63954	0.63977
L_3	0.67666	0.65704	0.65694

all values are in inches

specifications are taken as

$$VSWR \leq 1.01 \text{ for } 1.06 \text{ GHz} \leq \omega \leq 1.8 \text{ GHz} \tag{5.27}$$

The designable parameters for this problem are the height and length of each waveguide section. The fine model response at x_c^* is shown in Fig. 5.15. The first phase executed three successful iterations that required six fine model simulations. The response R'_f is shown in Fig. 5.16. The second phase executed four iterations (see Fig. 5.17). The response R_f^* is shown in Fig. 5.18. Table 5.3 shows the different designs.

5.6.4 Double-Folded Stub Filter

We consider the design of the DFS microstrip structure. See Fig. 3.2. L_1, L_2 and S are chosen as optimization variables. W_1 and W_2 are fixed at 4.8 mil. The design specifications are

$$|S_{21}| \geq -3 \text{ dB for } \omega \leq 9.5 \text{ GHz and } 16.5 \text{ GHz} \leq \omega \tag{5.28}$$

$$|S_{21}| \leq -30 \text{ dB for } 12 \text{ GHz} \leq \omega \leq 14 \text{ GHz} \tag{5.29}$$

The fine model is the structure simulated by HP HFSS ver. 5.2 through HP Empipe3D. We utilize the coarse model used in Chapter 4. This coarse model is shown in Fig. 4.18.

The fine model response at x_c^* is shown in Fig. 5.19. This figure shows a big shift between the optimal coarse response and the initial fine response. This signals considerable misalignment between the two models.

The first phase successfully carried out eight iterations that required twelve fine model simulations. The response R'_f is shown in Fig. 5.20. The mapping established in the first phase is utilized to get a good estimate of J_f and a switch to the second phase is carried out. The

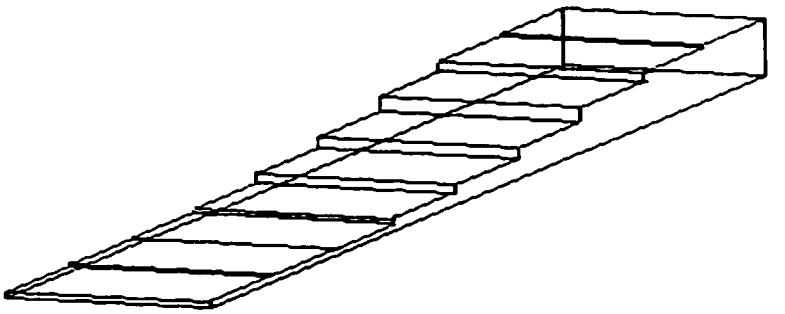

Fig. 5.14. The seven-section waveguide transformer.

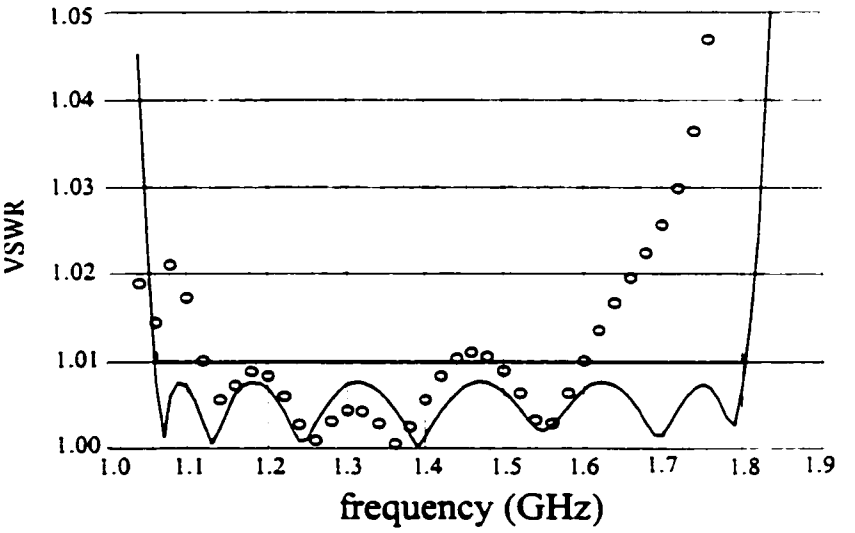

Fig. 5.15. The coarse response $\boldsymbol{R}_c^*$ (—) and the fine response $\boldsymbol{R}_f(\boldsymbol{x}_c^*)$ (o) for the seven-section waveguide transformer.

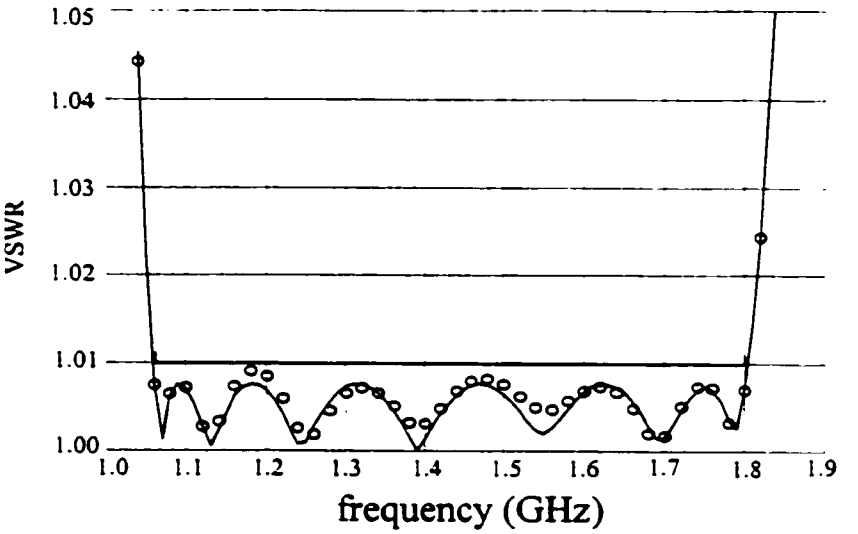

Fig. 5.16. The coarse response $\boldsymbol{R}_c^{\bullet}$ (—) and the fine response $\boldsymbol{R}'_f$ (o) for the seven-section waveguide transformer.

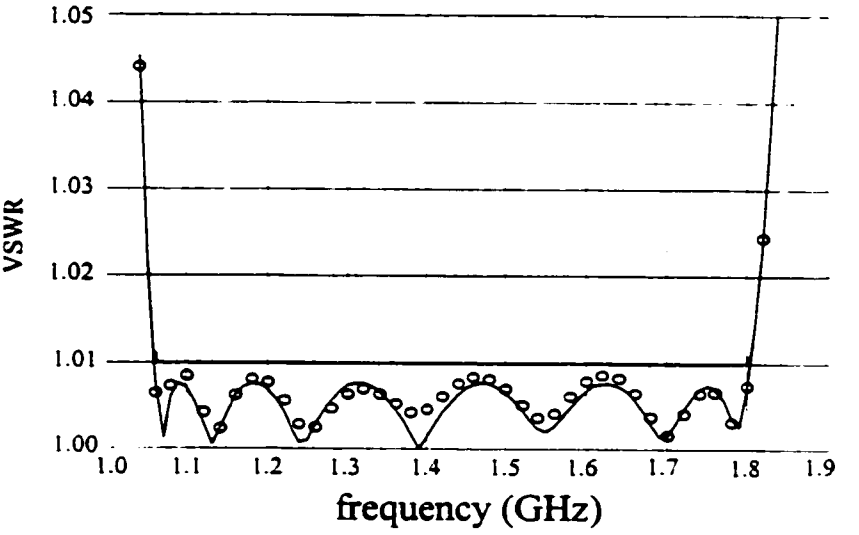

Fig. 5.17. The coarse response $\boldsymbol{R}_c^{\bullet}$ (—) and the fine response $\boldsymbol{R}''_f$ (o) for the seven-section waveguide transformer.

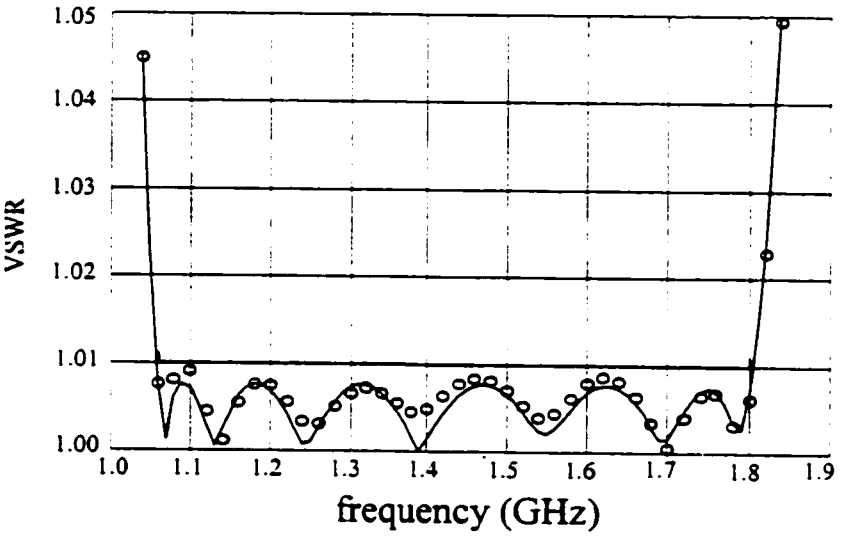

Fig. 5.18. The coarse response $\boldsymbol{R}_c^*$ (—) and the fine response $\boldsymbol{R}_f^*$ (o) for the seven-section waveguide transformer.

TABLE 5.3
THE OPTIMAL COARSE MODEL DESIGN AND THE DESIGNS OBTAINED DURING DIFFERENT PHASES OF THE HASM ALGORITHM FOR THE SEVEN-SECTION WAVEGUIDE TRANSFORMER

Parameter	x_c^*	x_f'	x_f''	x_f^*
b_1	7.86732	7.84126	7.84321	7.84319
b_2	6.61888	6.56661	6.56753	6.56746
b_3	4.68540	4.63369	4.63275	4.63267
b_4	2.91987	2.88266	2.88266	2.88268
b_5	1.81412	1.79307	1.79273	1.79272
b_6	1.27658	1.26697	1.26721	1.26723
b_7	1.06847	1.06475	1.06477	1.06474
L_1	7.10588	7.27059	7.27141	7.27145
L_2	7.12201	7.03866	7.04043	7.04047
L_3	7.11760	6.89568	6.89549	6.89552
L_4	7.12331	6.89253	6.89192	6.89189
L_5	7.12815	6.98273	6.97985	6.98000
L_6	7.12154	7.03160	7.03020	7.03023
L_7	7.12945	7.02606	7.02503	7.02509

all values are in cm

TABLE 5.4
THE OPTIMAL COARSE MODEL DESIGN, THE FINAL SPACE-MAPPED AND THE OPTIMAL FINE MODEL DESIGNS FOR THE DFS FILTER

Parameter	x_c^*	x_f'	x_f''	x_f^*
L_1	66.727	72.454	73.869	78.964
L_2	60.228	72.728	82.939	81.210
S	9.592	7.621	8.170	7.901

all values are in mil

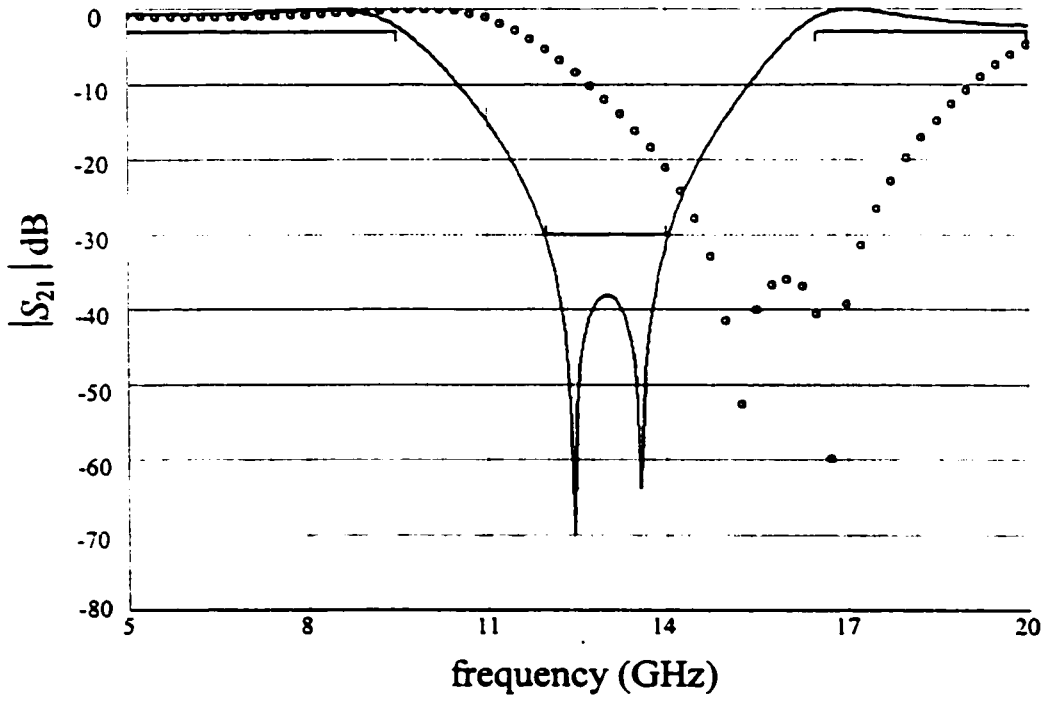

Fig. 5.19. The coarse response $\boldsymbol{R}_c^*$ (—) and the fine response $\boldsymbol{R}_f(\boldsymbol{x}_c^*)$ (o) for the DFS filter.

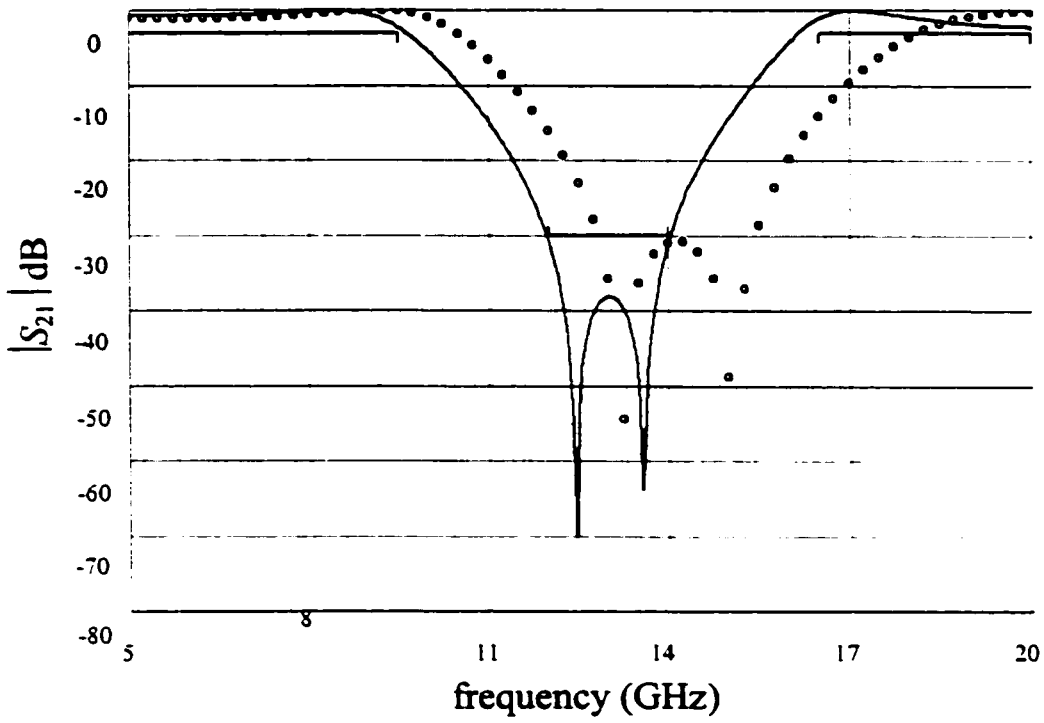

Fig. 5.20. The coarse response $\boldsymbol{R}_c^*$ (—) and the fine response $\boldsymbol{R}'_f$ (o) for the DFS filter.

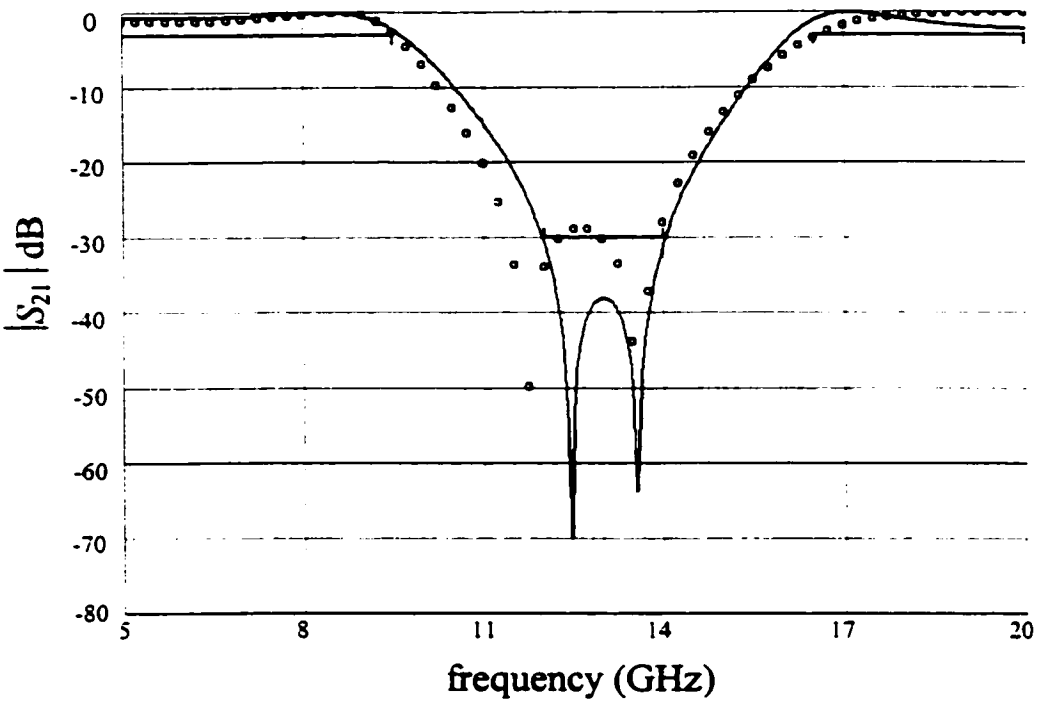

Fig. 5.21. The coarse response R_c^* (—) and the fine response R^*_f (o) for the DFS filter.

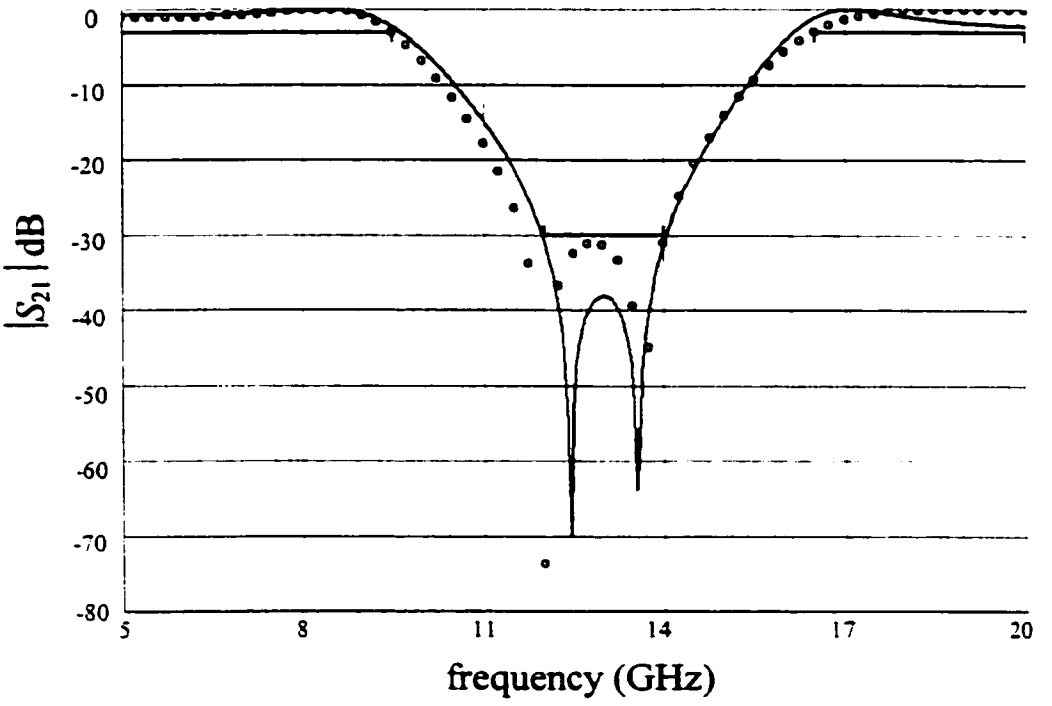

Fig. 5.22. The coarse response R_c^* (—) and the fine response R_f^* (o) for the DFS filter.

response R^*_f (Fig. 5.21) shows a significant improvement in the response. The design x^*_f is then taken as the starting point for the minimax optimizer. The response R^*_f is shown in Fig. 5.22. The designs are given in Table 5.4.

5.7 CONCLUSIONS

In this chapter, we present the Hybrid Aggressive Space Mapping (HASM) optimization algorithm. The algorithm is designed to handle severely misaligned cases. It enables switching from SM optimization to direct optimization if SM fails. The direct optimization phase utilizes all the available information accumulated by SM optimization about the mapping between the coarse and fine model spaces. The algorithm also enables switching back from direct optimization to space mapping if SM is converging. The connection between SM and direct optimization is based on a lemma that relates the mapping and the derivatives of the coarse and fine model responses. An original approach for the prediction of the starting point of the parameter extraction optimization problem is also utilized. This approach improves the uniqueness of the extraction step and consequently enhances the convergence of the algorithm. The algorithm is successfully demonstrated through the design of waveguide transformers and filters.

6

SURROGATE MODEL-BASED SPACE MAPPING OPTIMIZATION

6.1 INTRODUCTION

In this chapter, we present a Surrogate Model-based-Space Mapping (SMSM) algorithm [43, 44] for microwave circuit optimization. It integrates two distinct optimization approaches: SM optimization and surrogate-based optimization [45-49]. Both approaches aim at efficiently optimizing an accurate and time-intensive model, e.g., a full-wave Electromagnetic (EM) simulator. SM exploits the existence of a less accurate but fast coarse model. It formulates the design problem as a system of nonlinear equations. On the other hand, surrogate-based optimization exploits an approximate model in iteratively solving the original design problem. This model may be a less accurate physically-based model or algebraic model [47].

Our SMSM algorithm combines both approaches. The original design problem is solved using a surrogate model. This model is a convex combination of a mapped coarse model and a linearized fine model. The accuracy of the surrogate model is improved in every iteration using the generated fine model simulations.

Recent developments in Space Mapping-based Neuromodeling (SMN) [50] and Generalized Space Mapping (GSM) modeling [51] exploit frequency-sensitive mappings. This approach is reported to improve the accuracy of SM-based models. SMSM exploits this concept in constructing the mapped coarse model. Here, the coarse and fine models are simulated

at different sets of frequencies. This approach handles significant response shifts efficiently.

A number of examples are successfully solved. They include a Rosenbrock example, a capacitively-loaded two-section 10:1 impedance transformer [83], a DFS filter and an HTS filter.

6.2 SPACE MAPPING OPTIMIZATION VS. SURROGATE-BASED OPTIMIZATION

We denote the fine model responses at a point $\boldsymbol{x}_f \in \Re^{n\times 1}$ and frequency ω by $\boldsymbol{R}_f(\boldsymbol{x}_f, \omega) \in \Re^{N_r\times 1}$. These responses may include the real and imaginary parts of S_{11}, etc. The response vector $\boldsymbol{R}_f \in \Re^{m\times 1}$ denotes the responses at all N_ω simulation frequencies where $m=N_r N_\omega$. The original design problem is

$$\boldsymbol{x}_f^* = arg\left\{ \min_{\boldsymbol{x}_f} U(\boldsymbol{R}_f(\boldsymbol{x}_f)) \right\} \tag{6.1}$$

where U is the objective function and $\boldsymbol{x}_f^*$ is the optimal fine model design. Solving (6.1) using direct optimization methods, e.g. [12], is prohibitive due to the intensive simulation time of the fine model.

SM optimization exploits the existence of a fast but less accurate coarse model of the circuit. The first step in SM-based optimization algorithms is to obtain the optimal coarse model design $\boldsymbol{x}_c^*$. SM optimization obtains a space-mapped design $\overline{\boldsymbol{x}}_f$ whose response matches $\boldsymbol{R}_c^*$. $\overline{\boldsymbol{x}}_f$ is a solution of the nonlinear system of equations (2.29)

The previously discussed SM-based optimization algorithms solve (2.29) iteratively. ASM predicts a new iterate $\boldsymbol{x}_f^{(i+1)} = \boldsymbol{x}_f^{(i)} + \boldsymbol{h}^{(i)}$ by utilizing the quasi-Newton iteration (2.31). The TRASM algorithm minimizes $\left\| \boldsymbol{f}(\boldsymbol{x}_f^{(i+1)}) \right\|$ using least squares within a trust region. The ith

iteration of the algorithm is given by (3.7). The new iterates are accepted only if they are descent directions for $\|f^{(i)}\|$. The HASM algorithm addresses the problem of a poor coarse model. It utilizes a two phase algorithm. The first phase exploits a TRASM strategy. The second phase minimizes $\|R_f(x_f)-R_c^*\|_2$ through direct least-squares optimization.

Alternatively, an expensive model can be optimized indirectly by using a surrogate model [45-49]. This surrogate model may be a less accurate physics-based model or a polynomial approximation of the fine model. We denote the surrogate model in the ith iteration by $R_s^{(i)}(x_f) \in \Re^{m\times 1}$. The step taken is obtained by solving

$$h^{(i)} = arg\left\{ \min_{h^{(i)}} U(R_s^{(i)}(x_f^{(i)} + h^{(i)})) \right\}, \|h^{(i)}\| \le \delta^{(i)} \tag{6.2}$$

where $U(R_s^{(i)}(x_f^{(i)} + h^{(i)}))$ is the value of the objective function evaluated using the surrogate model at the point $x_f^{(i)} + h^{(i)}$. The point $x_f^{(i)} + h^{(i)}$ is then validated using fine model simulation. It is accepted if it improves the fine model objective function. Otherwise, the accuracy of $R_s^{(i)}(x_f)$ should be improved. Different strategies can be utilized for improving the surrogate model accuracy. One strategy utilizes only the validation fine model simulations. Additional fine simulations may be generated to improve the surrogate model in certain directions of the parameter space.

6.3 THE SURROGATE MODEL

In the ith iteration, the SMSM algorithm utilizes a surrogate model expressed as a convex combination between a Linearized Fine Model (LFM) and a Mapped Coarse Model (MCM) $R_m^{(i)}(x_f)$. It is given by

$$\boldsymbol{R}_s^{(i)}(\boldsymbol{x}_f) = \eta^{(i)}\,\boldsymbol{R}_m^{(i)}(\boldsymbol{x}_f) + (1-\eta^{(i)})(\boldsymbol{R}_f(\boldsymbol{x}_f^{(i)}) + \boldsymbol{J}_f^{(i)}\Delta\boldsymbol{x}_f),\ \eta^{(i)} \in [0,1] \tag{6.3}$$

$\boldsymbol{J}_f^{(i)} \in \Re^{m\times n}$ is an approximation to the Jacobian of fine model responses at $\boldsymbol{x}_f^{(i)}$. The parameter $\eta^{(i)}$ determines which model is favored. If $\eta^{(i)}=1$, the surrogate model becomes a MCM. If $\eta^{(i)}=0$, the surrogate model becomes a LFM. $\forall\eta^{(i)} \in (0,1)$, the surrogate model exploits both approximations. The LFM part in (6.3) ensures that the algorithm will work if the coarse model is poor or even wrong.

The MCM $\boldsymbol{R}_m^{(i)}(\boldsymbol{x}_f)$ utilizes the linear frequency-space mapping

$$\boldsymbol{R}_f(\boldsymbol{x}_f,\omega_j) \approx \boldsymbol{R}_m^{(i)}(\boldsymbol{x}_f,\omega_j) = \boldsymbol{R}_c(\boldsymbol{P}^{(i)}(\boldsymbol{x}_f,\omega_j), P_\omega^{(i)}(\boldsymbol{x}_f,\omega_j)),\ j=1, 2, \ldots, N_\omega \tag{6.4}$$

where

$$\begin{bmatrix}\boldsymbol{P}^{(i)}(\boldsymbol{x}_f,\omega_j)\\ P_\omega^{(i)}(\boldsymbol{x}_f,\omega_j)\end{bmatrix} = \begin{bmatrix}\boldsymbol{B}^{(i)} & \boldsymbol{s}^{(i)}\\ \boldsymbol{t}^{(i)T} & \sigma^{(i)}\end{bmatrix}\begin{bmatrix}\Delta\boldsymbol{x}_f\\ \omega_j\end{bmatrix} + \begin{bmatrix}\boldsymbol{c}^{(i)}\\ \gamma^{(i)}\end{bmatrix}, \tag{6.5}$$

and $\Delta\boldsymbol{x}_f = \boldsymbol{x}_f - \boldsymbol{x}_f^{(i)}$. The parameters $\boldsymbol{B}^{(i)} \in \Re^{n\times n}$, $\boldsymbol{s}^{(i)} \in \Re^{n\times 1}$, $\boldsymbol{t}^{(i)} \in \Re^{n\times 1}$, $\boldsymbol{c}^{(i)} \in \Re^{n\times 1}$, $\sigma^{(i)} \in \Re^{1\times 1}$ and $\gamma^{(i)} \in \Re^{1\times 1}$ are the mapping parameters. ω_j is the jth simulation frequency, j=1, 2, ..., N_ω. Here, a fine model point $\boldsymbol{x}_f$ and frequency ω_j correspond to a coarse model point $\boldsymbol{P}^{(i)}(\boldsymbol{x}_f,\omega_j)$ and coarse model frequency $P_\omega^{(i)}(\boldsymbol{x}_f,\omega_j)$. Notice that (6.5) defaults to the frequency-insensitive mapping utilized by the ASM, TRASM and HASM algorithms if $\boldsymbol{s}^{(i)} = \boldsymbol{t}^{(i)} = \boldsymbol{0}$, $\sigma^{(i)}=1$ and $\gamma^{(i)}=0$.

The advantage of utilizing (6.5) is illustrated by Fig. 6.1 for a single response case. It is required to extract the coarse point $\boldsymbol{x}_c$ corresponding to a given fine point $\boldsymbol{x}_f$. Previous SM-based algorithms utilize the PE procedure

$$x_c = arg\left\{ \min_{x_c} \left\| R_f(x_f) - R_c(x_c) \right\| \right\} \tag{6.6}$$

Fig. 6.1(a) shows also the coarse model response at the starting point for (6.6). The PE optimizer may not have enough information to align the almost disjoint responses. However, the responses could align perfectly if a frequency transformation $\omega_c = P_\omega(\omega)$ is applied to the coarse model frequency axis. This implies that the two models are simulated over different frequency ranges. Fig. 6.1(b) illustrates possible aligned results. It follows that (6.5) allows another degree of freedom in aligning the coarse and fine models.

The mapping parameters in (6.5) are obtained such that the MCM approximates the fine model over a region of fine model parameters and frequency. They are obtained through the optimization procedure

$$[B^{(i)}, s^{(i)}, t^{(i)}, \sigma^{(i)}, c^{(i)}, \gamma^{(i)}] = arg\left\{ \min_{B, s, t, \sigma, c, \gamma} \left\| \begin{bmatrix} e_1^T & e_2^T & \cdots & e_{N_p}^T \end{bmatrix}^T \right\| \right\} \tag{6.7}$$

$$e_k = R_m(x_f^{(k)}) - R_f(x_f^{(k)}) \;\; \forall\, x_f^{(k)} \in V^{(i)}, \tag{6.8}$$

where $V^{(i)}$ is a set of fine model points whose cardinality is $|V^{(i)}| = N_p$ and $e_k \in \Re^{m\times 1}$. The set $V^{(i)}$ is constructed through an iterative process. Initially, we set $V^{(i)} = \{x_f^{(i)}\}$. The two conditions

$$\frac{(x_f - x_f^{(i)})^T (x_f^{(k)} - x_f^{(i)})}{\|(x_f - x_f^{(i)})\| \|x_f^{(k)} - x_f^{(i)}\|} \le 1 - \varepsilon \;\; \forall\, x_f^{(k)} \in V^{(i)} \text{ and } \; 0 < \|x_f - x_f^{(i)}\| < \delta_e \tag{6.9}$$

are checked $\forall\, x_f \in S_f^{(i)}$, the set of simulated fine model points up to the ith iteration. The

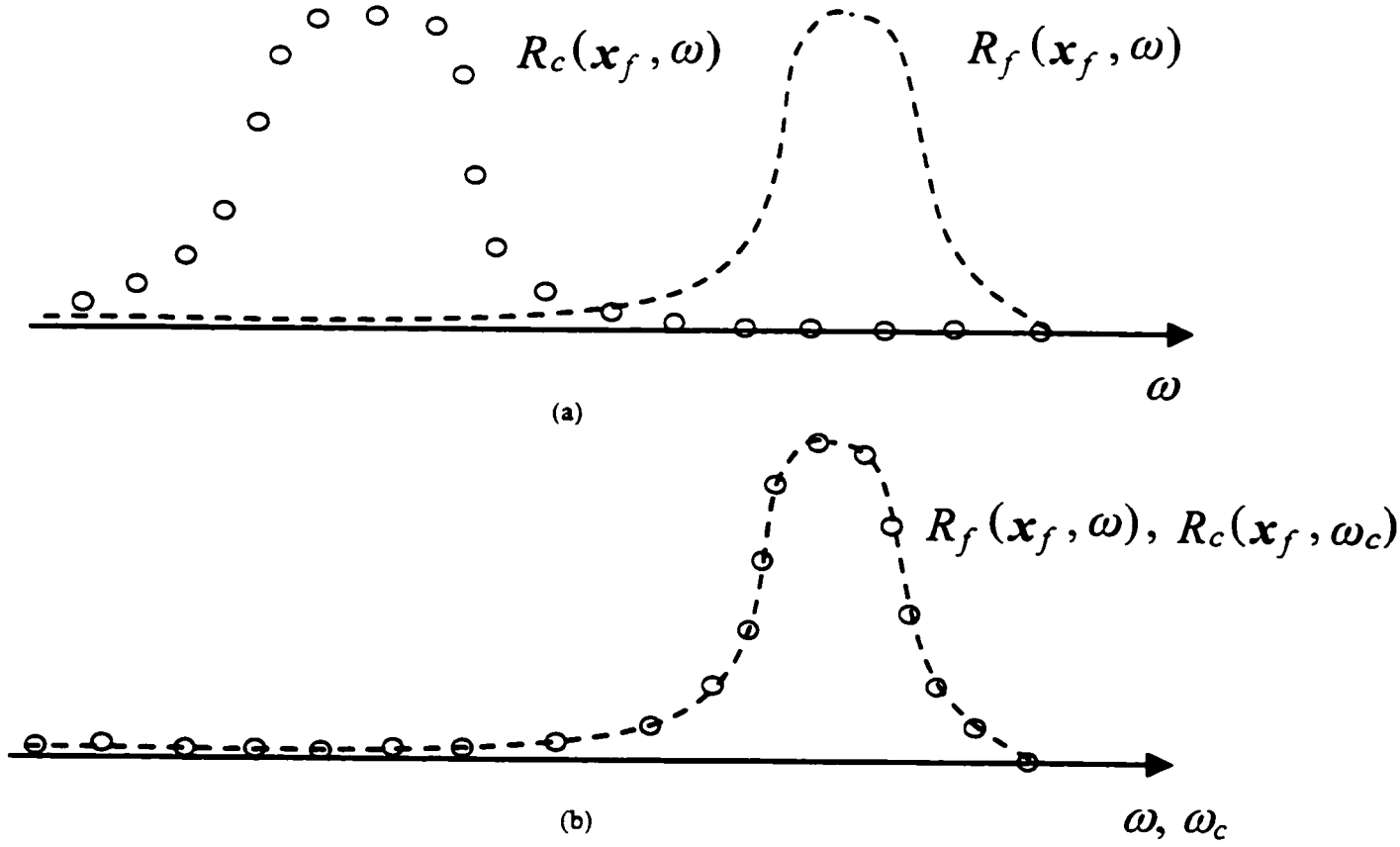

Fig. 6.1. Illustration of the frequency-sensitive mapping concept: (a) a significant frequency band shift exists between fine and coarse model responses at the initial iteration and (b) the coarse model frequency is transformed such that both responses match.

first condition ensures better coverage by the points in $V^{(i)}$. The second condition rejects points outside an δ_e neighborhood of $x_f^{(i)}$. We denote δ_e as the extraction radius.

If the (i-1)th iteration is unsuccessful, the coarse model approximation should be improved. This is important to guarantee a successful iteration in the ith iteration. However, no improvement is possible if (6.9) results in $V^{(i)} = V^{(i-1)}$. In this case, an additional perturbation Δx is generated by the algorithm. Δx is obtained by solving

$$\Delta x = arg\left\{ \min_{\Delta x \in S_v} \max_{x_f^{(k)} \in V^{(i)}} \frac{\Delta x^T \left(x_f^{(k)} - x_f^{(i)} \right)}{\|\Delta x\| \left\| x_f^{(k)} - x_f^{(i)} \right\|} \right\} \tag{6.10}$$

where

$$S_v = \left\{ \pm \delta_e \frac{v^{(i)}}{\|v^{(i)}\|} \middle| J_f^{(i)T} J_f^{(i)} v^{(i)} = \tau^{(i)} v^{(i)} \text{ and } \tau^{(i)} > 0 \right\} \tag{6.11}$$

The point $x_f^{(i)} + \Delta x$ is then added to $V^{(i)}$. The APE algorithm, discussed in Chapter 4, adopted a similar approach in generating new perturbations. The construction of $V^{(i)}$ is illustrated in Fig. 6.2.

6.4 THE SMSM ALGORITHM

The ith iteration of the algorithm proceeds as follows. First, the set $V^{(i)}$ is constructed. The mapping parameters are then estimated using the optimization procedure (6.7)-(6.8). The suggested step $h^{(i)}$ is obtained by solving (6.2), where the surrogate model is given by (6.3). Notice that (6.2) utilizes only coarse model simulations and can be solved using traditional optimization methods.

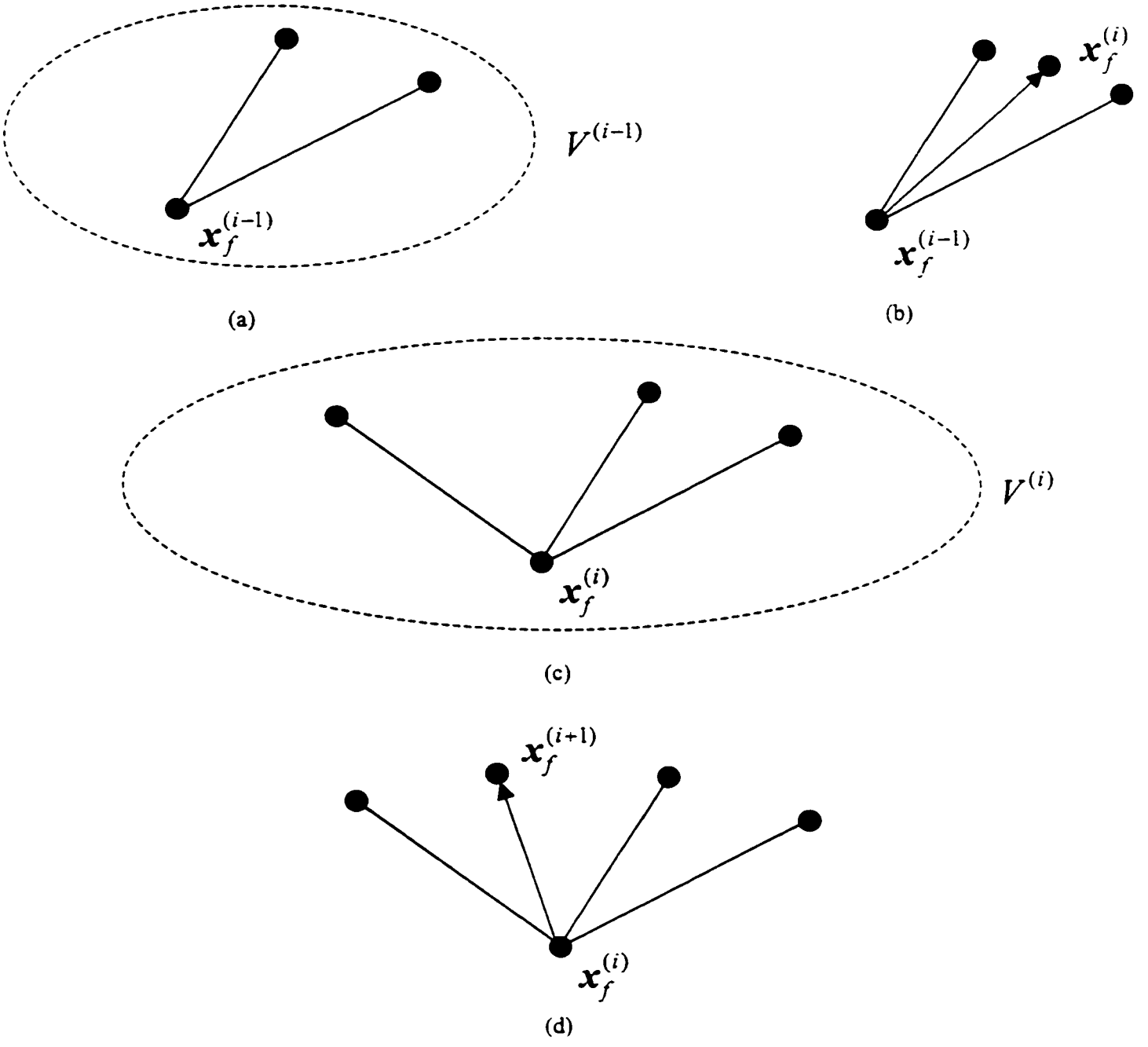

Fig. 6.2. Illustration of the selection of the parameter extraction points; (a) in the $(i-1)$th iteration, we have the point $x_f^{(i-1)}$ and the set $V^{(i-1)}$, (b) a new point is generated by the algorithm that does not satisfy the success criterion, (c) $x_f^{(i-1)}$ becomes $x_f^{(i)}$, the previous perturbation $h^{(i)}$ is excluded from $V^{(i)}$ and the algorithm generates an alternative perturbation and (d) the set $V^{(i)}$ is used to extract new mapping parameters and predict a successful iterate.

If the response $\boldsymbol{R}_c^*$ is good enough, we may be satisfied with a design for which $\boldsymbol{R}_f(\boldsymbol{x}_f) \approx \boldsymbol{R}_c^*$. In this case, we select U as $\|\boldsymbol{R}_f(\boldsymbol{x}_f) - \boldsymbol{R}_c^*\|$. However, if the optimality of the design is the main concern, U may be selected as the generalized minimax objective function [12].

$\boldsymbol{h}^{(i)}$ is accepted if it improves the objective function. Otherwise, it is rejected. The parameters $\boldsymbol{J}_f^{(i)}$, $\delta^{(i)}$ and $\eta^{(i)}$ are updated in every iteration. Broyden's formula [6] is used to update $\boldsymbol{J}_f^{(i)}$. Initially, we set $\boldsymbol{J}_f^{(1)} = \boldsymbol{J}_c^*$, the Jacobian of the coarse model response at $\boldsymbol{x}_c^*$. The trust region $\delta^{(i)}$ is updated based on the ratio between the actual reduction r_a in U and the predicted reduction r_p. The ratio

$$\rho = \frac{r_a}{r_p} = \frac{U(\boldsymbol{R}_f(\boldsymbol{x}_f^{(i)})) - U(\boldsymbol{R}_f(\boldsymbol{x}_f^{(i)} + \boldsymbol{h}^{(i)}))}{U(\boldsymbol{R}_s^{(i)}(\boldsymbol{x}_f^{(i)})) - U(\boldsymbol{R}_s^{(i)}(\boldsymbol{x}_f^{(i)} + \boldsymbol{h}^{(i)}))} \tag{6.12}$$

is thus evaluated at the end of each iteration. If $\rho \geq 0.75$, the surrogate model has good accuracy and we set $\delta^{(i+1)} = \pi_1 \delta^{(i)}$, $\pi_1 > 1.0$. If $\rho \leq 0.10$, we set $\delta^{(i+1)} = \pi_2 \delta^{(i)}$, $0 < \pi_2 < 1.0$. Otherwise, we set $\delta^{(i+1)} = \delta^{(i)}$. $\eta^{(i)}$ is updated to favor the more accurate model, either the LFM or the MCM. It is initialized by $\eta^{(1)} = 1$. The utilized update is

$$\eta^{(i+1)} = \frac{\|\boldsymbol{E}_l^{(i)}\|}{\|\boldsymbol{E}_l^{(i)}\| + \|\boldsymbol{E}_m^{(i)}\|} \tag{6.13}$$

where $\boldsymbol{E}_m^{(i)} = \boldsymbol{R}_m^{(i)}(\boldsymbol{x}_f^{(i)} + \boldsymbol{h}^{(i)}) - \boldsymbol{R}_f(\boldsymbol{x}_f^{(i)} + \boldsymbol{h}^{(i)})$ and $\boldsymbol{E}_l^{(i)} = \boldsymbol{R}_f(\boldsymbol{x}_f^{(i)}) + \boldsymbol{J}_f^{(i)} \boldsymbol{h}^{(i)} - \boldsymbol{R}_f(\boldsymbol{x}_f^{(i)} + \boldsymbol{h}^{(i)})$ define the prediction error using the MCM and the LFM, respectively. The SMSM algorithm terminates if n+1 consecutive unsuccessful iterations are carried out or if $\|\boldsymbol{h}^{(i)}\|$ becomes sufficiently small. Fig. 6.3 illustrates one iteration of the algorithm.

Our SMSM algorithm can be summarized by the following steps.

Step 1 Given $\boldsymbol{x}_f^{(1)} = \boldsymbol{x}_c^*$, $\eta^{(1)} = 1$, $\delta^{(1)}$, δ_e, $\boldsymbol{J}_f^{(1)} = \boldsymbol{J}_c^*$ and i=1.

Step 2 Construct $V^{(i)}$.

Step 3 Apply the optimization procedure (6.7)-(6.8) to obtain the mapping parameters.

Step 4 Obtain the suggested step $\boldsymbol{h}^{(i)}$ by solving (6.2).

Step 5 If $U(\boldsymbol{R}_f(\boldsymbol{x}_f^{(i)} + \boldsymbol{h}^{(i)})) < U(\boldsymbol{R}_f(\boldsymbol{x}_f^{(i)}))$, set $\boldsymbol{x}_f^{(i+1)} = \boldsymbol{x}_f^{(i)} + \boldsymbol{h}^{(i)}$ else $\boldsymbol{x}_f^{(i+1)} = \boldsymbol{x}_f^{(i)}$.

Step 6 Update $\boldsymbol{J}_f^{(i)}$, $\delta^{(i)}$ and $\eta^{(i)}$.

Step 7 If the stopping criterion is satisfied stop.

Step 8 Set i=i+1 and go to step 2.

A flowchart of the algorithm is shown in Fig. 6.4.

6.5 EXAMPLES

6.5.1 The Rosenbrock Example

We applied the SMSM algorithm to the Rosenbrock function [82]. This analytic example is frequently used as a test example for optimization algorithms. The coarse model is selected as

$$R_c = 100\left(x_{c.2} - x_{c.1}^2\right)^2 + \left(1 - x_{c.1}\right)^2 \tag{6.14}$$

An affine transformation of parameters is utilized in the fine model. This model is given by

$$R_f(\boldsymbol{x}_f) = R_c(\boldsymbol{x}_c), \quad \begin{bmatrix} x_{c.1} \\ x_{c.2} \end{bmatrix} = \begin{bmatrix} 1.1 & -0.2 \\ 0.2 & 0.9 \end{bmatrix} \begin{bmatrix} x_{f.1} \\ x_{f.2} \end{bmatrix} - \begin{bmatrix} -0.3 \\ 0.3 \end{bmatrix} \tag{6.15}$$

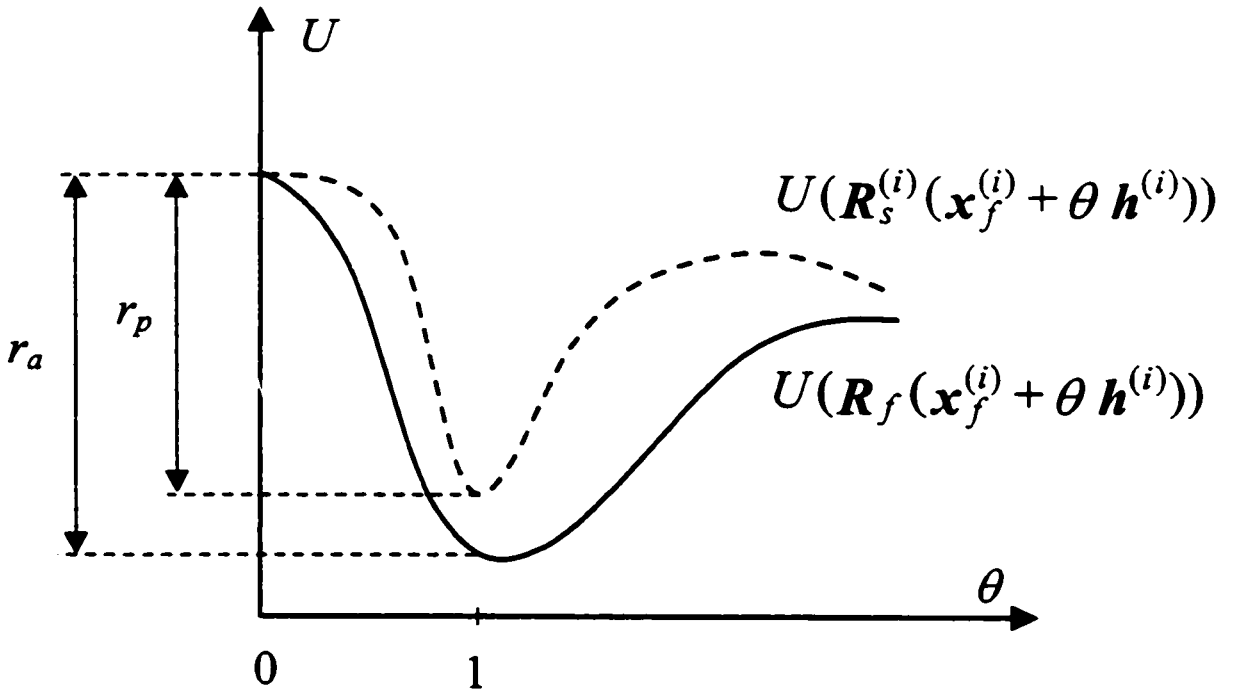

Fig. 6.3. Illustration of the ith iteration of the SMSM algorithm.

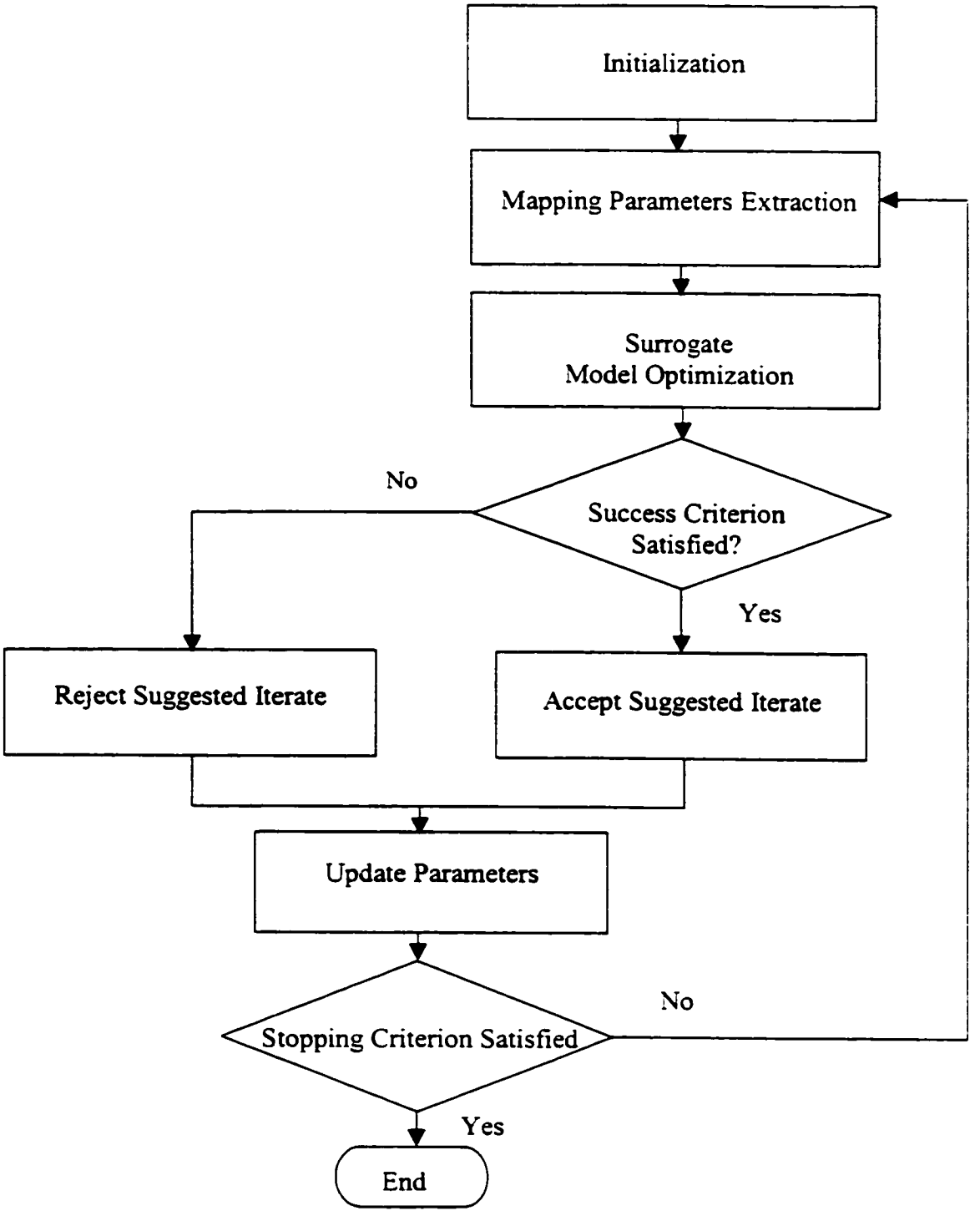

Fig. 6.4 A flowchart of the SMSM algorithm.

The target of the optimization process is to minimize R_f. The contours of U for both models are shown in Figs 6.5 and 6.6. We assume that R_f corresponds to zero "frequency". The algorithm executed eight iterations. Only nine fine model simulations are needed. The initial trust region and extraction radius are $\delta^{(1)} = \|x_c^*\|_\infty$ and $\delta_e = 5\|x_c^*\|_\infty$, respectively. The final mapping is given by

$$B^{(9)} = \begin{bmatrix} 1.10000 & -0.20000 \\ 0.197229 & 0.90049 \end{bmatrix},\ c^{(9)} = \begin{bmatrix} 1.00139 \\ 1.00285 \end{bmatrix},\ s^{(9)} = \begin{bmatrix} 0 \\ 0 \end{bmatrix},\ t^{(9)} = \begin{bmatrix} 0 \\ 0 \end{bmatrix},$$
$$\sigma^{(9)} = 1.0,\ \gamma^{(9)} = 0 \text{ and } \eta^{(9)} = 0.99999 \tag{6.16}$$

The final parameters given in (6.16) show that the mapping (6.15) is successfully recovered. The initial and final fine model designs are given in Table 6.1. The value of U in each iteration is shown in Fig. 6.7.

6.5.2 A Capacitively-Loaded 10:1 Impedance Transformer [83]

We consider the design of a capacitively-loaded 10:1 impedance transformer. The fine and coarse models are shown in Figs. 6.8 and 6.9, respectively. The values of the capacitances are given in Table 6.2. Design specifications are

$$|S_{11}| \le 0.50 \text{ for } 0.5 \text{ GHz} \le \omega \le 1.5 \text{ GHz} \tag{6.17}$$

The electrical lengths of the two transmission lines at 1.0 GHz are selected as designable parameters. The characteristic impedances are kept fixed at the optimal values given in Table 6.3. Both models make use of the ideal transmission line model available in OSA90/hope. Eleven frequency points were simulated per sweep. We utilized the real and imaginary parts of S_{11} in the optimization procedure (6.7)-(6.8). The initial trust region size and extraction radius are $\delta^{(1)} = 0.09\|x_c^*\|_\infty$ and $\delta_e = 0.09\|x_c^*\|_\infty$, respectively. The algorithm executed five iterations.

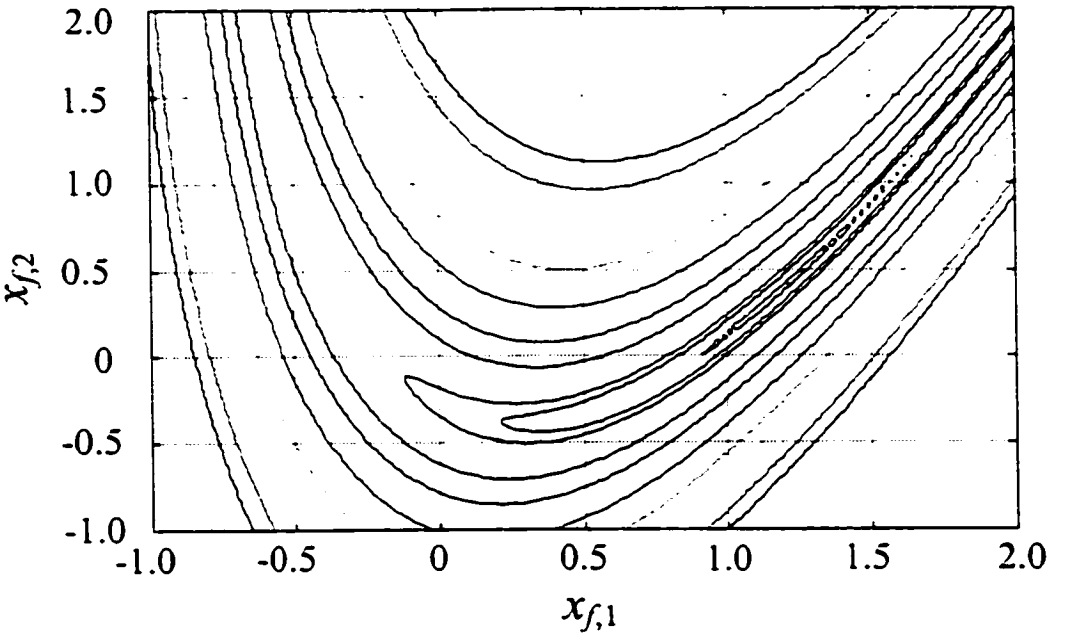

Fig. 6.5. The contours of U for the fine model of the Rosenbrock example.

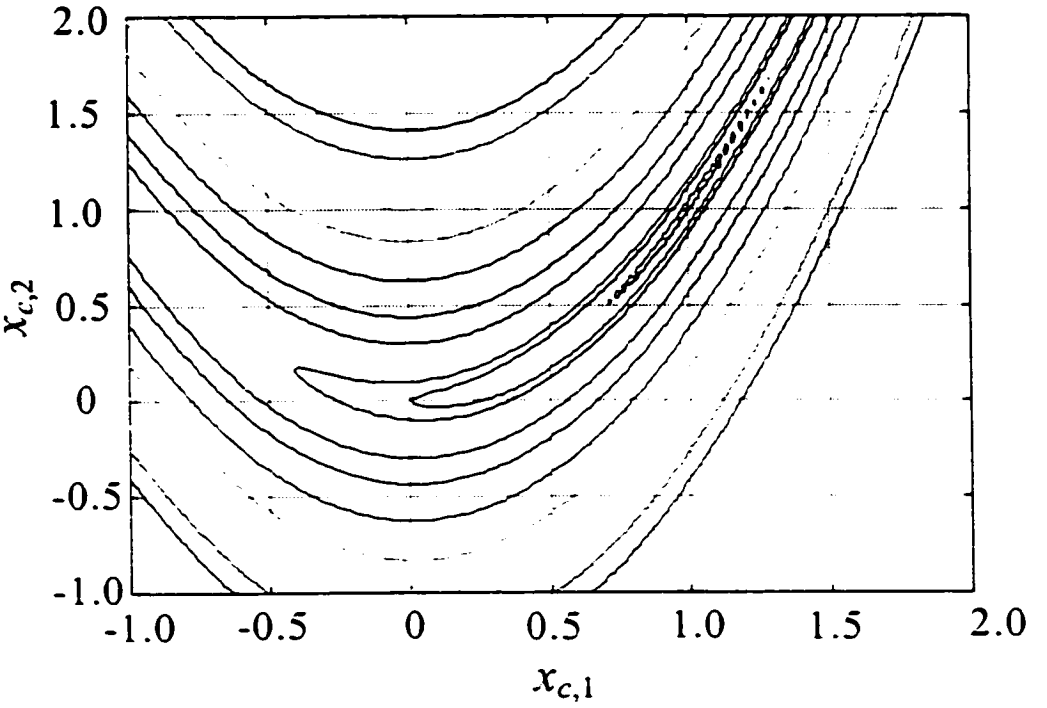

Fig. 6.6. The contours of U for the coarse model of the Rosenbrock example.

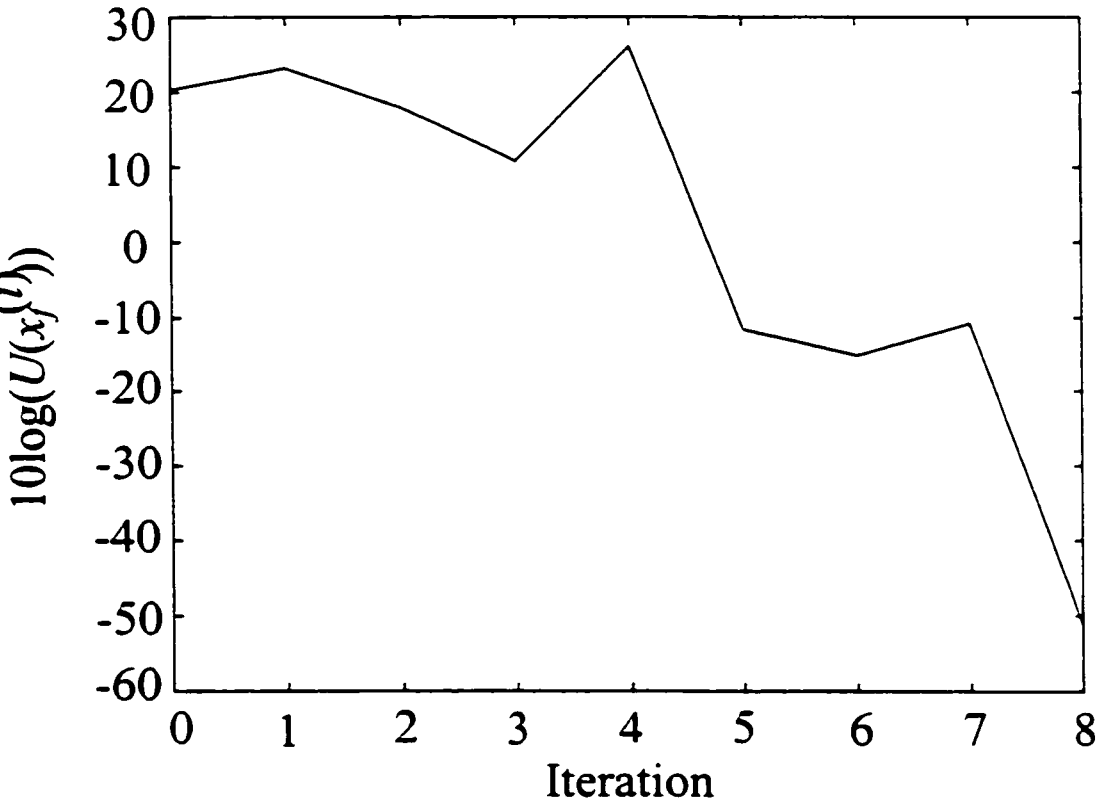

Fig. 6.7. The value of U in each iteration for the Rosenbrock example.

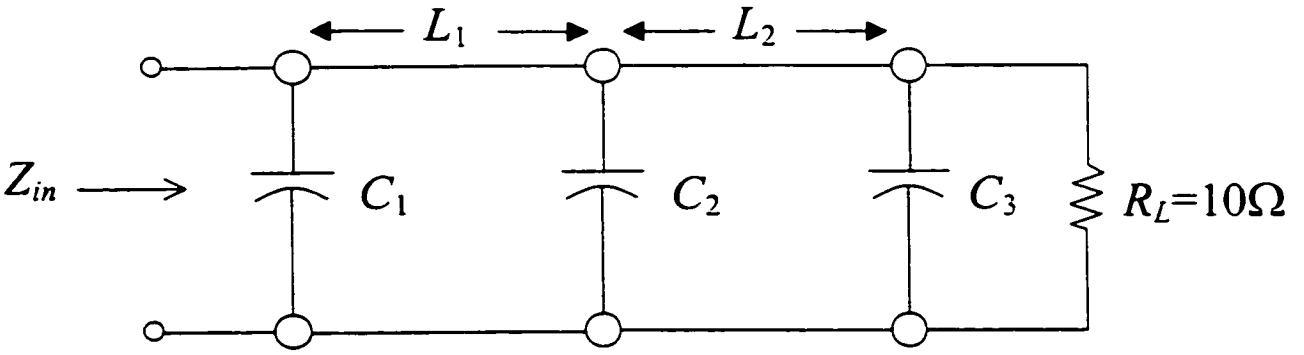

Fig. 6.8. The fine model of the capacitively-loaded 10:1 impedance transformer.

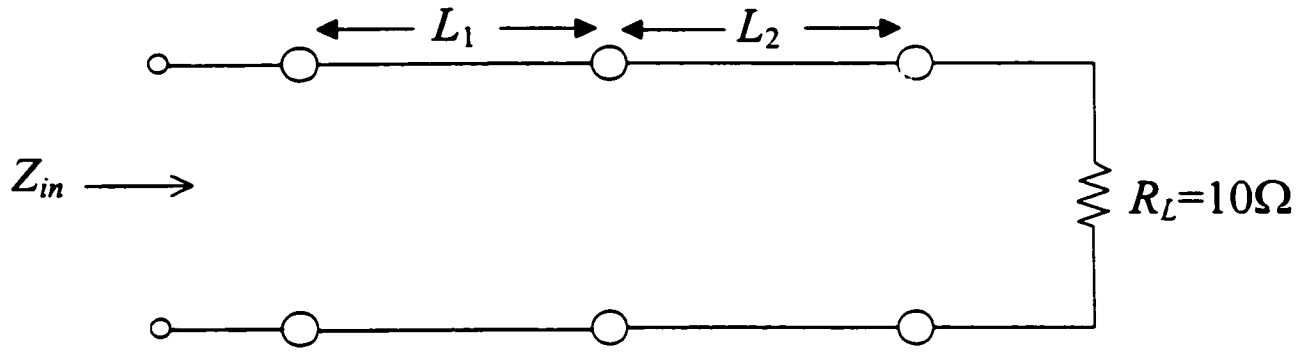

Fig. 6.9. The coarse model of the capacitively-loaded 10:1 impedance transformer.

TABLE 6.1
INITIAL AND FINAL FINE MODEL DESIGNS FOR THE ROSENBROCK FUNCTION

Parameter	$x_f^{(1)}$	$x_f^{(9)}$
$x_{f,1}$	1.0	1.27520
$x_{f,2}$	1.0	0.50037

TABLE 6.2
THE FINE MODEL CAPACITANCES FOR THE CAPACITIVELY-LOADED IMPEDANCE TRANSFORMER

Capacitance	Value
C_1	10
C_2	10
C_3	10
all values are in pF	

TABLE 6.3
THE CHARACTERISTIC IMPEDANCES FOR THE CAPACITIVELY-LOADED IMPEDANCE TRANSFORMER

Impedance	Value
Z_1	2.23615
Z_2	4.47230
all values are in Ohm	

TABLE 6.4
THE FIRST THREE DESIGNS FOR THE CAPACITIVELY-LOADED IMPEDANCE TRANSFORMER

Parameter	$x_f^{(1)}$	$x_f^{(2)}$	$x_f^{(3)}$
L_1	90.0000	81.9000	81.59880
L_2	90.0000	81.9000	74.38324
all values are in degrees			

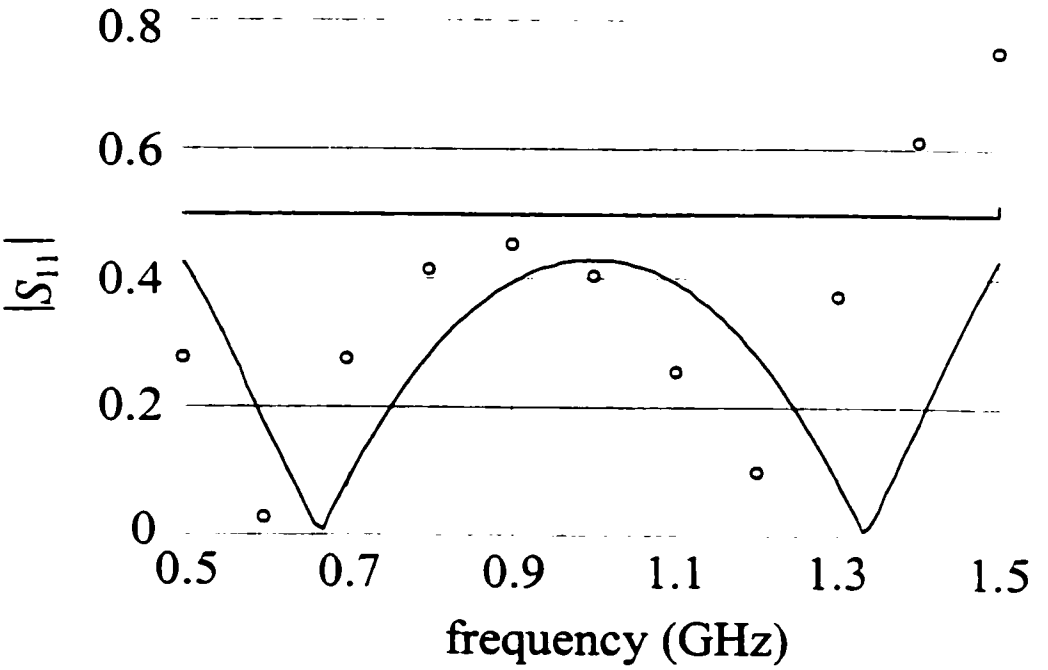

Fig. 6.10. The optimal coarse model response (—) and the fine model response (o) at the starting point for the capacitively-loaded 10:1 impedance transformer.

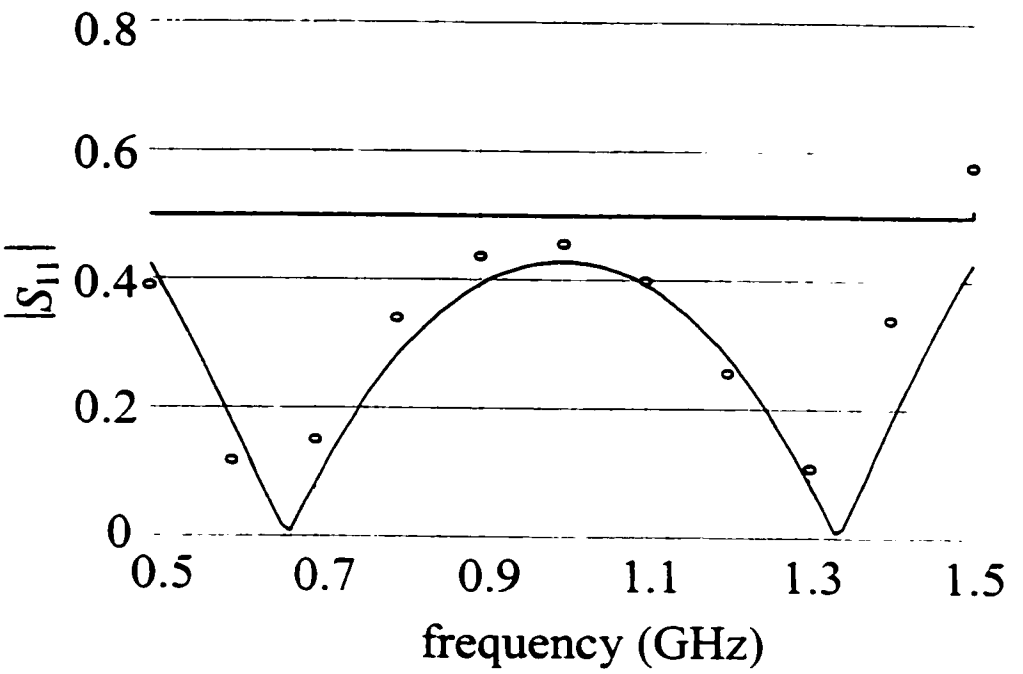

Fig. 6.11. The optimal coarse model response (—) and the fine model response (o) at the end of the first successful iteration for the capacitively-loaded 10:1 impedance transformer.

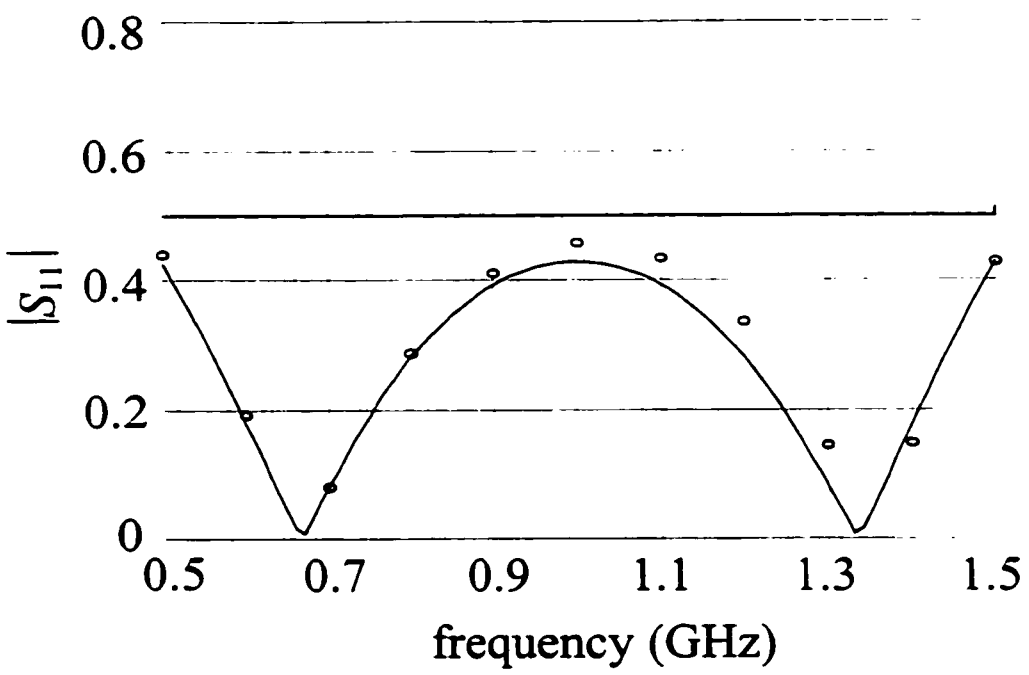

Fig. 6.12. The optimal coarse model response (—) and the fine model response (o) at the end of the second successful iteration for the capacitively-loaded 10:1 impedance transformer.

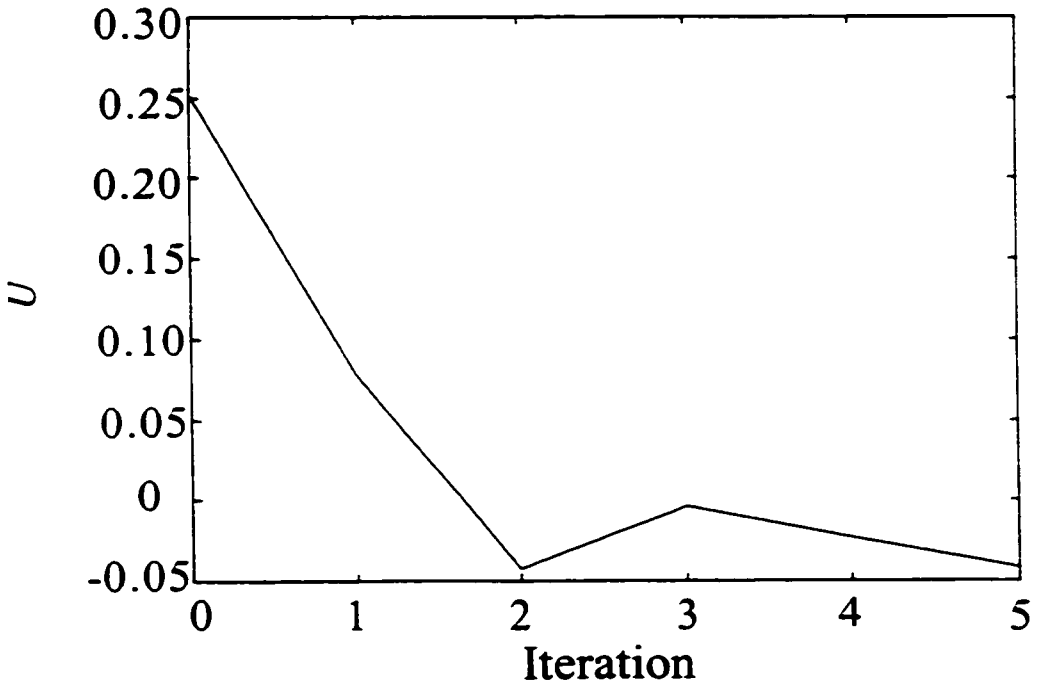

Fig. 6.13. The change of U with each iteration for the 10:1 impedance transformer.

Only the first two are successful. The total number of fine model simulations is seven. The first three designs are shown in Table 6.4. The corresponding responses are shown in Figs. 6.10, 6.11 and 6.12. The value of the U in every iteration are shown in Fig. 6.13. The final mapping is given by

$$\boldsymbol{B}^{(6)} = \begin{bmatrix} 1.12886 & 0.19245 \\ -0.17669 & 1.19167 \end{bmatrix},\ \boldsymbol{c}^{(6)} = \begin{bmatrix} 84.52643 \\ 87.95123 \end{bmatrix},\ \boldsymbol{s}^{(6)} = \begin{bmatrix} -0.06863 \\ 0.06035 \end{bmatrix},$$
$$\boldsymbol{t}^{(6)} = \begin{bmatrix} -0.00026 \\ -0.00212 \end{bmatrix},\ \sigma^{(6)} = 1.03243 \text{ and } \gamma^{(6)} = 0.00983 \tag{6.18}$$

6.5.3 The Double-Folded Stub Filter

The DFS fine model utilizes Sonnet's ***em*** through Empipe (See Fig. 3.2). We utilize the coarse model shown in Fig 4.18. The design specifications for this problem are given by (5.28)-(5.29).

L_1, L_2 and S are selected as designable parameters. W_1 and W_2 are fixed at 4.8 mil. Only eleven frequency points are utilized per frequency sweep. The mapping parameters are obtained using the real and imaginary parts of S_{21}. The initial trust region and extraction radius are $\delta^{(1)} = 0.09\left\|\boldsymbol{x}_c^*\right\|_\infty$ and $\delta_e = 0.09\left\|\boldsymbol{x}_c^*\right\|_\infty$, respectively. The width S is scaled by a factor of 6.0 to make the problem better conditioned.

The design procedure is carried out with the interpolation option of Empipe disabled. Here, every iterate is snapped to the nearest on-grid point. The SMSM algorithm carried out only 16 iterations. A total of 18 calls to Empipe (18 ***em*** simulations) were needed. The initial and final designs are given in Table 6.5. The corresponding responses are shown in Figs. 6.14 and 6.15, respectively. The value of U in each iteration is shown in Fig. 6.16. The final mapping is given by

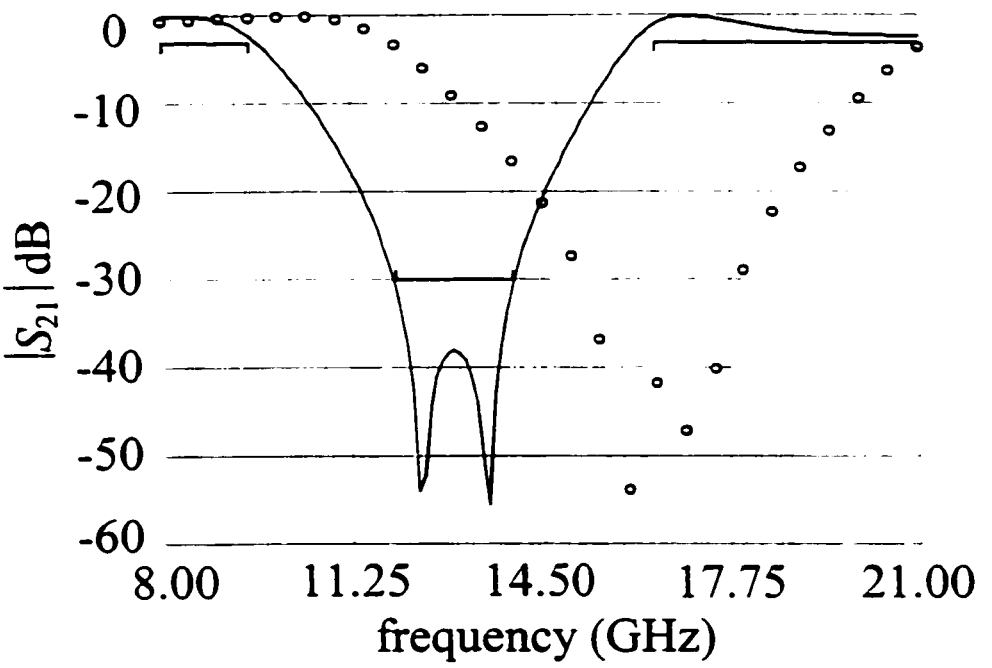

Fig. 6.14. The optimal coarse model response (—) and the fine model response (o) at the starting design for the DFS filter.

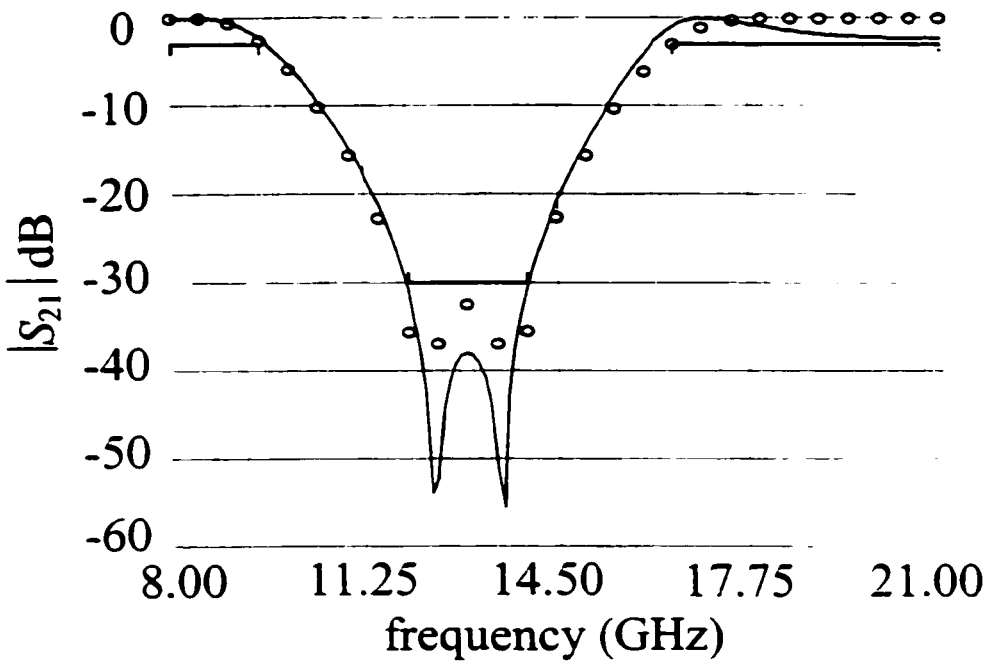

Fig. 6.15. The optimal coarse model response (—) and the fine model response (o) at the final design for the DFS filter.

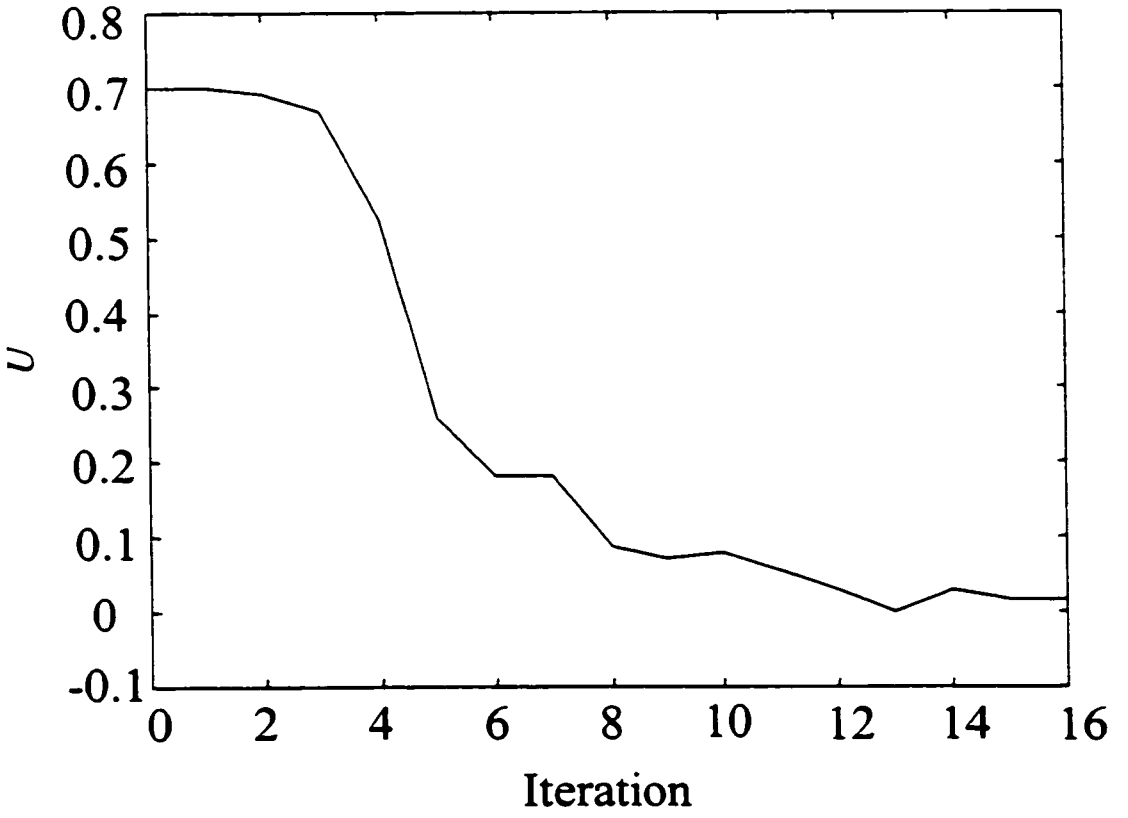

Fig. 6.16. The value of U in every iteration for the DFS filter.

$$B^{(17)} = \begin{bmatrix} 1.03074 & 0.11174 & 0.00031 \\ -0.20595 & 0.96384 & 0.00365 \\ -0.35144 & 0.34204 & 0.78257 \end{bmatrix},\ c^{(17)} = \begin{bmatrix} 236.1134 \\ 21.5218 \\ 74.8218 \end{bmatrix},$$

$$s^{(17)} = \begin{bmatrix} 0.44639 \\ 0.70939 \\ 0.50045 \end{bmatrix},\ t^{(17)} = \begin{bmatrix} 0.03854 \\ -0.01167 \\ 0.00439 \end{bmatrix},\ \sigma^{(17)} = 1.13771 \text{ and } \gamma^{(17)} = -0.55168 \tag{6.19}$$

6.5.4 The HTS Filter

We also consider the HTS filter. This filter is illustrated in Fig. 3.5. The design specifications are

$$|S_{21}| \le 0.05 \text{ for } \omega \le 3.967 \text{ GHz and } 4.099 \text{ GHz} \le \omega$$
$$|S_{21}| \ge 0.95 \text{ for } 4.008 \text{ GHz} \le \omega \le 4.058 \text{ GHz} \tag{6.20}$$

The designable parameters are L_1, L_2, L_3, S_1, S_2 and S_3. We take L_0 = 50 mil and W = 7 mil. The coarse model exploits the empirical models of microstrip lines, coupled lines and open stubs available in OSA90/hope (see Fig. 3.6). The fine model employs the method of moments simulator ***em*** through Empipe. We utilized the real and imaginary parts of both S_{11} and S_{21} in the optimization procedure (6.7)-(6.8). The initial trust region is $\delta^{(1)} = 0.20\left\|x_c^*\right\|_\infty$. The δ_e-neighborhood is selected as an n-dimensional box. This takes into account that the response is more sensitive to the lengths than the widths. The interpolation option of Empipe is disabled to make the optimization time reasonable.

We solved this problem for two different cases. For the first case, the substrate dielectric is assumed lossless and a relatively coarse grid size is used. The material and physical parameters values used in both OSA90/hope and in ***em*** are shown in Table 6.6. SMSM simulates the fine model at 16 frequency points. Starting from the snapped optimal coarse

TABLE 6.5
THE INITIAL AND FINAL DESIGNS FOR THE DFS FILTER WITHOUT INTERPOLATION

Parameter	$x_f^{(1)}$	$x_f^{(17)}$
S	9.60	6.4
L_2	60.80	84.8
L_1	67.2	86.4
all values are in mils		

TABLE 6.6
MATERIAL AND PHYSICAL PARAMETERS FOR THE HTS FILTER

Model Parameter	First Case		Second Case	
	OSA90/hope	*em*	OSA90/hope	*em*
substrate dielectric constant	23.425	23.425	23.425	23.425
substrate thickness (mil)	19.9516	19.9516	20	20
shielding cover height (mil)	∞	250	∞	250
Conducting material thickness	0	0	0	0
Substrate dielectric loss tangent	0	0	3.0e-5	3.0e-5
Resistivity of metal (Ωm)	0	0	0	0
Surface roughness of metal	0	—	0	—
Magnetic loss tangent	—	0	—	0
Surface reactance (Ω/sq)	—	0	—	0
x-grid cell size (mil)	—	1.00	—	1.00
y-grid cell size (mil)	—	1.75	—	1.00

TABLE 6.7
THE INITIAL AND FINAL DESIGNS OF THE FINE MODEL FOR THE HTS FILTER (FIRST CASE)

Parameter	$x_f^{(1)}$	$x_f^{(8)}$
L_1	188.00	188.00
L_2	198.00	192.00
L_3	189.00	187.00
S_1	22.75	22.75
S_2	99.75	78.75
S_3	112.00	91.00
all values are in mils		

TABLE 6.8
THE INITIAL AND FINAL DESIGNS OF THE FINE MODEL FOR THE HTS FILTER (SECOND CASE)

Parameter	$x_f^{(1)}$	$x_f^{(5)}$
L_1	188	196
L_2	198	184
L_3	189	195
S_1	22	23
S_2	99	79
S_3	112	90
all values are in mils		

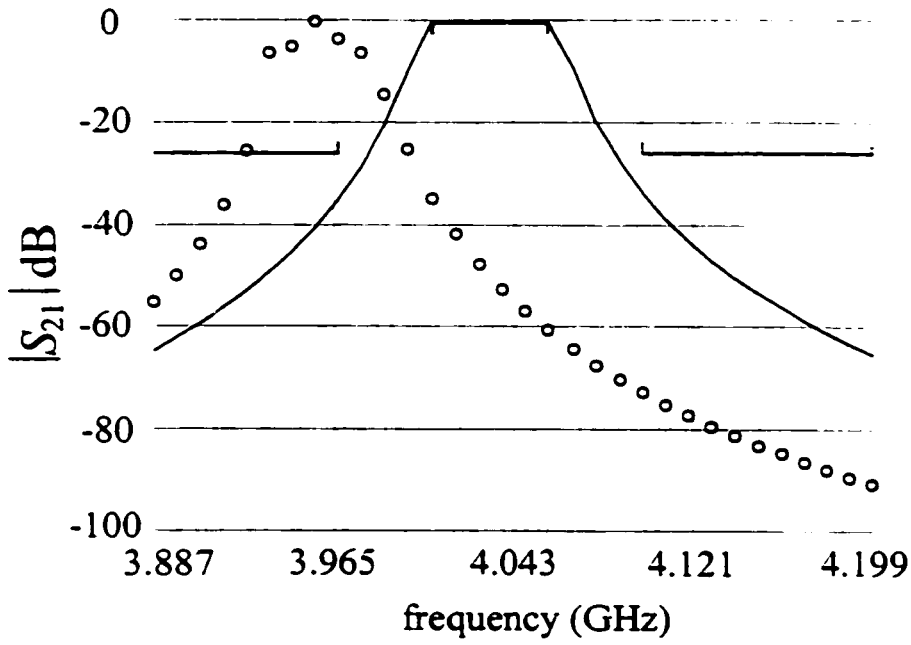

Fig. 6.17. The optimal coarse model response (—) and the fine model response (o) at the initial design for the HTS filter (first case).

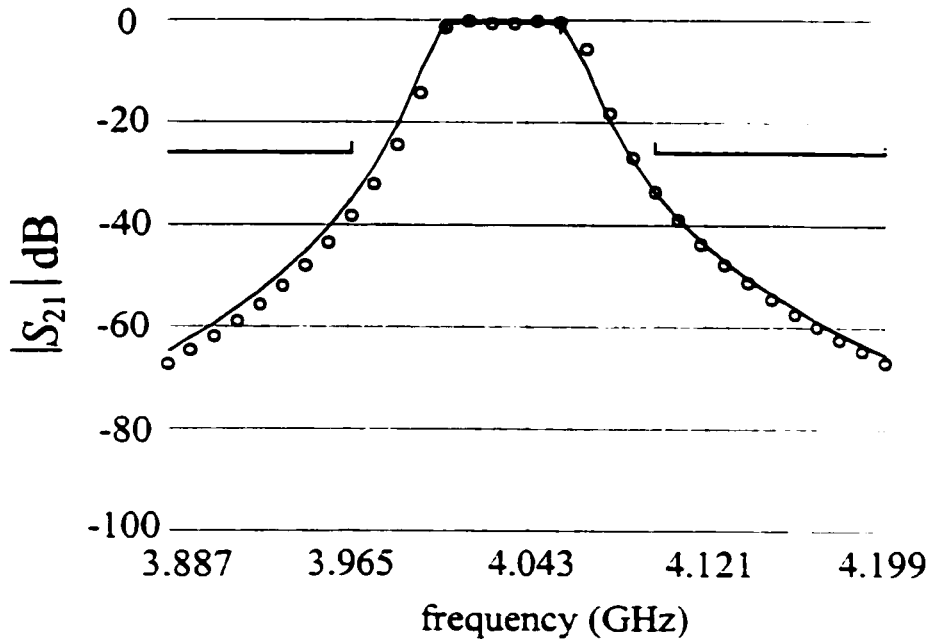

Fig. 6.18. The optimal coarse model response (—) and the fine model response (o) at the final design for the HTS filter (first case).

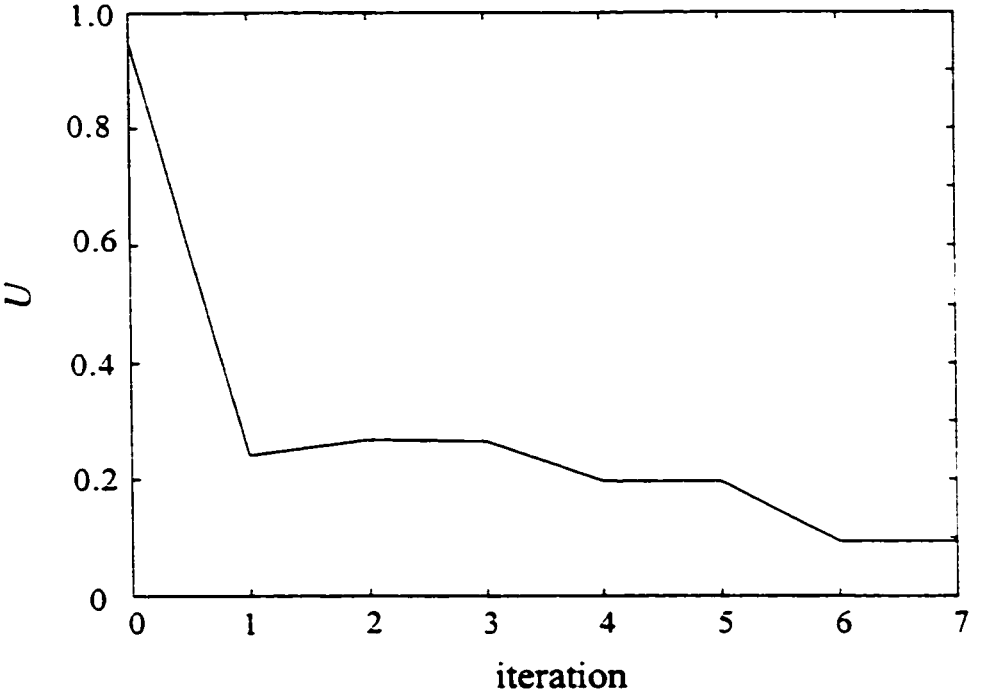

Fig. 6.19. The value of U in every iteration for the HTS filter (first case).

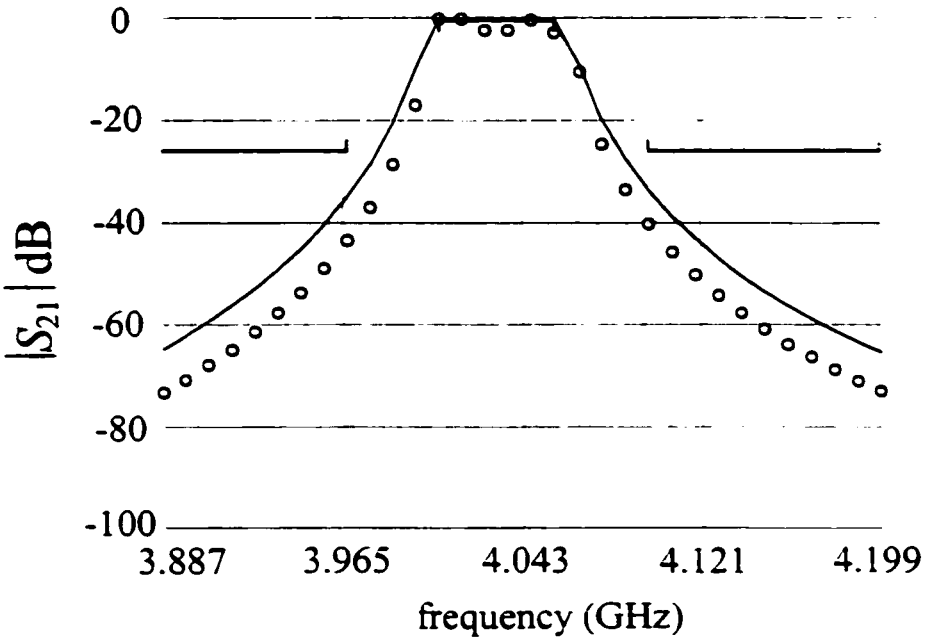

Fig. 6.20. The optimal coarse model response (—) and the fine model response (o) at the end of the first iteration for the HTS filter (first case).

design, the final design is reached in 7 iterations only. A total of 7 fine model simulations are used. The initial and final designs are given in Table 6.7. The corresponding responses are shown in Figs 6.17 and 6.18, respectively. The value of the objective function in each iteration is shown in Fig. 6.19.

Fig. 6.20 illustrates the fine model response at the end of the first iteration. It is seen that the fine model response is well aligned in the proper band using only one fine model simulation. This illustrates the power of SMSM in handling significant frequency shifts. The final mapping is given by

$$\boldsymbol{B}^{(8)} = \begin{bmatrix} 1.08894 & 0.00855 & -0.01082 & 0.01422 & -0.07505 & -0.00979 \\ -0.00481 & 0.96627 & -0.00695 & 0.00912 & -0.03234 & -0.00592 \\ 0.00828 & -0.00831 & 0.97551 & -0.01433 & 0.02963 & 0.00955 \\ -0.01513 & 0.01509 & -0.02016 & 1.04437 & 0.01671 & -0.01747 \\ -0.01324 & 0.01320 & -0.01766 & 0.02317 & 1.03175 & -0.01541 \\ -0.01401 & 0.01400 & -0.01869 & 0.02453 & 0.00672 & 0.95969 \end{bmatrix},$$

$$\boldsymbol{c}^{(8)} = \begin{bmatrix} 180.61046 \\ 190.38887 \\ 180.53859 \\ 23.96889 \\ 98.89007 \\ 113.32096 \end{bmatrix}, \quad \boldsymbol{t}^{(8)} = \boldsymbol{s}^{(8)} = \boldsymbol{0}, \quad \sigma^{(8)} = 1.07264, \quad \gamma^{(8)} = -0.12873 \tag{6.21}$$

The problem is resolved taking into account the substrate losses and using a finer grid as shown in Table 6.6. Here, the fine model is simulated over 9 frequency points only. The final design is reached in 4 iterations that required only 5 model simulations. The initial and final designs are given in Table 6.8. The corresponding responses are shown in Figs. 6.21 and 6.22, respectively. The values of the objective function in every iteration are shown in Fig. 6.23. The final mapping is given by

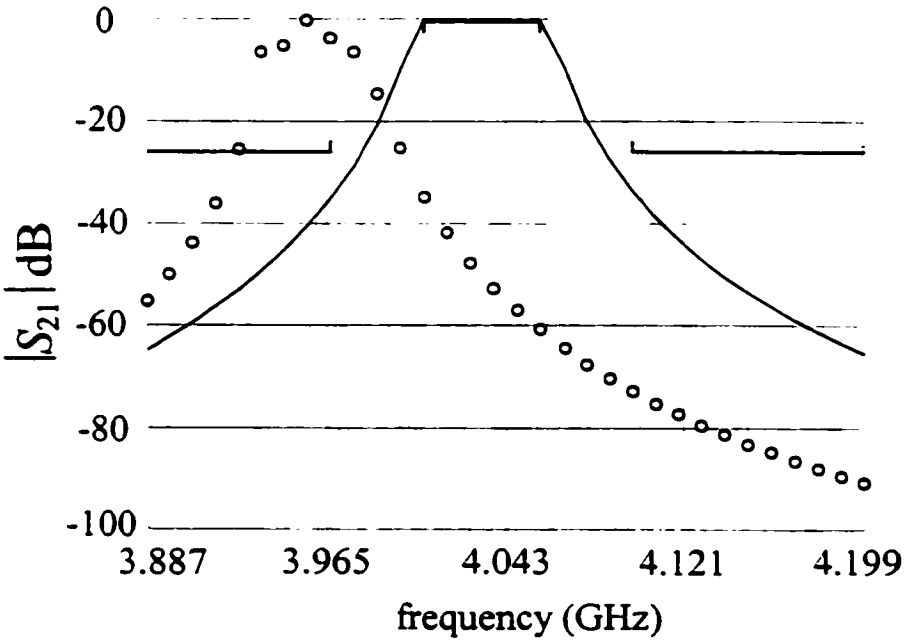

Fig. 6.21. The optimal coarse model response (—) and the fine model response (o) at the initial design for the HTS filter (second case).

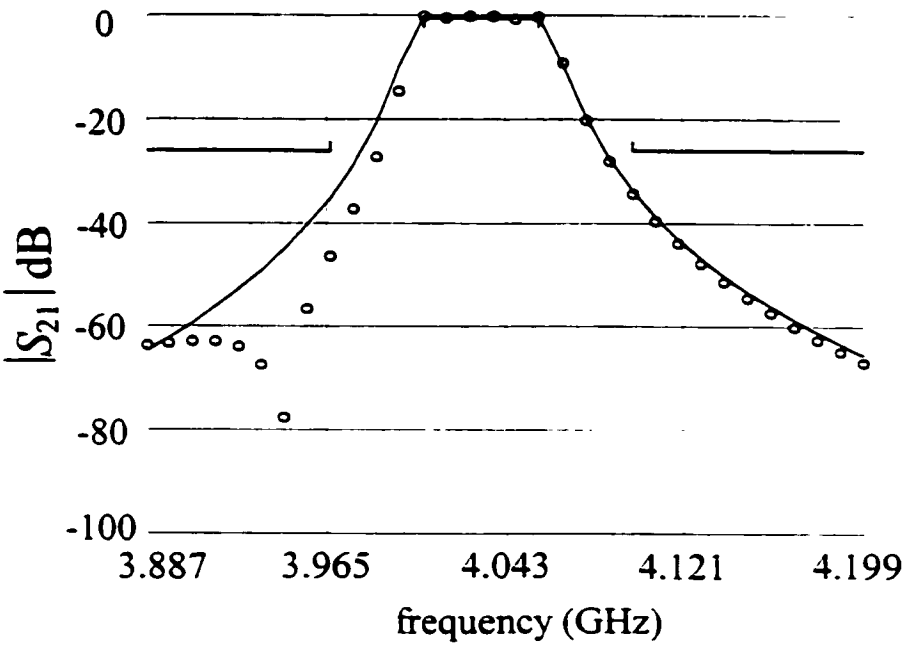

Fig. 6.22. The optimal coarse model response (—) and the fine model response (o) at the final design for the HTS filter (second case).

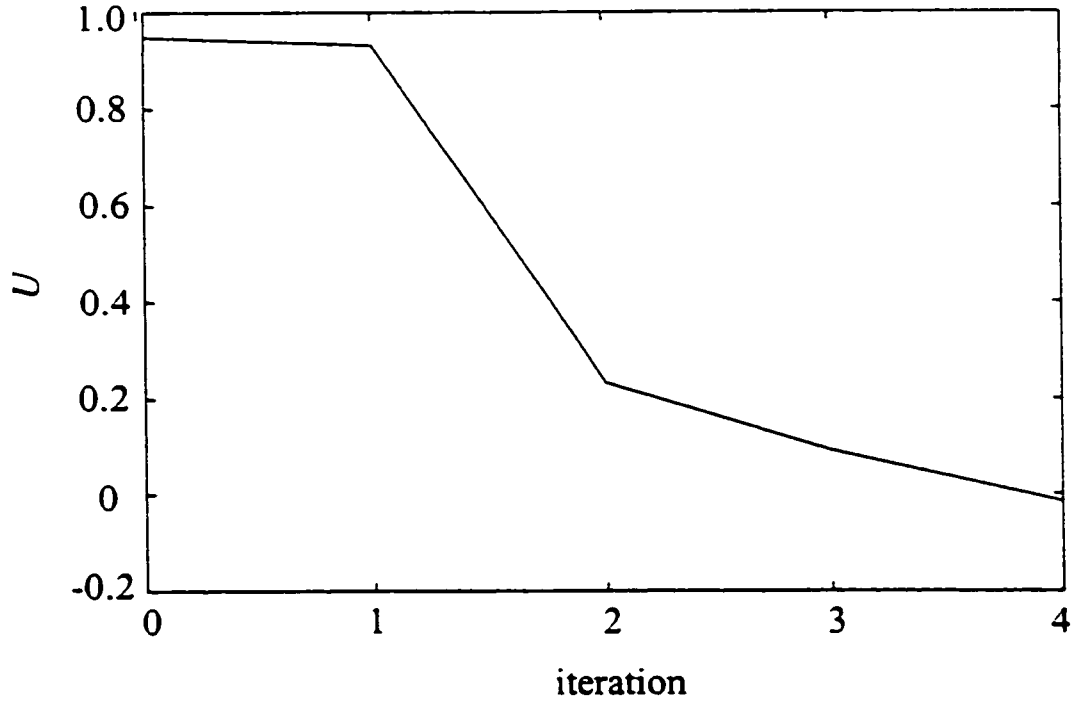

Fig. 6.23. The value of U in every iteration for the HTS filter (second case).

$$\boldsymbol{B}^{(5)} = \begin{bmatrix} 1.05301 & 0.00431 & -0.01655 & 0.03619 & -0.00836 & 0.03555 \\ 0.00490 & 0.95554 & 0.00673 & 0.00290 & 0.00322 & -0.01593 \\ -0.00702 & 0.00230 & 1.04096 & -0.00433 & -0.00400 & 0.02236 \\ -0.00083 & 0.00041 & -0.00119 & 0.99243 & -0.00057 & 0.00249 \\ -0.01196 & 0.00400 & -0.01577 & 0.01405 & 0.99812 & 0.03589 \\ -0.00691 & 0.00237 & -0.00920 & -0.00400 & -0.00465 & 1.33652 \end{bmatrix},$$

$$\boldsymbol{c}^{(5)} = \begin{bmatrix} 187.64378 \\ 183.51110 \\ 187.54660 \\ 24.06764 \\ 102.04845 \\ 104.05073 \end{bmatrix}, \quad \boldsymbol{t}^{(5)} = \boldsymbol{s}^{(5)} = \boldsymbol{0}, \quad \sigma^{(5)} = 1.08403, \quad \gamma^{(5)} = -0.17298 \tag{6.22}$$

6.6 CONCLUSIONS

We presented a Surrogate Model-based Space Mapping (SMSM) algorithm for efficient optimization of microwave circuits. The SMSM algorithm integrates SM optimization with surrogate model-based optimization. It exploits a surrogate model in the form of a convex combination of a mapped coarse model and a linearized fine model. The mapped coarse model utilizes a linear frequency-sensitive mapping. During optimization, the coarse and fine models are simulated over different frequency ranges. This approach is shown to be powerful especially if significant response shift exists. SMSM is successfully illustrated through the design of microwave filters and transformers.

7

CONCLUSIONS

This thesis has presented recent advances in Space Mapping (SM) optimization of microwave circuits. SM optimization aims at efficiently optimizing a time-intensive fine model using mainly coarse model simulations while maintaining the confidence supplied by fine model simulations.

Chapter 2 concerned itself with reviewing some of the basic concepts of circuit optimization. We briefly discussed the different types of error norms and their minimization algorithms. The basic concept of SM optimization was introduced. We reviewed the first two SM-based optimization algorithms; the original SM algorithm and Aggressive Space Mapping (ASM). The nonuniqueness problem of Parameter Extraction (PE) and its effect on the convergence of SM optimization were addressed. We illustrated the ASM algorithm through the design of a microwave impedance transformer.

Chapter 3 addressed the Trust Region Aggressive Space Mapping (TRASM) algorithm. TRASM integrates a trust region methodology with ASM. A Levenberg-Marquardt approach is used to convert this problem to a linear system of equations. The Recursive Multi-Point parameter Extraction (RMPE) procedure utilized by TRASM was also presented. This procedure makes use of the available mapping and fine model points. We illustrated the TRASM algorithm through the design of microwave filters and transformers.

Chapter 5 concerned itself with addressing the case of a poor coarse model. A lemma that relates the developed mapping to the fine and coarse model derivatives was presented. Through this lemma, we showed that SM-based optimization algorithms indirectly approximate the fine model derivatives using the coarse model derivatives and the available mapping. The

Hybrid Aggressive Space Mapping (HASM) algorithm exploits this lemma to handle the poor coarse model case. The two-phase approach utilized by HASM is explained. HASM was illustrated through a number of examples.

The PE problem is thoroughly reviewed in Chapter 4. We illustrated the Multi-Point Extraction (MPE) procedure used for enhancing the uniqueness of PE. This approach matches the responses of the fine and coarse models at a number of perturbed points. The Aggressive Parameter Extraction (APE) algorithm was reviewed. APE automates the selection of perturbations that are likely to impact the uniqueness of PE. APE was illustrated through the parameter extraction of a number of coarse models.

The SM-based optimization algorithms addressed in Chapters 2, 4 and 5 formalize the design problem as a nonlinear system of equations. These algorithms also utilize a frequency-insensitive mapping. During the course of the optimization algorithm, the fine and coarse models are simulated at different points but at the same set of frequencies. The Surrogate Model-based Space Mapping (SMSM) optimization algorithm, presented in Chapter 6, generalizes these concepts. SM optimization is formulated as a general optimization problem of a surrogate model. The construction of this surrogate model was explained. The algorithm also utilizes a frequency-sensitive linear mapping. We showed that this approach is powerful especially if significant response shift exists. The SMSM algorithm has been implemented in the *SMX* [90] engineering modeling and optimization system.

The theoretical work in this thesis has been amply supported by examples. Known difficult analytical examples were used to test the feasibility and robustness of the respective algorithm. Practical problems were also used to show the efficiency and engineering relevance of the algorithms discussed. For most of the practical examples, the fine model is presented by an Electromagnetic (EM) simulator. The coarse models are mainly empirical/circuit-theoretic models. The microwave literature is rich with models that can be utilized as coarse models.

The algorithms presented in this thesis can be implemented by any microwave engineer. MATLAB, for example, can be used for this purpose. A data link between the simulator and the optimizer has to be established for fast and accurate data transfer. This data link is a simulator-dependent and must be created for every utilized simulator.

We expect that more research will be carried out in SM optimization technology. We foresee that this research will lead to the following developments:

1. Making the SM optimization of arbitrary microwave structures feasible through
   - Automating the generation of coarse models by utilizing rational function approximation and equivalent circuit approximation. Currently, the generation of coarse models is the user's responsibility.
   - Developing a theory for the optimality and convergence properties of SM optimization.
2. Exploiting Artificial Neural Networks (ANN) in SM Optimization. A pioneering work [91, 92] approximates the mapping within a region of interest using ANN. ANN can approximate frequency-sensitive mappings of any order of nonlinearity.
3. Application of SM optimization and efficient derivative estimation to the design of antenna structures, CoPlanar Waveguide (CPW) structures and Multi-Layer (ML) circuits. Problems of special interest are the automated design of printed-circuit antennas and CPW and ML filters.

BIBLIOGRAPHY

[1] J.E. Dennis, Jr., and J.J. Moré, "Quasi-Newton methods, motivation and theory," *SIAM Rev.*, vol. 19, 1977, pp. 46-89.

[2] C.G. Broyden, "Quasi-Newton methods and their application to function minimization," *Math. Comp.*, vol. 21, 1967, pp. 368-381.

[3] W.C. Davidon, "Variable metric method for minimization," Rep. ANL-5900 Rev., *Argonne National Laboratories*, Argonne, IL, 1959

[4] R. Fletcher and M.J.D. Powell, "A rapidly convergent descent method for minimization," *Comput. J.*, vol. 6, 1963, pp. 163-168.

[5] P.E. Gill and W. Murray, "Quasi-Newton methods for unconstrained minimzation," *J. Inst. Math. Appl.*, vol. 9, 1972, pp. 91-108.

[6] C.G. Broyden, "A class of methods for solving nonlinear simultaneous equations," *Math. Comp.*, vol. 19, 1965, pp. 577-593.

[7] R. Flectcher and C.M. Reeves, "Function minimisation by conjugate gradients," *Comput. J.*, vol. 7, 1964, pp. 149-154.

[8] D. Le, "A fast and robust unconstrained optimization method requiring minimum storage," *Math. Program.*, vol. 32, 1985, pp. 41-68.

[9] J.E. Dennis, Jr., and R.B. Schnabel, *Numerical Methods for Unconstrained Optimization and Nonlinear Equations*. New Jersey: Prentice-Hall, 1983.

[10] A.D. Waren, L.S. Lasdon and D.F. Suchman, "Optimization in engineering design," *Proc. IEEE*, vol. 55, 1967, pp. 1885-1897.

[11] W. Murray and M.L. Overton, "A projected Lagrangian algorithm for nonlinear ℓ_1 optimization," *SIAM J. Scient. Stat. Comp.*, vol. 2, 1981, pp. 207-224.

[12] J.W. Bandler, W. Kellermann and K. Madsen, "A superlinearly convergent minimax algorithm for microwave circuit design," *IEEE Trans. Microwave Theory Tech.*, vol. MTT-33, 1985, pp. 1519-1530.

[13] D. Angew, "Improved minimax optimization for circuit design," *IEEE Trans. Circuits Syst.*, vol. CAS-28, 1981, pp. 791-803.

[14] J.W. Bandler, S.H. Chen, S. Daijavad, W. Kellermann, M. Renault and Q.J. Zhang, "Large scale minimax optimization of microwave multiplexers," *Proc. European Microwave Conf.* (Dublin, Ireland), 1986, pp. 435-440.

[15] C. Charalambous, "Minimax design of recursive digital filters," *Computer Aided Design*, vol. 6, 1974, pp. 73-81.

[16] C. Charalambous and A.R. Conn, "Optimization of microwave networks," *IEEE Trans. Microwave Theory Tech.*, vol. MTT-23, 1975, pp. 834-838.

[17] J. Hald and K. Madsen, "Combined LP and quasi-Newton methods for minimax optimization," *Math. Program.*, vol. 20, 1981, pp. 49-62.

[18] K. Madsen, H. Schjaer-Jacobson and J. Voldby, "Automated minimax design of networks," *IEEE Trans. Circuits Syst.*, vol. CAS-22, 1975, pp. 791-796.

[19] M.R. Osborne and G.A. Watson, "An algorithm for minimax optimization in the nonlinear case," *Comput. J.*, vol. 12, 1969, pp. 63-68.

[20] J.W. Bandler, S.H. Chen and K. Madsen, "An algorithm for one-sided ℓ_1 optimization with application to circuit design centering," *Proc. IEEE Int. Symp. Circuits Syst.* (Espoo, Finland), 1988, pp. 1795-1798.

[21] J.W. Bandler, W. Kellermann and K. Madsen, "A nonlinear ℓ_1 optimization algorithm for design, modeling and diagnosis of networks," *IEEE Trans. Circuits Syst.*, vol. CAS-34, 1987, pp. 174-181.

[22] J. Hald and K. Madsen, "Combined LP and quasi-Newton methods for nonlinear ℓ_1 optimization," *SIAM J. Numer Anal.*, vol. 22, 1985, pp. 68-80.

[23] M.R. Osborne and G. A. Watson, "On an algorithm for discrete nononlinear ℓ_1 optimization," *Comput. J.*, vol. 14, 1971, pp. 184-188.

[24] J.W. Bandler, S.H. Chen and S. Daijavad, "Microwave device modeling using efficient ℓ_1 optimization: a novel approach," *IEEE Trans. Microwave Theory Tech.*, vol. MTT-34, 1986, pp. 1282-1293.

[25] J.W. Bandler and C. Charalambous, "Practical least *p*th optimization of networks," *IEEE Trans. Microwave Theory Tech.*, vol. MTT-20, 1972, pp. 834-840.

[26] J.W. Bandler, S.H. Chen, R.M. Biernacki, L. Gao, K. Madsen and H. Yu, "Huber optimization of circuits: a robust approach," *IEEE Trans. Microwave Theory Tech.*, vol. 41, 1993, pp. 2279-2287.

[27] ***em***™, Sonnet Software, Inc., 1020 Seventh North Street, Suite 210, Liverpool, NY 13088.

[28] *Maxwell Eminence*™, Version 4.02, Ansoft Corporation, Four Station Square, Suite 660, Pittsburgh, PA 15219, USA.

[29] HP HFSS™, HP EESof, now Agilent Technologies, 1400 Fountaingrove Parkway, Santa Rosa, CA 95403-1799.

[30] J.W. Bandler, R.M. Biernacki, S.H. Chen, P.A. Grobelny and R.H. Hemmers, "Space mapping technique for electromagnetic optimization," *IEEE Trans. Microwave Theory Tech.*, vol. 42, 1994, pp. 2536-2544.

[31] J.W. Bandler, R.M. Biernacki, S.H. Chen, R.H. Hemmers and K. Madsen, "Electromagnetic optimization exploiting aggressive space mapping," *IEEE Trans. Microwave Theory Tech.*, vol. 43, 1995, pp. 2874-2882.

[32] J.W. Bandler, R.M. Biernacki and S.H. Chen, "Fully automated space mapping optimization of 3D structures," *IEEE MTT-S Int. Microwave Symp. Dig.* (San Francisco, CA), 1996, pp. 753-756.

[33] M.H. Bakr, J.W. Bandler, R.M. Biernacki, S.H. Chen and K. Madsen, "A trust region aggressive space mapping algorithm for EM optimization," *IEEE MTT-S Int. Microwave Symp. Dig.* (Baltimore, MD), 1998, pp. 1759-1762.

[34] M.H. Bakr, J.W. Bandler, R.M. Biernacki, S.H. Chen and K. Madsen, "A new space mapping algorithm for EM optimization" *TRIO Meeting* (Ottawa, ON), 1998.

[35] M.H. Bakr, J.W. Bandler, R.M. Biernacki and S.H. Chen, "Automated electromagnetic optimization for RF, wireless and microwave circuits," *CITO Retreat* (Hamilton, Ontario), 1998.

[36] M.H. Bakr, J.W. Bandler, R.M. Biernacki, S.H. Chen and K. Madsen, "A trust region aggressive space mapping algorithm for EM optimization," *IEEE Trans. Microwave Theory Tech.*, vol. 46, 1998, pp. 2412-2425.

[37] J.W. Bandler, M.H. Bakr, N. Georgieva, M.A. Ismail and D.G. Swanson., Jr., "Recent results in electromagnetic optimization of microwave components, including microstrip T-junctions," *Proc. 15th Annual Review of Progress in Applied Computational Electromagnetics ACES* 99 (Monterey, CA), 1999, pp. 326-333.

[38] M.H. Bakr, J.W. Bandler, N. Georgieva and K. Madsen, "A hybrid aggressive space mapping algorithm for EM optimization," *IEEE MTT-S Int. Microwave Symp. Dig.* (Anaheim, CA), 1999, pp. 265-268.

[39] J.W. Bandler, M.H. Bakr and J.E. Rayas-Sánchez, "Accelerated optimization of mixed EM/circuit structures," *Proc. Workshop on Advances in Mixed Electromagnetic Field and Circuit Simulation, IEEE MTT-S Int. Microwave Symp.* (Anaheim, CA), 1999.

[40] M.H. Bakr, J.W. Bandler, N. Georgieva and K. Madsen, "A hybrid aggressive space mapping algorithm for EM optimization," *IEEE Trans. Microwave Theory Tech.*, vol. 47, 1999, pp. 2440-2449.

[41] M.H. Bakr, J.W. Bandler and N. Georgieva, "An aggressive approach to parameter extraction," *IEEE MTT-S Int. Microwave Symp. Dig.* (Anaheim, CA), 1999, pp. 261-264.

[42] M.H. Bakr, J.W. Bandler and N. Georgieva, "An aggressive approach to parameter extraction," *IEEE Trans. Microwave Theory Tech.*, vol. 47, 1999, pp. 2428-2439.

[43] M.H. Bakr, J.W. Bandler, K. Madsen, J.E. Rayas-Sánchez and J. Søndergaard, "Space mapping optimization of microwave circuits exploiting surrogate models," *IEEE MTT-S Int. Microwave Symp. Dig.* (Boston, MA), 2000, pp. 1785-1788.

[44] M.H. Bakr, J.W. Bandler, K. Madsen, J.E. Rayas-Sánchez and J. Søndergaard, "Space mapping optimization of microwave circuits exploiting surrogate models," *IEEE Trans. Microwave Theory Tech.*, December 2000.

[45] A.J. Booker, J.E. Dennis, Jr., P.D. Frank, D. B. Serafini, V. Torczon and M.W. Trosset, "A rigorous framework for optimization of expensive functions by surrogates," *Structural Optimization*, vol. 17, 1999, pp. 1-13.

[46] M.W. Trosset and V, Torczon, "Numerical optimization using computer experiments," Technical Report 97-38, *ICASE, NASA Langley Research Center*, Hampton, Virginia 23681-2199, 1997.

[47] V. Torczon and M.W. Trosset, "Using approximations to accelerate engineering design optimization," Technical Report 98-33, *ICASE, Langley Research Center*, Hampton, Virginia 23681-2199, 1998.

[48] J.E. Dennis, Jr., and V. Torczon, "Managing approximation models in optimization," Technical Report 95-19, *Department of Computational and Applied Mathematics*, Rice University, Houston, Texas 77005-1892, 1995.

[49] N. Alexandrov, J.E. Dennis, Jr., R.M. Lewis and V. Torczon, "A trust region framework for managing the use of approximation models in optimization," *Structural Optimization*, vol. 15, 1998, pp. 16-23.

[50] J.W. Bandler, M.A. Ismail, J.E. Rayas-Sánchez and Q.J. Zhang, "Neuromodeling of microwave circuits exploiting space mapping technology," *IEEE Trans. Microwave Theory Tech.*, vol. 47, 1999, pp. 2417-2427.

[51] J.W. Bandler, N. Georgieva, M.A. Ismail, J.E. Rayas-Sánchez and Q. J. Zhang, "A generalized space mapping tableau approach to device modeling," 29th *European Microwave Conf.* (Munich, Germany), 1999, vol. 3, pp. 231-234.

[52] J.W. Bandler and S.H. Chen, "Circuit optimization: the state of the art," *IEEE Trans. Microwave Theory Tech.*, vol. 36, 1988, pp. 424-443.

[53] J.W. Bandler and M.R.M. Rizk, "Optimization of electrical circuits," *Math. Program. Study*, vol. 11, pp. 1-64, 1979.

[54] G.C. Temes and D.Y.F. Zai, "Least *p*th approximation," *IEEE Trans. Circuit Theory*, vol. CT-16, 1969, pp. 235-237.

[55] P. Huber, *Robust Statistics*. New York: Wiley, 1981.

[56] H. Ekblom and K. Madsen, "Algorithms for nonlinear Huber estimation," *BIT*, vol. 29, 1989, pp. 60-76.

[57] C. Charalambous, "Nonlinear least *p*th optimization and nonlinear programming," *Math. Program.*, vol. 12, 1977, pp. 195-225.

[58] J.W. Bandler and A.E. Salama, "Fault diagnosis of analog circuits," *Proc. IEEE*, vol. 73, 1985, pp. 1279-1325.

[59] J.J. Moré, "Recent developments in algorithms and software for trust region methods," in *Mathematical Programming, the State of the Art*, Springer Verlag, 1982, pp. 258-287.

[60] K. Madsen, "An algorithm for minimax solution of overdetermined systems of non-linear equations," *J. Inst. Math. Appl.*, vol. 16, 1975, pp. 321-328.

[61] K. Madsen and H. Schjær-Jacobsen, "Singularities in minimax optimization of networks," *IEEE Trans. Circuits and Syst*, vol. CAS-23, 1976, pp. 456-460.

[62] J.W. Bandler, "Optimization of design tolerances using nonlinear programming," *J. Optimization Theory and Applications*, vol. 14, 1974, pp. 99-114.

[63] J.W. Bandler, P.C. Liu and H. Tromp, "A nonlinear programming approach to optimal design centering, tolerancing and tuning," *IEEE Trans. Circuits Syst.*, vol. CAS-23, 1976, pp. 155-165.

[64] J.W. Bandler and H.L. Abdel-Malek, "Optimal centering, tolerancing and yield determination via updated approximations and cuts," *IEEE Trans. Circuits Syst.*, vol. CAS-25, 1978, pp. 853-871.

[65] H.L. Abdel-Malek and J.W. Bandler, "Yield optimization for arbitrary statistical distributions, Part I: Theory," *IEEE Trans. Circuits Syst.*, vol. CAS-27, 1980, pp. 245-253.

[66] H.L. Abdel-Malek and J.W. Bandler, "Yield optimization for arbitrary statistical distributions, Part II: Implementation," *IEEE Trans. Circuits Syst.*, vol. CAS-27, 1980, pp. 253-262.

[67] J.W. Bandler, R.M. Biernacki, S.H. Chen, S. Ye and P.A. Grobelny, "Multilevel multidimensional quadratic modeling for yield-driven electromagnetic optimization," *IEEE MTT-S Int. Microwave Symp. Dig.* (Atlanta, GA), 1993, pp. 1017-1020.

[68] S. Bila, D. Baillargeat, S. Verdeyme and P. Guillon, "Automated design of microwave devices using full em optimization method," *IEEE MTT-S Int. Microwave Symp. Dig.* (Baltimore, MD), 1998, pp. 1771-1774.

[69] A.M. Pavio, "The electromagnetic optimization of microwave circuits using companion models," *Proc. Workshop on Novel Methodologies for Device Modeling and Circuit CAD, IEEE MTT-S Int. Microwave Symp.* (Anaheim, CA), 1999.

[70] M.H. Bakr, J.W. Bandler, R.M. Biernacki and S.H. Chen, "Design of a three-section 3:1 microstrip transformer using aggressive space mapping," Report SOS-97-1-R, *Simulation*

Optimization Systems Research Laboratory, McMaster University, Hamilton, Canada, 1997.

[71] OSA90/hope™ Version 4.0, formerly Optimization Systems Associates Inc., P.O. Box 8083, Dundas, ON, Canada, L9H 5E7, 1997, now Agilent Technologies, 1400 Fountaingrove Parkway, Santa Rosa, CA 95403-1799.

[72] Empipe3D™, Version 4.0, formerly Optimization Systems Associates Inc., P.O. Box 8083, Dundas, ON, Canada, L9H 5E7, 1997, Chapter 5, now Agilent Technologies, 1400 Fountaingrove Parkway, Santa Rosa, CA 95403-1799.

[73] K. Levenberg, "A method for the solution of certain problems in least squares," *Quart. Appl. Math.*, vol. 2, 1944, pp. 164-168.

[74] D. Marquardt, "An algorithm for least-squares estimation of non-linear parameters," *SIAM J. Appl. Math.*, vol. 11, 1963, pp. 431-441.

[75] J.J. Moré and D.C. Sorenson, "Computing a trust region step," *SIAM J. Sci. Stat. Comp.*, vol. 4, 1983, pp. 553-572.

[76] J.C. Rautio, Sonnet Software, Inc., 1020 Seventh North Street, Suite 210, Liverpool, NY 13088, Private Communication, 1992.

[77] Empipe™ Version 4.0, formerly Optimization Systems Associates Inc., P.O. Box 8083, Dundas, Ontario, Canada L9H 5E7, now Agilent Technologies, Hewlett-Packard Company, 1400 Fountaingrove, Parkway, Santa Rosa, CA 95403-1799.

[78] J.W. Bandler, R.M. Biernacki, S.H. Chen, W.J. Gestinger, P.A. Grobelny, C. Moskowitz and S.H. Talisa, "Electromagnetic design of high-temperature superconducting filters," *Int. J. Microwave and Millimeter-Wave CAE*, vol. 5, 1995, pp. 331-343.

[79] J.W. Bandler, "Computer optimization of inhomogeneous waveguide transformers," *IEEE Trans. Microwave Theory Tech.*, vol. MTT-17, 1969, pp. 563-571.

[80] *Empipe3D™ Manual*, Version 4.0, formerly Optimization Systems Associates Inc., P.O. Box 8083, Dundas, ON, Canada, L9H 5E7, 1997, Chapter 5, now Agilent Technologies, 1400 Fountaingrove Parkway, Santa Rosa, CA 95403-1799.

[81] MATLAB®, The Math. Works, Inc., 24 Prime Park Way, Natick, MA 01760.

[82] R. Fletcher, *Practical Methods of Optimization*. New York: Wiley, Second Edition, 1987.

[83] J.W. Bandler, "Optimization methods for computer-aided design," *IEEE Trans. Microwave Theory Tech.*, vol. MTT-17, 1969, pp. 533-552.

[84] HP Empipe3D™ Version 5.2, Agilent Technologies, 1400 Fountaingrove Parkway, Santa Rosa, CA 95403-1799, 1998.

[85] C.S. Walker, *Capacitance, Inductance and Crosstalk Analysis*. Norwood, MA: Artech House, 1990.

[86] M. Kirschning, R. Jansen and N. Koster, "Measurement and computer-aided modeling of microstrip discontinuities by an improved resonator method," *IEEE MTT-S Int. Microwave Symp. Dig.* (Boston, MA), 1983, pp. 495-497.

[87] L. Young and B.M. Schiffman, "A useful high-pass filter design," *Microwave J.*, vol. 6, 1963, pp. 78-80.

[88] G.L. Matthaei, L. Young and E.M. T. Jones, *Microwave Filters, Impedance-Matching Network and Coupling Structures*. New York: McGraw-Hill, First Edition, 1964.

[89] N. Marcuvitz, *Waveguide Handbook*. New York: McGraw-Hill, First Edition, 1951, p. 221.

[90] *SMX, Simulation Optimization Systems Research Laboratory*, McMaster University, Hamilton, Canada, 2000.

[91] M.H. Bakr, J.W. Bandler, M.A. Ismail, J.E. Rayas-Sánchez and Q.J. Zhang, "Neural space mapping optimization of EM microwave structures," *IEEE MTT-S Int. Microwave Symp. Dig.* (Boston, MA), 2000, pp. 879-882.

[92] M.H. Bakr, J.W. Bandler, M.A. Ismail, J.E. Rayas-Sánchez and Q.J. Zhang, "Neural space mapping optimization for EM-based design," *IEEE Trans. Microwave Theory Tech.*, December 2000.

Subject Index

Aggressive Parameter Extraction (APE), 1, 2, 61, 72, 73, 75, 90, 96, 138, 168

Double Folded Stub (DFS) filter, 2, 27, 32, 34, 35, 61, 85, 92, 93, 94, 96, 125, 129, 130, 131, 132, 135, 150, 154

em, 2, 20, 27, 32, 34, 36, 37, 80, 150, 153, 154

Empipe, 32, 150, 153

Full rank, 68, 72, 108

Generalized Space Mapping, 135

Hessian matrix, 71

High Temperature Superconducting (HTS) filter, 2, 27, 33, 37, 38, 39, 42, 61, 80, 86, 87, 88, 89, 90, 91, 135, 153, 154, 155, 156, 157, 159

HP HFSS, 2, 27, 55, 56, 57, 92, 117, 121, 125

Huber norm, 9

Huber optimization, 10

Hybrid Aggressive Space Mapping (HASM), 102, 103, 105, 111, 115, 117, 120, 129, 133, 168

Interpolation, 32

Jacobian matrix, 68, 115

Linearized Fine Model (LFM), 135, 140

Locally nonunique minimum, 69, 73

Locally unique minimum, 69, 71, 85

l_p norm, 10, 11, 12

l_1 norm, 10, 11, 12

l_2 norm, 10, 11, 12, 72, 73

l_∞ norm, 10, 11

Maxwell Eminence, 2, 27, 43, 46, 47, 50, 54

Mapped Coarse Model (MCM), 135, 136, 140

Monte Carlo, 59, 60, 61

Multi-Point Extraction (MPE), 27, 29, 31, 61, 67, 68, 69, 70, 71, 72, 78, 92, 103, 104, 105, 112, 114, 168

Objective function, 9, 28, 70, 71, 111, 113, 135, 140, 157, 158

OSA90/hope, 20, 36, 37, 80, 92, 121, 144, 153, 154

Parameter Extraction (PE), 1, 2, 24, 27, 61, 96, 103, 111, 113, 115, 160, 168

Perturbation, 29, 59, 61, 67, 69, 70, 71, 72, 73, 78, 108, 138

Recursive Multi-Point Extraction (RMPE), 27, 29, 30, 61, 112, 160

Responses, 1, 5, 6, 7, 8, 20, 24, 27, 31, 32, 36, 59, 67, 68, 69, 71, 80, 81, 85, 108, 111, 133, 135, 136, 150, 157, 158, 168

Rosenbrock function, 73, 76, 77, 104, 141

Single-Point Extraction (SPE), 15, 16, 18, 19, 28, 36, 61, 73, 85, 87, 92, 111, 112

Space Mapping-based NeuroModeling (SMN), 135

Specifications, 5, 6, 7, 9, 10, 20, 24, 32, 33, 55, 78, 80, 117, 125

Surrogate model, 1, 2, 168

TRASM, 1, 2, 27, 28, 32, 36, 43, 59, 61, 67, 102, 104, 105, 111, 135, 160, 168

Trust Region, 1, 2, 27, 61, 160

Yield, 10, 11, 61